Mechanisms involved in the fast combustion of organic powders : application to dust explosions

Matteo Pietraccini

Laboratoire Réactions et Génie des Procédés – CNRS (UMR 7274)

Ecole doctorale :
Science et Ingénierie des Molécules, des Produits, des Procédés et de l'Énergie

THESIS

Presented and defended publicly on:

December 9th, 2022

for obtaining the title of

Doctor of the University of Lorraine

Process, Product and Molecules Engineering

by

Matteo PIETRACCINI

Sustainable Process and Chemical Engineer

Mechanisms involved in the fast combustion of organic powders: application to dust explosions

---

Composition of the jury :

Referees:	Jean-François BRILHAC	Pr. - University of Haute-Alsace (President of the jury)
	Guy MARLAIR	HDR - INERIS
Members:	Gaëlle DUCOM	Dr. - INSA Lyon
	Agnès JANÈS	Dr. - CRAMIF Paris
	Luca MARMO	Dr. - Polytechnic of Turin
	Olivier DUFAUD	Pr. - University of Lorraine (Thesis Director)
	Pierre-Alexandre GLAUDE	Dr. - University of Lorraine – CNRS (Thesis Co-Director)
	Anthony DUFOUR	Dr. - University of Lorraine – CNRS (Thesis Supervisor)

She done already done had herses

RuPaul Charles

Acknowledgements

It is beyond difficult to thank everyone who participated professionally and personally in my thesis work, but I will still try my best.

I want to express my most sincere gratitude to my supervisors, Olivier, Pierre-Alexandre and Anthony, for showing me three different approaches to scientific research and, in general, to life. It has been challenging to have three voices echoing in my head, but I feel very enriched and lucky for had this opportunity. I cannot help to make a special mention of Olivier. He believed in me from the beginning and allowed me to experience many beautiful things during these three years, which will be fundamental for my future.

During these three years, many people stepped by the laboratory, and many left a permanent mark on my life. I want to thank Erika for everything we shared: coffee, gossip, stress, wine, gin-tonic, beautiful moments and much more. And may the odds be with her. I know for sure that we will keep on sharing beautiful moments. I want to thank Stephanie and Mathilde for every cold coffee, every minute we spent complaining, and every laugh. We formed a beautiful team (Totally Spies). I want to thank all the BJC, the past, the present and the future. I want to thank Andres for his movie choice, recipes, and talent to kill every plant I gave him and for all the laughter. I want to thank the team SAFE for the coffee breaks and for making our 1st floor the best. I want to thank everyone who crossed my path for making this experience unique and unforgettable.

A huge thanks to my family for always supporting me. The distance was often a non-negligible obstacle to overcome, but we always managed to support each other.

And, of course, I want to thank Monia for all the support she gave me during these challenging years and, in general, for being part of my life.

Abstract

It was on a misty night on the 14th of December 1785 that a *"spontaneous inflammation"*, as described later by Count Morozzo Della Rocca, occurred in a bakery in Turin, Italy. From that episode, considered the first-ever documented accident caused by a dust explosion, the scientific community has built a profound knowledge of this phenomenon. However, the comprehension of the numerous physical and chemical mechanisms involved is still not complete. The aim of this work is to identify the processes that have a primary role in organic dust explosions, study them and propose experimental tools to characterise them better. Choosing operating conditions coherent with those encountered during a dust explosion will be crucial.

First, a large selection of organic powders was dispersed in a Godbert-Greenwald furnace to quantify their tendency to agglomerate when suspended as a dust cloud. The pulse pressure played a major role in determining agglomeration or deagglomeration. Dispersion tests were also carried out in the same apparatus at higher temperatures to focus on another fundamental brick of organic dust fast combustion: the pyrolysis process. The reaction products were collected and analysed, constituting the input data for a pyrolysis lumped mechanism. Additionally, the potential synergy between the gaseous pyrolysis product and solid phases was investigated by performing hybrid mixture explosion tests in the 20L sphere. The role of solid and condensable pyrolysis products was also included. Lastly, unstretched flame speed, determined in the 20L sphere and a vertical semi-open tube, was compared to that estimated in a micro-fluidised bed burner. The latter was characterised in terms of fluidisation regimes to generate a stable flow of pyrolysis products, oxidised subsequently in the burner.

A deeper understanding of the single phenomena involved in an organic dust explosion led to a deeper comprehension of the global one by avoiding the "black-box approach". The agglomeration process, the pyrolysis and oxidation mechanisms, the behaviour of the hybrid mixture generated during an explosion and the flame propagation step are fundamental bricks that were profoundly studied in this work and can build a solid and complete model tailored for dust explosions.

Resumé

C'est par une nuit brumeuse du 14 décembre 1785 qu'une "*inflammation spontanée*", telle que décrite plus tard par le comte Morozzo Della Rocca, s'est produite dans une boulangerie à Turin, en Italie. Depuis cet épisode, considéré comme le premier accident documenté causé par une explosion de poussière, la communauté scientifique a construit une profonde connaissance de ce phénomène. Cependant, la compréhension des mécanismes physico-chimiques impliqués n'est pas encore complète. L'objectif de ce travail est d'identifier les processus qui jouent un rôle primaire dans les explosions de poussières organiques, de les étudier et de proposer des outils expérimentaux pour mieux les caractériser. Le choix de conditions opératoires cohérentes avec celles rencontrées lors d'une explosion de poussières sera crucial.

Dans un premier temps, une sélection de poudres organiques a été dispersée dans un four Godbert-Greenwald afin de quantifier leur tendance à s'agglomérer lorsqu'elles sont en suspension sous forme de nuage de poussière. La pression du pulse a joué un rôle majeur dans la détermination de l'agglomération ou de la désagglomération. Des tests de dispersion ont également été réalisés dans le même appareil à haute température afin de se concentrer sur une autre brique fondamentale de la combustion rapide des poussières organiques : la pyrolyse. Les produits de la réaction ont été collectés et analysés, constituant les données d'entrée d'un mécanisme condensé de pyrolyse. De plus, la synergie potentielle entre le produit gazeux de la pyrolyse et les particules a été étudiée en réalisant des tests d'explosion de mélanges hybrides dans la sphère de 20L. Le rôle des produits de solides et condensables a également été inclus. Enfin, la vitesse de la flamme non étirée, déterminée dans la sphère de 20L et dans un tube semi-ouvert vertical, a été comparée à celle estimée dans un brûleur couplé à un micro-lit fluidisé. Ce dernier a été caractérisé en termes de régimes de fluidisation pour générer un flux stable de produits de pyrolyse, oxydés ensuite dans le brûleur.

Une compréhension plus approfondie des phénomènes individuels impliqués dans une explosion de poussières organiques a permis de mieux appréhender le phénomène global en évitant l'approche de la "boîte noire". Le processus d'agglomération, les mécanismes de pyrolyse et d'oxydation, le comportement du mélange hybride généré lors d'une explosion et l'étape de propagation de flamme sont des briques fondamentales qui ont été étudiées en profondeur dans ce travail et qui permettent de construire un modèle solide et complet adapté aux explosions de poussière.

Contents

List of figures

List of tables

Preamble

General context

Powders have always characterised people's daily life and numerous industrial processes. Whether they are by-products, wastes, energy sources or working media, their unique features make them interesting materials for many purposes. For example, coal and wood dusts have been employed as an energy source for centuries; sawdust is inevitably present in all wood manufacturing sites; silica sand found fundamental roles in construction, glass production or fluidised bed reactors; the food industry is pervaded by powdered food, such as flour, starch, sugar, milk and coffee. Powder handling and manipulation are thus merged with several common and standard processes. A significant fraction of the powdered materials in the industry is constituted by organic powders, which are, by definition, combustible powders. Interest has grown in their regard, especially in the energy sector, due to their relatively high energy density. However, their utilisation is inevitably accompanied by risks to people, the environment and infrastructures. Being subdivided materials, they can cause problems to the respiratory system, generate fires, and, if specific conditions are satisfied, participate in dust explosions.

The XXth has been a turning century for dust explosions. The growing awareness and conscience toward these phenomena have increased the number of accident reports and scientific works. Nowadays, it is common knowledge to differentiate them from other accidental cases, such as gas explosions, self-heating processes and fireballs, since the physicochemical mechanisms involved are different, as well as the consequences on people, equipment and the environment. Hence, the industry needs a deep understanding of these phenomena to prevent them. Different approaches can be adopted and summed in three principal families:

- experimentation (lab-scale tests and experience feedback);
- modelling (transport phenomena equations, CFD and dimensionless number analysis);
- hybrid methods (a merger of the two).

According to needs and limitations, one approach may be preferred to another. Applying them to dust explosions means dealing with multiphasic heterogeneous explosible systems, considering numerous parameters interacting and changing in time and space. Nevertheless,

they are reproducible on a lab scale with some approximations, which must be considered in further analysis to establish their influence on the results.

Global approach of this work

Based on these premises, this work aims to study an organic dust explosion, identify the most significant phenomena involved and elaborate a method to characterize them. The simplification of the system is necessary to study the mechanisms involved in organic dust explosions. However, it is crucial to understand better which factors play a major role and which ones can be neglected. The first phase involves identifying the crucial steps that constitute the global process, dismantling it and allowing more punctual analyses. Their role will be thus examined, described and characterized by employing apparatuses typically used to assess the flammability, explosibility, and explosion severity. A focus on these instruments' versatility will be included by proposing original modifications and novel uses. During this stage, dimensionless numbers will be exploited to characterize the multiple regimes potentially encountered in a dust explosion, as in Di Benedetto (Di Benedetto et al. 2010). The parameters ruling on these regimes (i.e. particle size, temperature, ignition energy, etc.) will be studied and directly related to the experimental results regarding ignition sensitivity and explosion severity. The work of Cuervo Rodriguez (Cuervo Rodriguez 2018) will be used as an inspiration to carry out this study. A modelling part will complete the experimental study, and functional parameters will be determined to widen the range of applicability.

Experimental strategy

Intending to study the physical-chemical mechanisms involved in an organic dust explosion, it is mandatory to reproduce the characteristic features of these phenomena:

- High subdivision degree (particle sizes inferior to 200 µm, approximately);
- Short time scales (in the order of magnitude of 100-200 ms);
- Suspension of the powder (the reacting unit is a dust cloud).
- High particle heating rates (greater than 1000°C per second)

The apparatuses commonly used to determine the ignition sensitivity and explosion severity parameters seem to be the optimal choice to fulfil the tasks. First, they have been broadly described, studied and revised, offering rich scientific works that can be used as a

comparison to validate the results and inspire new research strategies. Moreover, they are relatively versatile to be modified and adapted to specific needs. The setups chosen for this work are the Godbert-Greenwald oven, the Hartmann tube and the 20-L sphere. They allowed the investigation of multiple phenomena involved in an organic dust explosion: particle agglomeration, de-agglomeration and segregation in a dust cloud, ignition, fast pyrolysis and combustion, hybrid mixture explosions and flame propagation. This last was also examined in a different apparatus: a micro-fluidised bed. Although it does not allow studying the behaviour of a dust cloud, it will enable recreating a short time scale process involving highly subdivided materials (powders). The characteristics of these four apparatuses are comparable yet different. The 20L sphere is a standard setup broadly and thoroughly studied. Still, it does not allow the control of the conditions at which an explosion occurs, obtaining global results that can only be exploited through semi-empirical relationships. The G-G furnace is a free-fall system that imposes the reactor's temperature and the dust cloud residence time. Therefore, finer control of the operating conditions is possible. In addition, the vertical propagation tube determines a dust cloud's flame speed. Results are global, but they can directly be calculated from experiments. Finally, the fluidised bed represents a slightly different setup but allows the separation of pyrolysis and oxidation steps, generating a continuous regime test complementary to the others.

Manuscript structure

The following chapters will present the most relevant results of this thesis, which were redacted in the form of scientific publications, except for Chapter 1. Hence, some parts, for example the "Materials and Methods" sections, may be repeated throughout the manuscript. In addition, a brief introduction will be added to each part to indicate its context and purpose and the points previously discussed to simplify the reader's journey. It should also be noted that the preliminary work of this thesis has already been the subject of publications which will not be repeated extensively in this manuscript. The ensemble of the published works during the PhD period is reported afterwards.

- **Chapter 1** is dedicated to a literature review, where a critical analysis of the background of dust explosions is carried out, pointing out the reasons that promoted the development of this domain in industrial safety. Furthermore, the most sensitive features of a dust explosion will be introduced, with particular attention to biomass powders.

- **Chapter 2** presents the work entitled "*A travel through space and time in the Godbert-Greenwald furnace: the evolution of a dust cloud particle size distribution*". It focuses on the characterization of the modification that occurs to the particle size distribution (PSD) of a dust cloud in an apparatus currently used for ignition sensitivity tests.
- The work entitled "*Study of flash pyrolysis and combustion of biomass powders using the Godbert-Greenwald furnace: an essential step to better understand organic dust explosions*" constitutes **Chapter 3**. The apparatus employed in the previous chapter is now used to characterize flash pyrolysis and combustion step in an organic dust explosion. This work was submitted to *Process Safety and Environmental Protection*.
- Results presented in **Chapter 4** go under the title *"Making hybrid mixture explosions a common case"*, and they were exploited for proposing hybrid mixtures as a tool to study the role of pyrolysis in an organic dust explosion. The work was submitted to a special issue of *Journal of Loss Prevention in the Process Industries*.
- In the following chapter, **Chapter 5**, biomass pyrolysis in a micro-fluidized bed was compared to fast biomass oxidation in the same apparatus, focusing on the process operability. The work's title is *"Effect of air on the operability of biomass pyrolysis in a micro-fluidized bed"*. The results and conclusions of this part will be exploited in the next chapter. The publication will be submitted to Energy&Fuels in the early 2023.
- Finally, in **Chapter 6**, the flame propagation step becomes the protagonist in the study titled *"A three-way experimental method to determine the laminar flame speed of organic powders"*. A comparison between three experimental approaches for determining the laminar flame speed of a biomass powder was made. Modelling was also used to support the results.
- In **Chapter 7**, some general conclusions summarize the main results of these works, enlightening their relative roles in determining the mechanisms involved in biomass dust explosions. Several perspectives and ideas for future studies are then proposed.
- Supplementary material and results are presented in the **Annexes**.

List of publications

The table below resumes the publications developed during the PhD, including those that were not considered in this thesis manuscript, which were the object of international conferences.

Authors	Pietraccini, Delon, Santandrea, Pacault, Glaude, Dufour and Dufaud
Title	*Determination of heterogeneous reaction mechanisms: A key milestone in dust explosion modelling*
Journal	Journal of Loss Prevention in the Process Industries 73 (2021)
DOI	10.1016/j.jlp.2021.104589
Status	Published
Authors	Pietraccini, Santandrea, Verdonck, Dufour, Glaude and Dufaud
Title	*Dust Explosions: A New Path To Estimate The Explosibility Characteristics Of An Organic Powder*
Journal	2021 AIChE Spring Meeting and 17th Global Congress on Process Safety proceeding
DOI	Scopus
Status	Published
Authors	Pietraccini, Badu, Glaude, Dufour and Dufaud
Title	*Organic Dust Explosions: Is It All Just About Pyrolysis?*
Journal	Chemical Engineering Transactions 90 (2022)
DOI	10.3303/CET2290037
Status	Published
Authors	Pietraccini, Danzi, Marmo, Glaude, Dufour and Dufaud
Title	*Particle Size Distribution in a Godbert-Greenwald Furnace: Experiments and Modelling*
Journal	Chemical Engineering Transactions 90 (2022)
DOI	10.3303/CET2290079
Status	Published
Authors	Pietraccini, Badu, Tait, Glaude, Dufour, Dufaud
Title	*Study of flash pyrolysis and combustion of biomass powders using the Godbert-Greenwald furnace: An essential step to better understand organic dust explosions*
Journal	Process Safety and Environmental Protection
DOI	10.1016/j.psep.2022.11.041
Status	Published
Authors	Pietraccini, Glaude, Dufour, Marmo, Danzi and Dufaud
Title	*A travel through space and time in the Godbert-Greenwald furnace: the evolution of a dust cloud particle size distribution*
Journal	Powder Technology
DOI	-
Status	To be submitted
Authors	Pietraccini, Glaude, Dufour and Dufaud
Title	*Making hybrid mixture explosions a common case*
Journal	Journal of Loss Prevention in the Process Industries
DOI	-
Status	Under review

Authors	Pietraccini, Glaude, Dufour and Dufaud
Title	*Effect of air on the operability of biomass pyrolysis in a micro-fluidized bed*
Journal	Energy & Fuels
DOI	-
Status	To be submitted
Authors	Pietraccini, Glaude, Dufour and Dufaud
Title	*A three-way experimental method to determine the laminar flame speed of organic powders*
Journal	-
DOI	-
Status	To be submitted

CHAPTER 1

Summary

The first chapter is dedicated to a general description of the current knowledge about dust explosions, focusing on those involving organic powders. After a brief discussion about the definitions of an explosion, the global phenomenon is described by dividing it into fundamental steps: particle heating, pyrolysis, oxidation and flame propagation were chosen as such. This part is followed by the accidentology, a journey between the major accidents caused by a dust explosion. Next, the latter was studied more in detail via the parameters usually used to characterise it, starting with those related to the ignition sensitivity. The tendency of a dust cloud to be ignited is a function of its interaction with the surrounding environment. It is thus fundamental to understand and estimate the probability of ignition. Once it occurs, the explosion severity becomes the main characterising parameter. Information and notions presented in this chapter are meant to support and complete the experimental results obtained in the following.

Resumé

Le premier chapitre est consacré à une description générale des connaissances actuelles sur les explosions de poussières, en se concentrant sur celles impliquant des poudres organiques. Après une brève discussion sur les définitions d'une explosion, le phénomène global est décrit en le divisant en étapes fondamentales : échauffement de la particule, pyrolyse, oxydation et propagation de flamme. Cette partie est suivie de l'accidentologie, un parcours entre les accidents majeurs liés à une explosion de poussières. Ensuite, elles seront étudiées plus en détail via les paramètres habituellement utilisés pour les caractériser, à commencer par ceux liés à la sensibilité à l'inflammation. La tendance d'un nuage de poussière à s'enflammer est fonction des interactions avec le milieu environnant, un aspect fondamental pour estimer la probabilité d'inflammation et comprendre comment la matière organique sous forme de poudre interagit avec le milieu qui l'entoure. Une fois l'inflammation survenue, la gravité de l'explosion devient le principal paramètre de caractérisation. Les informations et notions présentées dans ce chapitre sont destinées à supporter et compléter les résultats expérimentaux obtenus dans la suite.

Definition and Features of biomass dust explosions

1. General aspects of dust explosions

1.1 Definition

The answer to the question "What is a dust explosion?" is simple and complex at the same time. The discussion has its roots in the controversy over the ambiguous definition of an explosion. According to the ISO 80079-36:2016 standard, an explosion is "a sudden increase of pressure and temperature, due to oxidation or other exothermic reaction", but also a "rapid temperature and pressure rise resulting in an audible spherically propagating pressure wave". The EN 13237:2012 standard for potentially explosive atmospheres defines an explosion as an "abrupt oxidation of decomposition reaction producing an increase in temperature, pressure or both simultaneously". The EN 1127-1:2019 standard for explosive atmospheres compares an explosion and a fire: "In contrast to burning in a fire, an explosion is essentially a self-sustained propagation of the reaction zone (flame) through the explosive atmosphere". Blasquez (Blazquez and Thorn 2010) follow the same path and analyse the difference between a fire and an explosion to define it: "An explosion is a violent release of energy caused by a physical or chemical reaction. It is accompanied by a rapid increase in pressure and usually temperature. The high speed of reaction distinguishes the explosive reaction from ordinary combustion". Moreover, the NFPA 69 standard on Explosion prevention systems describes an explosion as "The bursting or rupture of an enclosure or a container due to the development of internal pressure from a deflagration". As stated in Eckhoff (Eckhoff 2003), this phenomenon's definitions can be classified into two categories: the first one is more focused on the overpressure, and the blast wave originated from the release of chemical or mechanical energy; the second one concentrates on those explosions caused by a chemical energy release and, thus, on its causes". A definition is then proposed: "An explosion is an exothermal chemical process that, when occurring at constant volume, gives rise to a sudden and significant pressure rise".

Finding the globally accepted definition is far from being straightforward. The numerous and constantly changing situations involving an explosion have led to a versatile definition, which must be adaptable to a specific context, as proposed by Eckhoff (Eckhoff 2003). As for the dust explosions, the main character is the combustible fraction's solid state and subdivision

degree. Any combustible solid can originate a dust explosion if a high enough subdivision degree is reached, i.e. if it presents itself in the form of a powder. The principal parameter used to quantify the subdivision degree is the particle size or, more generally, the characteristic length of the particles. Generally speaking (and omitting the specific case of nanoparticles), the smaller the particle size, the faster the combustion process is, which translates into a higher flame propagation rate and, hence, a higher explosion severity. Eckhoff (Eckhoff 2003) fixed around 100 μm as the order of magnitude to classify a powder as explosible. However, one of the keys to understanding dust explosions lies in the difference between the terms "explosible" and "explosive". The "Committee of Experts on the Transport of Dangerous Goods and on the Globally Harmonized System of Classification and Labelling of Chemicals" (Committee of Experts on the Transport of Dangerous Goods and on the Globally Harmonized System of Classification and Labelling of Chemicals 2012) of the United Nations studied this distinction to clarify the classification of dangerous materials. As a result, they reported two definitions that are consistent with common knowledge:

- "Explosible" must be intended as "capable of being exploded";
- "Explosive" is "related to, characterised by, or operated by an explosion".

To conclude, an explosible dust can be either explosive or not, but an explosive dust is always explosible. The conditions for making an explosible dust explosive are several and are presented in the next section.

1.2 Phenomenology

A small size of particles of a solid combustible is insufficient to make it explosive. Since dust explosions are combustion phenomena, the conditions resumed by the fire triangle must be fulfilled simultaneously as well. So, an oxidiser is required to trigger a combustion process, and an ignition source must furnish the sufficient amount of energy to overcome the kinetic barrier associated with these reactions. The oxidiser must be able to access the combustible phase, whose concentration must lie in a specific range. The powder cannot be in a quiescent state and needs to be dispersed to be in the proper reacting interval. The particulate solid phase must then be suspended in a gaseous phase, generating an airborne dust cloud. At this state, the system can ignite. However, since an explosion is characterised by an overpressure leading to a burst wave, a system can be considered explosive only with the right level of confinement. All the necessary conditions for a dust explosion to occur are summarised in Figure 1-1.

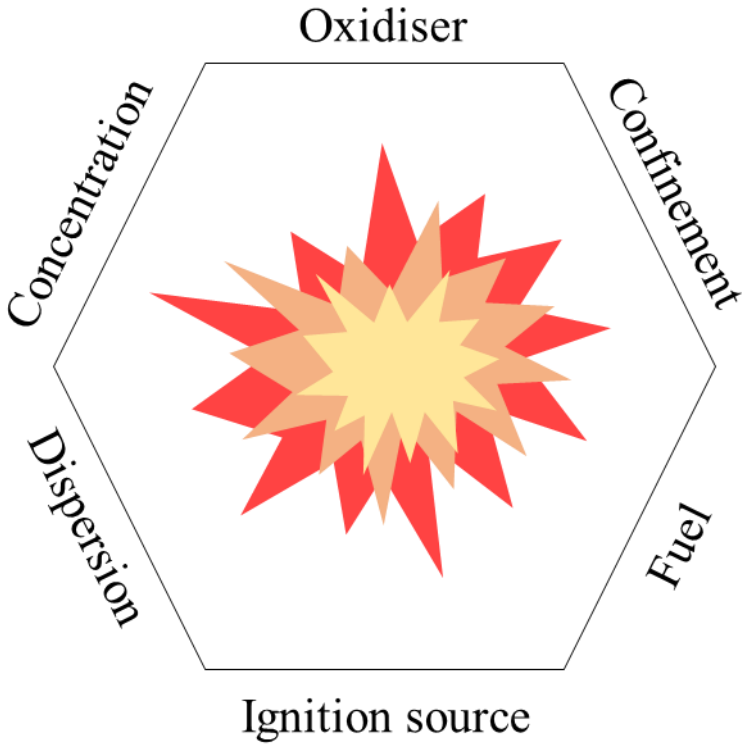

Figure 1-1 - The dust explosion hexagon

The sensitivity of a powder to ignition corresponds to the ease with which it can ignite. It is related to the probability associated with the following three-way system: ignition source, oxygen concentration and explosibility domain. Considering the powder dispersed in a gaseous phase in the form of a dust cloud, several parameters can be determined experimentally to quantify each system element, as described hereafter. The dust cloud can encounter several ignition sources: electrical sparks, hot surfaces, glowing bodies, flames, static electricity discharges, hotspots, friction particles, etc. The energy furnished by the source must be high enough to trigger the ignition and sustain the flame propagation. The ignition source from an electrical phenomenon is characterized by the Minimum Ignition Energy (MIE). In contrast, those related to heat sources are characterized by the Minimum Ignition Temperature (MIT). The minimum oxygen concentration required to propagate a flame within a dust cloud is considered through the Limiting Oxygen Concentration (LOC).

Finally, the explosion domain is defined by the Minimum Explosible Concentration (MEC). It corresponds to the minimum dust concentration that allows flame propagation within the cloud. If the MEC can be determined experimentally without accuracy and repeatability issues, a maximum explosible concentration is intrinsically complicated to estimate. In fact, creating a stable airborne cloud at high dust concentrations is far from straightforward due to

sedimentation, segregation and significant inter-particle interactions, which reduce the homogeneity of the dust concentration in the apparatus. Moreover, to propose a maximum concentration would suggest that it is possible to safely operate at higher concentrations, which is false. As for the explosion severity, two parameters are currently globally employed: the maximum explosion overpressure (P_{max}) and the maximum rate of explosion pressure rise ($(dP/dt)_{max}$). Together, they characterize the blast wave generated by a dust explosion and the powder involved in the accidental phenomenon. The P_{max} is related to the energy released by the fast combustion process; hence it is related to its thermodynamics. On the other hand, the $(dP/dt)_{max}$ is related to the rate of the reactions involved and, thus, to its kinetics.

1.3 Accidentology

One of the first documented accidents caused by a dust explosion was reported in the Memoires de l'Académie Royale des Sciences de Turin (Italy) in 1788 by the count Carlo Lodovico Morozzo Della Rocca. He investigated an explosion that occurred on December 14th, 1785, in a bakery in Turin that caused two injuries. He went there personally to collect precious information and to interrogate the witnesses. After a meticulous inspection, Count Morozzo noticed that the flour was drier than usual. The owner confirmed that they had never had such dry flour that year. Even though he never defined the phenomenon as a dust explosion, referring to it as "spontaneous inflammations" (as reported in Figure 1-2), he proposed to introduce a class of substances incapable of inflaming by themselves but ignitable with a flame, defining then the ignition phenomenon of a powder (Royal Academy of Science 1788).

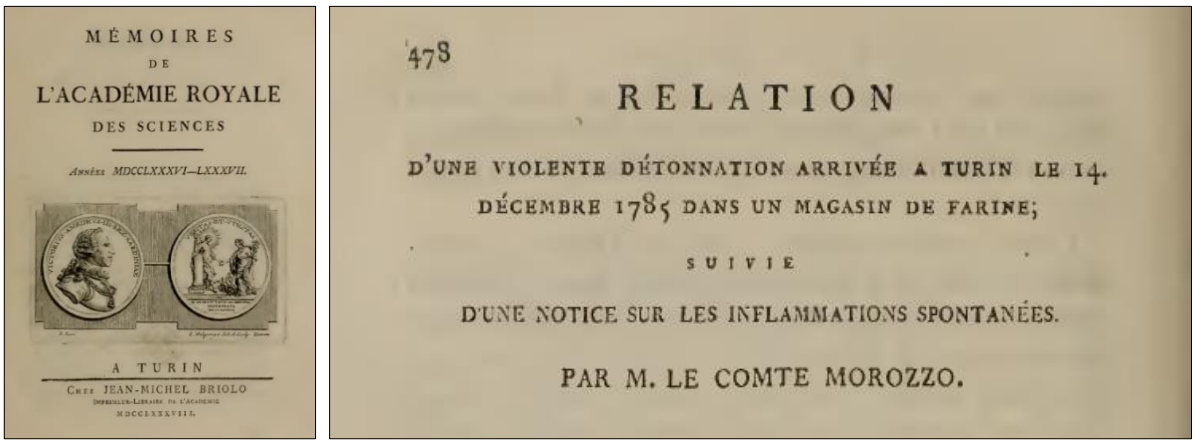
MÉMOIRES
DE
L'ACADÉMIE ROYALE
DES SCIENCES
Année MDCCLXXXVI—LXXXVII.
A TURIN
Chez JEAN-MICHEL BRIOLO
478
RELATION
D'UNE VIOLENTE DÉTONNATION ARRIVÉE A TURIN LE 14. DÉCEMBRE 1785 DANS UN MAGASIN DE FARINE;
SUIVIE
D'UNE NOTICE SUR LES INFLAMMATIONS SPONTANÉES.
PAR M. LE COMTE MOROZZO.

Figure 1-2 - Memoires de l'Académie Royale des Sciences de Turin, published in 1788, where the first dust explosion was documented.

In 1878, Nature published a text by F. E. L. (not identified author, F. E. L. 1878), who "noticed a letter by A. Mackennah on an explosion of malt dust in a grinding machine". The ignition source was unknown, and some observations were made about the milling operating conditions, the dynamics and the effects of the explosions. The solution adopted to reduce the explosion risk was to create several holes on the wood conveying lines to allow a free current of air, to prevent the solid from smouldering. In 1881, "The cause of colliery explosions" was published in Nature, a study of the character and dynamics of coal dust explosions. In addition, several experimental works are reported. They were performed to reproduce characteristic conditions encountered in the galleries and to determine the flame propagation speed, with and without firedamp, composed essentially of methane, carbon dioxide and nitrogen. Finally, the effect of the coal dust was assessed, and, as reported in the article, "it appears then that dust of any kind, as a finely-divided solid, can operate in determining the explosion of an otherwise harmless mixture of gas and air [...]". By the end of the XIX century, the Second Industrial Revolution generated a significant increase in coal extraction and consumption, and the explosion risk associated with coal mines caught the scientific community's attention. Furthermore, as depicted by Chen (Chen and Bhatt 2019), a complexification of the industrial sector has occurred, especially in the petrochemical industry and technology. As a result, many experimental works and case studies on the fire and explosion risk associated with powder handling, conveying and transporting were published, as reported in Figure 1-3 (built via Dimensions).

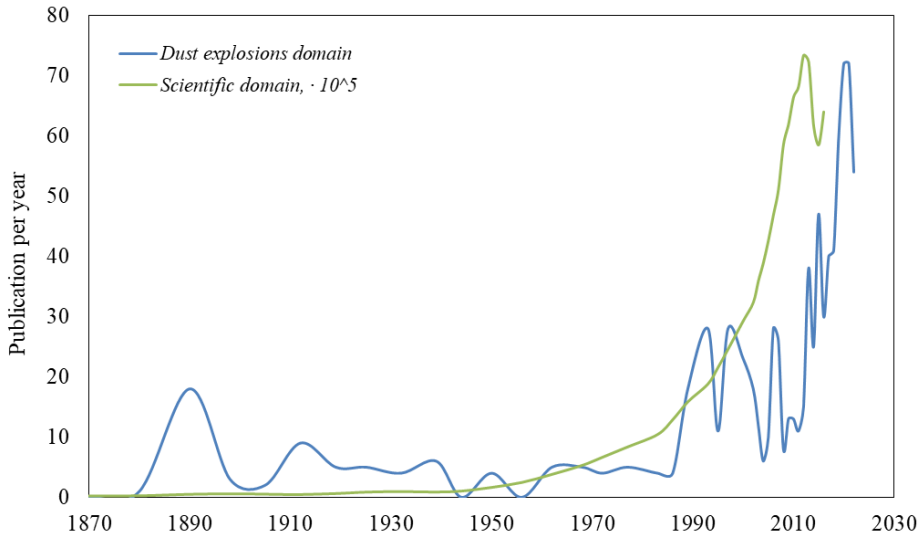

Figure 1-3 - Publications per year in the dust explosion and scientific domains (built via Dimensions)

Although industrials became increasingly aware of its risk and researchers continued to provide qualitative and quantitative analysis of this phenomenon, dust explosions remained an actual problem, strictly enveloping the industrial reality. Numerous accidents worldwide involved dust explosions, as non-exhaustively reported in Table 1-1. As can be seen, the nature of the powder varies significantly according to the production sector: pharmaceutics, wood manufacturing, cereal distribution, energy production, material storage and coal extraction are only a few examples of the variety of industrial branches that are potentially sensitive to dust explosions. "Learning by doing" and "experience feedback" are effective approaches to improving and deepening the knowledge of a scientific field. However, exploiting them in the dust explosion domain means dealing with unpleasant and potentially catastrophic scenarios, which cannot be the sole source of information. As reminded by Eckhoff (Eckhoff 2003), the awareness of the dust explosion risk is more profound among those who experienced such an accidental phenomenon. At the same time, it is also possible to attain a genuine appreciation of this hazard by understanding how it can manifest in daily life. Hence, case studies and accident reports constitute a fundamental key to unlock the right motivation for minimizing the probability associated with dust explosions.

A precise and complete accident report is necessary to analyse the context, identify the most critical unitary operations and deduce the explosion's origin. Nonetheless, finding unprecise and incomplete files about an accident is not improbable. Causes are disparate, principally because of two aspects:

- The complexity of the scenarios of dust explosions;
- An incomplete experience feedback.

For example, considering the reported dust explosions in agriculture between 2006 and 2020 in the United States (Purdue University), as reported in Figure 1-4, the number of accidents in which no ignition source was identified or identifiable constitutes 66% of the total number of accidents. Moreover, according to the Combustible Dust Incident Report 2020 (Cloney 2020) and to Eckhoff (Eckhoff 2003), determining the unitary operation where the explosion originated might be equally challenging. The number of accidents (between 2017 and 2020) associated with an unknown location of the ignition point was on the same order of magnitude as the other locations (see Figure 1-5 and Figure 1-6). Likewise, not even the nature of the powder involved in the explosion has always been reported. Between 5 and 10% of accidents each year were not characterized by the type of dust involved, as indicated in Figure 1-7.

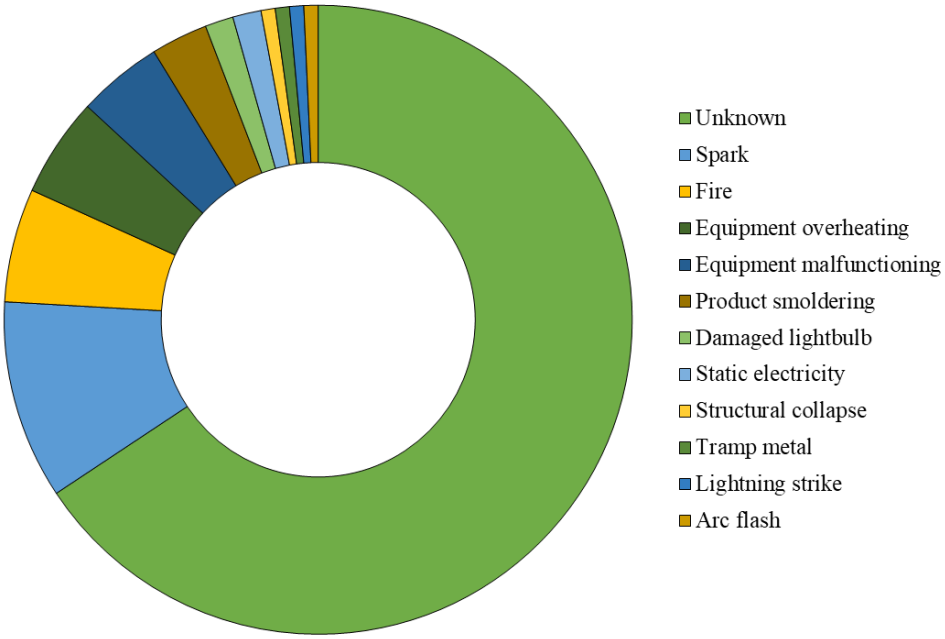

Figure 1-4 - Ignition sources of dust explosions occurred in the agricultural sector in US, from 2006 to 2020 (Purdue University)

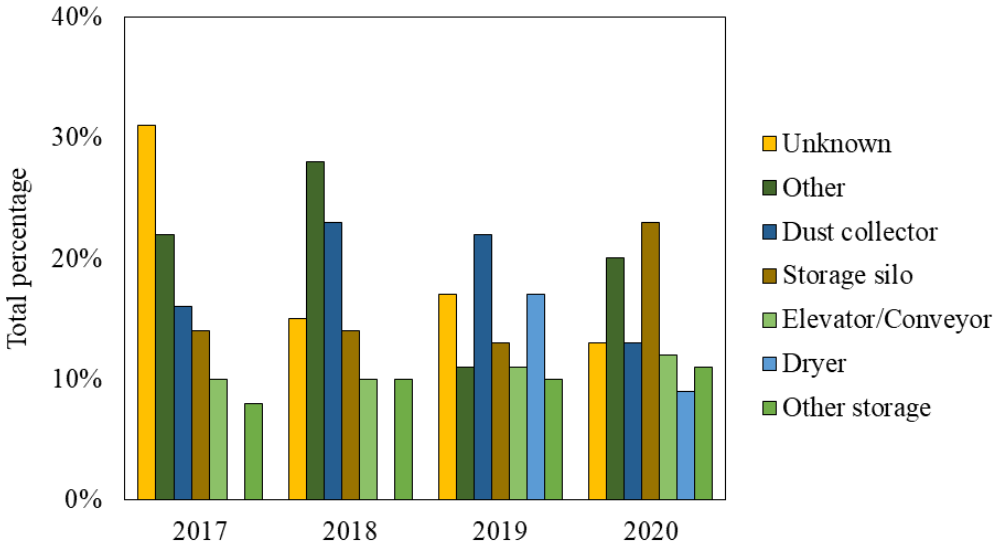

Figure 1-5 - Locations of dust explosion origin point, from 2017 to 2020 worldwide (Cloney 2020)

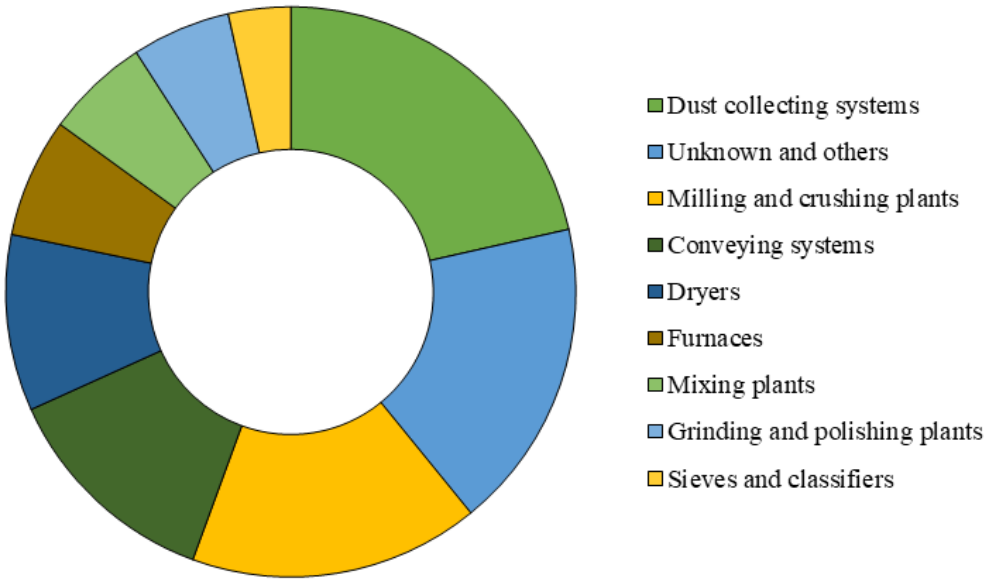

Figure 1-6 - Frequency of dust explosions in Germany between 1965 and 1985, according to the unitary operation involved (Eckhoff 2003)

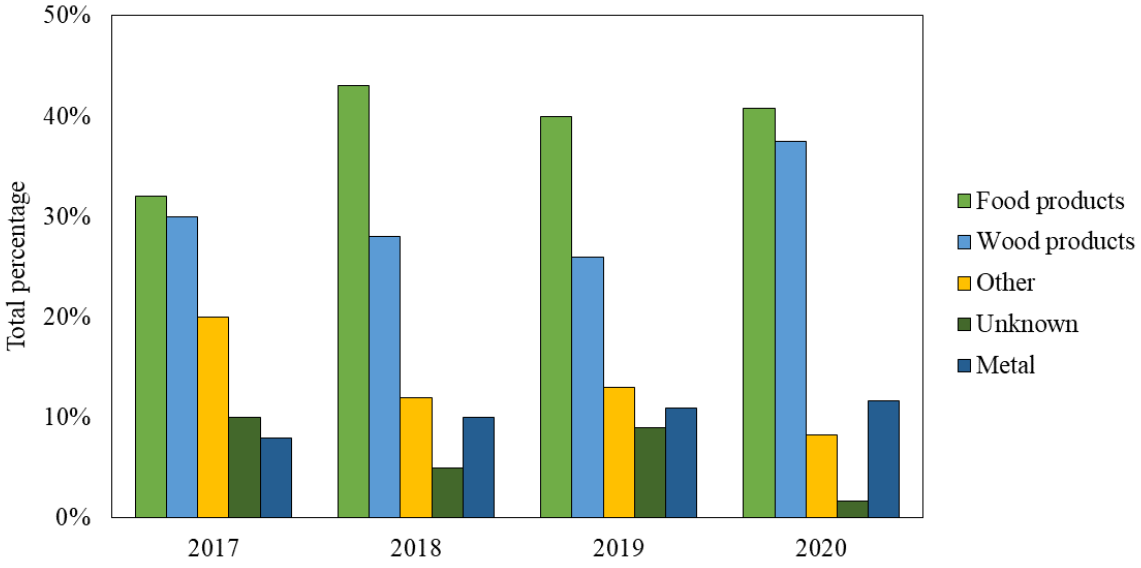

Figure 1-7 - Combustible dusts involved in explosions, from 2017 to 2020 (Cloney 2020)

Table 1-1 - A non-exhaustive list of dust explosion accidents in the industry

Year	Location	Dust involved	Most probable cause
1872	Glasgow, Scotland, UK	Cereal grain dust	Cereal feeding stopped, two millstones started to overheat, spark ignited the flour, fan sent flames into the exhaust box, explosion propagated everywhere
1878	Minneapolis, Minnesota, USA	Flour	Friction between two milestones, spark and ignition of the flour
1919	Port Colborne, Ontario, Canada	Grain dust	Unknown ignition source, several dust explosions in the grain elevator
1921	Mount Mulligan, Australia	Coal dust	Miners were using open flame lights, ignition of a coal dust cloud
1942	Benxi, China	Methane/Coal dust	Gas and coal dust explosion, many workers trapped inside by the Japanese, who did not fully evacuate the mine
1970	Stavanger, Norway	Wheat grain dust	Smouldering phenomena in the bucket elevators or welding on the outside of the grain feed duct
1972	Bremanger, Norway	Silicon dust	A small hole in a steel pipe for conveying Si powder was made with an acetylene/oxygen torch and ignited the powder deposited internally
1973	Gullaug, Norway	Aluminum dust	Inerting system inadequate, oxygen concentration too high, spark in the screw tube, violent explosion
1975	Norway	Fish meal dust	Electric arcs in an empty silo, whose internal walls were covered by fish meal dust
1976	Kambo, Norway	Barley or Oats dust	Burning or glowing material generated by overheated hammer mill dropped in the bucket elevator
1976	Oslo, Norway	Malted barley dust	Primary explosion in a silo cell
1979	Bremen, Germany	Wheat flour	Cable fire, ignition of a flour cloud
1980	St. Joseph, Missouri, USA	Cereal dust	Exposed wires due to repeated filling-discharge cycles, electric arc between the lower-level indicator in a silo cell
1980	St. Paul, Minesota, USA	Cereal dust	Electric arcing during the unloading of grain trucks
1980	Fonda, Iowa, USA	Corn dust	Poor electrical contact between grounding clamp and grounded elevator casing, generation of a hotspot
1980	Lägerdorf, Germany	Methane/Coal dust	Methane release, primary explosion, dispersion of deposited powder, secondary explosion
1980	Muhansk Oblast, Ukraine	Methane/Coal dust	Gas and coal dust explosion
1981	Corpus Christi, Texas, USA	Sorghum dust	Smouldering lumps entered in a bucket elevator
1983	Anglesley, UK	Aluminum dust	Unknown ignition source, the (secondary) explosion started on the stream 1 and propagate thanks to dust deposits
1984	St Bernardino County, California, USA	Methane/Coal dust	Hotspot originated by a smouldering combustion, flammable atmosphere in the silo

1985	Stavanger, Norway	Rapeseed pellet dust	Smouldering gas explosion in the silo cell
1985	Not specified	Methanol, Acetone, Penicillin Powder	Two operators were charging penicillin powder into a reactor containing a mixture of acetone and methanol, an explosion occurred at the reactor man-hole
1987	Oslo, Norway	Malted barley dust	Smouldering phenomena in a dust filter, packing dust in the unloading screw at the filter bottom
1987	Tomylovo, Russia	Sunflower seed dust	Smouldering gas explosion in the silo cell
1987	Harbin, China	Linen flax dust	Unknown ignition source, the explosion originated in one of the nine dust collectors
1988	Stavanger, Norway	Wheat grain dust	Slight offset in the elevation system, dust heated up, some glowing fragments dropped into the grain deposit and initiated the smouldering combustion
1988	Not specified	Toluene/powder mixture	An operator was charging a toluene-wet powder to the hot dryer, electrostatic discharge, explosion occurred at the charge chute
1988	Not specified	Acetone/Powder	A technician closed a vacuum drier and started rotation, after some minutes, an explosion occurred. Investigations revealed that the dryer man-hole cover was not fully fastened and thus air must have entered. The ignition source was probably an electrostatic discharge. No nitrogen inerting was used
1989	Not specified	Wood, paper, glue and products for agriculture	A pyromaniac set on fire some papers and packing materials. The fire was nearly extinguished when a dust explosion occurred and the fire spread again
1997	Not specified	Corn dust	Explosion of flammable dust in a silo of corn
1997	Not specified	Ethyl Acetate, Nitrocellulose, Pigments	Two workers were loading with nitrocellulose a mixer containing ethyl acetate, using a hopper of a worm feeder equipped with a shielded (explosion protected) motor. Small fires developed following the ignition of flammable materials (rags, ink tanks, resins, pigments) present in the hall (hangar)
1997	Not specified	Wood dust	During a loading operation of a combustion installation, an explosion occurred on the bottom-side of the drag-chain conveyor. Probably the explosion was ignited through a flame-transmission from the furnace
1998	Not specified	Thioridazine Hydrochloride	An operator was pouring thioridazine hydrochloride from a sack in the feedbox of a mixer, ignition and explosion
1999	Not specified	Wood dust	Fire and explosion in a chipboard production plant
1999	Not specified	Suplhur, Iron dust	Ignition of powder clouds created by local overheating. The drying vaporiser and silo caught fire, and the washing water pipes were destroyed
2001	Not specified	Nitrobenzene, Ludigol	Explosion in a dryer, spray nozzles in the dryer was switched from nitrogen to ambient air
2001	Not specified	Animal feed dust	Discharging of colza press cakes, fire and subsequent explosion at the base of a conveyor
2002	Not specified	Wood dust	Explosion in an empty fireproof wood chip silo occurred its door was opened for a control, some residual powder ignited
2003	Kinston, North Carolina, USA	PE dust	Dust layer onto the ceiling, generation of a dust cloud, ignition

2003	Not specified	Grass meal dust	Smouldering nest, dust explosion. The shock wave generated caused approx. 3/4 of the roof deck to collapse, killing two firemen
2003	Not specified	Plastic dust	Fine plastic powder caused massive blast, killing six workers
2005	Not specified	Hydrogen/Silicon dust	Explosion in a silicon dust suspension container, plant totally destroyed
2006	Not specified	Pentaerythrite dust	Three workers opened the manhole of one chamber of a silos for inspection, some product fell on the ground taking fire, first explosion. Further product slid down from the silo, and was dispersed in the air by the ventilators placed under the silo, the air-pentaerythrite mixture ignited, explosion.
2008	Port Wentworth, Georgia, USA	Sugar dust	Primary explosion in a building used to store sugar prior to packaging, secondary explosion involved the silo cells
2010	Not specified	Antrachinon dust/vapour	Spark of static electricity in closed space of production line, which contained the mix of vapour and dust of anthrachinon. Problems in the electrical grounding
2011	Not specified	Azobisisobutyronitril dust	During a filling procedure, AIBN was released in the form of a dust cloud, which then ignited, injuring the employee working in the area. A second deflagration occurred when three open AIBN drums, which were near the reactor, ignited by brush discharge
2014	Kunshan, China	Metal polishing dust	Fire ignited the metal polishing dust
2014	Not specified	Nitrocellulose	An explosion occurred in the transfer pump and the piping linking storage tank B5 with the pycnometer tank during the transfer of nitrocellulose granules in the medium of water between these tanks. The investigations showed that the explosion had created detonation conditions in the pump and the vertical pipes downstream of the pump
2015	Cheshire, UK	Wood dust	Unknown ignition source, three explosions probably caused by deposits on the floor
2015	Arteixo, Spain	SM 75 ROQUAT dust	Deflagration occurred in the stainless-steel reactor (capacity 3000 L)
2015	Not specified	Charcoal dust	A shelter housed a grinding mill (not in use at the time of the explosion) and a concrete mixer used for fine milling charcoal. The only operation in progress in the area was the fine milling of charcoal
2016	Abbotsford, British Columbia, Canada	Wood dust	Firefighters were trying to mitigate the fire, dust explosion engulfed one of them
2017	Not specified	Sulphur-fungicide dust	Alarms pointed to an explosion in the filter recovering dust from the unit's ventilation network and the opening of that dust filter's explosion vents. A fire then broke out in the filter
2022	Sehmatal, Germany	Aluminum dust	Deflagration during grinding work
2022	Bergerac, France	Nitrocellulose dust	Unknown ignition source, several explosions and a subsequent fire
2022	Archbold, Ohio, USA	Wood dust	Unknown ignition source, two silos involved in the explosion
2022	Sevierville, Tennessee, USA	Nickel-Aluminum dust	Nickel aluminum powder likely exploded, and the fire was contained by their fire suppression system

2022	Hardy, Iowa, USA	Sulphur dust	Material was moving through a pit to an elevated mixing bin
2022	Whiteville, North Carolina, USA	Wood dust	Dust collector blocked, a worker tried to clear the blockage, explosion
2022	Santa Catarina, Brazil	Wood dust	The explosion occurred in a silo that stores sawdust
2022	Coshocton, Ohio, USA	Grain dust	The explosion occurred near the grain drier, no injuries
2022	Peoria, Illinois, USA	Grain dust	Three 150-foot silos were leaning over, one collapsed; a second silo later collapsed, and fire developed in a third silo, creating worries about another explosion

1.4 Fundamental steps

Dust explosions are complex and fast processes. Therefore, a certain degree of simplification is necessary to model such a phenomenon. Eckhoff (Eckhoff 2003) pointed out the existence of two types of dust flames: the Nusselt and the volatile flames. The first one is characterised by heterogeneous combustion sustained by the oxygen diffusion toward the particle's surface, leading to premixed combustion on a macroscopic scale constituted by local diffusion flames. On the other hand, a volatile flame considers the devolatilisation of the particles, the mix with the oxidiser and the combustion as in a premixed flame. In this work, the approach proposed by Rockwell (Rockwell and Rangwala 2013) and reported by Skjold (Skjold 2022) will be adopted to describe the combustion behaviour of a dust cloud, a premixed combustible system with non-premixed substructures. In general, dust explosions can be classified into two families: organic and metal dust explosions. The phenomena involved in each are different, and they depend on several characteristics of the powders. Metal particle combustion is usually described by Glassman's criterion, which compares the metal boiling point (T_{bm}) and the boiling—dissociation temperature of its oxide (T_{bo}) (Brzustowski and Glassman 1964):

- Vapour phase reaction, if $T_{bm} > T_{bo}$;
- Particle surface reaction, if $T_{bm} < T_{bo}$.

Yetter (Yetter et al. 2009) also reported the latest integrations to this criterium to consider the flame temperature limitations due to the vaporization-dissociation of the oxide, which must be compared to the reaction heat provided by the metal oxidation exothermic reaction. The principal combustion regimes of metal particles are graphically represented in Figure 1-8

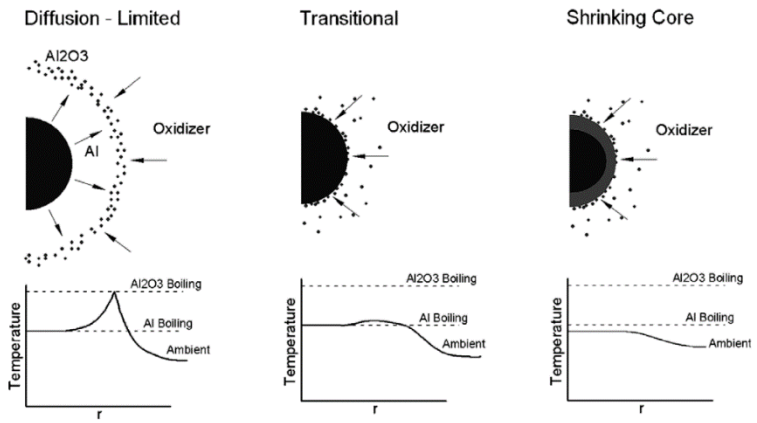

Figure 1-8 - Schematic representation of the combustion regimes of a metal (aluminum) particle (from (Bazyn, Krier, and Glumac 2007))

As for organic dust explosion, the approach chosen to present the global phenomenon is to decompose it into its elemental bricks: particle heating, pyrolysis, oxidation and flame propagation. Within a dust cloud, the exposition of the particles to an ignition source translates into an increase in their temperature. The heat transfer rules this step, and it is strictly dependent on the physical properties of the ignition source (temperature, emissivity, shape), the gaseous phase surrounding the particles (velocity, turbulence, transmissivity, thermal diffusivity) and the particles themselves (thermal conductivity, porosity, tortuosity, particle size and shape). As the particle temperature increases, chemical reactions can eventually be triggered, and, for organic materials, they usually correspond to pyrolysis, a devolatilization process that generates lighter species. An example of the devolatilization onset temperature of organic materials is reported in Table 1-2.

As soon as the concentration of the pyrolysis products in the gaseous/vapour phase enters the flammability domain, the ignition source might ignite the mixture and trigger the flame propagation and, more in general, the dust explosion phenomenon. This step corresponds to the oxidation step, which involves an oxidizer species, often represented by the oxygen in the air. The exothermicity of the oxidation reactions rapidly increases the temperature of particles and the gaseous phase, which in turn rapidly increases the radiative heat transfers within the dust cloud. A flame front, a pre-heating and a post-combustion zone are identifiable during this process, called flame propagation. The four steps are graphically represented in Figure 1-9.

Table 1-2 - Devolatilization onset temperatures for some organic materials

Material	Devolatilization onset T, °C	Source
Sodium alginate	211	Guerretta et al. 2019
Cellulose	305-311	Barud et al. 2007
Sucrose	240	Wang et al. 2014
Miscanthus straw	210	Jeguirim et al. 2010
Teak wood	195	Oluoti et al. 2014
Obobo wood	197	Oluoti et al. 2014
Olive pomace	192	Pietraccini et al. 2021

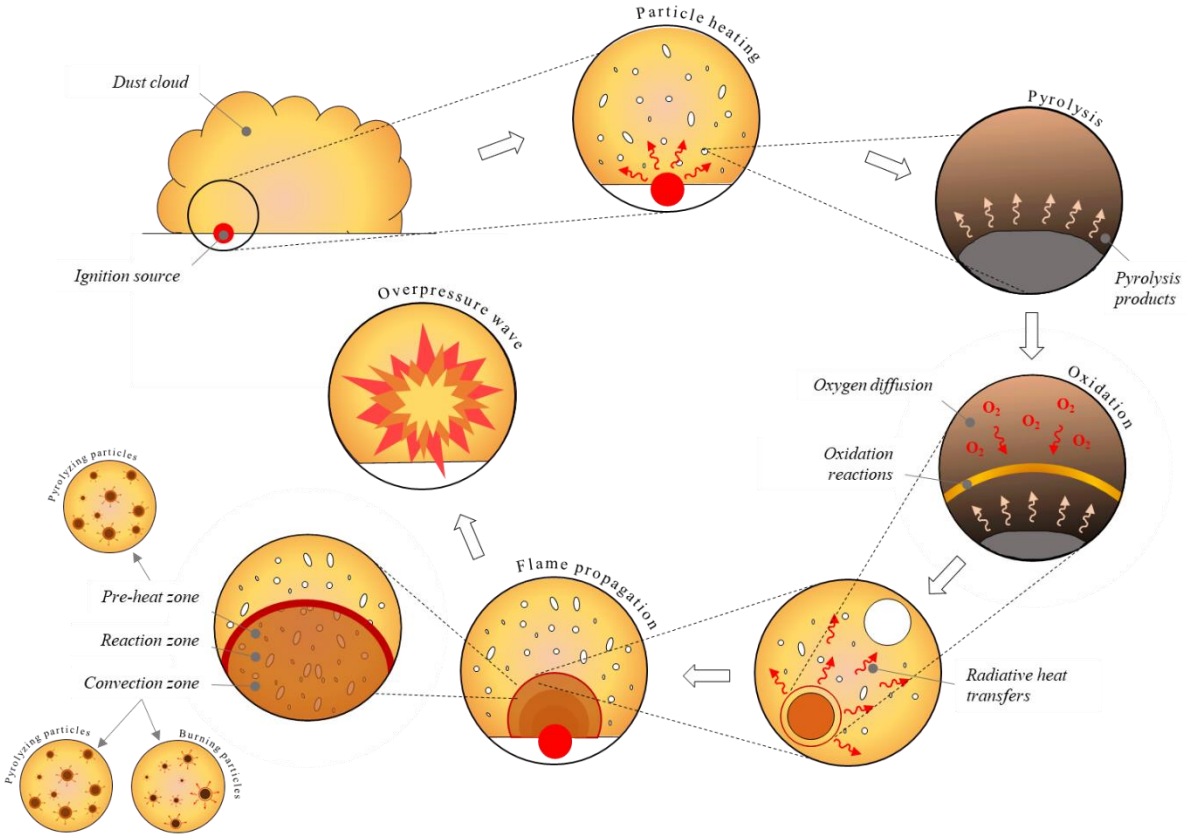

Figure 1-9 - Schematic representation of the fundamental steps of an organic dust explosion

1.5 Powder Particle Size Distribution

Since the dimension of the particles that form a powder is not unique, a fundamental element to characterise it is its Particle Size Distribution (PSD). It corresponds to the frequency of the relative amounts of particles associated with each size class chosen. It can be calculated on a mass/volume, surface or number basis, i.e. the mass/volume, the surface or the number of the particles are considered to determine the relative fractions belonging to a specific size class. A powder's PSD is a fundamental feature that intervenes in the definition of, for instance, its bulk density, solubility, flowability, mechanical, thermal and kinetic properties. For simplicity reasons, specific values are extracted from the PSD to represent it in a synthetic way instead of associating a statistical function. Moreover, parameters can be calculated to characterise the distribution and its shape. They are several, and the more commonly used ones are presented in Figure 1-10 and Table 1-3.

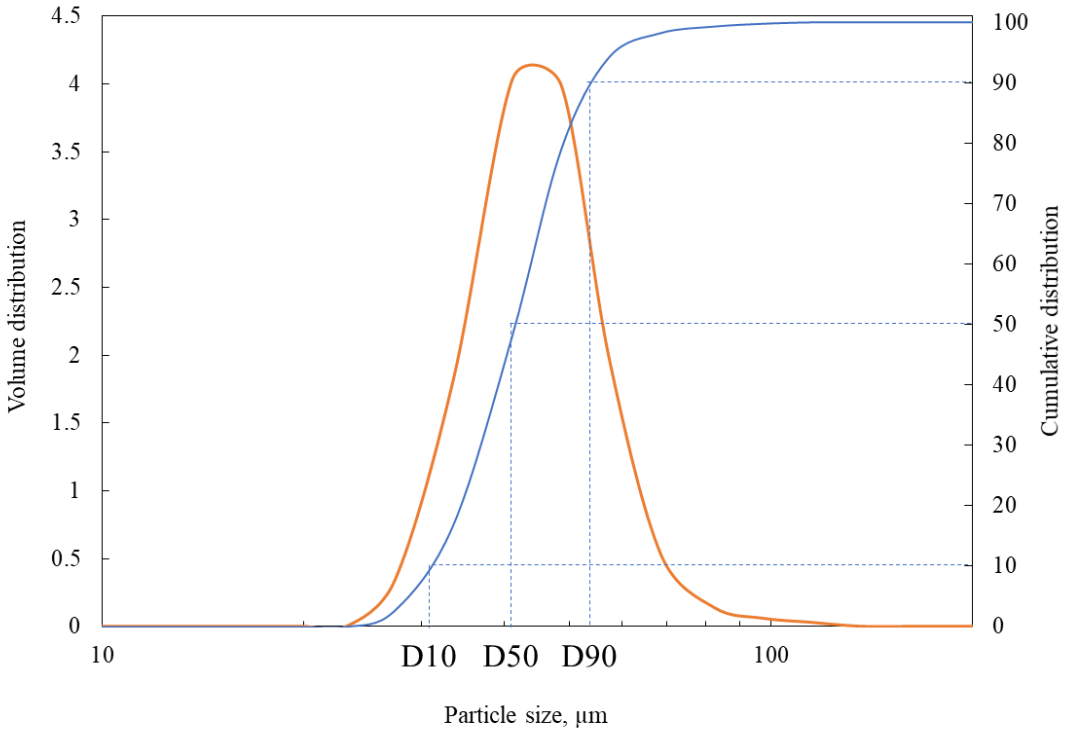

Figure 1-10 - Definition of the D10, D50 and D90 of a Particle Size Distribution

Table 1-3 - Definition of characteristic diameters and parameters of a Particle Size Distribution

Value	**Symbol**	**Definition**	**Utilisation**
10% diameter	D10	The 10% of the elements of the population are below this diameter	To represent the finer fraction in a volume distribution
50% diameter	D50	The median diameter	To represent the powder's median diameter
90% diameter	D90	The 90% of the elements of the population are below this diameter	To represent the coarser fraction in a volume distribution
Sauter diameter	D[3,2]	Surface area moment mean	The central point of the frequency around which the distribution would rotate. Used in surface-related phenomena
De Brouckere diameter	D[4,3]	Volume (or Mass) moment mean	The central point of the frequency around which the distribution would rotate. Used in volume-related phenomena
Span	-	(D90 - D10) / D50	The normalised width of the distribution
Skewness	-	$E = \left[\left(\frac{X - \bar{X})}{\sigma}\right)^{3}\right]$	The asymmetry of the distribution
Kurtosis	-	$E = \left[\left(\frac{X - \bar{X})}{\sigma}\right)^{4}\right]$	The distance of the considered distribution from a normal distribution

2. Ignition sensitivity

As mentioned in Section 1.1.2, electrical sparks, incandescent bodies, hotspots, mechanical friction heating, and hot surfaces are potential causes of dust cloud ignition. This section presents the parameters used to characterize and quantify a dust cloud's ignition sensitivity.

2.1 Minimum Ignition Energy

2.1.1 Context and Definition

The MIE corresponds to the minimum energy delivered by an electrical spark necessary to ignite an explosive atmosphere. The spark is then the vector that delivers a specific amount of energy for the ignition. The simplicity of generating an electric spark and covering a broad range of operating conditions (see Figure 1-11) made the electric spark widely used worldwide for simulating ignition phenomena. In Figure 1-11 the energy values associated to some common ignition sources are reported, in comparison to the typical ranges for dust and vapour/gas explosions.

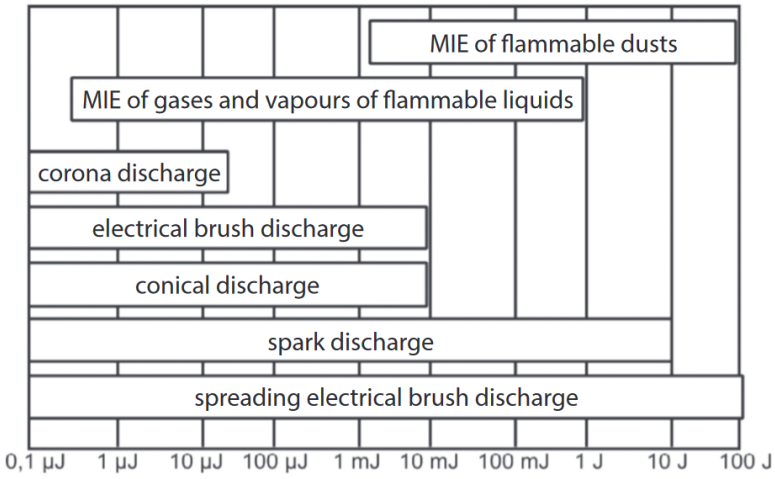

Figure 1-11 - MIE ranges for combustible dusts and gas/vapours, in comparison to the energy ranges associated to the typical source of ignition in industry (Bielawski 2020)

2.1.2 Experimental setups and procedure

ASTM E2019-03:2007 and ISO/IEC 80079-20-2:2016 (ISO/IEC 80079-20-2 2016a) are the standardized procedure currently employed in the MIKE 3 apparatus (Figure 1-12). Through a system of seven condensers, the spark energy can be varied from 1 to 1000 mJ. The dust is dispersed from the bottom of the cylindrical tube upwards, and the amount used in each test ranges between 300 and 1500 mg, to study the behaviour of the cloud at different dust concentrations. In fact, the Ignition Energy (IE) shows a minimum point (MIE) when plotted as a function of the dust concentration: for low concentrations, the high interparticle distance reduces the probability to sustain a flame propagation; for high concentrations, the energy furnished by the spark is absorbed by too many particles for igniting the mixture; for intermediate concentrations, around the stoichiometric concentration, the ignition can occur and the flame can propagate.

However, the dust concentration in a dust cloud changes in space and over time, which means that the ignition delay (the time between the dispersion and the spark generation) must also be an operating condition to be varied, in order to change the turbulence level at the moment of the ignition. The value fixed by the standard procedure is 120 ms. Several works on the influence of the delay time on the dust concentration near the electrodes were published. Danzi (Danzi et al. 2021) proposed an experimental procedure based on high-speed video analysis to estimate the local average concentration of the dust cloud and to choose the right delay time corresponding to the highest ignition sensibility.

The evaluation of the MIE of a dust is straightforward, but it hides some thorny issues peculiar to all dust explosions and due to their special and time heterogeneity. Four steps constitute a single test:

- Verification of the electrical circuit (blank tests) to assure the correct sequence during the actual test;
- Preparation of the test, by weighting the powder, placing it at the bottom of the glass cylinder and assembling the apparatus;
- Parameters setting and dispersion of the powder with compressed air;
- Spark generation between the two electrodes to ignite (or not) the dust cloud; a test is negative after ten no-ignition tests.

  A complete series of experiments aims to find a minimum in the ignition energy-concentration curve, at different turbulence levels (or ignition delay times).

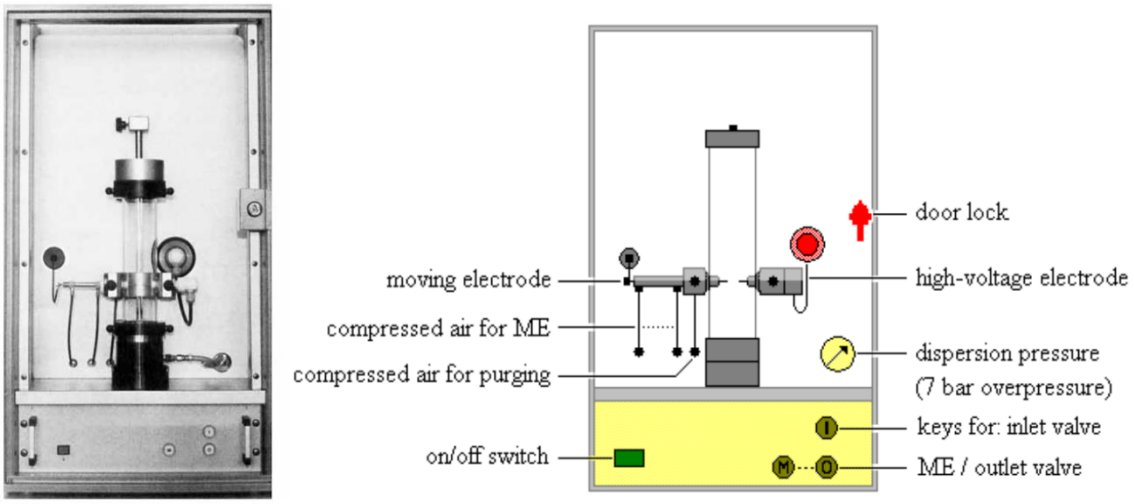

Figure 1-12 - Photos and Schematic representation of the MIKE 3 apparatus, employed for the determination of the MIE of a dust

2.1.3 Influencing parameters

Several parameters influence the final result: the ambient temperature, the oxygen content and the presence of combustible gases, the particle size distribution. The last parameter is known to be a crucial parameter that determines the ignition sensitivity of a powder. In particular, the mean particle diameter D50 plays a key role in the MIE, as illustrated in Figure 1-13. The MIE also decreases as the oxygen concentration increases. As Wu (Wu et al. 2022) reported, the MIE can decrease by three orders of magnitude, increasing the oxygen concentration by 9 mol% in a coal dust cloud. Moreover, they also found that the inhibiting effect of nitrogen is weaker than that of CO_2, which means that the composition of the gaseous phase in the dust cloud has a major role in the ignition sensitivity. Finally, if the dust is part of a hybrid mixture, the vapour and/or the gas concentration has a non-negligible influence on the MIE. Wu (Wu et al. 2022) evaluated the influence of small concentration of H_2 and CH_4 on the MIE of a coal dust, obtaining non-negligible effects even at very low gas concentrations. Their results are consistent with those reported by Siwek (Siwek and Cesana 1995), who focused on the effects of propane on several powders' ignition sensitivity. As for H_2 and CH_4 on coal dust, propane sensibly reduces the MIE, as shown in Figure 1-14. A parallel can be drawn with the appearance of pyrolysis gases in a dust cloud.

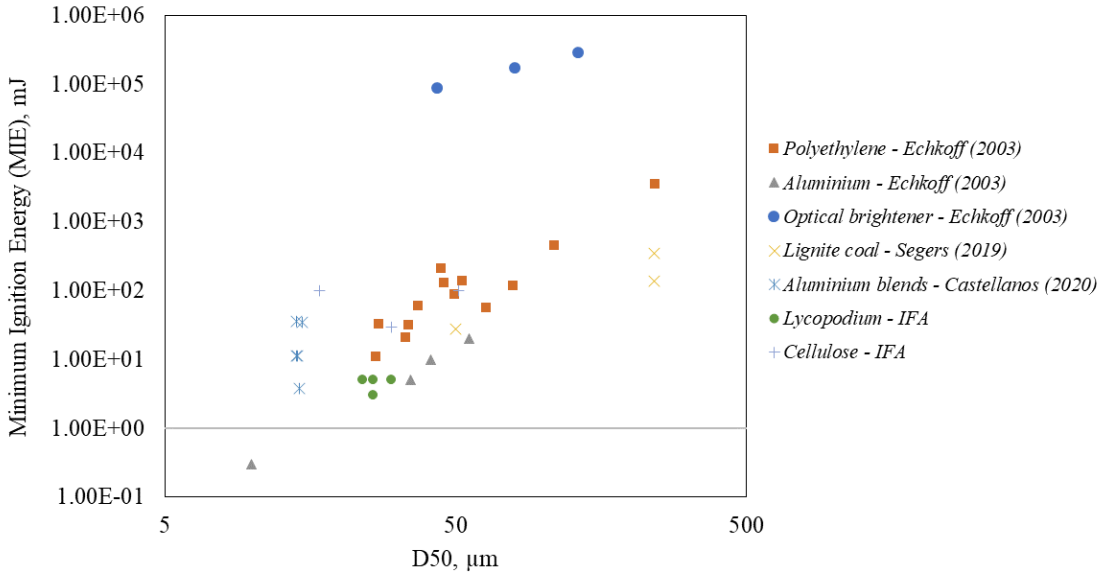

Figure 1-13 - MIEs of several powders as a function of their D50

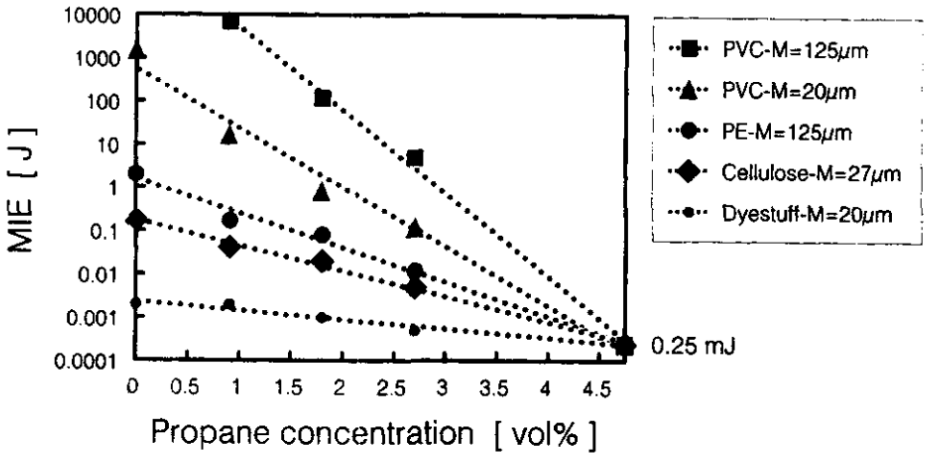

Figure 1-14 - Influence of propane concentration on several powders' MIE (from (Siwek and Cesana 1995)).

2.1.4 Modelling

Modelling is currently used to estimate the MIE to support the experimental data and add an information layer, as in Li (Li et al. 2020), Chaudhari (Chaudhari et al. 2019) and Ackroyd (Ackroyd et al. 2011). They all proposed MIE evaluation models to define how the ignition sensitivity changes as a function of the oxygen concentration, also as a theoretical basis for building inerting systems in the industry. Eckhoff (Eckhoff 2019a) reported several theories for predicting the MIEs of dust clouds, and they all present limitations due to necessary

simplifications of the analysed systems. The most impacting one is the complexity of obtaining a homogeneous concentration field in the MIKE 3, mainly close to the electrodes during the spark generation, which contributes to the probabilistic feature of the ignition process.

2.2 Minimum Ignition Temperature

2.2.1 Context and Definition

Powders can exhibit autoignition phenomena when their temperature is high enough to trigger an oxidation reaction. The limit beyond which it might occur is the Minimum Ignition Temperature (MIT). This value assumes two different significations when the powder is dispersed in a gaseous phase or the form of a dust layer. In the first case, the interparticle distance is larger; thus, the more important resistance to heat transfer usually translates into a higher MIT. The combustion processes are profoundly different in the two cases: due to different heat transfer limitation, particles residence times and flame/particle interactions. Dust layers self-heating is also called smouldering (combustion). Unfortunately, this phenomenon is widespread in the industry and often triggers fires and dust explosions (see Table 1-1). Self-heating of dust layer is not in the scope of this study and will not be developed here. The heat sources in both cases can assume several forms: hot surfaces, glowing bodies, hotspots and flames are only a few examples that can be found in the industry. They might be situated near a welding station, on the outer surface of a compressor, a heat exchanger, inside a burner or an oven. The temperature associated with a specific location or apparatus is directly compared to the MIT, allowing a straightforward fire and explosion risk analysis in the framework of DSEAR/ATEX regulation.

2.2.2 Experimental setups and procedure

The MIT of a dust cloud is a fundamental parameter for assessing powders' ignition sensitivity and designing experimental setups, operations and industrial processes, making them intrinsically safer. The study of MIT has most of its roots in coal mining, which involved several accidents related to coal-methane hybrid explosions during the Second Industrial Revolution. Nowadays, two apparatuses are employed to measure the MIT of a dust cloud: the Godbert-Greenwald (G-G) furnace and the BAM oven.

As described by Eckhoff (Eckhoff 2019b), many setups have been proposed over the years before the global standardization of the G-G oven. Some of them are shown in Figure 1-15. In 1935, Godbert and Greenwald (Godbert and Greenwald 1935) compared the flammability of two coals from the United Kingdom and the United States, focusing on the finer coal particles' role. They slightly modified an already-existing experimental apparatus to perform the tests. It was constituted by a vertical cylindrical chamber, approximately 3 cm large and 20 cm long. It was heated up using a nichrome wire, and an outer metal shell held the tube. Diatomaceous earth was used for thermal insulating between the two layers. In 1952, Godbert (Godbert 1952) proposed a standard apparatus for determining the MIT of coal dust, fixing the characteristics for the current Godbert-Greenwald apparatus. The BAM oven is a different version of the vertical-chamber apparatus, and it presents a horizontal chamber. It was standardized by the *Bundesanstalt fur Materialprufung* (BAM, German Federal Institute for Testing Materials). It is also currently employed for determining the MIT of a dust cloud. The chamber has a diameter of 6 cm, is 12.5 cm long, and is electrically heated. Its characteristic feature is a slightly concave parabolic metal disk (the smaller surface is about 20 cm^2) placed coaxially in the chamber. Its temperature is measured with a thermocouple, corresponding to the test's reference temperature. Compared to the vertical chamber in the G-G oven, BAM oven's horizontal chamber is shorter and larger, which might have translated into a dust cloud residence time too short for triggering any ignition. Contrarily, placing a deflecting disk in the chamber means increasing the dust cloud residence time, allowing eventual ignitions to occur, as well as potentially changing the cloud PSD due to fragmentation or agglomeration.

In both cases, the test procedure is similar:

- Temperature setting and powder weighting;
- Preparation of the dispersion, by placing the powder in the special container;
- Dispersion of the powder in the heated chamber;
- Evaluation of the results: if an audible and visible flame exits the setup within ten seconds (for BAM / ISO 80079-20-2) from the dispersion, the test is considered positive; otherwise, it is negative.

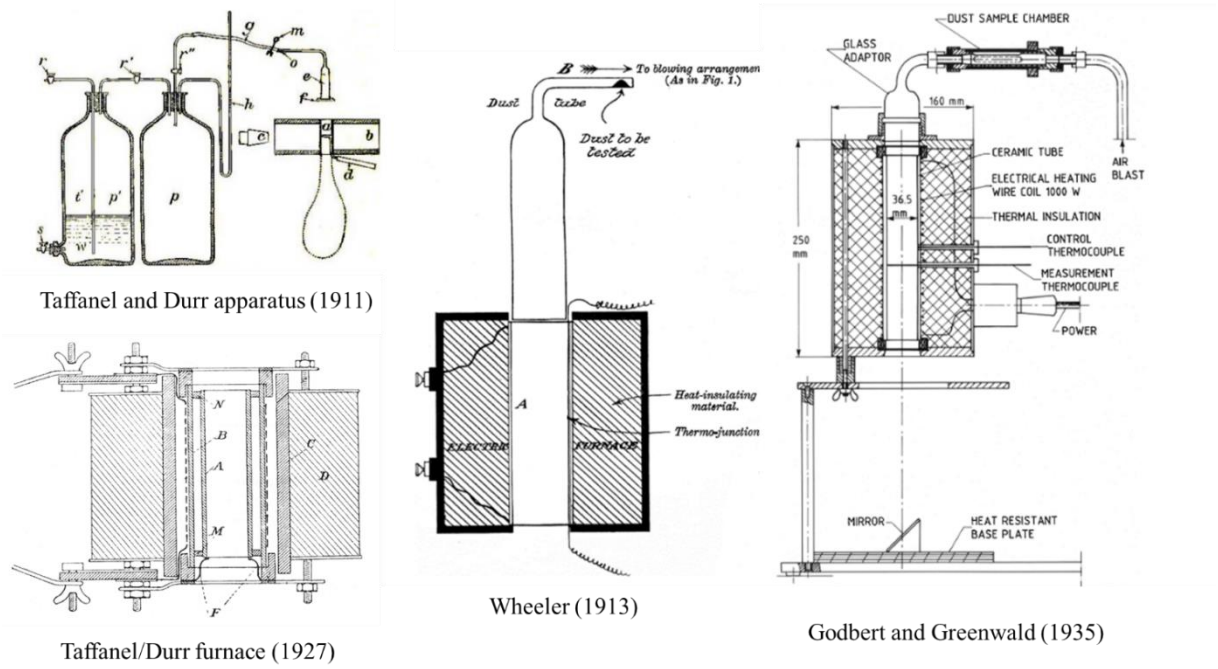

Figure 1-15 - Apparatuses developed to determine the MIT of dust cloud; the Godbert-Greenwald oven is the one to the right

In the lab protocol, mass, dispersion pressure and temperature are changed to investigate a wide range of scenarios and find the worst one associated with the "most vigorous" flame. The values for the MIT of several powders are reported in Table 1-4. Due to their structural differences, the MITs determined with BAM and G-G ovens differ. As Siwek (Siwek and Cesana 1995) reported, results are lower by using the first setup. It might be due to a longer residence time in the heated chamber, a higher turbulence level due to the deflecting disk, or the higher ignition probability of the flue gases eventually generated by powder deposits in the chamber. The difference is visible in Figure 1-16. Similarly to the MIE determination, the procedure for determining the MIT provide for changing several operating conditions to find the scenario associated with the higher ignition probability. Mass of powder, pressure dispersion and temperature are varied (according to the standard procedure) between 0.1 and 0.3 g, 0.1 and 0.5 barg, 150 and 1000°C, respectively. The minimum temperature at which ignition is observed corresponds to the MIT.

2.2.3 Influencing parameters

The particle size profoundly influences the MIT of a powder. As for the MIE, finer particles are responsible for increasing the ignition sensitivity of the dust cloud. As found by Sha (Sha et al. 2021), who worked on the ignition sensitivity of coal dust, and as reported in

Table 1-4, their contribution can decrease the MIT from 610 to 520°C for a diminution of the mean particle size from 75 to 25 µm. Similar results were reported in Yu (Yu et al. 2019), whose work was also focused on the minimum ignition temperature of coal dusts, and in Arshad (Arshad et al. 2021), in which the ignition sensitivity of corn starch was tested.

Apart from the particle size, the MIT is also influenced by the dust concentration in the heated chamber (i.e. the amount of dust injected) and the dispersion pressure. Therefore, many works focused on quantifying their contribution to the ignition temperature, such as Arshad (Arshad et al. 2021), Yu (Yu et al. 2019) and Azam (Azam and Mishra 2019). From their results, it can be concluded that:

- A minimum value of MIT is noticeable for a specific concentration, likely corresponding to the equilibrium point between the number of fine particles (i.e. higher probability of ignition) and the heat sink effect at high concentrations;
- The MIT decreases with the dispersion pressure, which might be related to deagglomeration phenomena within the dust cloud.

Table 1-4 - MITs of several powders of interest for this study

Material	**D50, µm**	**MIT (G-G), °C**	**MIT (BAM), °C**	**Source**
Wheat grain dust	36	290		Ramírez et al. 2009
Barley grain dust	34	290		Ramírez et al. 2009
Alfalfa dust	39	300		Ramírez et al. 2009
Soybean dust	52	300		Ramírez et al. 2009
Olive pomace	60	590	540	Pietraccini et al. 2021
Cellulose	46	530		IFA Database
Cellulose	33	540		IFA Database
Cellulose	30		430	IFA Database
Cellulose	17		430	IFA Database
Wood dust	98	410		IFA Database
Coal dust	25	520		Sha et al. 2021
Coal dust	37	550		Sha et al. 2021
Coal dust	53	580		Sha et al. 2021
Coal dust	75	610		Sha et al. 2021
Pine sawdust	52	300-310		Liu et al. 2019
Cupressus funebris	40	290-300		Liu et al. 2019

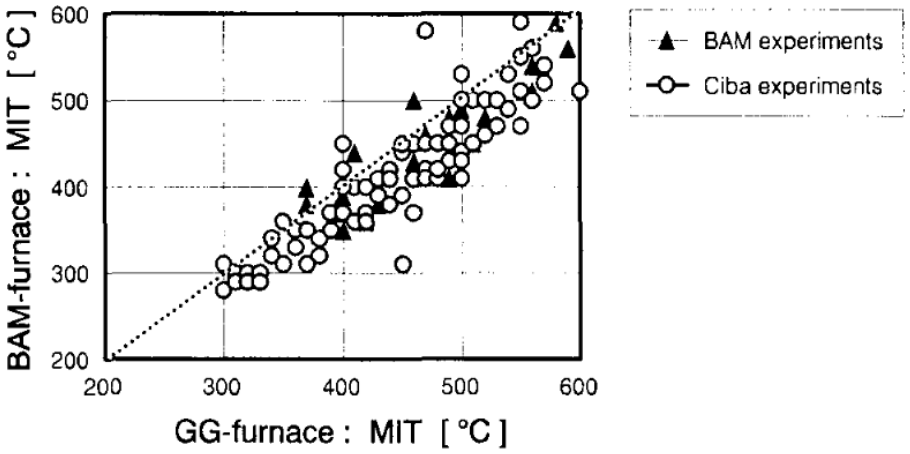

Figure 1-16 - Comparison between the MITs determined with the BAM and the G-G oven (Ciba experiments) (from Siwek and Cesana 1995)

2.2.4 Modelling

The MIT determination is a time-consuming test, and multiple parameters can intervene in the ignition behaviour of a dust cloud. Aiming to consider their influence, add an information layer to the experimental data and eventually estimate the MIT of a powder, several predictive models have been proposed. Addai (Addai et al. 2016) presented seven, based on different ignition criteria and assumptions, and compared three to experimental results. They agreed well with the models, as shown in Figure 1-17. A different approach was followed by Arshad (Arshad et al. 2021). Statistical analysis and artificial neural networks were merged to estimate the MIT of some powders. Results showed good agreement with the experimental data, proving that, despite its stochastic feature, the ignition phenomenon and sensitivity can be successfully described and modelled by calculating the associated parameters. However, kinetic data are almost always taken from slow-heating analysis, whose operating conditions are incompatible with those encountered during a dust explosion. Moreover, fundamental phenomena, such as agglomeration, pyrolysis product yield, and dust cloud mean conversion must be considered to perform a complete analysis.

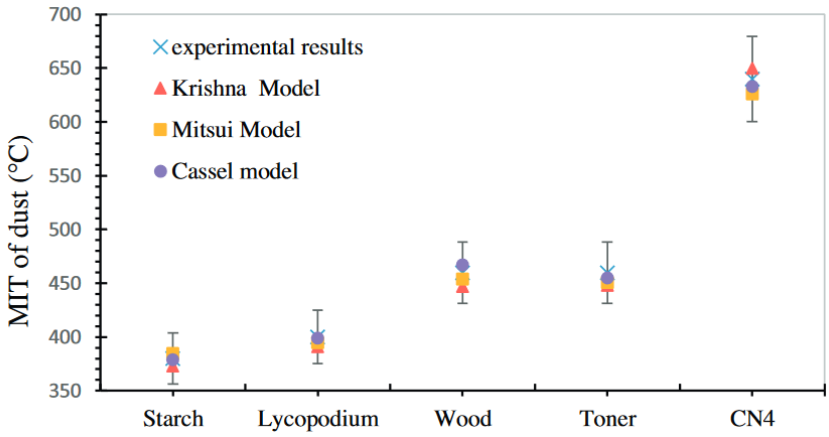

Figure 1-17 - Comparison between experimental MITs and values obtained with three models (Addai et al. 2016)

2.3 Minimum Explosive Concentration

2.3.1 Context and Definition

A powder's Minimum Explosible Concentration (MEC) corresponds to the minimum dust concentration below which no flame can propagate within the dust cloud. It strictly depends on the dispersion procedure, the ignition's turbulence level, the powder's nature and the presence of a gas or vapour phase. It is largely used in industry to design apparatuses and unitary operations, making them intrinsically explosion-safe.

2.3.2 Experimental setups and procedure

The standard apparatus for determining the MEC is the 20L sphere (see Figure 1-18) and the standard procedure is the EN 14034-3 (EN 14034-3 2006). It provides for starting the test at a known explosive dust concentration, progressively reducing it by 50%. The minimum value at which an explosion was recorded corresponds to the MEC. In the 20L vessel, an explosion corresponds to an increment of at least 0.3 bar compared to the initial pressure right before the ignition (usually corresponding to 1 bar).

Although its apparent simplicity, the experimental measurement of the MEC is far from straightforward. Abbas (Abbas et al. 2022a) stated that numerous biases and interferences related to the standard procedure and apparatuses might lead to unrealistically low values, such as heterogeneity of the dust concentration and a too high turbulence level. Therefore, they developed a vertical top-open acrylic glass tube to measure the MEC in a homogeneous and uniform dust suspension. Moreover, the setup can be associated with a dust concentration measuring system.

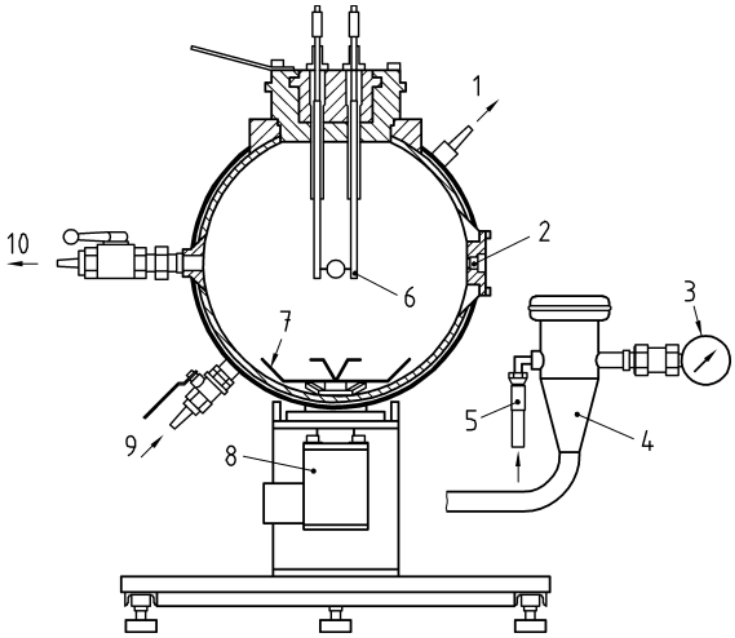

1	*Water outlet*	*5*	*Air inlet*	*8*	*Fast-acting valve*
2	*Pressure sensors*	*6*	*Ignition source*	*9*	*Water inlet*
3	*Manometer*	*7*	*Rebound nozzle*	*10*	*Outlet (air, reaction products)*
4	*Dust container (0,6 dm^3)*				

Figure 1-18 - Standard 20L vessel

2.3.3 Influencing parameters

Particle size is one of the main powder characteristics that play a significant role in the MEC. The smaller the particle size, the lower the MEC, as reported in Eckhoff (Eckhoff 2003). Considering a constant dust concentration and ignition energy, decreasing the mean particle diameter means increasing the fraction of finer particles, associated with a lower characteristic heating time. The result is a lower amount of energy per particle necessary to attain those

temperatures at which devolatilization reactions occur. Results presented by Altwal (Altwal and Véchot 2021) confirm this effect of the particle size on the MEC. Furthermore, they pointed out discrepancies between the values obtained with the 20L sphere and the Hartmann tube, which might lead to over- or underestimation of the ignition sensitivity of a powder.

If the dust is part of a hybrid mixture, the influence of the gaseous/vapour phase composition cannot be neglected. Several works assessed the tendency of combustible vapours and gases to decrease the MEC of the mixture under the MEC of pure dust (Addai et al. 2015; Kim et al. 2020; Zhao et al. 2020).

2.3.4 Modelling

Predicting dust's MEC signifies studying an entity characterized by a high stochastic behaviour. Multiple works focused on understanding the principal phenomena involved, trying to isolate the parameters with a major role in order to simplify the system. For example, Klippel (Klippel et al. 2014) tried to describe the loading process of a silo, estimating the zones associated with an explosive concentration, especially where the MEC might place in the silo. A comparison between experimental and modelling data was made, leading to a general agreement. An uncertainty was nonetheless present, mainly deriving from the strict dependency of the dust dispersion on the test conditions (i.e. air humidity). Finally, the MEC of hybrid mixtures is widely studied and modelled, even though the phenomenon's complexity and the lack of knowledge regarding the interaction between gaseous, vapours and solid combustible species make the simplification hypothesis strictly necessary (Abbas et al. 2019).

2.4 Limiting Oxygen Concentration

2.4.1 Context and Definition

The flame propagation phenomenon within a dust-air cloud strictly depends on the equivalent ratio (ER): in rich mixtures (ER > 1), the oxygen represents the limiting reactant, and its quenching effect slows down the flame propagation; in lean mixtures (ER < 1), the low dust concentration translates in a high inter-particle distance, and nitrogen inerting effect becomes relatively more important, which partially quenches the flame slowing down its propagation. The minimum oxygen concentration that allows flame propagation is the Limiting Oxygen Concentration (LOC). It is primarily employed in industry to reduce the intrinsic ignition risk of an explosive system. As an example, in Table 1-5 are reported the maximum

oxygen concentrations allowed for inerting with N_2. According to the dust's chemical nature and particle size, the composition of the inerting atmosphere must be carefully chosen to prevent fires and explosions intrinsically. This notion can also be useful in gasification or during pyrolysis in a partially oxidising atmosphere

Table 1-5 - Maximum oxygen concentration allowed for inerting storage units with nitrogen (Eckhoff 2003)

Powder	**Median particle diameter, µm**	**Max O_2 concentration, %vol**
Cellulose	22	9
Cellulose	51	11
Waste from wood cutting	130	14
Wood	27	10
Pea flour	25	15
Maize starch	17	9
Waste from malted barley	25	11
Starch derivative	24	14
Wheat flour 550	60	11
Brown coal	42	12
Brown coal	63	12
Brown coal	66	12
Brown coal briquette dust	51	15
Bituminous coal	17	14
Ground hops	500	17
Hops draff	490	18
Polyethylene HD	26	10
Methyl cellulose	29	15
Methyl cellulose	49	14
Methyl cellulose	70	10
Aluminum	22	5
Aluminum	22	6
Ferrosilicon	17	7
Ferrosilicon	21	12
Magnesium alloy	21	3
Soot	<10	12
Soot	<10	12
Soot	13	12
Soot	16	12

2.4.2 Experimental setups and procedure

The standard apparatus for determining the LOC is the 20L sphere (see Figure 1-18), and the standard procedure is the EN 14034-4. It provides for classically starting the test with the selected dust and air and progressively reducing the oxygen concentration by using an inert gas (often nitrogen). The minimum oxygen concentration at which an explosion was recorded corresponds to the LOC. In the 20L vessel, an explosion corresponds to an increment of at least 0.3 bar compared to the initial pressure right before the ignition (usually corresponding to 1 bar).

2.4.3 Influencing parameters

An explosive system's LOC is dependent on its ignition energy. Therefore, MIE and MIT intervene to modify the minimum oxygen concentration at which a system can explode, according to the following relationship (Equation (1)) presented in Siwek (Siwek and Cesana 1995) (see Figure *1-19*):

$$LOC = 1.62 \cdot \log MIE\,[1+(MIT / 273)] + 12.9 \qquad (1)$$

Addai (Addai et al. 2019) also found similar results, underlining the role of the ignition energy in determining the LOC. They worked on several hybrid mixtures of fifteen dusts, isopropanol, acetone and methane, using pyrotechnical igniters of 10 J, 2 and 10 kJ. Results were diverse: using the less energetic ones, LOC values were always sensibly higher, while for the highest ignition energy, they decreased. Moreover, the LOC of the hybrid mixtures differed from the pure dusts, often even leading to LOC lower than solvents and methane.

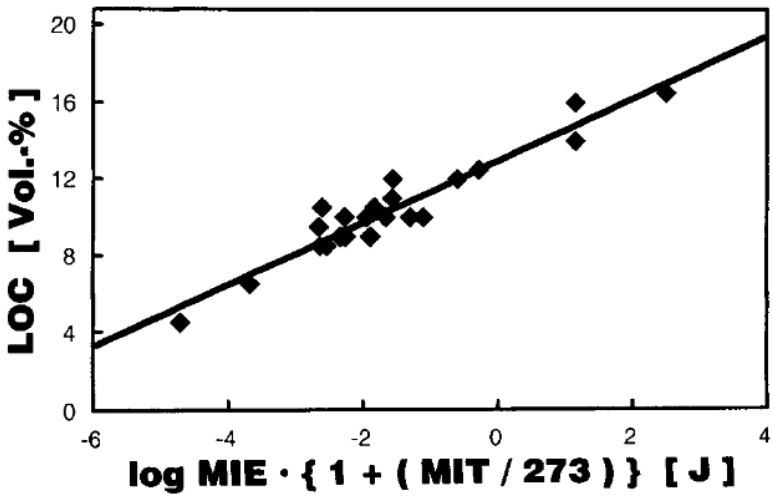

Figure 1-19 - Correlation between the LOC, MIE and MIT of a dust (from Siwek and Cesana 1995)

2.4.4 Modelling

Since determining a powder's LOC is time-consuming, reliable results estimated with models and calculations constitute an appealing approach for the industry. Therefore, Krause (Krause et al. 1992) elaborated a simple approach to calculate the LOC of a powder based on some of its physicochemical properties, such as the elemental analysis, MEC and heat of reaction. They also compared the calculated results with experimental ones, finding a satisfactory agreement (Krause et al. 2016).

3. Explosion severity

3.1 Content and Definition

Unfortunately, although numerous precautions can be adopted to reduce the ignition sensitivity of explosive systems, the experience feedback from the industry provides solid proof that dust explosions occur (Table 1-1). Lack of awareness and poor maintenance are only two of the causes responsible for these accidents. Hence, it is always rigidly necessary to consider the explosion's scenario and its consequences on people, equipment and the environment. Two parameters characterize the explosion severity: the maximum explosion overpressure (P_{max}) and the maximum rate of pressure rise ($(dP/dt)_{max}$). P_{max} corresponds to the maximum overpressure attained during an explosion test series, while $(dP/dt)_{max}$ translates to the maximum rate of the explosion overpressure rise in a test series. These two parameters are employed to design the venting systems and to estimate the damages due to an explosion scenario.

Hartmann and his research team made the first documented attempt at determining the dust explosion severity in a closed-bomb apparatus in 1943 (Hartmann, Nagy, and Brown 1943). They conceived a 1.2 L closed cylindrical chamber in which dust was dispersed from the bottom upwards and ignited by a continuous electrical spark. A second chamber was added at the top to allow the flame to propagate and to record the pressure-time profile. However, Eckhoff (Eckhoff 1984) in 1984 assessed that numerous copies of the Hartmann apparatus were realized worldwide, leading to many different setups with a strong influence on the rate of pressure rise. Consequently, the agreement between laboratory results in the U.S.A. and Europe was poor. In 1971 Bartknecht underlined the inadequateness of the Hartmann bomb for industrial design (Bartknecht 1971), proposing a $1m^3$ apparatus for the determination of the explosion parameters. Nevertheless, because of its higher volume and price and the necessary

modifications to the dust injection, the $1m^3$ was not broadly used. Nonetheless, in 1996, Siwek (Siwek 1996) defined the $1m^3$ chamber as the standard vessel for testing the dust explosion severity, reporting that 70 examples were being used that year worldwide. He also assessed the increasing use of another vessel: the 20L apparatus (see Figure 1-18). In 1977 Bartknecht and Siwek (Siwek 1977) proposed a smaller spherical vessel for determining dust explosion parameters comparable with those obtained in the 1 m^3 chamber. In order to define its optimal volume, they started with a 5L bomb and continued with a 10L one, ending with the 20L chamber, which is currently the most used standard vessel for quantifying the explosion severity of dusts. The volume of an explosion test apparatus can reach up to 250 m^3.

As pointed out by Eckhoff (Eckhoff 1985) and Nagy (Nagy et al. 1969), the influence of the chamber volume on the explosion parameters is not negligible. Therefore, to uniformize the results and to carve out the influence of the volume, the commonly adopted law is the cubic law:

$$K_{St} = (dP/dt)_{max} \cdot V^{1/3} \qquad bar.m.s^{-1} \qquad (2)$$

where K_{St} is the deflagration index. This relationship was established considering two dust explosions (associated thus with the same burning velocity) in two vessels with different volumes. Several hypotheses were made to obtain Equation (2) (Eckhoff 1985):

- The explosive gas mixtures are identical, homogeneous and quiescent;
- The ignition sources are punctual and activated at the sphere centres simultaneously at time t = 0;
- The sphere walls are assumed to be perfect heat insulators;
- The flame propagation rate is low enough to ensure complete spatial pressure equilibrium throughout the vessels at any instant.

The influence of the apparatus on the explosion severity is nonetheless non-negligible, as depicted by Skjold (Skjold 2018). In Figure 1-20, the K_{St} determined in the 20L sphere is compared to that obtained in the $1m^3$ sphere, showing a high dispersion of the data and a factor-2 region defining it.

Although these hypotheses might not be entirely compatible with dust explosions, the K_{St} is widely used and accepted in the scientific literature as a comparison and classification tool. The EN 14034-2 standard procedure defines it and the laboratory protocol to determine it.

Moreover, the deflagration index allows classifying a powder in four classes, as depicted into Table 1-6.

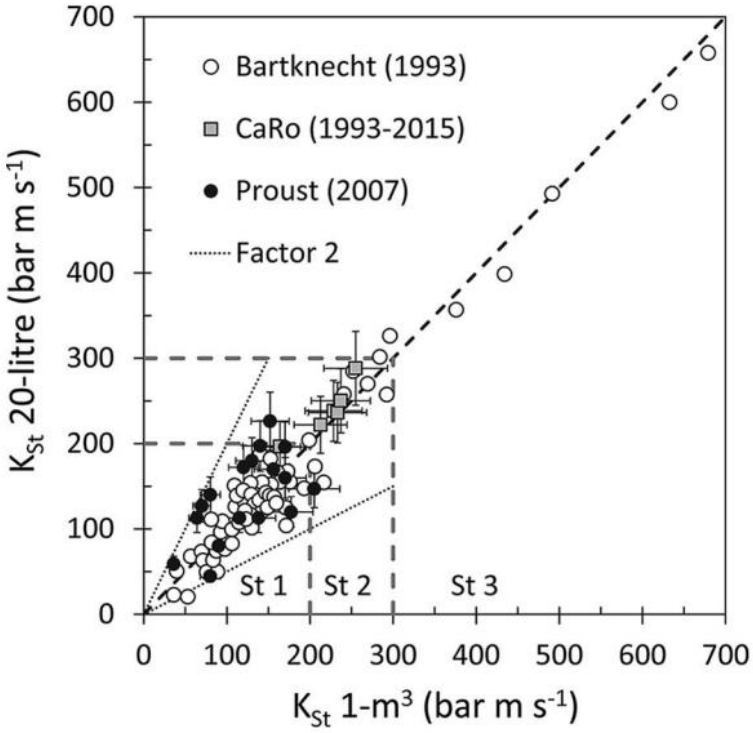

Figure 1-20 - Comparison between the K_{St} values determined in the 20L vessel and those determined in the 1m^3 vessel (Skjold 2022)

Table 1-6 - Classification of a powder according to its deflagration index

Dust class	K_{St}, bar.m.s^{-1}	Characteristic
-	0	No explosion
St 1	$0 < K_{St} \leq 200$	Weak explosion
St 2	$0 < K_{St} \leq 300$	Strong explosion
St 3	$K_{St} > 300$	Very strong explosion

3.2 Experimental setups and procedure

Both P_{max} and $(dP/dt)_{max}$ are determined in the 20L sphere following the EN 14034-1 and EN 14034-2 standard procedures, respectively (EN 14034-1 2004; EN 14034-2 2006). The dust is weighted and placed in the dust container. Then, the chosen pyrotechnical igniters are

fixed to the special metallic bars that allow placing the ignition source at the centre of the sphere. The vessel is sealed with the lid, and the internal pressure is reduced with a vacuum pump. The test can be started as soon as the internal pressure attains 0.4 bar (as specified in the standard). Next, the dust container is pressurized to 21 bar, and an electro-valve opens and allows the dust to disperse in the sphere. After an imposed ignition delay time (t_v), the cloud is ignited. Two pressure sensors detect the pressure during the test. During an explosion in the 20L chamber, the pressure-time profile exhibits the characteristic trend shown in Figure 1-21, used to define several values and parameters associated with this curve, according to the EN 14034-2 standard procedure.

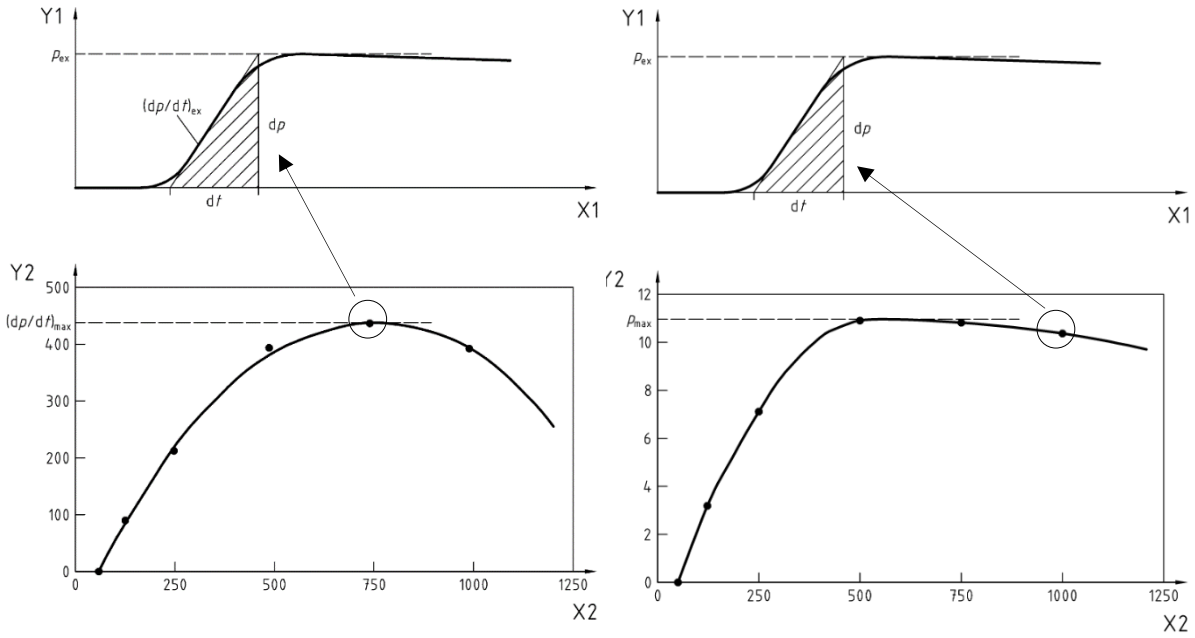

Y1 explosion overpressure p

Y2 rate of explosion pressure rise $(dp/dt)_{ex}$, in $bar.s^{-1}$

X1 time t

X2 dust concentration C, in $g.m^{-3}$

Y1 explosion overpressure p

Y2 explosion overpressure p_{ex}, in bar

X1 time t

X2 dust concentration C, in $g.m^{-3}$

Figure 1-21 - An example of typical curves associated to a dust explosion in the 20L chamber

3.3 Influencing parameters

The particle size distribution influences the explosion severity as with the other parameters. In particular, the explosion behaviour of dusts seems affected by the combination of its PSD features: median value, D_{32}, skewness, kurtosis and span.

Eckhoff (Eckhoff 2003) presented the influence of the PSD median value on the explosion severity of polyvinyl chloride (PVC) and polyethylene (PE). Two major characteristics influenced their behaviour: the presence of chlorine in PVC and the median value. Halogens usually have a retarding effect on flame propagation, causing the $(dP/dt)_{max}$ to decrease around 50 µm rapidly. PE's P_{max} showed a different decreasing trend but a similar trend considering the $(dP/dt)_{max}$. In conclusion, both polymers' explosion parameters decrease with the median particle size. As underlined by Tascon (Tascón 2018), D50 and negative skewness promote the explosion parameters of aluminum and coal dusts. A PSD more centred on finer particles is then responsible for increasing both P_{max} and $(dP/dt)_{max}$, as also presented by Dufaud (Dufaud et al. 2010). Since flame propagation is strictly associated with radiative heat transfer within the dust cloud, which depends on the exchange surface of the bodies involved, the result of small median particle size, a negative kurtosis or a combination of both is an increment of the flame front speed, thus a high $(dP/dt)_{max}$. Moreover, finer particles are more prone to react completely, releasing a higher energy content and increasing the P_{max} value. In coarser particles, the internal conduction characteristic time scale rises significantly and prevents particles from converting entirely. The particle size does not only influence the kinetics directly but also via agglomeration. Finer particles have a more significant tendency to form clustery structures (e.g. due to Van der Waals forces), therefore increasing the effective particle sizes reacting within the dust cloud (Eckhoff 2003). Bagaria (Bagaria et al. 2016) studied the effect of the dispersion in the 20L sphere on the agglomeration importance of three organic powders, enlightening the influence of both the dispersion process and nominal dust concentration (Figure 1-22).

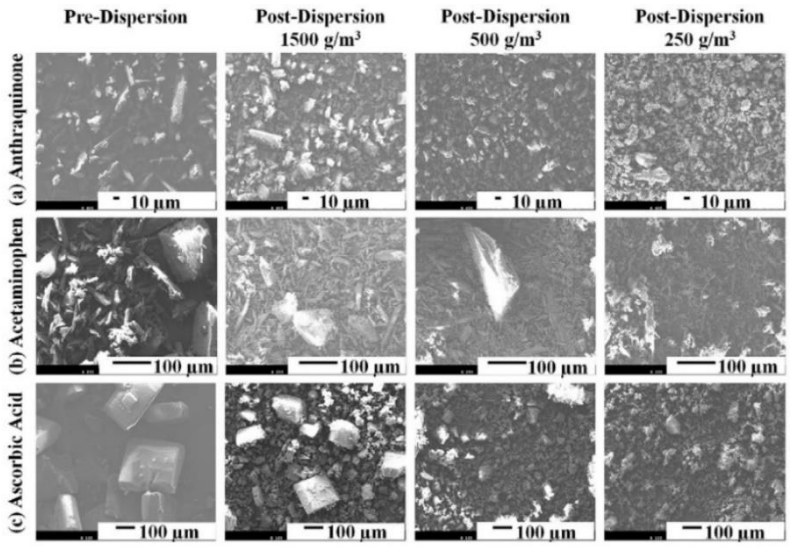

Figure 1-22 - SEM images of pre- and post-dispersion sample in the 20L sphere, at different dust concentration (Bagaria et al. 2016)

Moreover, the particle shape is an essential characteristic that plays a fundamental role in determining the parameters previously presented. Therefore, morphology and characteristic lengths are vital in dust explosions, especially when complex geometries are involved. Several works (Marmo 2010; Marmo et al. 2018; Salatino et al. 2012) focused on determining flammability and explosion severity of textile fibres, whose peculiar feature is to present intricated geometries. In these cases, the main challenge is to develop a method to determine the characteristic lengths involved in the physicochemical mechanisms and then analyse their thermal behaviour. According to the phenomenon studied, the definition of the proper characteristic length can lead to different results due to particle shape differences. For instance, considering a cylindrical and a spherical particle, the characteristic dimensions will be the thickness for the first and the diameter for the second. Moreover, volume- and surface-based PSD can be adapted to be consistent with the phenomenon considered.

The moisture content is a further factor determining a reduction of a dust explosion severity (in the case of organic compounds). Eckhoff (Eckhoff 2003) reduced its effect to three main consequences:

- Heating and evaporation of water act like a heat sink;
- Water vapour mixes with the pyrolysis products, reducing their reactivity;
- Inter-particle cohesive interactions are enhanced, leading to larger effective particles;
- Fuel concentration reduction.

Yuan (Yuan et al. 2014) showed the heat-sink role of the moisture in the explosion severity of four coal dust, whose explosion parameters are notably reduced. Sheenan (Sheehan et al. 2022) characterized the influence of the moisture content on the unloading process of powdered sugar cane bagasse, showing a significant reduction of the fines as it increases.

The oxygen concentration does not act only on the MIE but also on the explosion dynamics, becoming a non-negligible parameter for determining P_{max} and $(dP/dt)_{max}$. Eckhoff (Eckhoff 2003) and Mittal (Mittal 2013) reported its effect on coal dust samples, showing decreasing P_{max} and $(dP/dt)_{max}$ as a function of the oxygen concentration. Both the kinetics and the energy released during the explosion are thus affected by it.

It is common knowledge that hybrid mixtures have a peculiar explosion behaviour. The interactions between their components are not linear and not simple to study and explain, especially considering the explosion parameters. For example, Figure 1-23 depicts the maximum rate of pressure rise of magnesium stearate/ethanol hybrid mixtures, showing peaks and valleys associated with multiple phenomena. P_{max} is known for being slightly influenced by the presence of a combustible gas or vapour phase, but $(dP/dt)_{max}$ echoes the critical changes

in the explosion dynamics (Bartknecht 1971; Dufaud et al. 2008). Garcia-Agreda (Garcia-Agreda et al. 2011) elaborated an explosion regime diagram that defines the roles of the combustible dust and gas (in this work, nicotinic acid and methane, respectively). It is shown in Figure 1-24, and five zones constitute it:

- A no-explosion zone, delimited by Le Chatelier's curve;
- A synergic explosion zone, where the K_{St} is the result of a synergic combination of dust and gas;
- A dust-driven explosion zone, where the solid phase primarily determines the K_{St} (also K_h for a hybrid mixture);
- A gas-driven explosion zone, where the gaseous fuel primarily determines the K_{St} (also K_h for a hybrid mixture);
- A dual-fuel explosion zone, where both fuels contribute to the explosion.

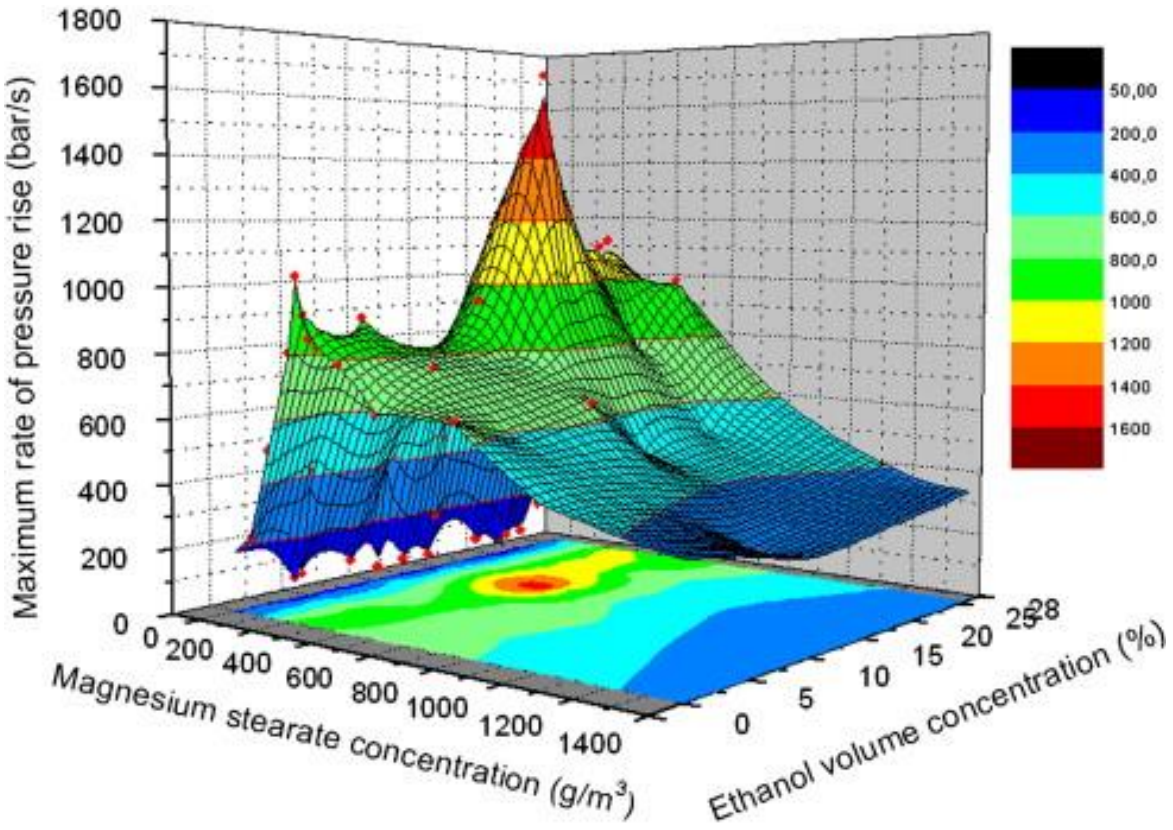

Figure 1-23 - Representation of the maximum rate of pressure rise of magnesium stearate/ethanol hybrid mixtures (Dufaud et al. 2009)

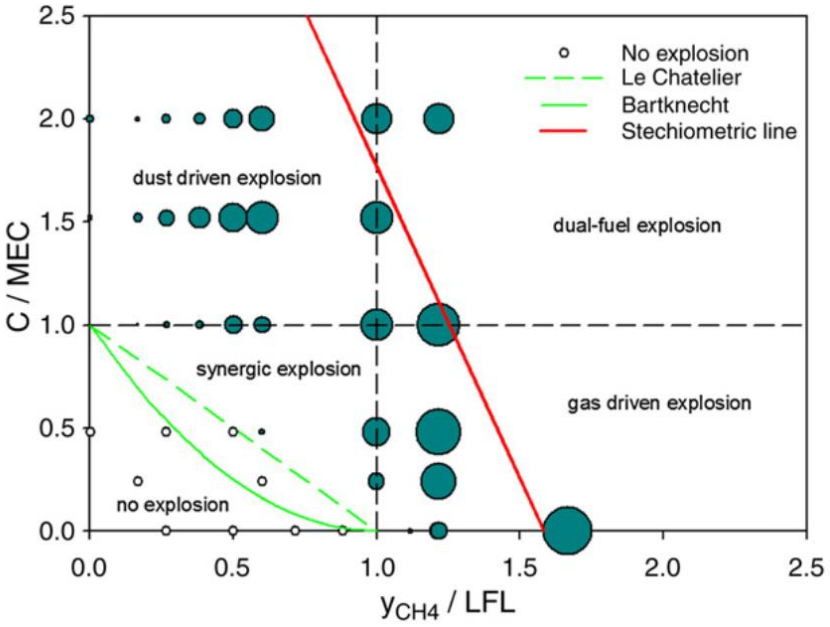

Figure 1-24 - Explosion regime chart for nicotinic acid/methane hybrid mixtures (Garcia-Agreda et al. 2011); MEC and LFL correspond to the Minimal Explosion Concentration and the Lower Flammable Limit, respectively.

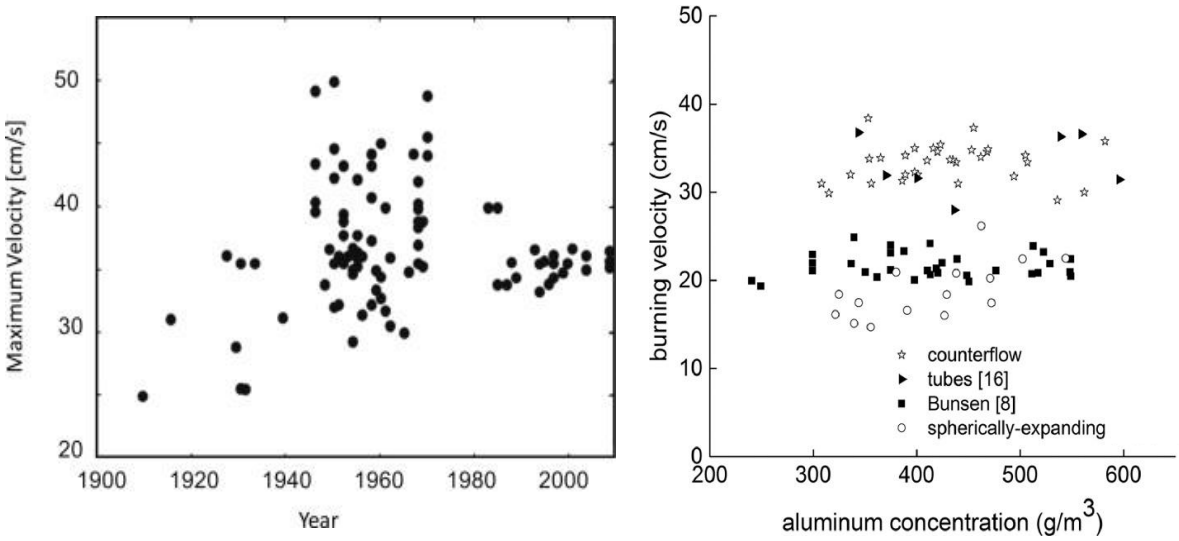

Figure 1-25 - Measurements of the maximum flame speed for a methane-air mixture (to the left) and burning velocities of aluminum dust-air mixture measured with different experimental setups (Julien et al. 2017; Ranzi et al. 2012)

3.4 Modelling

The experimental determination of fundamental variables involved in dust explosion phenomena is not exempt from variability in space and time. As presented in Figure 1-25, for

example, the measure of methane-air mixture laminar burning velocity has led to uneven values over time, while the choice of the setup and the concentration have a strong influence on the final value. To model and simulate a dust explosion hides then significant challenges that need to be considered. Skjold (Skjold 2022) stressed out several significant points in modelling dust explosions:

- The complexity of determining fundamental combustion properties for transient, turbulent and particle-laden flow, typical of dust explosion scenarios;
- The significant variability between repeated experiments;
- The sensitivity to slight variations in the initial boundary conditions;
- The resolution of complex internal geometries coupled to important external areas (venting systems, openings, etc.).

On this premise, several works in the literature proposed approaches to model a dust explosion. Cheng (Cheng et al. 2020) developed a CFD model to describe the flame propagation phenomenon of corn starch in a vertical square tube 50 cm long. Since the volatilization mechanism of corn starch is not well known, they assumed a global chemical formula to represent the volatile matter of the solid phase ($C_{4.51}H_{10}O_{4.51}$) and a composition of volatiles (CH_4 = 13.33 mol%; CO_2 = 13.33 mol%; CO = 34.46 mol%; H_2 = 39.99 mol%). CFD modelling results are coherent with the experimental high-speed videos, but observed and simulated spatial flame velocities showed some discrepancies, especially after 60-70 ms from the ignition.

Di Benedetto (Di Benedetto and Russo 2007) studied the flame propagation in cellulose, corn starch and polyethylene dust clouds. They based their CFD modelling on both volatile analysis (sampled in the propagation tube) and literature references, comparing it to experimental data and other simulations found in the literature. Figure 1-26 resumes their work on corn starch: the discrepancies between models, experimental data and approaches underlined the complexity of the objective, subject to several changing operating parameters. Finally, Copelli (Copelli et al. 2019) developed a method based on heat and mass balance on a single particle and volatiles, also considering the effect of the ignition source (pyrotechnical igniters). A comparison between the experimental and the predicted results is reported in Table 1-7. The model seems to slightly overestimate the K_{St}, but the relative deviation respects the limits imposed by the EN 14034-2:2006 standard.

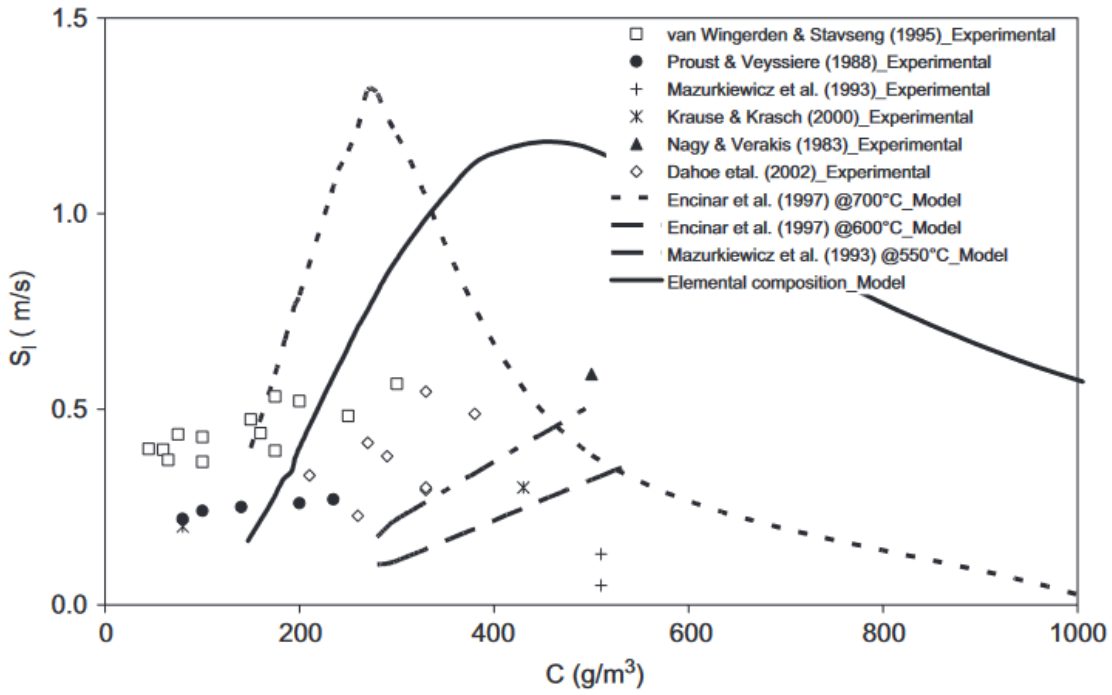

Figure 1-26 – Comparison between experimental and simulation results of the laminar burning velocity in a corn starch dust cloud, as function of the dust concentration (from (Di Benedetto and Russo 2007))

Table 1-7 - Experimental and predicted K_{St} values (adapted from (Copelli et al. 2019))

Dust	**Median diameter µm**	**K_{St} EXP bar.m.s^{-1}**	**K_{St} MOD bar.m.s^{-1}**	**Relative deviation**	**Deviation allowed (EN 14034-2:2006)**
Aspirin	25	217	220	-1.4%	± 10%
Cork	42	202	200	1.0%	± 10%
Corn	54	132	131	0.8%	± 12%
Niacin	37	215	220	-2.3%	± 10%
Polyehtylene	28	133	147	-10.5%	± 12%
Polystyrene	20	218	216	0.9%	± 10%
Sugar	37	138	155	-12.3%	± 12%
Wheat	57	62	63	-1.6%	± 20%

4. Biomass dusts

In the previous section, it has been shown the importance of biomass sector's role in organic dust explosions. This section will present biomass's global context, principal features, and major processes involved in its thermo-chemical valorisation. Focusing on the pyrolysis chemical mechanisms will finally link the study of organic dust explosions.

4.1 Socio-ecological and economic context

The second half of the XXth century has been characterized by deep industrialization and significant growth of the population, which have continued until today. While the population grew by approximately 1 billion per decade, the world Gross Domestic Product (GDP), usually used to represent the health of national and global economies, started to rise linearly at the end of the century. On the other hand, energy consumption slightly decreased during the 90s but rose substantially from 2000 to today. Figure 1-27 reports GDP and energy consumption normalized to the global population.

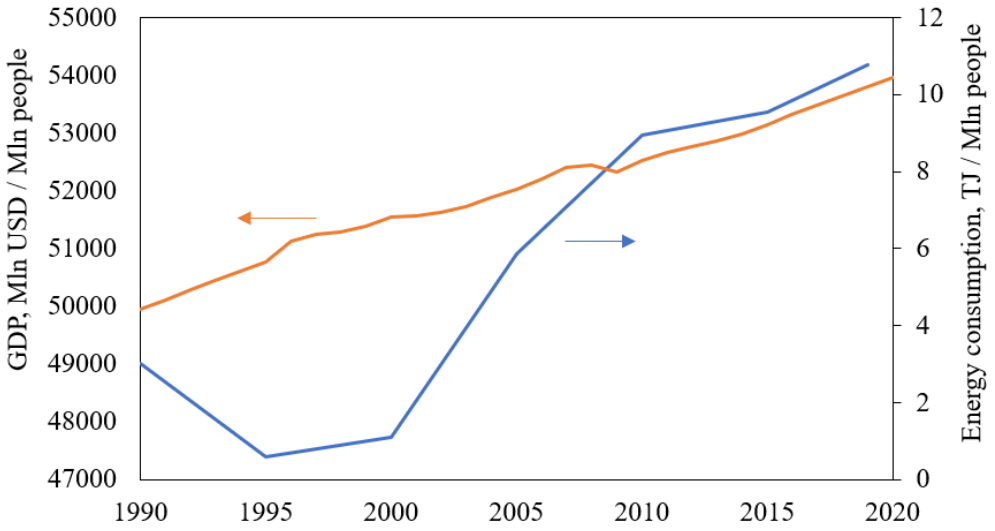

Figure 1-27 - Industrialization process and energy consumption between 1990 and 2020 (from EEA, IEA, UN Department of Economic and Social Affairs)

In this climate of continuous growth, energy became a primary need. The technological development allowed it to diversify its production, even though fossil sources continue to cover a wide range of the global energy supply, as presented in Figure 1-28. The final consumption (Figure 1-29) is constituted mainly by oil products, such as gasoline and diesel. Energy from biomass (bioenergy) and waste accounts for about 10% of the total energy consumption in 2019. Among the renewable energies, bioenergy has caught the attention of numerous countries as an energy vector. It will continue to grow in the future, as esteemed by a European research team during the development of ENSPRESO (ENergy System Potentials for Renewable Energy SOurces) (Ruiz et al. 2019). Unfortunately, although bioenergy and renewables gained a deep global interest, investments between 2011 and 2020 have significantly decreased, as clearly presented in Figure 1-30. Moreover, investments in bioenergy suffered a particularly dramatic decline, partially due to a lack of interest in the production systems and a lack of technological innovation. Consequently, it kept the cost of many renewable energies constant while others significantly decreased, as can be deduced from Figure 1-31.

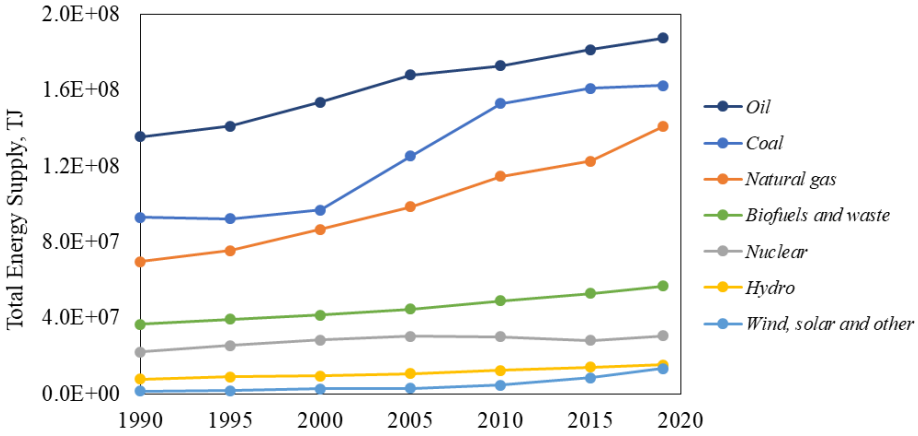

Figure 1-28 - World Total Energy Supply between 1990 and 2020 sorted by production technology (IEA Report 2021)

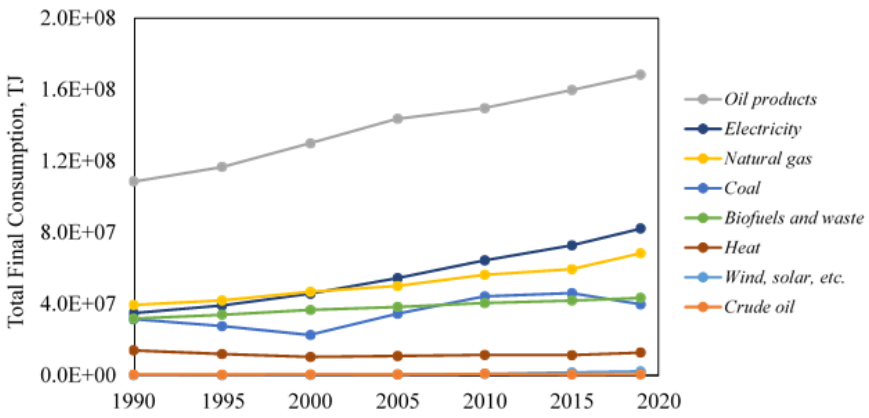

Figure 1-29 - World Total Final Consumption sorted by source (IEA Report 2021)

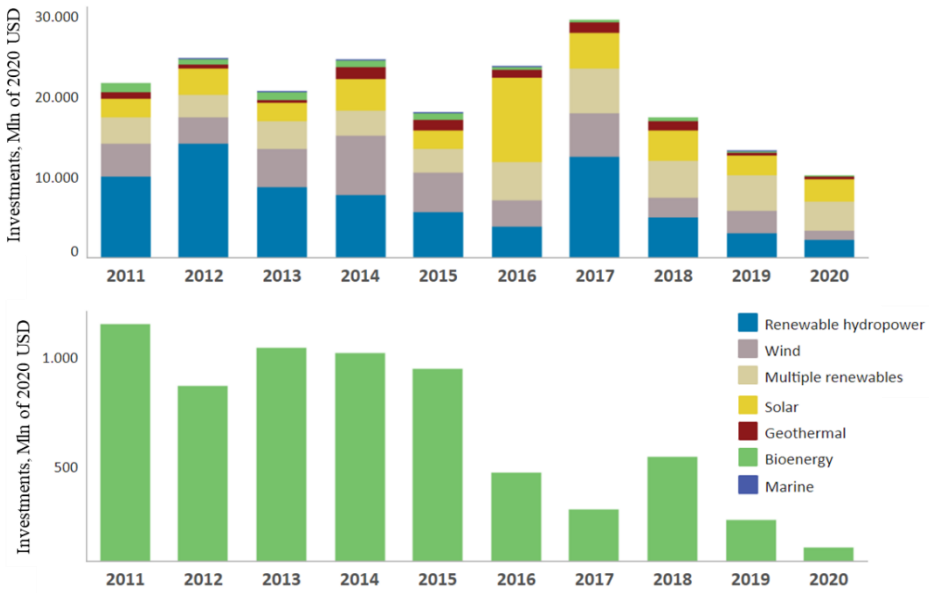

Figure 1-30 - Total investments in renewables energies, worldwide between 2011 and 2020 (IRENA 2021)

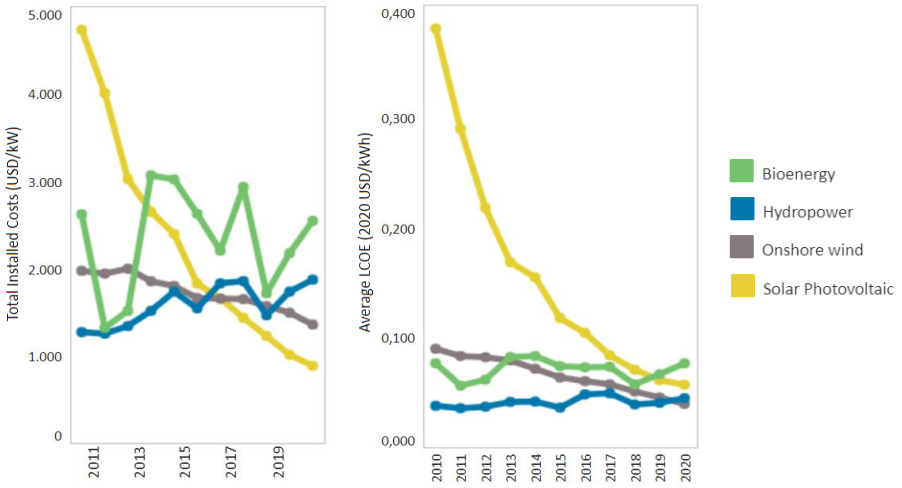

Figure 1-31 - Total installed cost and average Levelized Cost of Energy (LCOE) for bioenergy, hydro-, onshore wind and solar photovoltaic power (IRENA 2021)

4.2 General aspects of biomass

The term "biomass" has its roots in the first half of the XXth century. The Russian mineralogist Vladimir Ivanovič Vernadskij was the first to introduce the idea of grouping all living beings together in a single word. Still, the actual forging of this term is attributed to the

oceanographer Reinhard Demoll (Demoll 1927). As it suggests (from Greek βίος, bìos = "life"), according to him, "biomass" corresponds to the entirety of the living organisms on Earth (animals, plants, bacteria and fungi). With industrialisation and technological development in the post-war period, the definition of biomass slightly changed. Edomah (Edomah 2018) defined it as "the term used to describe any fuel derived from plants. This includes crop residues, wood, crops and animal waste". Biomass is now related to the energy production system. Finally, during the last two decades, a schism between the so-called "traditional" and "modern" or "non-conventional" biomasses pointed out the need to include wastes and by-products in this term, indirectly associated with the original "biomass". The IEA Market Report Series on Renewables (2021) (IEA 2021), for example, explicitly defines bioenergy (i.e. the energy directly or indirectly produced from biomass) as:

- A type of energy that comes "from solid, liquid, and gaseous biomass and municipal waste (renewable and non-renewable). It does not include plants that co-fire biomass with fossil fuels";
- A type of energy that "includes […] traditional uses of biomass".

To conclude, today's needs and urges changed the definition of biomass, which might continue to change in the future. Biomass can be classified according to its origin, as presented in Figure 1-32. Primary biomasses are associated with naturally grown, cultivated and harvested plants and can be divided into wood and non-wood based. Secondary biomasses are the by-products of physical, chemical and biological processes which aim to modify one or more characteristics of these materials. Finally, tertiary biomasses are represented by the wastes of post-consumer processes. Among these, the Solid Recovered Fuels (SRF) represent an increasingly-interesting energy source. SRF are based of the by-products of waste sorting.

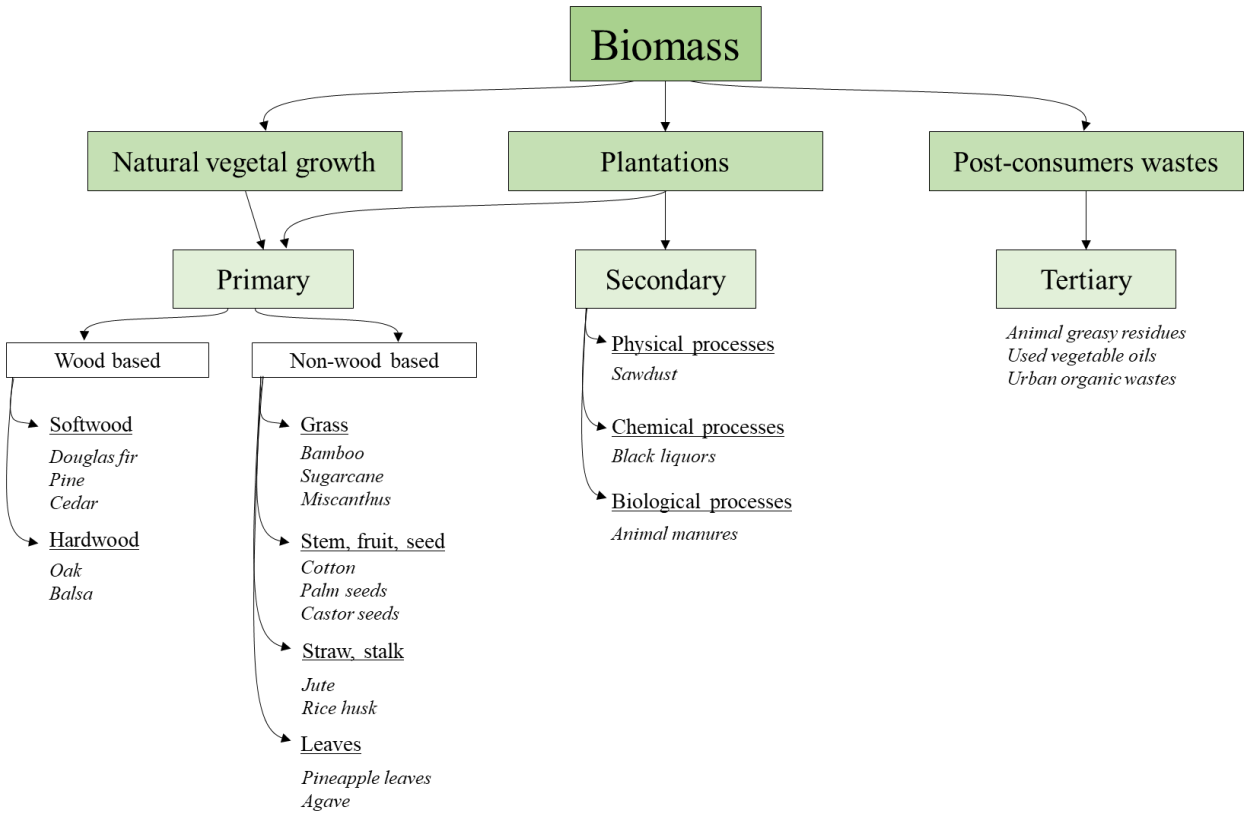

Figure 1-32 - Classification of biomass, adapted from (Kumari et al. 2021; Panwar, Pawar, and Salvi 2019; Yankov 2022)

Lignocellulosic biomass is the broadest range of biomass. It is mainly composed of carbon (C), hydrogen (H), oxygen (O), nitrogen (N) and sulphur (S), with a non-negligible percentage of inorganic matter, constituted essentially of Si, K, Mg, Na and Ca. The primary constituent of lignocellulosic biomass is water; thus, biomass drying processes represent a fundamental brick of its valorisation chain (Le Brech 2015). Secondly, lignin, cellulose and hemicellulose are the main components of the plant's cell wall. Their fractions depend on the species considered, as shown in Table 1-8.

Cellulose can be considered as the structure of the cell wall. It is the most abundant biopolymer on Earth, forming between 43 and 60% of the vegetal biomass. The chain of its molecule is constituted by β-D-glucopyranose monomeric units ($C_6H_{10}O_5$), held together by β(1,4) glyosidic bonds (Le Brech 2015), as shown in Figure 1-33. Hydrogen bonds and Van der Waals weak bonds establish between the chains, which explains the fibrous nature of cellulose and confers high crystallinity.

Hemicellulose indicates a large family of branched heteropolymers constituted by different monomeric units, as presented in Figure 1-33, including pentoses (arabinose, xylose),

hexoses (glucose, galactose and mannose), and a small amount of rhamnose and fructose. The composition of hemicellulose varies according to the species considered.

Lignin is an aromatic (phenolic) hetero-biomacromolecule constituted by long and chemically complex chains (see Figure 1-33). Three main monomers can be identified: p-coumaryl alcohol (unit H, hydroxyphenyl), coniferyl alcohol (unit G, guaiacyl), and sinapyl alcohol (unit S, syringyl) (Cassoni et al. 2022; Le Brech 2015; Serrano et al. 2019). The variability of the ratio between these monomers is high and is characteristic of the type of biomass. However, the exact structure of lignin is not precisely established yet (Le Brech 2015).

Table 1-8 - Agricultural biomasses and their composition in terms of lignin, hemicellulose and cellulose (Kumari et al. 2021)

Biomass	**Cellulose**	**Hemicellulose**	**Lignin**
Corn cobs and stalks	35–45	25–35	15–35
Jute	71	14	13
Wheat straw	30	50	15
Sisal	73	14	11
Rice straw	34	23	11
Switch grass	31	29	17
Bamboo	73	12	10
Barley straw	33.8	21.9	13.8
Corn cob	35	16.8	7
Cotton residues	58.5	14.4	21.5
Rice residues	36.2	19	9.9
Sugarcane	40	27	10
Wheat straw	32.9	24	8.9
Carrot	10.01	5.73	2.5
Cucumber	16.13	4.33	4.51

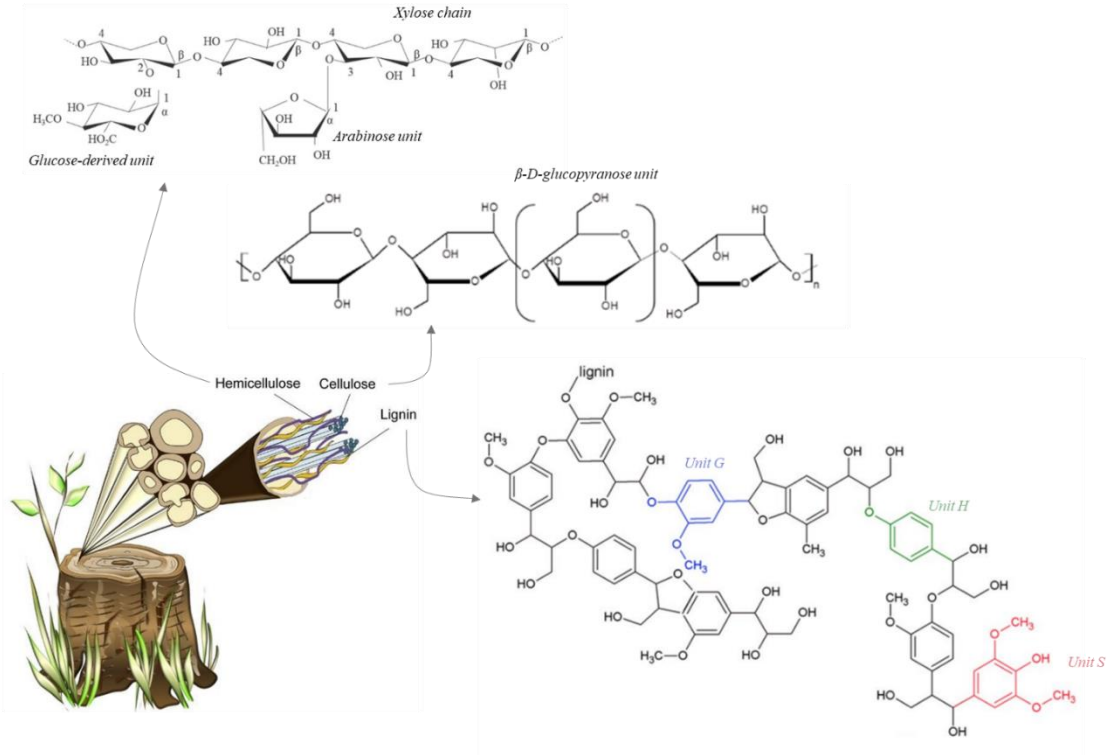

Figure 1-33 - Structure of lignocellulosic biomass and its main components (adapted from (Becker and Wittmann 2019; Benaimeche et al. 2020; Le Brech 2015; Serrano et al. 2019))

Lignocellulosic biomass also contains the so-called "extractives", a group of organic compounds that do not belong to the biopolymer families previously presented. Instead, they are often constituted by resins, tannins and pectins (Le Brech 2015), but also by Phenolic compounds, alkaloids, non-proteic aminoacids, terpenes and fatty acids (Ranzi et al. 2008).

Inorganic species can be found in the different tissues of lignocellulosic biomass. They are principally represented by Si, K, Ca, Mg, P, Cl, Fe and Na, in the form of oxalates, carbonates, sulphates, or bonded to macromolecules (Le Brech 2015).

4.3 Thermo-chemical valorisation of biomass

As the previous section shows, lignocellulosic biomasses are constituted by carbon-rich macromolecules associated with certain energy content. Other than being exploited as a material for their structure, they can be valorised to produce energy (heat and electricity), fuels (bio-oils, biofuels, bioethanol, biogas) or value-added chemicals and molecules. Figure 1-34 schematically represents the biochemical and thermal ways of valorisation.

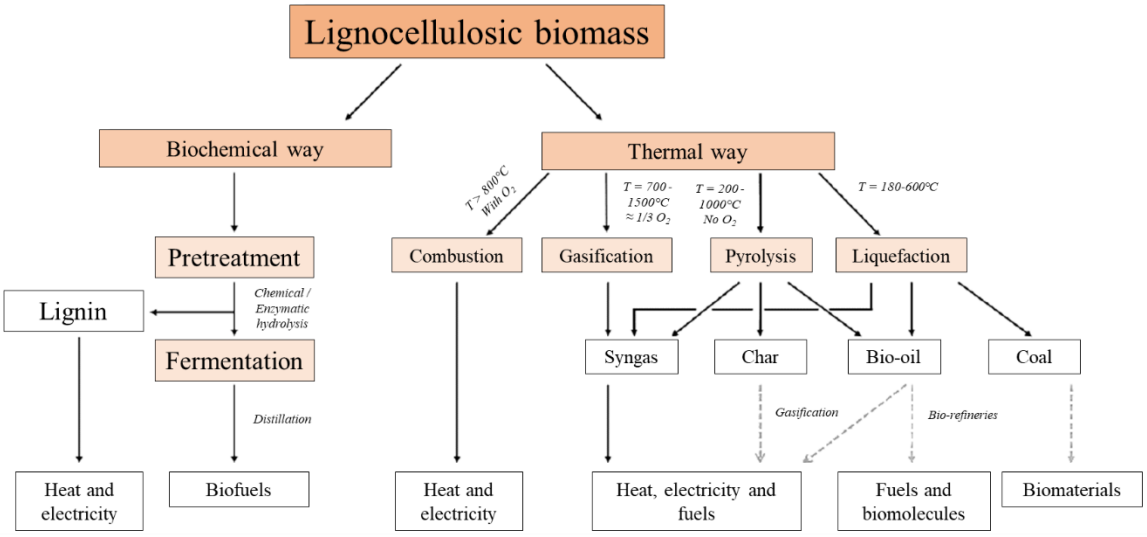

Figure 1-34 - Thermo-chemical ways to valorise the lignocellulosic biomass (adapted from (Le Brech 2015))

As for the biochemical ways, microorganisms are exploited to transform the biomass into energetically-interesting species, such as ethanol, methane or hydrogen. A pre-treatment is often necessary and fundamental to grant the microorganism access to the macromolecules required by their metabolism. Combustion is the complete oxidation of biomass to convert its chemical energy into thermal energy. H_2O and CO_2 are the most abundant gaseous products, while ashes constitute the solid combustion residues. It is the essential biomass conversion process, representing 97% of the bioenergy production in the world (Zhang, Xu, and Champagne 2010). Gasification aims to produce a syngas which can be further valorised to purified H_2, CH_4, liquid fuels or combined heat and power. The lignocellulosic biomass is converted into a gaseous phase (CO, CO_2, H_2, CH_4 and light hydrocarbons), a vapour phase (highly aromatic tars, water) and ashes in an oxidative atmosphere. Three processes can be identified according to their type: partial oxidation with air, oxygen and steam pyrolytic gasification. The diluting effect of nitrogen is not present in the second type. Still, with the third

one, the highest average calorific value of the gaseous fraction is attained (Bridgwater 2003). The gas can be purified to produce syngas ($CO + H_2$), used to produce liquid fuels, thermal energy and power via cleaner combustion, methane via methanation and hydrogen via purification. During a pyrolysis process, the lignocellulosic biomass is heated in an inert atmosphere to produce gaseous (mainly CO, CO_2, H_2 and CH_4), liquid (bio-oil and water) and solid (biochar) products. According to the operating conditions, the production of a phase can be promoted over the others. Section 1.4.4 will more deeply present this process and the reactions involved. A liquid-phase reaction medium characterizes liquefaction, aiming to convert biomass into lowly oxygenated bio-oils, which can be used to produce biofuels (Le Brech 2015). Biochar and gaseous products are generated as well.

4.4 Pyrolysis mechanisms and processes

4.4.1 Context and Definition

The term "*pyrolysis*" was coined from the Greek word "*πυρος, pyro*" ("fire") and "*λύσις, lysis*" ("separating"). It is a thermal conversion technique conducted in an inert atmosphere, applicable to the lignocellulosic biomass. The latter is heated up, and three product fractions are usually identifiable during and after the process: gaseous, liquid and solid. The relative yields strictly depend on the nature of the biomass but even more on the choice of the operating conditions. However, three govern the global phenomenon and, thus, the product yields:

- The reactor temperature.
- The heat flux at which the biomass is exposed.
- The residence time of the three fractions.

Bridgwater and Le Brech (Bridgwater 2003; Le Brech 2015) defined two types of pyrolysis:

- Fast pyrolysis (moderate temperature, around 500°C; short residence time, typically less than 2 s for the vapours; high heat flux, beyond 10 $kW.m^{-2}$);
- Slow pyrolysis (low temperature, between 300 and 500°C; very long residence time; low heat flux, less than 10 $kW.m^{-2}$).

This last classification is not globally recognised and adopted worldwide because it intrinsically depends on secondary operating conditions, such as the biomass particle size, its thermal conductivity and that of the gas used in the process, reactor design, and the moisture content of the solid. These parameters, in fact, influence the heating rate of the particle themselves,

determining the heating time and affecting the product yields. Fast pyrolysis is gaining more and more attention from the scientific community, especially for being associated with high yields of liquid product (Bridgwater 2003). According to Sikarwar (Sikarwar et al. 2017), the use of biomass for power generation will significantly grow in the future (see Figure 1-35). It likely influenced (and still influences) the biomass valorisation scientific domain, whose publications increased significantly in the last 20 years, as depicted in Figure 1-35. Ranzi (Ranzi et al. 2008) reported that large-scale gasification and pyrolysis units require deep knowledge in phenomenology modelling for designing and simulating reactor performances, understanding how pollutants form and evolve, and choosing strategies for adequate control. As previously presented, cellulose is the most abundant component of the lignocellulosic biomass. It was chosen as the primary powder sample to study the physical-chemical mechanisms involved during organic dust explosions, as presented in the next chapters. Since the pyrolysis step plays a vital role in this work, cellulose pyrolysis will be one of the main focuses of the following sections and chapters. A general presentation of lignin and hemicellulose pyrolysis will be nonetheless given. A concluding section on lignocellulosic biomass is presented.

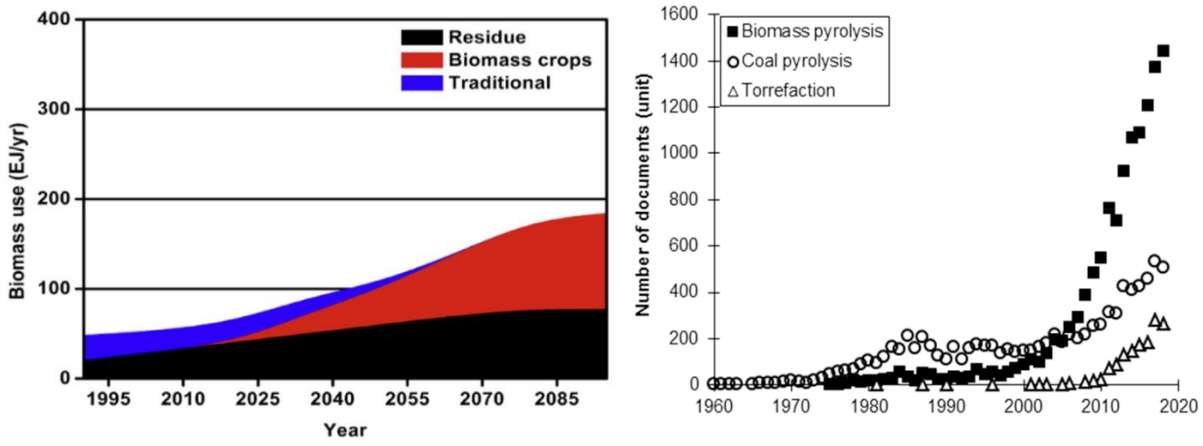

Figure 1-35 – To the left, the biomass use for energy production; to the right, the number of scientific documents focused on biomass, coal pyrolysis and torrefaction (from (Gouws et al. 2021; Sikarwar et al. 2017))

4.4.2 Cellulose pyrolysis

It is not easy to precisely identify the origin of the study of cellulose pyrolysis. However, one of the first documented goals corresponds to Pictet and Sarasin's work (Pictet and Sarasin 1918) in 1918. They isolated an unknown compound in cellulose distillation tars, which was baptized "levoglucosan". It represented the most abundant product, and it immediately caught the scientific community's attention, which widely studied its generation mechanisms.

In 1965, Broido and Kilzer (Kilzer 1965) have studied the cellulose pyrolysis process in detail, stressing out two endothermal and an exothermal processes, corresponding to the formation of tars (mainly constituted by levoglucosan), dehydrated cellulose, and char, water and permanent gases, respectively. During the 1960s and 70s, Shafizadeh focused his studies on determining the mechanisms involved in the first stage of cellulose pyrolysis and, in 1968, published a mechanism involving concurrent and consecutive reactions (Shafizadeh 1968). Following its path, in 1979, the Broido-Shafizadeh mechanism was published: it proposed a cellulose activation step necessary to allow the subsequent devolatilization reactions, paving the way for numerous future works. With the development of analytical techniques, the possibilities to better characterize gaseous and condensable products rose. In 1988, Piskorz's research team published a reaction mechanism representing the attempt to describe and predict the product distribution (Piskorz et al. 1988a). They used a fluidized bed fed with poplar wood or different celluloses. The temperature was varied between 400 and 650°C, and the gas phase residence time was kept below 1 s to reduce the secondary reactions in the gaseous phase. In 1987, Lédé (Lédé, Li, and Villermaux 1987) showed a fusion-like behaviour of the cellulose to generate a liquid intermediate, which was confirmed by Boutin (Boutin, Ferrer, and Lédé 1998) in 1998. They worked on cellulose pyrolysis using a radiative oven to produce a heat flux between 10^5 and $7 \cdot 10^6$ $W.m^{-2}$. Micro-imaging allowed identifying a yellowish liquid compound, referred to as Intermediate Liquid Compound (ILC). It is constituted by levoglucosan and other anhydrous-saccharides with polymerization degrees between 2 and 7 (Le Brech 2015). Table 1-9 resumes some of the cellulose pyrolysis mechanisms proposed in the scientific literature.

Table 1-9 - Various cellulose pyrolysis mechanisms over the years (adapted from (Le Brech 2015))

Mechanism	Reactions	Observations
Broido and Kilzer (1965)	Cellulose → Tars	280 – 340°C, Endothermic
	Cellulose → Dehydrated cellulose	200 – 280°C, Endothermic
	Dehydrated cellulose → Char, CO, CO_2, H_2O, etc.	Exothermic
Broido and Shafizadeh (1979)	Cellulose → Active cellulose	No phase change
	Active cellulose → Char, gaseous products	-
	Active cellulose → Tars	-
Diebold (1980)	Cellulose → Active cellulose	Chain breaking
	Cellulose → Char, H_2O, gaseous products	-
	Active cellulose → Primary vapours	-
	Active cellulose → Gaseous products	-
	Active cellulose → Char, H_2O, gaseous products	-
	Primary vapours → Secondary vapours, gaseous products	-
	Cellulose → Depolymerized cellulose	> 450°C, Rapid heating

Waterloo (1988)	Cellulose → Char, H_2O, gaseous products	< 300°C, Slow heating
	Depolymerized cellulose → Anhydro-saccharides	Depolymerisation
	Depolymerized cellulose → Glyoxal, acetol, formic acid, etc.	Fragmentation, decarboxylation
Banyasz (2001)	Cellulose → Depolymerized cellulose	Depolymerization
	Cellulose → Dehydrated cellulose	Dehydration
	Dehydrated cellulose → Char	-
	Depolymerized cellulose → Tars, CO_2, char	-
	Depolymerized cellulose → Intermediate	High temperatures
	Intermediate → Hydroxyacetaldehyde	-
	Intermediate → Formaldehyde, CO	-
Wang and Garcia-Perez (2013)	Cellulose → Intermediate	-
	Intermediate → Levoglucosan, cellobiosan	-
	Intermediate → Dehydrated cellulose, H_2O	-
	Dehydrated cellulose → Condensed cellulose	-
	Condensed cellulose → Char	-

Condensed cellulose → Vapours	-
Condensed cellulose → CO, CO_2, H_2O	-

4.4.3 Hemicellulose pyrolysis

As previously discussed, hemicelluloses constitute a family of diverse molecules forming an intricate and branched structure in lignocellulosic biomass. As assessed in Le Brech (Le Brech 2015), this diversity generally determines a higher complexity associated with studying its thermal degradation. Moreover, their extraction sensibly alters their structure, which leads to molecules that represent less accurately the native hemicellulose in the lignocellulosic biomass. However, it is fundamental to include knowledge about the thermal degradation of the hemicelluloses in the study of biomass pyrolysis. Their decomposition typically starts at approximately 200°C and ends at 350°C (Le Brech 2015). Furthermore, the chemical bonds in the hemicellulose structure differ from those in the cellulose, which influences the thermal stability and, thus, the degradation temperature. At temperatures between 150 and 250°C, hemicelluloses are involved in dehydration and fragmentation reactions (Collard and Blin 2014; Shen, Gu, and Bridgwater 2010), producing principally formic acid, acetic acid and methanol. When the temperature rises and reaches 250-350°C, furfurals, levoglucosan and levogalactosan represent the most abundant species among the products (Hosoya, Kawamoto, and Saka 2007). For temperatures above 350°C, methane and methylphenols are detected (Jensen et al. 1998).

4.4.4 Lignin pyrolysis

Lignin thermal degradation occurs between 150 and 500°C (Yang et al. 2007). This broader range than cellulose and hemicelluloses is due to the high variability of its chemical bonds. Furthermore, in a similar way to hemicelluloses, its structure is impacted by the extraction methods. Lignin pyrolysis results thus in a complex phenomenon. At low temperatures (150-300°C), the modifications are focused on the aliphatic oxygenated chains, with the generation of formaldehyde, water, formic acid and CO_2 (Jakab et al. 1995; Kawamoto, Horigoshi, and Saka 2007; Q. Liu et al. 2008). For higher temperatures than 300°C, the aliphatic chains are totally converted (Sharma et al. 2004). Moreover, the phenolic units volatilise, and the residue is more and more condensed. Methane and methanol are produced (Evans and Milne 1986).

4.4.5 Lignocellulosic biomass pyrolysis

Biomass pyrolysis involves numerous chemical species (Evans and Milne 1986; Garcia-Perez et al. 2007), and each species participates in several reactions; precisely determining its characteristic chemical mechanisms is, thus, far from straightforward. Nonetheless, several

attempts have been made to model this complex phenomenon. As presented in Dufour (Dufour, 2007) (see Figure 1-36), the process is constituted of three main steps: primary pyrolysis and secondary and tertiary conversion. In the first one, the solid phase volatilizes, generating permanent gases (CO, CO_2 and H_2), primary molecules (primary tars), becoming char. Then, the primary tars are involved in a secondary conversion, which produces secondary tars and lighter species (H_2O, CO, CO_2, H_2 and C_{2+}). Finally, less oxygenated tertiary tars are generated during a tertiary conversion, along with CH_4, CO, CO_2, H_2 and soot particles. The temperature and the residence time of the vapours are the key parameters that rule over the process, defining the conversion stage of the biomass. In 2008, Ranzi (Ranzi et al. 2008) proposed a kinetic mechanism to describe the pyrolysis of lignocellulosic biomass. First, a simplification was adopted to reduce the complexity level of the system: independent pyrolysis of cellulose, hemicellulose and lignin are considered the major phenomena, and their combination is equivalent to the global. Furthermore, experimental data were selected to verify the results obtained with the model. Finally, mechanism was elaborated, revised and published in 2016 (Ranzi, Faravelli, and Manenti 2016a). Table 1-10 reports the acronyms used in the mechanism, and Table 1-11 reports the reactions that compose the mechanism. The proposed multistep model can predict the yields and the gaseous, condensable and solid products of the devolatilization of lignocellulosic biomass, considering the extractive contribution. Moreover, lumped pseudo species (G{CO}, G{CO_2}, G{H_2}, G{CH_3OH}, G{COH_2}, G{CH_4}, G{C_2H_4}) are included in the mechanism to represent the functional moieties in the condensed phase or in the solid matrix that can be released as gases, via desorption or vaporization.

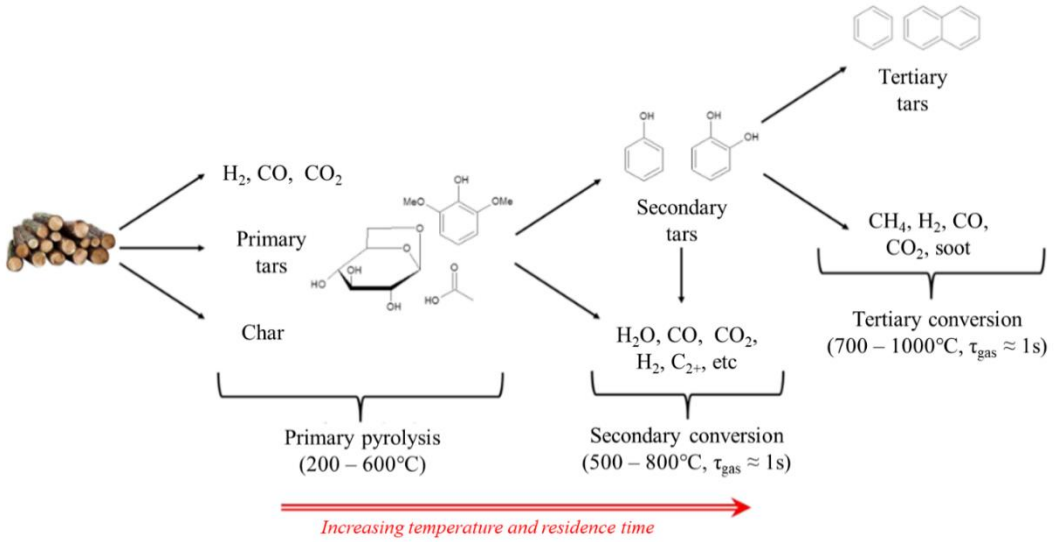

Figure 1-36 - Biomass pyrolysis mechanism (adapted from Dufour, 2007)

Table 1-10 - Acronyms of chemical species involved in the model proposed by (Ranzi et al.2017).

CELL	Cellulose
CELLA	Activated cellulose
HCE	Hemicellulose
HCE1	Hemicellulose intermediate 1
HCE2	Hemicellulose intermediate 2
GMSW	Glucomannan Softwood HCE
XYHW	Xylan Hardwood HCE
LIG	Lignin
LIG-C	Carbon-rich lignin
LIG-H	Hydrogen-rich lignin
LIG-O	Oxygen-rich lignin
LIG-CC	More carbon-rich lignin
LIG-OH	OH-rich lignin
TANN	Tannin
ITANN	3,5-dihydroxy-benzofuranone
HAA	Hydroxyacetaldehyde
GLYOX	Glyoxal
ACAC	Acetic acid
FURF	Furfural
HMFU	5-hydroxymethyl-furfural
ALD3	n-propionaldehyde
LVG	Levoglucosan
XYL	Xylose monomer
COUMARYL	Coumaryl alcohol
ACROL	Acrolein
FFA	Free fatty acid
FE2MACR	Sinapaldehyde
ACQUA	Water

Table 1-11 - Lignocellulosic biomass pyrolysis mechanism proposed by Ranzi et al. 2017.

	Reaction	A, s^{-1}	E_a, kcal.$kmol^{-1}$
Cellulose pyrolysis			
1	CELL → CELL A	$1.5 \cdot 10^{14}$	47000
2	CELL A → 0.4 HAA + 0.05 GLYOX + 0.15 CH3CHO + 0.15 CH3OH + 0.25 HMFU + 0.35 ALD3 + 0.3 CH2O + 0.36 CO2 + 0.61 CO + 0.05 H2 + 0.05 G{CH4} + 0.02 HCOOH + 0.93 H2O + 0.05 C3H6O2	$2.0 \cdot 10^{6}$	19100
3	CELL A → Levoglucosan	3.3 T	10000
4	CELL → 5 H2O + 6 Char	$6.5 \cdot 10^{7}$	31000
Hemicellulose pyrolysis			
5	GMSW → 0.70 HCE 1 + 0.30 HCE 2	$1 \cdot 10^{10}$	31000
6	XYHW → 0.35 HCE 1 + 0.65 HCE 2	$1 \cdot 10^{10}$	28500
7	HCE 1 → 0.6 XYLAN + 0.2 C3H6O2 + 0.12 GLYOX + 0.2 FURF + 0.4 H2O + 0.08 G{H2} + 0.16 CO	3 T	11000
8	HCE 1 → 0.4 H2O + 0.79 CO2 + 0.05 HCOOH + 0.69 CO + 0.01 G{CO} + 0.01 G{CO2} + 0.35 G{H2} + 0.3 CH2O + 0.9 G{COH2} + 0.625 G{CH4} + 0.375 G{C2H4} + 0.875 CHAR	$1.8 \cdot 10^{-3}$ T	3000
9	HCE 2 → 0.2 H2O + 0.275 CO + 0.275 CO2 + 0.4 CH2O + 0.1 C2H5OH + 0.05 HAA + 0.35ACAC + 0.025 HCOOH + 0.25 G{CH4} + 0.3 G{CH3OH} + 0.225 G{C2H4} + 0.4 G{CO2}+ 0.725 G{COH2}	$5 \cdot 10^{9}$	31500
Lignin pyrolysis			

10	LIG-C → 0.35 LIGCC + 0.1 COUMARYL + 0.08 PHENOL + 0.41 C2H4 + 1.0H2O + 0.7 G{COH2} + 0.3 CH2O + 0.32 CO + 0.495 G{CH4}	$1 \cdot 10^{11}$	37200
11	LIG-H → LIGOH + 0.5 ALD3 + 0.5 C2H4 + 0.2 HAA + 0.1 CO + 0.1 G{H2}	$6.7 \cdot 10^{12}$	37500
12	LIG-O → LIGOH + CO2	$3.3 \cdot 10^{8}$	25500
13	LIG-CC → 0.3 COUMARYL + 0.2 PHENOL + 0.35 HAA + 0.7 H2O + 0.65 CH4 + 0.6 C2H4 +H2 + 1.4 CO + 0.4 G{CO} + 6.75 CHAR	$1 \cdot 10^{4}$	24800
14	LIG OH → 0.9 LIG + H2O + 0.1 CH4 + 0.6 CH3OH + 0.05 G{H2} + 0.3 G{CH3OH} + 0.05 CO2 + 0.65 CO + 0.6 G{CO} + 0.05 HCOOH + 0.85 G{COH2} + 0.35 G{CH4} + 0.2 G{C2H4} + 4.25 CHAR	$1 \cdot 10^{8}$	30000
15	LIG → 0.7 FE2MACR + 0.3 ANISOLE + 0.3 CO + 0.3 G{CO} + 0.3 CH3CHO	4 T	12000
16	LIG → 0.6 H2O + 0.4 CO + 0.2 CH4 + 0.4 CH2O + 0.2 G{CO} + 0.4 G{CH4} + 0.5 G{C2H4} + 0.4 G{CH3OH} + 2 G{COH2} + 6 CHAR	$8.3 \cdot 10^{-2}$ T	8000
17	LIG → 0.6 H2O + 2.6 CO + 1.1 CH4 + 0.4 CH2O+C2H4 + 0.4 CH3OH	$1 \cdot 10^{7}$	8000
Extractives pyrolysis			
18	TGL → ACRO + 3 FFA	$7 \cdot 10^{12}$	45700
19	TANN → 0.85 PHENOL + 0.15 G{PHENOL} + G{CO} + H2O + ITANN	20	10000
20	ITANN → 5 CHAR + 2 CO + H2O + G{COH2}	$1 \cdot 10^{3}$	25000
Metaplastic			
21	G{CO2} → CO2	$1 \cdot 10^{6}$	24000
22	G{CO} → CO	$5 \cdot 10^{12}$	50000
23	G{COH2} → CO+H2	$1.5 \cdot 10^{12}$	71000

24	G{H2} → H2	$5 \cdot 10^{11}$	75000
25	G{CH4} → CH4	$5 \cdot 10^{12}$	71500
26	G{CH3OH} → CH3OH	$2 \cdot 10^{12}$	50000
27	G{C2H4} → C2H4	$5 \cdot 10^{12}$	71500
28	G{PHENOL} → PHENOL	$1.5 \cdot 10^{12}$	71000
Water evaporation			
29	ACQUA → H2O	1 T	8000

5. Biomass dust explosions

As presented in Section 1.1.3, explosion accidents that involve lignocellulosic biomass are frequent and can lead to disastrous scenarios. Considering then the increasingly important role of bioenergy in the energy transition, briefly seen in Sections 1.4.1 and 1.4.4, to better understand biomass dust explosions seem to be a non-negligible key for preventing a significant sector of industrial accidents from occurring. To include all the parameters previously presented in this chapter in the study of biomass dust explosions is beyond challenging, and it might represent an obstacle to accurately representing reality. As initially introduced, this work will be focused on merging an experimental and a theoretical approach, trying to predict the most representative parameters of a dust explosion. From a phenomenological point of view, a dust explosion is a fast combustion process associated with a time scale of approximately 100 ms. Therefore, a simplification is necessary to analyse such a transient, fast, complex, and dynamic system. In this work, as exposed in the previous sections, the pyrolysis step was chosen to be compared to the others by comparing the associated time scales. One of the main problems is the range of applicability of the pyrolysis mechanisms proposed in the literature. Although several works can be compared to the operating conditions typical of dust explosions (dispersion step, presence of a dust cloud, rapid heating, very short time scale), such as Boutin (Boutin et al. 1998), Piskorz (Piskorz et al. 2000a), Boutin (Boutin, Ferrer, and Lédé 2002a) and Luo (Luo et al. 2004), literature does not offer any work that respect them all. To model a biomass dust explosion using experimental apparatuses capable of reproducing its typical features means thus intrinsically including them in the experimental results and, secondarily, in the model results. As underlined by Ranzi (Ranzi et al. 2016a), other than the reactor temperature, the pyrolysis of lignocellulosic biomass particles strictly depends on the conversion degree of each one. When such a material is reduced to powder form, it must be associated with a particle size distribution. Finer and coarser particles respond differently to the operating conditions in a thermal conversion, primarily when associated with short residence times. It then determines a range of particle temperature conversion degrees, which consequently determines a range of products. In Figure 1-37, upper and lower limits of each product fraction zone represent the results considering the variability associated to the presence of fine and coarse particles.

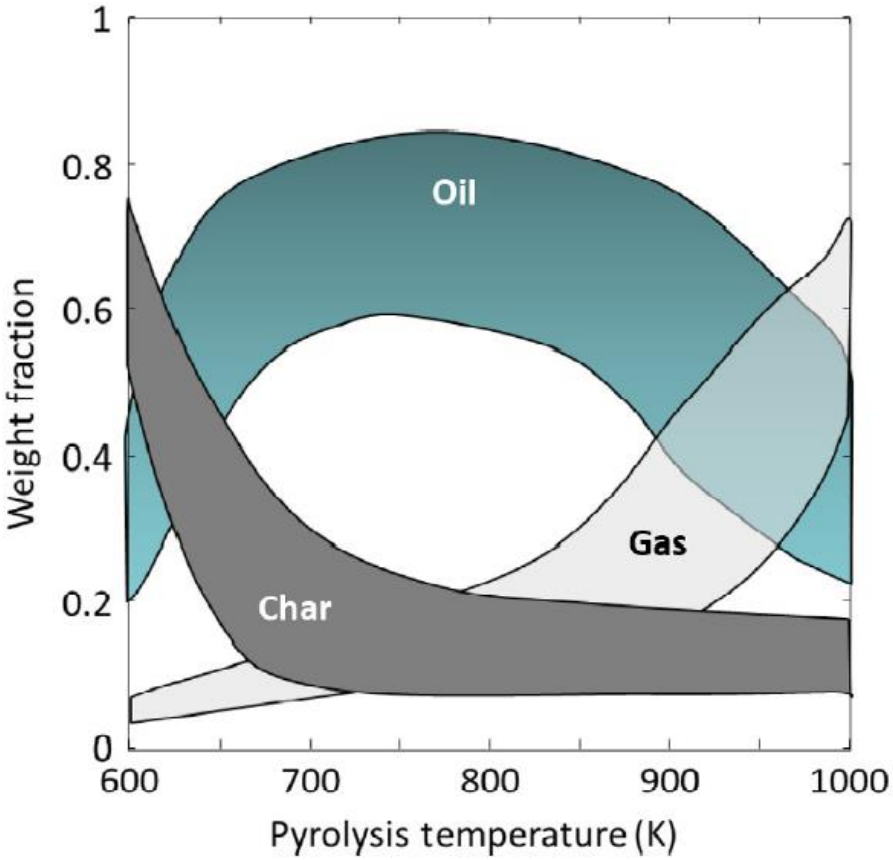

Figure 1-37 - Predicted yields of condensable, gaseous and solid product from fast pyrolysis of biomass (from Ranzi et al. 2016a)

6. Conclusions

In this first chapter, the complexity of studying organic dust explosions was depicted via the definition and analysis of the main parameters that define the inflammability and explosibility of an organic powder. Furthermore, the nature of the powder, its particle size distribution and the composition of the gaseous phase forming the dust cloud were described as the intrinsic features influencing the explosion risk, while the characteristics of the external environment positively or negatively interact with the dust cloud. Focusing on lignocellulosic biomass powder opens the horizons to enriching an increasingly attractive industrial domain. However, this organic matrix increases the system's complexity by increasing the number of chemical reactions involved in this ultra-fast oxidation process.

References

Abbas, Zaheer, Dieter Gabel, Arne Krietsch, and Ulrich Krause. 2022. 'Quasi-Static Dispersion of Dusts for the Determination of Lower Explosion Limits of Hybrid Mixtures'. *Journal of Loss Prevention in the Process Industries* 74:104640. doi: 10.1016/j.jlp.2021.104640.

Abbas, Zaheer, Ronald Zinke, Dieter Gabel, Emmanuel Kwasi Addai, Ardalan Fakhr Darbanan, and Ulrich Krause. 2019. 'Theoretical Evaluation of Lower Explosion Limit of Hybrid Mixtures'. *Journal of Loss Prevention in the Process Industries* 60:296–302. doi: 10.1016/j.jlp.2019.05.014.

A.Brzustowski, Thomas, and Irvin Glassman. 1964. 'Spectroscopic Investigation of Metal Combustion'. *Progress in Astronautics and Rocketry* 15:41–73. doi: https://doi.org/10.1016/B978-1-4832-2730-6.50008-7.

Ackroyd, Graham, Mike Bailey, and Robert Mullins. 2011. 'The Effect of Reduced Oxygen Levels on the Electrostatic Ignition Sensitivity of Dusts'. *Journal of Physics: Conference Series* 301:012034. doi: 10.1088/1742-6596/301/1/012034.

Addai, Emmanuel Kwasi, Martin Clouthier, Paul Amyotte, Muddasar Safdar, and Ulrich Krause. 2019. 'Experimental Investigation of Limiting Oxygen Concentration of Hybrid Mixtures'. *Journal of Loss Prevention in the Process Industries* 57:120–30. doi: 10.1016/j.jlp.2018.11.016.

Addai, Emmanuel Kwasi, Dieter Gabel, and Ulrich Krause. 2015. 'Explosion Characteristics of Three Component Hybrid Mixtures'. *Process Safety and Environmental Protection* 98:72–81. doi: 10.1016/j.psep.2015.06.013.

Addai, Emmanuel Kwasi, Dieter Gabel, and Ulrich Krause. 2016. 'Models to Estimate the Minimum Ignition Temperature of Dusts and Hybrid Mixtures'. *Journal of Hazardous Materials* 304:73–83. doi: 10.1016/j.jhazmat.2015.10.015.

Altwal, Jack M., and Luc N. Véchot. 2021. 'Experimental Study of the Influence of Particle Size on Minimum Explosible Concentration of Sulfur Dust'. *Journal of Loss Prevention in the Process Industries* 71:104507. doi: 10.1016/j.jlp.2021.104507.

Arshad, Ushtar, Syed Ali Ammar Taqvi, and Azizul Buang. 2021. 'Modelling of the Minimum Ignition Temperature (MIT) of Corn Dust Using Statistical Analysis and Artificial Neural Networks Based on the Synergistic Effect of Concentration and Dispersion Pressure'. *Process Safety and Environmental Protection* 147:742–55. doi: 10.1016/j.psep.2020.12.040.

Azam, Sikandar, and Devi Prasad Mishra. 2019. 'Effects of Particle Size, Dust Concentration and Dust-Dispersion-Air Pressure on Rock Dust Inertant Requirement for Coal Dust Explosion Suppression in Underground Coal Mines'. *Process Safety and Environmental Protection* 126:35–43. doi: 10.1016/j.psep.2019.03.030.

Bagaria, Pranav, Jiaqi Zhang, Entao Yang, Ashok Dastidar, and Chad Mashuga. 2016. 'Effect of Dust Dispersion on Particle Integrity and Explosion Hazards'. *Journal of Loss Prevention in the Process Industries* 44:424–32. doi: 10.1016/j.jlp.2016.11.001.

Bartknecht, W. 1971. *Brenngas- Und Staubexplosionen. Forschungsbereicht F45*. Koblenz: Bundesinstitut fiir Arbeitsschutz.

Barud, H. S., C. A. Ribeiro, Marisa S. Crespi, M. A. U. Martines, J. Dexpert-Ghys, R. F. C. Marques, Y. Messaddeq, and S. J. L. Ribeiro. 2007. 'Thermal Characterization of Bacterial Cellulose–

Phosphate Composite Membranes'. *Journal of Thermal Analysis and Calorimetry* 87(3):815–18. doi: 10.1007/s10973-006-8170-5.

Bazyn, Tim, Herman Krier, and Nick Glumac. 2007. 'Evidence for the Transition from the Diffusion-Limit in Aluminum Particle Combustion'. *Proceedings of the Combustion Institute* 31(2):2021–28. doi: 10.1016/j.proci.2006.07.161.

Becker, Judith, and Christoph Wittmann. 2019. 'A Field of Dreams: Lignin Valorization into Chemicals, Materials, Fuels, and Health-Care Products'. *Biotechnology Advances* 37(6):107360. doi: 10.1016/j.biotechadv.2019.02.016.

Benaimeche, Oussama, Nadhir Toubal Seghir, Łukasz Sadowski, and Mekki Mellas. 2020. 'The Utilization of Vegetable Fibers in Cementitious Materials'. Pp. 649–62 in *Encyclopedia of Renewable and Sustainable Materials*. Elsevier.

Bielawski, Jakub. 2020. 'Fire and Explosion Hazards Associated with Electrostatic Powder Coating'. *Zeszyty Naukowe SGSP* 75:23–36. doi: 10.5604/01.3001.0014.4266.

Blazquez, Estibaliz, and Chris Thorn. 2010. 'Fires and Explosions'. *Anaesthesia & Intensive Care Medicine* 11(11):455–57. doi: 10.1016/j.mpaic.2010.08.007.

Boutin, O., M. Ferrer, and J. Lédé. 1998. 'Radiant Flash Pyrolysis of Cellulose—Evidence for the Formation of Short Life Time Intermediate Liquid Species'. *Journal of Analytical and Applied Pyrolysis* 47(1):13–31. doi: 10.1016/S0165-2370(98)00088-6.

Boutin, Olivier, Monique Ferrer, and Jacques Lédé. 2002. 'Flash Pyrolysis of Cellulose Pellets Submitted to a Concentrated Radiation: Experiments and Modelling'. *Chemical Engineering Science* 57(1):15–25. doi: 10.1016/S0009-2509(01)00360-8.

Bridgwater, A. V. n.d. 'The Future for Biomass Pyrolysis and Gasification: Status, Opportunities and Policies for Europe'. 30.

Cassoni, Ana C., Inês Mota, Patrícia Costa, Marta W. Vasconcelos, and Manuela Pintado. 2022. 'Effect of Alkaline and Deep Eutectic Solvents Pretreatments on the Recovery of Lignin with Antioxidant Activity from Grape Stalks'. *International Journal of Biological Macromolecules* 220:406–14. doi: 10.1016/j.ijbiomac.2022.07.233.

Chaudhari, Purvali, Bharatvaaj Ravi, Pranav Bagaria, and Chad Mashuga. 2019. 'Improved Partial Inerting MIE Test Method for Combustible Dusts and Its CFD Validation'. *Process Safety and Environmental Protection* 122:192–99. doi: 10.1016/j.psep.2018.12.009.

Chen, Dongmei, and Yagyavalk Bhatt. 2019. *The Impacts of Industrialization on Freight Movement in China*. King Abdullah Petroleum Studies and Research Center. doi: 10.30573/KS--2019-DP57.

Cheng, Fangming, Zhuchuan Chang, Zhenmin Luo, Changchun Liu, Haitao Li, and Tao Wang. 2020. 'Numerical Study on Premixing Characteristics and Explosion Process of Starch in a Vertical Pipe under Turbulent Flow'. *Journal of Loss Prevention in the Process Industries* 68:104303. doi: 10.1016/j.jlp.2020.104303.

Cloney, Chris. 2020. *2020-Mid-Year-Combustible-Dust-Incident-Report-v5.Pdf*. Dust Safety Science.

Collard, François-Xavier, and Joël Blin. 2014. 'A Review on Pyrolysis of Biomass Constituents: Mechanisms and Composition of the Products Obtained from the Conversion of Cellulose, Hemicelluloses and Lignin'. *Renewable & Sustainable Energy Reviews* 38:594–608. doi: 10.1016/j.rser.2014.06.013.

Committee of Experts on the Transport of Dangerous Goods and on the Globally Harmonized System of Classification and Labelling of Chemicals. 2012. *Dust Explosion Hazards Guidance*. Item 2(a) of Provisional agenda. Geneva, Switzerland.

Copelli, Sabrina, Marco Barozzi, Martina Silvia Scotton, Anna Fumagalli, Marco Derudi, and Renato Rota. 2019. 'A Predictive Model for the Estimation of the Deflagration Index of Organic Dusts'. *Process Safety and Environmental Protection* 126:329–38. doi: 10.1016/j.psep.2019.04.012.

Cuervo Rodriguez, Nicolas. 2018. 'Influences of Turbulence and Combustion Regimes on Explosions of Gas-Dust Hydrid Mixtures'.

Danzi, Enrico, Franco Franchini, Olivier Dufaud, Matteo Pietraccini, and Luca Marmo. 2021. 'Investigation of the Fluid Dynamic of the Modified Hartmann Tube Equipment by High-Speed Video Processing'. *Chemical Engineering Transactions* 86:367–72. doi: 10.3303/CET2186062.

Demoll, Reinhard. 1927. *Betrachtungen Über Produktionsberechnungen*. 18.

Di Benedetto, A., and P. Russo. 2007. 'Thermo-Kinetic Modelling of Dust Explosions'. *Journal of Loss Prevention in the Process Industries* 20(4–6):303–9. doi: 10.1016/j.jlp.2007.04.001.

Di Benedetto, A., P. Russo, P. Amyotte, and N. Marchand. 2010. 'Modelling the Effect of Particle Size on Dust Explosions'. *Chemical Engineering Science* 65(2):772–79. doi: 10.1016/j.ces.2009.09.029.

Dimensions. n.d. 'App.Dimensions.Ai/Discover/Publication'. Retrieved (https://app.dimensions.ai/discover/publication).

Dufaud, O., L. Perrin, M. Traore, S. Chazelet, and D. Thomas. 2009. 'Explosions of Vapour/Dust Hybrid Mixtures: A Particular Class'. *Powder Technology* 190(1–2):269–73. doi: 10.1016/j.powtec.2008.04.046.

Dufaud, O., M. Traoré, L. Perrin, S. Chazelet, and D. Thomas. 2010. 'Experimental Investigation and Modelling of Aluminum Dusts Explosions in the 20 L Sphere'. *Journal of Loss Prevention in the Process Industries* 23(2):226–36. doi: 10.1016/j.jlp.2009.07.019.

Dufaud, Olivier, Laurent Perrin, and Mamadou Traore. 2008. 'Dust/Vapour Explosions: Hybrid Behaviours?' *Journal of Loss Prevention in the Process Industries* 4.

Dufour, Anthony. 2007. 'Optimisation de la production d'hydrogène par conversion du méthane dans les procédés de pyrolyse/gazéification de la biomasse'.

Eckhoff, Rolf K. 2003. 'Assessment of Ignitability, Explosibility, and Related Properties of Dusts by Laboratory-Scale Tests'. Pp. 473–548 in *Dust Explosions in the Process Industries*. Elsevier.

Eckhoff, Rolf K. 2003. *Dust Explosions in the Process Industries*. 3rd edition. Elsevier.

Eckhoff, Rolf K. 2019a. 'Measurement of Minimum Ignition Energies (MIEs) of Dust Clouds – History, Present, Future'. *Journal of Loss Prevention in the Process Industries* 61:147–59. doi: 10.1016/j.jlp.2019.05.001.

Eckhoff, Rolf K. 2019b. 'Origin and Development of the Godbert-Greenwald Furnace for Measuring Minimum Ignition Temperatures of Dust Clouds'. *Process Safety and Environmental Protection* 129:17–24. doi: 10.1016/j.psep.2019.06.012.

Eckhoff, Rolf K. n.d. 'Use of (DP/Dt)Max from Closed-Bomb Tests for Predicting Violence of Accidental Dust Explosions in Industrial Plants'. 10.

Edomah, Norbert. 2018. 'Economics of Energy Supply'. P. B9780124095489116000 in *Reference Module in Earth Systems and Environmental Sciences*. Elsevier.

EN 14034-1. 2004. *Determination of Explosion Characteristics of Dust Clouds - Part 1: Determination of the Maximum Explosion Pressure Pmax of Dust Clouds*.

EN 14034-2. 2006. *Determination of Explosion Characteristics of Dust Clouds - Part 2: Determination of the Maximum Rate of Explosion Pressure Rise (Dp/Dt)Max of Dust Clouds*.

EN 14034-3. 2006. *Determination of Explosion Characteristics of Dust Clouds - Part 3: Determination of the Lower Explosion Limit LEL of Dust Clouds*.

Evans, Robert J., and Thomas A. Milne. n.d. 'Molecular Characterization of the Pyrolysis of Biomass'. *Pyrolysis of Biomass* 15.

F. E. L. 1878. 'Explosive Dust'. *Nature*, February.

Garcia-Agreda, A., A. Di Benedetto, P. Russo, E. Salzano, and R. Sanchirico. 2011. 'Dust/Gas Mixtures Explosion Regimes'. *Powder Technology* 205(1–3):81–86. doi: 10.1016/j.powtec.2010.08.069.

Garcia-Perez, M., A. Chaala, H. Pakdel, D. Kretschmer, and C. Roy. 2007. 'Characterization of Bio-Oils in Chemical Families'. *Biomass and Bioenergy* 31(4):222–42. doi: 10.1016/j.biombioe.2006.02.006.

Godbert, A. L. 1952. *Standard Apparatus for Determining the Inflammability of Coal Dusts and Mine Dusts*. Research Report 58. Safety in Mines Reasearch Establishment (British).

Godbert, A. L., and H. P. Greenwald. 1935. *Effect of Fineness of Coal and Inert Dusts on the Inflammability of Coal Dusts*. Washington, US: United States Department of the Interior - Bureau of mines.

Gouws, S. M., M. Carrier, J. R. Bunt, and H. W. J. P. Neomagus. 2021. 'Co-Pyrolysis of Coal and Raw/Torrefied Biomass: A Review on Chemistry, Kinetics and Implementation'. *Renewable and Sustainable Energy Reviews* 135:110189. doi: 10.1016/j.rser.2020.110189.

Guerretta, Federico, Giuliana Magnacca, Flavia Franzoso, Pavlo Ivanchenko, and Roberto Nisticò. 2019. 'Sodium Alginate Conversion into Char via Pyrolysis at the Onset Temperature'. *Materials Letters* 234:339–42. doi: 10.1016/j.matlet.2018.09.127.

Hartmann, I., J. Nagy, and H. r. Brown. 1943. *Inflammability and Explosibility of Metal Powders*. 3722. US Bureau of Mines.

Hosoya, T., H. Kawamoto, and S. Saka. 2007. 'Pyrolysis Behaviors of Wood and Its Constituent Polymers at Gasification Temperature'. *Journal of Analytical and Applied Pyrolysis* 78(2):328–36. doi: 10.1016/j.jaap.2006.08.008.

IEA. 2021. *IEA Market Report Series - Renewables 2021 - Definitions and Notes*.

ISO/IEC 80079-20-2. 2016. *Explosive Atmospheres - Part 20-2: Material Characteristics - Combustible Dusts Test Methods*.

Jakab, E., O. Faix, F. Till, and T. Székely. 1995. 'Thermogravimetry/Mass Spectrometry Study of Six Lignins within the Scope of an International Round Robin Test'. *Journal of Analytical and Applied Pyrolysis* 35(2):167–79. doi: 10.1016/0165-2370(95)00907-7.

Jeguirim, Mejdi, Sophie Dorge, Angélique Loth, and Gwenaëlle Trouvé. 2010. 'Devolatilization Kinetics of Miscanthus Straw from Thermogravimetric Analysis'. *International Journal of Green Energy* 7(2):164–73. doi: 10.1080/15435071003673641.

Jensen, Anker, Kim Dam-Johansen, Marek A. Wójtowicz, and Michael A. Serio. 1998. 'TG-FTIR Study of the Influence of Potassium Chloride on Wheat Straw Pyrolysis'. *Energy & Fuels* 12(5):929–38. doi: 10.1021/ef980008i.

Julien, Philippe, Sam Whiteley, Michael Soo, Samuel Goroshin, David L. Frost, and Jeffrey M. Bergthorson. 2017. 'Flame Speed Measurements in Aluminum Suspensions Using a Counterflow Burner'. *Proceedings of the Combustion Institute* 36(2):2291–98. doi: 10.1016/j.proci.2016.06.150.

Kawamoto, H(Kyoto Univ (Japan)), S. Horigoshi, and S. Saka. 2007. 'Pyrolysis Reactions of Various Lignin Model Dimers'. *Journal of Wood Science* 53(2):168–74. doi: 10.1007/s10086-006-0834-z.

Kilzer, F. J. n.d. 'Speculations on the Nature of Cellulose Pyrolysis'. 13.

Kim, Wookyung, Satoshi Anraku, Takuma Endo, and Kwangseok Choi. 2020. 'Flammability and Flame Propagation of Propane/L-Leucine Powder Hybrid Mixtures'. *Powder Technology* 372:694–702. doi: 10.1016/j.powtec.2020.05.107.

Klippel, Alexander, Martin Schmidt, Olaf Muecke, and Ulrich Krause. 2014. 'Dust Concentration Measurements during Filling of a Silo and CFD Modeling of Filling Processes Regarding Exceeding the Lower Explosion Limit'. *Journal of Loss Prevention in the Process Industries* 29:122–37. doi: 10.1016/j.jlp.2014.02.006.

Krause, U., D. Weinart, and P. Wöhrn. 1992. 'Rechnerische Und Graphische Bestimmung Der Sauerstoffgrenzkonzentration Explosionsfähiger Staub/Luft-Gemische (Computational and Graphical Determination of the Limiting Oxygen Concentration of Explosible Dust/Air Mixtures)'. *Staub – Reinhaltung Der Luft* 52:361.

Krause, Ulrich, Emmanuel Kwasi Addai, and Dieter Gabel. 2016. 'Determination of the Limiting Oxygen Concentration of Dust/Air and Hybrid Mixtures Based on Thermochemical Properties'. doi: 10.13140/RG.2.1.4293.9127.

Kumari, Kanchan, Anshika Singh, Deepak Marathe, and Priya Pariyar. 2021. 'Agricultural Biomass as Value Chain Developers in Different Sectors'. Pp. 467–509 in *Advanced Technology for the Conversion of Waste into Fuels and Chemicals*. Elsevier.

Le Brech, Yann. 2015. 'Analyse Des Mécanismes Primaires de Pyrolyse de La Biomasse'. Université de Lorraine, Nancy.

Lede, J., Huai Li, and J. Villermaux. 1987. 'Fusion-like Behaviour of Biomass Pyrolysis'.

Li, Haitao, Xiaokun Chen, Jun Deng, Chi-Min Shu, Chia-Ho Kuo, Yongchuan Yu, and Xiangyu Hu. 2020. 'CFD Analysis and Experimental Study on the Effect of Oxygen Level, Particle Size, and Dust Concentration on the Flame Evolution Characteristics and Explosion Severity of Cornstarch Dust Cloud Deflagration in a Spherical Chamber'. *Powder Technology* 372:585–99. doi: 10.1016/j.powtec.2020.05.117.

Liu, Aihua, Jieyun Chen, Xiaofei Huang, Junjiang Lin, Xiaochun Zhang, and Wenbin Xu. 2019. 'Explosion Parameters and Combustion Kinetics of Biomass Dust'. *Bioresource Technology* 294:122168. doi: 10.1016/j.biortech.2019.122168.

Liu, Qian, Shurong Wang, Yun Zheng, Zhongyang Luo, and Kefa Cen. 2008. 'Mechanism Study of Wood Lignin Pyrolysis by Using TG–FTIR Analysis'. *Journal of Analytical and Applied Pyrolysis* 82(1):170–77. doi: 10.1016/j.jaap.2008.03.007.

Luo, Z., S. Wang, Y. Liao, and K. Cen. 2004. 'Mechanism Study of Cellulose Rapid Pyrolysis'. *Industrial & Engineering Chemistry Research* 43(18):5605–10. doi: 10.1021/ie030774z.

Marmo, Luca. 2010. 'Case Study of a Nylon Fibre Explosion: An Example of Explosion Risk in a Textile Plant'. *Journal of Loss Prevention in the Process Industries* 23(1):106–11. doi: 10.1016/j.jlp.2009.06.006.

Marmo, Luca, Roberto Sanchirico, Almerinda Di Benedetto, Valeria Di Sarli, Daniela Riccio, and Enrico Danzi. 2018. 'Study of the Explosible Properties of Textile Dusts'. *Journal of Loss Prevention in the Process Industries* 54:110–22. doi: 10.1016/j.jlp.2018.03.003.

Mittal, Manju. 2013. 'Limiting Oxygen Concentration for Coal Dusts for Explosion Hazard Analysis and Safety'. *Journal of Loss Prevention in the Process Industries* 26(6):1106–12. doi: 10.1016/j.jlp.2013.04.012.

Nagy, J., J. W. Conn, and H. C. Verakis. 1969. *Explosion Development in a Spherical Vessel*. *7279*. U.S. Bureau of Mines.

Oluoti, Kehinde Olubukola, Tobias Richards, T. R. K. Doddapaneni, and D. Kanagasabapathi. 2014. 'Evaluation of the Pyrolysis and Gasification Kinetics of Tropical Wood Biomass'. *BioResources* 9(2):2179–90. doi: 10.15376/biores.9.2.2179-2190.

Panwar, N. L., Ashish Pawar, and B. L. Salvi. 2019. 'Comprehensive Review on Production and Utilization of Biochar'. *SN Applied Sciences* 1(2):168. doi: 10.1007/s42452-019-0172-6.

Pictet A. and Sarasin J. 1918. 'Distillation of Cellulose and Starch in Vacuo'. *Helv. Chim.* Acta 1.

Pietraccini, Matteo, Enrico Danzi, Luca Marmo, Albert Addo, and Paul Amyotte. 2021. 'Effect of Particle Size Distribution, Drying and Milling Technique on Explosibility Behavior of Olive Pomace Waste'. *Journal of Loss Prevention in the Process Industries* 71:104423. doi: 10.1016/j.jlp.2021.104423.

Piskorz, J., P. Majerski, D. Radlein, A. Vladars-Usas, and D. S. Scott. 2000. 'Flash Pyrolysis of Cellulose for Production of Anhydro-Oligomers'. *Journal of Analytical and Applied Pyrolysis* 56(2):145–66. doi: 10.1016/S0165-2370(00)00089-9.

Piskorz, Jan, Desmond St. A. G. Radlein, Donald S. Scott, and Stefan Czernik. 1988. 'Liquid Products from the Fast Pyrolysis of Wood and Cellulose'. Pp. 557–71 in *Research in Thermochemical Biomass Conversion*, edited by A. V. Bridgwater and J. L. Kuester. Dordrecht: Springer Netherlands.

Purdue University. n.d. *Agricultural Dust Explosions Database*. Purdue University.

Ramírez, Álvaro, Javier García-Torrent, and Pedro J. Aguado. 2009. 'Determination of Parameters Used to Prevent Ignition of Stored Materials and to Protect against Explosions in Food Industries'. *Journal of Hazardous Materials* 168(1):115–20. doi: 10.1016/j.jhazmat.2009.02.013.

Ranzi, E., T. Faravelli, and F. Manenti. 2016. 'Pyrolysis, Gasification, and Combustion of Solid Fuels'. Pp. 1–94 in *Advances in Chemical Engineering*. Vol. 49. Elsevier.

Ranzi, E., A. Frassoldati, R. Grana, A. Cuoci, T. Faravelli, A. P. Kelley, and C. K. Law. 2012. 'Hierarchical and Comparative Kinetic Modeling of Laminar Flame Speeds of Hydrocarbon

and Oxygenated Fuels'. *Progress in Energy and Combustion Science* 38(4):468–501. doi: 10.1016/j.pecs.2012.03.004.

Ranzi, Eliseo, Alberto Cuoci, Tiziano Faravelli, Alessio Frassoldati, Gabriele Migliavacca, Sauro Pierucci, and Samuele Sommariva. 2008. 'Chemical Kinetics of Biomass Pyrolysis'. *Energy & Fuels* 22(6):4292–4300. doi: 10.1021/ef800551t.

Ranzi, Eliseo, Paulo Eduardo Amaral Debiagi, and Alessio Frassoldati. 2017. 'Mathematical Modeling of Fast Biomass Pyrolysis and Bio-Oil Formation. Note I: Kinetic Mechanism of Biomass Pyrolysis'. *ACS Sustainable Chemistry & Engineering* 5(4):2867–81. doi: 10.1021/acssuschemeng.6b03096.

Rockwell, Scott R., and Ali S. Rangwala. 2013. 'Modeling of Dust Air Flames'. *Fire Safety Journal* 59:22–29. doi: 10.1016/j.firesaf.2013.03.006.

Royal Academy of Science. 1788. *Mémoires de l'Académie Royale Des Sciences à Turin. Mémoire*. Turin, Italy.

Ruiz, P., W. Nijs, D. Tarvydas, A. Sgobbi, A. Zucker, R. Pilli, R. Jonsson, A. Camia, C. Thiel, C. Hoyer-Klick, F. Dalla Longa, T. Kober, J. Badger, P. Volker, B. S. Elbersen, A. Brosowski, and D. Thrän. 2019. 'ENSPRESO - an Open, EU-28 Wide, Transparent and Coherent Database of Wind, Solar and Biomass Energy Potentials'. *Energy Strategy Reviews* 26:100379. doi: 10.1016/j.esr.2019.100379.

Salatino, Piero, Almerinda Di Benedetto, Riccardo Chirone, Ernesto Salzano, and Roberto Sanchirico. 2012. 'Analysis of an Explosion in a Wool-Processing Plant'. *Industrial & Engineering Chemistry Research* 51(22):7713–18. doi: 10.1021/ie2023614.

Serrano, Luis, Juan Antonio Cecilia, Cristina García-Sancho, and Araceli García. 2019. 'Lignin Depolymerization to BTXs'. *Topics in Current Chemistry* 377(5):26. doi: 10.1007/s41061-019-0251-6.

Sha, Di, Yucheng Li, Xihua Zhou, and Ruiqing Li. 2021. 'Variation of Ignition Sensitivity Characteristics of Non-Stick Coal Dust Explosions'. *International Journal of Low-Carbon Technologies* 16(1):125–34. doi: 10.1093/ijlct/ctaa046.

Shafizadeh, F. 1968. 'Pyrolysis and Combustion of Cellulosic Materials'. Pp. 419–74 in *Advances in Carbohydrate Chemistry*. Vol. 23. Elsevier.

Sharma, Ramesh K., Jan B. Wooten, Vicki L. Baliga, Xuehao Lin, W. Geoffrey Chan, and Mohammad R. Hajaligol. 2004. 'Characterization of Chars from Pyrolysis of Lignin'. *Fuel (Guildford)* 83(11):1469–82. doi: 10.1016/j.fuel.2003.11.015.

Sheehan, M., E. Antunes, B. Seligmann, and C. Weight. 2022. 'The Influence of Moisture Content on Dust Generation in Falling Curtains of Sugarcane Bagasse Fiber'. *Powder Technology* 397:117001. doi: 10.1016/j.powtec.2021.11.045.

Shen, D. K., S. Gu, and A. V. Bridgwater. 2010. 'Study on the Pyrolytic Behaviour of Xylan-Based Hemicellulose Using TG–FTIR and Py–GC–FTIR'. *Journal of Analytical and Applied Pyrolysis* 87(2):199–206. doi: 10.1016/j.jaap.2009.12.001.

Sikarwar, Vineet Singh, Ming Zhao, Paul S. Fennell, Nilay Shah, and Edward J. Anthony. 2017. 'Progress in Biofuel Production from Gasification'. *Progress in Energy and Combustion Science* 61:189–248. doi: 10.1016/j.pecs.2017.04.001.

Siwek, R. 1977. ‘20L Laborapparatur ftir die Bestimmung der ExplosionskenngrSssen brennbarer Staube’. Technikum Winterthur, Technikum Winterthur.

Siwek, Richard. 1996. ‘Determination of Technical Safety Indices and Factors Influencing Hazard Evaluation of Dusts’. *Journal of Loss Prevention in the Process Industries* 9(1):21–31. doi: 10.1016/0950-4230(95)00057-7.

Siwek, Richard, and Christoph Cesana. 1995. ‘Ignition Behavior of Dusts: Meaning and Interpretation’. *Process Safety Progress* 14(2):107–19. doi: 10.1002/prs.680140205.

Skjold, Trygve. 2018. ‘Dust Explosion Modeling: Status and Prospects’. *Particulate Science and Technology* 36(4):489–500. doi: 10.1080/02726351.2017.1389790.

Skjold, Trygve. 2022.‘Dust Explosion Modelling: Challenges and Limitations’. Presented at the DUST EXPLOSION SAFETY FOR THE PROCESS INDUSTRY Online workshop organised by RISE, January 21, Online edition.

Smil, Vaclav. n.d. *Energy Transitions: Global and National Perspectives*. 2nd ed. Praeger.

Tascón, Alberto. 2018. ‘Influence of Particle Size Distribution Skewness on Dust Explosibility’. *Powder Technology* 338:438–45. doi: 10.1016/j.powtec.2018.07.044.

Wang, Chao, Binlin Dou, Yongchen Song, Haisheng Chen, Mingjun Yang, and Yujie Xu. 2014. ‘Kinetic Study on Non-Isothermal Pyrolysis of Sucrose Biomass’. *Energy & Fuels* 28(6):3793–3801. doi: 10.1021/ef500940q.

Wu, Dejian, Arne Krietsch, Martin Schmidt, and Ulrich Krause. 2022. ‘Effect of Oxygen Concentration, Inert Gas and CH4/H2 Addition on the Minimum Ignition Energy of Coal Dusts’. *Journal of Loss Prevention in the Process Industries* 77. doi: https://doi.org/10.1016/j.jlp.2022.104772.

Yang, Haiping, Rong Yan, Hanping Chen, Dong Ho Lee, and Chuguang Zheng. 2007. ‘Characteristics of Hemicellulose, Cellulose and Lignin Pyrolysis’. *Fuel (Guildford)* 86(12):1781–88. doi: 10.1016/j.fuel.2006.12.013.

Yankov, Dragomir. 2022. ‘Fermentative Lactic Acid Production From Lignocellulosic Feedstocks: From Source to Purified Product’. *Frontiers in Chemistry* 10:823005. doi: 10.3389/fchem.2022.823005.

Yetter, Richard A., Grant A. Risha, and Steven F. Son. 2009. ‘Metal Particle Combustion and Nanotechnology’. *Proceedings of the Combustion Institute* 32(2):1819–38. doi: 10.1016/j.proci.2008.08.013.

Yu, Hongkun, Cheng Wang, Lei Pang, Yangyang Cui, and Dongping Chen. 2019. ‘Inhibiting Effect of Coal Fly Ash on Minimum Ignition Temperature of Coal Dust Clouds’. *Journal of Loss Prevention in the Process Industries* 61:24–29. doi: 10.1016/j.jlp.2019.05.018.

Yuan, Jingjie, Wenyun Wei, Weixing Huang, Bing Du, Long Liu, and Jiahua Zhu. 2014. ‘Experimental Investigations on the Roles of Moisture in Coal Dust Explosion’. *Journal of the Taiwan Institute of Chemical Engineers* 45(5):2325–33. doi: 10.1016/j.jtice.2014.05.022.

Zhang, Linghong, Chunbao (Charles) Xu, and Pascale Champagne. 2010. ‘Overview of Recent Advances in Thermo-Chemical Conversion of Biomass’. *Energy Conversion and Management* 51(5):969–82. doi: 10.1016/j.enconman.2009.11.038.

Zhao, Peng, Xin Tan, Martin Schmidt, Aizhu Wei, Weixing Huang, Xinming Qian, and Dejian Wu. 2020. ‘Minimum Explosion Concentration of Coal Dusts in Air with Small Amount of

CH4/H2/CO under 10-KJ Ignition Energy Conditions'. *Fuel* 260:116401. doi: 10.1016/j.fuel.2019.116401.

CHAPTER 2

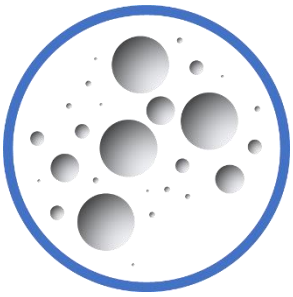

Summary

As shown in Chapter 1, particle size plays a starring role in many phenomena involved in dust explosions, and it is a primary influencing parameter. Chapter 2 studies the agglomeration and de-agglomeration tendencies of several selected organic powders when dispersed to form a dust cloud. Experiments and modelling were employed to characterise and quantify their behaviour. A setup well-known in the dust explosion research domain was adopted to perform the tests: the Godbert-Greenwald furnace. Some original modifications were also made to study the influence of the sedimentation process, to enlighten such apparatus's versatility, and to enlighten the significant influence of agglomeration and dispersion on the results obtained with the G-G furnace.

Resumé

Comme le montre le chapitre 1, la taille des particules joue un rôle déterminant dans de nombreux phénomènes liés aux explosions de poussières, et c'est un paramètre sensible essentiel qui ne peut être négligé. Le chapitre 2 étudie les tendances à l'agglomération et à la désagglomération de plusieurs poudres organiques sélectionnées lorsqu'elles sont dispersées pour former un nuage de poussière. Des expériences et la modélisation ont été utilisées pour caractériser et quantifier leur comportement. Une installation bien connue dans le domaine de la recherche sur les explosions de poussières a été adoptée pour effectuer les tests : le four Godbert-Greenwald. Des modifications originales ont également été apportées afin d'étudier l'influence du processus de sédimentation, de démontrer la polyvalence de cet appareil, et de souligner l’influence significative de l’agglomération et de la dispersion sur les résultats obtenus avec le four G-G.

A travel through space and time in the Godbert-Greenwald furnace: the evolution of a dust cloud particle size distribution

Matteo Pietraccini [1], Pierre-Alexandre Glaude [1], Anthony Dufour [1], Luca Marmo [2], Enrico Danzi [2], Olivier Dufaud[1,]*

** Corresponding author:* olivier.dufaud@univ-lorraine.fr

[1] *Université de Lorraine, CNRS, LRGP, F-54000 Nancy, France*

[2] *Politecnico di Torino, Dipartimento di Scienza Applicata e Tecnologia, Torino, Italy*

Abstract

Minimum Ignition Temperature (MIT) is a fundamental parameter for estimating the ignition sensibility of a dust cloud. However, the standard apparatuses available for its experimental determination strongly influence the final results. This work aims to assess the role of a Godbert-Greenwald furnace in the agglomeration, deagglomeration and fragmentation phenomena that occurs in the setup itself. A modified horizontal configuration was also conceived to enlighten the effect of sedimentation. Several organic powders were chosen for the study. Dispersion tests were carried out at different pulse pressure (0.1, 0.3, 0.5 and 1 barg). The average dust cloud residence time in the setup was estimated: according to the amount of powder injected and the pulse pressure, it varied from 120 to 330 ms. Entanglement was observed for coarser cellulose particles, while surface cohesion forces characterised the agglomerates of finer cellulose, glucose and ascorbic acid particles. The latter was also characterised by a strong deagglomeration and fragmentation, especially at 0.5 and 1 barg. Biot, Pyrolysis and Damköhler numbers were then used to analyse the effects of cellulose agglomeration and deagglomeration at higher temperatures. At 600K, the pyrolysis is the rate-limiting step, but from 700K, the external heat transfer becomes the rate-limiting step, which would not happen without agglomeration.

Graphical abstract

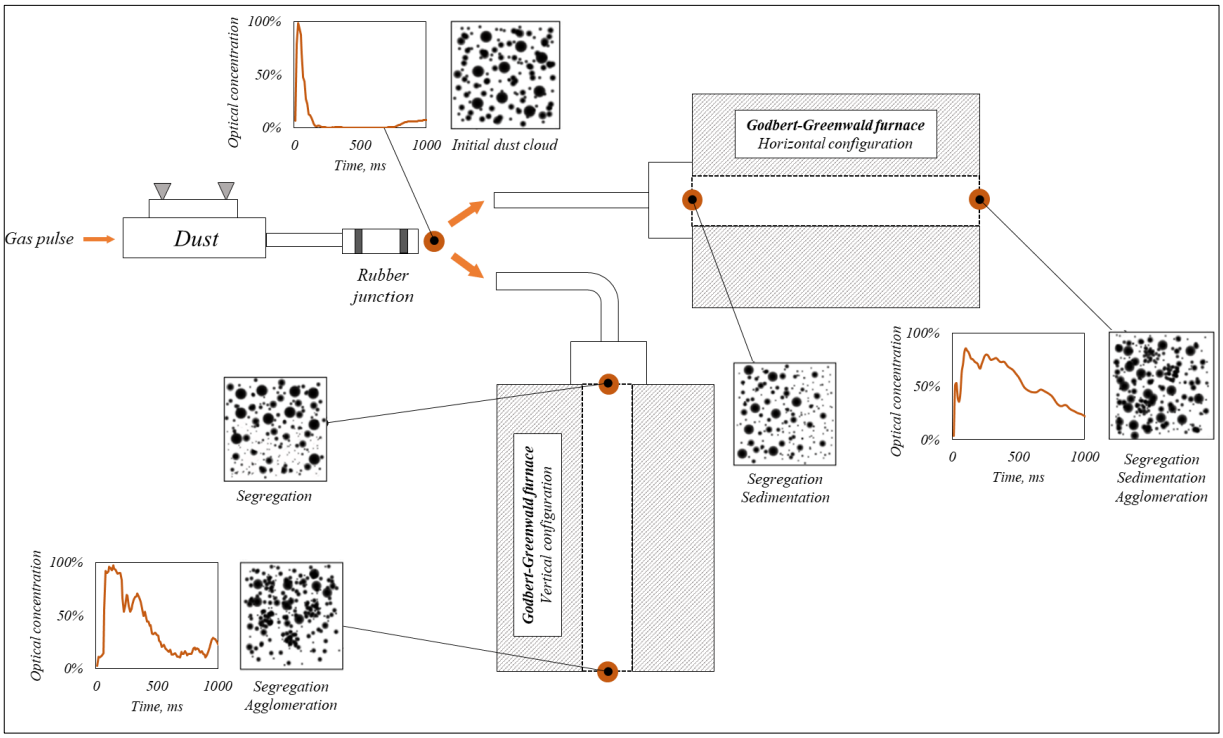

1. Introduction

Dust clouds may lead to an explosion phenomenon if an appropriate source of energy is furnished. This energy source can assume the form of electric sparks, heated surfaces, flames, mechanical friction or ember, and it must reach a minimum level of energy to trigger an actual ignition. Depending on the type of ignition source considered by the risk assessment, two parameters can be considered: Minimum Ignition Energy (MIE) and Minimum Ignition Temperature (MIT). They correspond respectively to the lowest energy of an electrical spark and the lowest temperature of a hot surface that will cause the ignition of a dust cloud and subsequent flame propagation. In their review article, Yuan (Yuan et al. 2015) showed that almost 45% of dust explosions were caused by flames or local temperature rise phenomena. Two experimental setups are currently used to determine the MIT: the Godbert-Greenwald (G-G) and the BAM oven. Both are constituted by a dust container, a gas-pulse generation system, a heated element and a controlling box. Both apparatuses share a similar experimental procedure: the temperature of the heated element is set, the powder is placed in a container, an air pulse is generated leading to a cloud of dust coming into contact with the hot surface of the

furnace. The test is considered negative if no flame is visible after a set period of time (10 seconds for BAM oven (ISO/IEC 80079-20-2 2016b)), otherwise, it is considered positive.

This short summary of the standard procedures used to determine the MIT stresses the influence of the set-up configuration and the dispersion pressure. Both operating parameters are known to lead to potential modification of the particle size distribution (PSD) of the powder, as a function of the occurrence of fragmentation or agglomeration phenomena. For instance, Sanchirico (Sanchirico et al. 2015) and Di Sarli (Di Sarli et al. 2019) highlighted the impact of the nozzle and pressure on the PSD change before and after dust dispersion in the 20L sphere. Murillo also observed fragmentation in this set-up, whereas dust agglomeration was visible in the modified Hartmann tube (Murillo 2013), confirming that the same powder, subjected to different dispersion procedures, can exhibit different behaviours. In the case of MIT determination, the main differences between the two setups are the orientation of the heated element and the dispersion procedure: in the BAM oven, the dust is blown using a rubber bulb against a metallic surface placed within the horizontal heated element; in the G-G furnace, the powder is dispersed by an air pulse (from 10 to 50 kPa - ISO/IEC 80079-20-2 standard (ISO/IEC 80079-20-2 2016b)) in a vertical heated tube. The fluid dynamics, particles-wall interactions, segregation and sedimentation phenomena involved are thus greatly different. Hence, PSD differences between both set-ups are expected, which can impact the MIT values. Few studies were dedicated to the determination of the PSD evolution during MIT determination. Bu (Bu et al. 2020) observed no particle breakage due to the dispersion in the Godbert-Greenwald furnace. However, the experimental method used was based on a comparison between the PSD of the powder before and after dispersion, collecting the powder in a beaker, which does not exclude the phenomena of fragmentation on impact at the bottom of the container or re-agglomeration before post-dispersion analysis.

In addition, the nature, shape and initial PSD of the powder can also influence the PSD, and more generally the properties – turbulence level, heterogeneity, etc – of the dust cloud. It is especially the case with fibres (Marmo et al. 2018) wet powders and nanoparticles (Eckhoff 1985), which shows significant evolution of their PSD when dispersed. Hence, the tendency of the powder to generate a dust cloud can be related to the dust cloud concentration, heterogeneity and thus, explosivity (Eckhoff 1985; Klippel et al. 2013). This ability is called “dustiness” and can be measured through standard tests, such as the rotating drum, the continuous drop or the vortex shaker (EN 17199-5 2019:17199). As demonstrated in the previous paragraph, the dustiness is not a physical property and also depends on the environmental and operating

conditions (Klippel et al. 2015). Eckhoff (Eckhoff 2013) and Bu (Bu et al. 2020) also used the concept of dispersibility, based on the work necessary to completely dispersed powder agglomerates. Marmo (Marmo et al. 2018) proposed a dustability index, notably related to the ability of a powder to generate a dust cloud in the Hartmann tube and related it to its ignition sensitivity.

Little work has been done on the evolution of the PSD during the dust dispersion in the G-G furnace and, to our knowledge, none has used a non-intrusive *in-situ* method to determine this potential evolution. This work suggests an experimental approach to investigate the space-time evolution of an organic dust cloud PSD during MIT determination in a standard G-G furnace. Both the influences of the operating conditions (dispersion pressure, heating element orientation -horizontal or vertical) and of the powder properties (initial PSD, particle nature) are studied. Furthermore, a model is proposed to study and quantify the tendency of a powder to agglomerate and deagglomerate when dispersed in the G-G furnace. The impact on the MIT is also highlighted.

2. Materials and Methods

2.1 Experimental setup

Dispersion tests were performed in both the standard and the “modified G-G furnace”, i.e. in which the cylindrical chamber was rotated by 90 degrees and connected to the dust container through a straight inox junction (Figure 2-1). This last part was realized with the exact internal dimensions as the glass elbow of the standard configuration. These two configurations will make it possible to highlight the possible influences of the elbow and the orientation of the furnace on the PSD. Each test consisted of the dispersion of 0.2 g of powder at room temperature. The gas pulse pressure varied between 0.1 and 1 bar. The first point was eventually changed to 0.2 bar if the dispersibility of the powder was too low to assure a complete dispersion of the sample placed in the dust container. Dry compressed air was used as dispersion gas. The space dependency of the dust cloud PSD was studied by performing *in-situ* analyses at different locations, chosen to enlighten the various setup-to-particle and the particle-to-particle interactions. As indicated in Figure 2-1, the "primary PSD" of the dust cloud was measured at location 1, which represents the result of the dispersion and the interaction between powder and the dust container's internal walls. At this point, it should be stressed that the dust container was designed to limit the levels difference between the rubber junction and the inner part of the

container, which improves the dispersion efficiency and limit residual powder deposits. The effects of the junction (straight or elbow) was highlighted at locations 2a and 2b. Positions 1 and 2b were then considered equivalent, which was verified for several samples. Finally, the sum of the effects of the setup on the PSD was underlined in locations 3a and 3b.

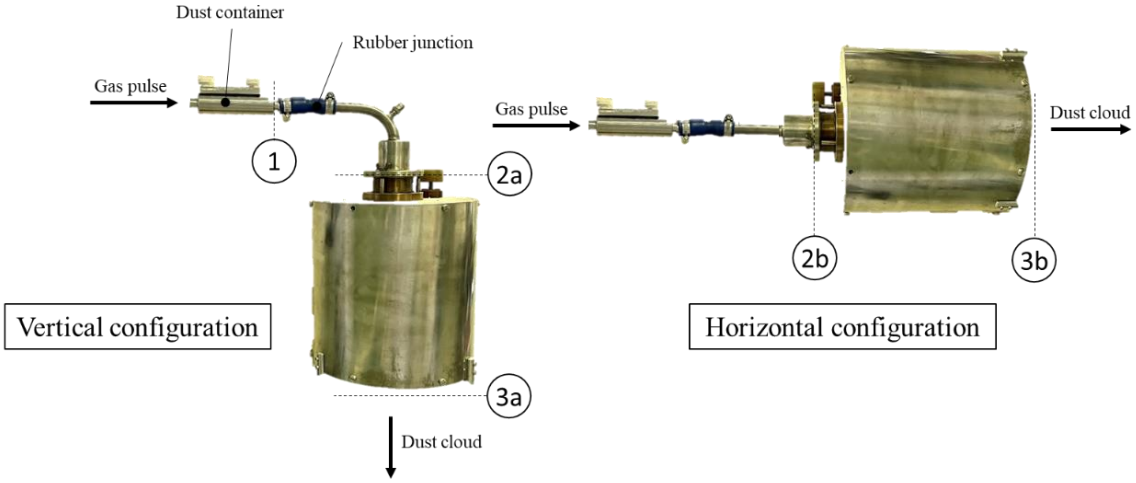

Figure 2-1 - The two configurations of the G-G furnace setup used in this work

2.2 In-situ PSD analysis

A Helos laser diffraction sensor was employed to carry out *in-situ* PSD measurements (Sympatec GmbH). The time evolution of the cloud PSD was measured at each location each 0.5 ms but the measurements were merged in 10 ms steps, for a total duration set at 1 s. This choice was made to focus on the most significant time range in terms of dust concentration and turbulence level. After this delay, the variability of the dust cloud characteristics appears to be negligible. Analyses were performed using a lens (called R5), whose measurement boundaries correspond to 0.5 and 875 µm. The signal analysis is based on the enhanced Fraunhofer Enhanced Evaluation (FREE), which is a parameter free method (i.e. the knowledge of the real and imaginary parts of the refractive index is not necessary).

2.3 Dust cloud residence time

The average residence time of the powder in the vertical chamber ($\bar{\tau}$) is crucial and necessary information to characterize the dynamics of the flow passing in the standard G-G apparatus. Due to the heterogeneity of the cloud and the complexity of the particle-particle interactions, two approaches were adopted to determine $\bar{\tau}$:

- A theoretical one, built from the Bernoulli equation applied between Location 1 and 3a, aimed to determine $\bar{\tau}$ in no-slip conditions between the gaseous and the solid phase (particles);
- An experimental one, based on high-speed videos of the powder dispersion, which allowed to consider the various interactions.

The theoretical approach was developed considering the dust cloud as if it was formed solely by a gaseous phase with no particles. Its apparent density was calculated by a weighted average between the air and the powder (here, Avicel ph 10 cellulose) as a function of the nominal dust concentration. The contribution of the solid phase to the dust cloud inertia was considered. Furthermore, the obstacles that the dust cloud encounters on its path in the G-G furnace (change of directions, narrowing and enlargement) and the dynamic friction onto the internal walls were also considered in this study.

The experimental part consisted in placing a high-speed camera (Mikrotron MotionBLITZ Eo Sens mini), set to an acquisition rate of 200 frames-per-second (fps), to record the dispersion of the powder at the entrance and the exit of the set-up. A transparent rubber junction placed at Position 1 (Figure 2-1) allowed the visualization of the dust cloud ahead from the furnace. The powder moves along the furnace in a "plug" flow whose axial dispersion increases as it approaches the exit (Figure 2-2). A mean entry time was defined as the average between the time at which the first particles passing through the transparent junction were perceptible (point A) and the time at which the last particles were visualized (point B). In the same way, a mean exit time was defined at the bottom of the furnace (points C and D). Finally, the difference between the two times gave $\bar{\tau}$. MotionBLITZ Director2 software was used for high-speed video treatment. Tests were performed with 0.2, 0.4 and 0.6 g of cellulose, varying the dispersion pressure from 1.3 to 1.8 bar. Each test was performed twice for repeatability purposes.

2.4 Minimum Ignition Temperature determination

The Minimum Ignition Temperature (MIT) of the samples was determined by following the ISO 80079-20-2 standard procedure. Dispersion pressure and PSD were varied to point out their role directly in the ignition phenomenon and thus on the MIT. As the dispersion of some powders, of larger size or density, may be incomplete at very low pressure (0.1 barg), the study did not consider this value. Instead, 0.2, 0.5 and 1 barg were selected to study the effect of a low-, intermediate- and high-pressure dispersion on the MIT.

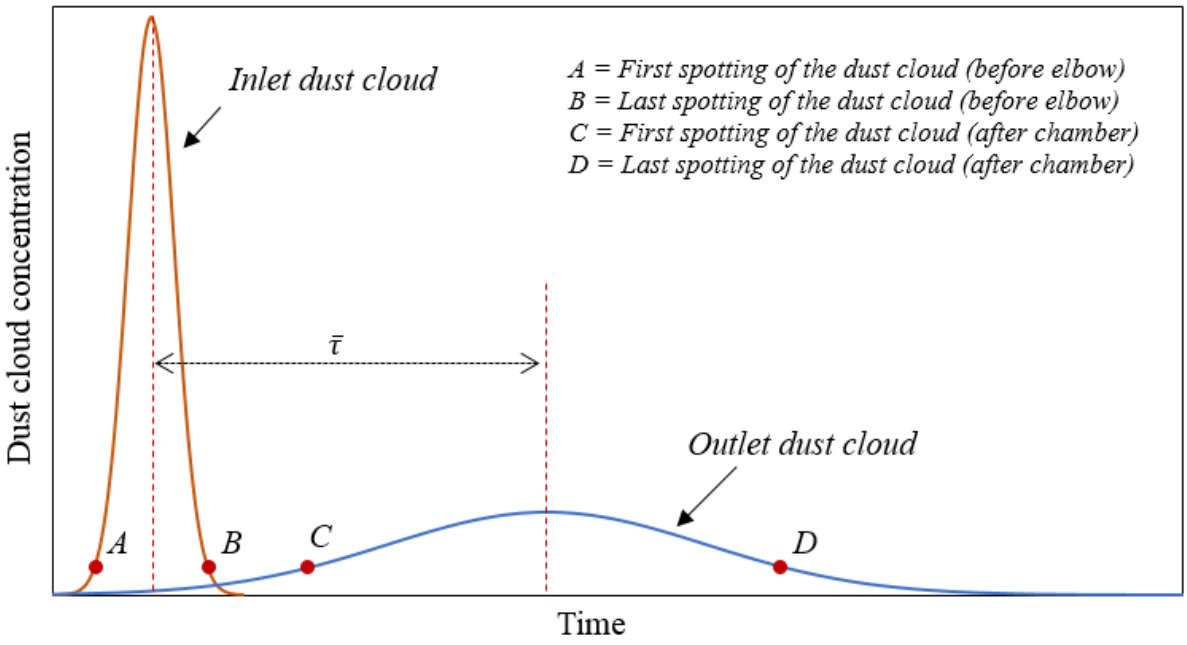

Figure 2-2 - Schematic representation of the procedure for estimating experimentally the mean dust cloud residence time in the setup

2.5 Powders

2.5.1 Choice of the samples

Nine organic powders were chosen with regard to their nature, shape and mechanical properties (brittle, hard, etc.): four microcrystalline celluloses (Avicel ph 101, 102, 105 and Vivapur 200), wheat starch, glucose, ascorbic acid and glass beads.

The four cellulose samples were chosen to focus on the sole influence of the PSD, avoiding any interference due to the different nature or shape of the powders. These four shared the same particle shape and chemical composition and differed only in their PSD. The behaviour of the cellulose was then compared to that of wheat starch, which shares the same monomer (-[$C_6H_{10}O_5$]-) but a diverse molecular structure: linear for cellulose, which translates into fibrous and more elongated particles, and branched for starch, which on the other hand leads to more spherical particles.

Due to its extensive use in the agro- and food-processing industry, its different crystalline structure and its availability on the market, glucose was also chosen to be compared to the first two biopolymers. Used in the food and pharmaceutical industries, ascorbic acid was included in the study as it was defined as very brittle (i.e. high brittleness index) by Bagaria (Bagaria et

al. 2019) in a previous study performed on closed explosion vessels. Finally, glass beads were used as a reference and calibration powder for their tendency not to form any inter-particle bond and, therefore, to represent a "non-agglomeration and non-fragmentation scenario". It should be noted that lycopodium could also have been used as a reference (Bagaria et al. 2019).

The choice of the powders was also made according to their dispersibility, which corresponds to their tendency to form an airborne cloud stable in a specific time. Bu (Bu et al. 2020a) associated it with the dustiness of a powder, and Eckhoff (Eckhoff 2003) defined it as the ratio between the efficiency of dispersion (k - ranging from 0 to 1) and the minimum work needed to break all the inter-particle bonds (W_{min}):

- k = 0 if the inter-particles interactions are strong enough to prevent the dust cloud from forming, regardless of the mechanical work applied to the powder;
- k = 1 if there is no inter-particle interaction and particles are part of the dust cloud as a single unit (no agglomerates).

It should be stressed that while the definitions of dispersability and dustiness used by the previous authors are consistent, the analytical means of determining them differ. Therefore, the dispersability defined here, does not correspond to the dustiness measured by the international standards (EN EN 15051 or EN 17199).

2.5.2 Sieving step

In addition to the raw samples, a sieving step was carried out to characterize and compare the contribution of the different fractions to the PSD modifications. 20, 56, 112 and 180 µm sieves were employed. Each fraction was subjected to the same dispersion tests as the original samples. It is well known that a sieving process can suffer from experimental interferences or limitations related to elongated particles, fibres or high agglomeration tendencies. In both cases, the PSD of the sieved fraction might not sufficiently represent the expected PSD (larger or smaller particles than expected). To overcome this problem, the PSD of each fraction was measured ex-situ after the sieving step (as depicted in 2.5.3).

2.5.3 Characterization of the samples

The naked-eye appearance of the powders was studied by employing a Canon EOS 2000D camera to consider their overall tendency to agglomerate in the container where they are stocked. In addition, a 5 Mp Dino-lite Pro HR digital microscope was employed to highlight the particles' shape and outer appearance. Finally, Scanning Electronic Microscopy (SEM) was

performed with a JEOL JSM-649-LV to investigate the particle surface and the structure and morphology of the agglomerates potentially formed.

The "original" PSD was determined ex-situ with a Malvern Mastersizer 3000 equipped with an Aero S dry dispersion unit. 2-bar compressed air and a high vibration feeding system were employed in this unit to attain the maximum level of dispersion and the minimum presence of agglomerates.

2.6 Agglomeration and deagglomeration modelling

The particle-to-particle interactions in a transient and heterogeneous system as a dust cloud are complex to model. Neglecting the particles transportation and focusing exclusively on the agglomeration/fragmentation phenomena simplifies the system, but several physical interactions must still be considered. According to the classification proposed by Rumpf (Rumpf 1962), agglomeration can be related to van der Waals forces, electrostatic and magnetic bonds, and mechanical interlocking due to shape-related entanglement. For instance, the last phenomenon will be considered to explain the behaviour of fibrous particles as cellulose. Furthermore, Capes (Capes 1980) reported that the particle-to-particle electrostatic interactions are on a lower order of magnitude than magnetic bonds, which, in turn, are significantly smaller than van der Waals interactions for many powdered materials. Hence, for the sake of simplicity, Van der Waals forces will only be considered in this study.

Agglomeration and deagglomeration phenomena were studied and modelled, considering several gas-to-particle interactions exerted by the airflow on the particle surface. The rotary, turbulent and inertia stresses have been selected, evaluated and compared to the agglomerates' strength. To determine the latter, Rumpf (Rumpf 1962), Kendall (Kendall 1988) and Weiler (Weiler et al. 2010) theories were selected to explain the deagglomeration mechanisms observed. They are graphically represented in Figure 2-3. Several assumptions must be made to simplify the approach:

- Particles are approximated with mono-sized spheres with a diameter of d_p;
- All the agglomerates share the same porosity ε_p;
- Assessment of the parameters related to Van der Waals forces (i.e. Hamaker constant H, the cut-off of separation h_p)

Rumpf model considers that the breakage occurs along a transversal section that divides the agglomerate into two parts without considering its shape and dimension. All the inter-particle bonds break simultaneously, and the cohesion strength can be written as:

$$\sigma_{agg,R} = \frac{3}{64}\left(\frac{1-\varepsilon_p}{\varepsilon_p}\right)\frac{H}{d_p\, {h_p}^2} \quad (1)$$

where ε_p is the porosity of the agglomerate and d_p is the primary particle diameter.

Kendall model describes deagglomeration as a more gradual phenomenon involving a small fraction of unitary particles at a time and proposes the cohesion strength to be equal to:

$$\sigma_{agg,K} = 15.6\,\frac{(1-\varepsilon_p)^4}{d_p}\,\frac{H}{12\pi\, {h_p}^2} \quad (2)$$

Finally, a total breakage of the agglomerate in its primary particles is proposed by Weiler model, implicitly stating that the cohesion strength is sensibly higher than in the other two theories and equal to:

$$\sigma_{agg,W} = \frac{(1-\varepsilon_p)}{\epsilon_p}\,\frac{F_c}{2\, {d_{agg}}^2}\left[\left(\frac{d_{agg}}{d_p}\right)^3 - \frac{4\left(1-\frac{arcos(b)}{180^\circ}\right)}{b^2}\right] \quad (3)$$

where d_{agg} is the agglomerate diameter, F_c the cohesion force (here limited to Van der Waals forces), and $b = \frac{d_p}{d_{agg}-d_p}$.

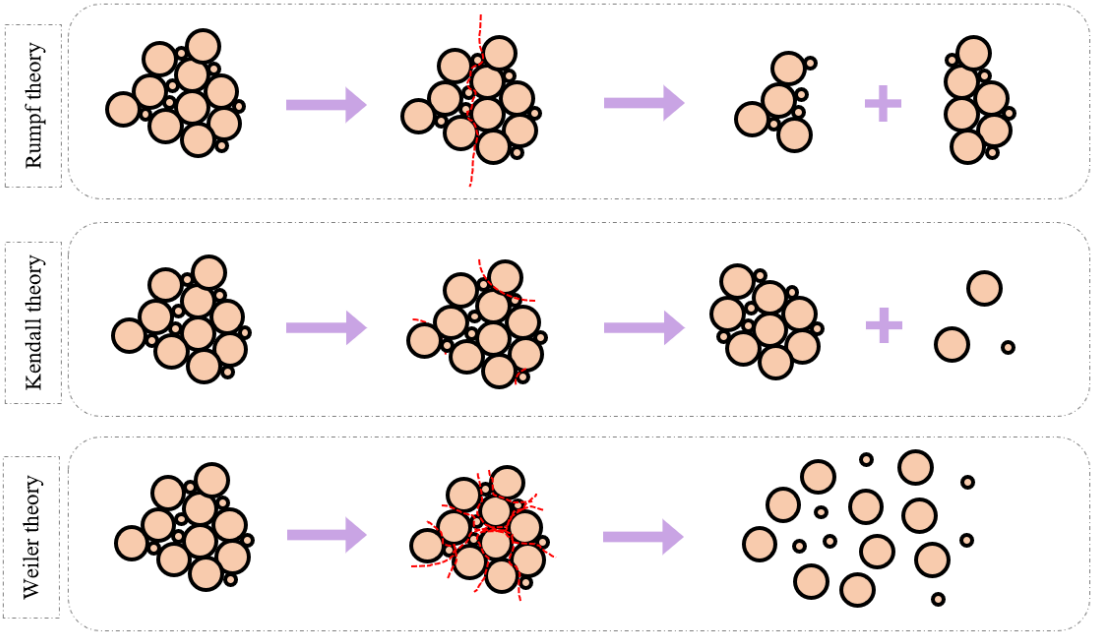

Figure 2-3 – Representations of agglomerate breakage theories selected for this work

3. Results and Discussion

3.1 Characterization of the samples

Figure 2-4 resumes the naked-eye appearance, the digital and the SEM analysis performed on the samples. Table 2-1 shows the characteristic diameters (D10, D50 and D90 - volume-based size distribution) of the samples, as well as the skewness (Tascón 2018) and kurtosis values. All samples' distributions presented positive skewness and kurtosis: for all powders, the contribution of finer particles is more critical than larger ones, and distributions are relatively narrow.

As can be noticed from the first series of images, Avicel ph 105, glucose and ascorbic acid naturally tend to form lumpy structures. The digital microscopy highlights some differences in the particle shape. Since the chemical structure of cellulose is linear, all the cellulose samples presented fibrous and elongated particles. On the other hand, wheat starch particles are associated with an ellipsoidal shape, characterized by a slight concavity. Skewness and kurtosis values do not vary in a significant way for the cellulose samples (they range from 1.87 to 2.18 and from 4.96 and 6.14, respectively), but they reach higher values for wheat starch (2.95 and 10.05, respectively), meaning a narrower PSD more centred on smaller particle sizes. Glucose and ascorbic acid particles presented a profoundly different particle shape, characterized by sharp edges, which can be related to the crystalline nature of these powders.

Even though the dynamic of the agglomeration process in the G-G oven is different from the phenomena that may naturally occur in a storage container, the SEM images were integrated into the study of the different agglomeration modes of the powders. The four celluloses showed that for smaller particle sizes (for Avicel ph 105 and 101), the overall tendency is to form smaller lumpy structure, which might be the result of inter-particles surface weak bonds, whilst the larger particles (for Avicel ph 102 and especially Vivapur 200) tend to entangle. Despite this diversity, all four cellulose samples present a similar span value, varying from 1.82 to 2.02. It might signify that both modes are responsible for the agglomeration, and both intervene in the four samples. Nonetheless, according to the particle size, one can take over the other and rule the global agglomeration phenomenon, entanglement being especially predominant for large fibres.

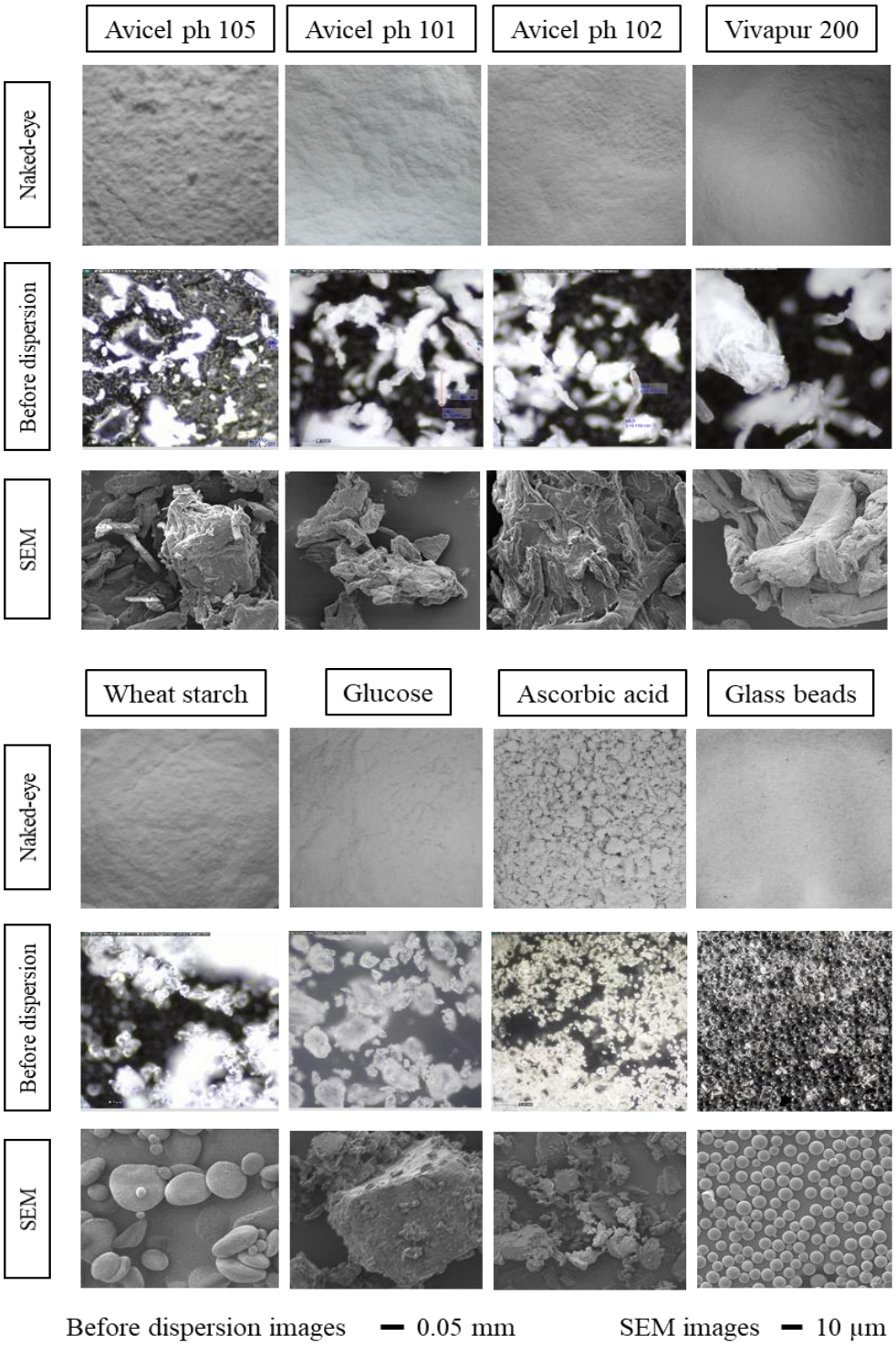

Figure 2-4 - Naked-eye photos, digital and electronic microscope images of the samples.

Table 2-1 - Characteristic diameters and parameters of the powder samples before dispersion in the furnace.

Sample	D10, µm	D50, µm	D90, µm	Span	Skewness	Kurtosis
Avicel ph 105	8	21	47	1.86	2.18	6.14
Avicel ph 101	21	59	140	2.02	1.91	4.96
Avicel ph 102	28	101	232	2.02	1.87	4.97
Vivapur 200	65	219	463	1.82	2.13	6.06
Wheat starch	12	20	33	1.05	2.95	10.05
Glucose	17	119	434	3.50	1.21	2.83
Ascorbic acid	4	15	45	2.73	1.69	4.20
Glass beads	36	42	49	0.33	5.97	37.16

3.2 Dispersion tests

3.2.1 Dust cloud residence time

A theoretical and experimental study of the residence time of a cellulose dust cloud was carried out in the standard configuration of the G-G oven. Results are reported in Figure 2-5. As it can be deduced from the graph, the two approaches have led to curves with different trends and values in different orders of magnitude. As the dispersion pressure increases, the theoretical residence time decreases proportionally to $P^{-0.5}$. Moreover, by raising the concentration of the dust, the apparent density increases, but the final result does not change significantly (discrepancies range between 1 and 5 ms).

On the other hand, the experimental dust cloud residence time showed an unexpected trend. All three curves show a raising part followed by a decrease, and all three curves seemed to converge towards the same value (approximately 230 ms). The first phase of increasing residence time, which may seem counter-intuitive, is related to the low efficiency of the powder dispersion mechanism at low pressures. Indeed, deposits can be observed in the horizontal part of the experimental set-up, which decreases the amount of powder dispersed in the furnace: the delay between C and D decreases (Figure 2-2), which reduces residence time. After reaching a maximum, the kinetic energy associated with the gas pulse becomes high enough to take over the global phenomenon and to reduce the residence time, as observed for the theoretical residence time. The turbulence level should also be taken into account: for smaller Reynolds

numbers (i.e. for low pressures), the energy dissipation is higher than for larger ones (i.e. for high pressures). Hence, a significant kinetic energy loss and a low dispersion efficiency might be responsible for the highest residence times, whilst a lower dissipation and a more efficient dispersion might be responsible for the lowest ones. In the next section, a quantitative analysis of the dust-gas flow turbulence will be carried out, with a focus on the eventual solid-gas phase detachment. It should also be underlined that ISO 80078-20-2 proposes dispersion pressures ranging from 10 to 50 kPa, the latter value corresponding to the maximum residence time observed for 0.2 g of cellulose (Figure 2-5).

3.2.2 Dust cloud dynamics

In order to study and characterize the fluid dynamics of the dust cloud, two dimensionless numbers were employed: the Reynolds (Re) and particle Stokes (St_p) numbers. Re allows quantifying the level of turbulence in the gas-solid flow whereas St_p compares two time-scales: the time required by a particle to react to changes in the fluid flow (particle relaxation time, τ_p) and a characteristic time of the fluid (fluid time scale, τ_f). Therefore, St_p allows to define and quantify the tendency of a particle to follow the fluid flow. The two dimensionless numbers are defined in Equations (4) and (5).

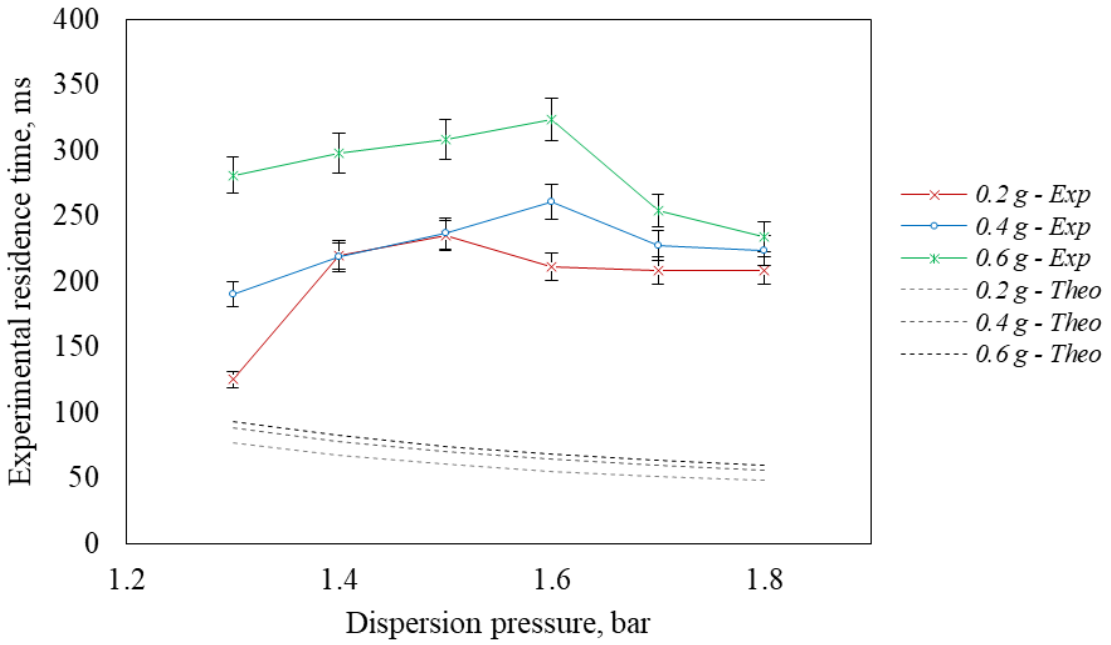

Figure 2-5 - Experimental and theoretical dust cloud residence times as a function of the dispersion pressure, for three different injected masses of cellulose.

$$Re = \frac{\rho_b \, u \, d_r}{\mu_g} \quad ; \quad St_p = \frac{\tau_p}{\tau_f} = \frac{\rho_p \, {d_p}^2}{18 \, \mu_g} \frac{u}{\delta} \qquad (4) \text{ and } (5)$$

where ρ_b is the dust-air bulk density, u the bulk velocity, d_r the reactor diameter, d_p the particle diameter and μ_g the dynamic viscosity of air.

It is well known that the choice of τ_f (i.e. $\frac{\delta}{u}$) is far from being simple because a fluid flow, especially a turbulent one, can be characterized by several time scales, such as the integral, the Kolmogorov and the viscous time scale (Wang and Manhart 2012). Regarding the information available experimentally, the choice fell on the integral time scale. It represents the fluctuations of a turbulent flow by considering the average lifetime of the largest eddies. It can be determined by dividing the characteristic length of the system surrounding the particles (δ) by the bulk velocity (u). Since the powder density and the gas characteristics did not vary much from test to test, the following average parameters will be considered for the rest of the study and especially for the assessment of the Stokes number St_p (Figure 2-6): a bulk density of 1500 $kg.m^{-3}$, a gas viscosity of $1.8 \cdot 10^{-5}$ Pa.s and a characteristic length of 0.026 m (the diameter of the cylindrical vertical chamber, here considered the space scale of the largest eddies). The bulk velocity u was determined experimentally. Results showed that Re varied between $9.9 \cdot 10^6$ and $12 \cdot 10^6$, indicating a high turbulence level in the vertical chamber of the G-G furnace. By integrating the PSD in the study, it is also possible to enlighten the particle size heterogeneity typical of a dust cloud. Figure 2-6 reports the St_p of a "surrogate powder" having the characteristics described previously, as well as the PSD for ascorbic acid, Avicel ph 105 and glucose, chosen as examples of powders with a different PSD. Considering the PSD of ascorbic acid, all the particles are associated with a St_p lower than 12. Approximately 84% of the particles are related to a $St_p < 1$, reflecting the tendency of the majority of this sample to follow the path of the gas flow without detachment between the two phases. As for the Avicel ph 105, this percentage decreased at 25%, while among the complementary fraction, particles reach values of $St_p \approx 200$. The detachment between particles and gas flow is significantly crucial for this sample. Finally, for glucose, whose PSD is characterized by a wide PSD (span equal to 3.50), 20% of the particles are associated with a St_p below the unity, but at the same time, the coarser fraction reaches 1000. The fact that some large particles or agglomerates do not follow the flow lines induces mechanical stresses that can lead to the fragmentation of brittle structures.

Re granted access to complementary information characterising the dust cloud flow: the convective heat transfer coefficient h. Through Equation (6), it was possible to estimate an average h = 44 $W.m^{-1}.K^{-1}$, which is consistent with other works that exploited similar experimental setups (Dufour et al. 2009a).

$$Nusselt\ (Nu) = \frac{hL}{\lambda_g} = 3.66 + \frac{0.0668\ Re\ Pr\left(\frac{D}{L}\right)}{1+0.04\left[Re\ Pr\left(\frac{D}{L}\right)\right]^{\frac{2}{3}}} \quad (6)$$

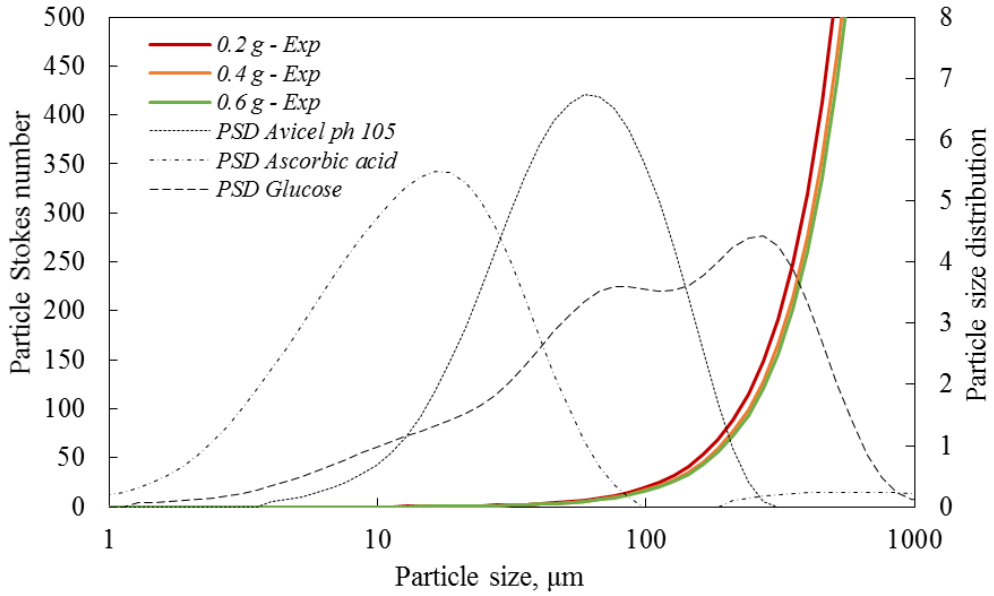

Figure 2-6 – PSD of ascorbic acid, Avicel ph 101 and glucose and evolution of the Stokes number of a "surrogate powder" as a function of the particle size

3.2.3 Influence of the setup

Results are reported in Figure 2-7, Figure 2-8, Figure 2-9 and Figure 2-10, which respectively correspond to the measurements performed at Position 1, 2a, 3a and 3b on Avicel ph 105. For each graph, the characteristic diameters (D10, D50 and D90) were extracted from each PSD curve and plotted as a function of the time. Results for the glass beads are reported in Figure S 1 in Annex 1: they confirm that there is no agglomeration or fragmentation for these powders. The heterogeneity in time and space of a dust cloud leads intrinsically to a specific particle size variability, noticeable in all curves. Furthermore, the optical concentration registered by the laser sensor during the analysis was plotted as well as a function of the time. As defined in Kohler (2010) (Köhler et al. 2010), in a laser diffraction analysis, the optical concentration is the extinction of the laser beam in focus. Therefore, it allows locating the time

region where the particle concentration is at its highest, neglecting the dust cloud tail formed by particles still in suspension. For the glass beads, the study of the evolution of the optical concentration also made it possible to highlight deposition phenomena in the horizontal part of the tube (decrease in concentration at the furnace outlet) at low dispersion pressure.

As shown by previous studies (Pietraccini et al. 2022), a fragmentation phenomenon, more or less significant according to the physico-chemical characteristics of the powders, can be observed during the suspension process, at the exit of the dust container. For example, the D50 of ascorbic acid decreases from 15 to 9 µm while that of glucose drops from 119 to 77 µm; the intensity of the effect depends of course on the dispersion pressure. The fragmentation phenomenon is even more intense with large crystalline particles, as for example with fructose. Some less brittle powders, such as celluloses, are less affected by such decrease in PSD on exiting the container or can even be prone to entanglement at high pressures. But other elements of the G-G furnace may have an influence on the PSD of the cloud. Figure 2-7 shows that there is a slight difference between the PSD of Avicel ph 105 before and after the elbow in the vertical configuration. However, as previously said, the characteristic diameters did not change significantly and are comparable to the original PSD, showing that no significant agglomeration or fragmentation phenomena occurred up to this point. As for the optical concentration, the high and narrow peak observed at Position 1 seemed to widen to some extent, which might be due to a slight segregation of the particles according to their size. The increase of the characteristic diameters around 700 ms was probably due to few large particles suspended exiting the dust container, as it should be kept in mind that the volume-D90 can be greatly affected by the presence of a single large particle. Thereafter, the curves relative to Position 2a (Figure 2-8) and 3a (Figure 2-9) enlightened a significant modification of the PSD of the cellulose cloud: a critical agglomeration tendency is noticeable, leading to an average increment of all three characteristic diameters of more than 100%. Such increase is due to the wall-particle interactions and the entanglement phenomena occurring in the cylindrical chamber. Concerning the curves determined in the horizontal configuration (Figure 2-10), an overall agglomeration tendency is still noticeable, but the particle size did not increase as much as in the vertical chamber; e.g. D50 reaches 270 µm after 500 ms in the vertical configuration compared to 50 µm in the horizontal configuration. It must be stressed that in the horizontal configuration, the contribution of the sedimentation phenomena to the modification of the PSD is far from negligible. Size, shape and apparent density play a substantial role in defining the free-fall velocity of a particle: as they come together as a result of fibre entanglement, the agglomerates

formed by the cellulose are low in density and have a large external surface area, which is subject to flow and friction. Moreover, as previously said, dust deposits have been observed at low dispersion pressures in the horizontal configuration, which tends to reduce the presence of large particles at the exit of such set-up. The shape and low density of cellulose agglomerates might also explain the slight increases around 500 ms after the vertical chamber (Figure 2-9) and around 800 ms after the horizontal chamber (Figure 2-10): some of the agglomerates are slowed down by the increasing drag forces, but managed to exit the chamber.

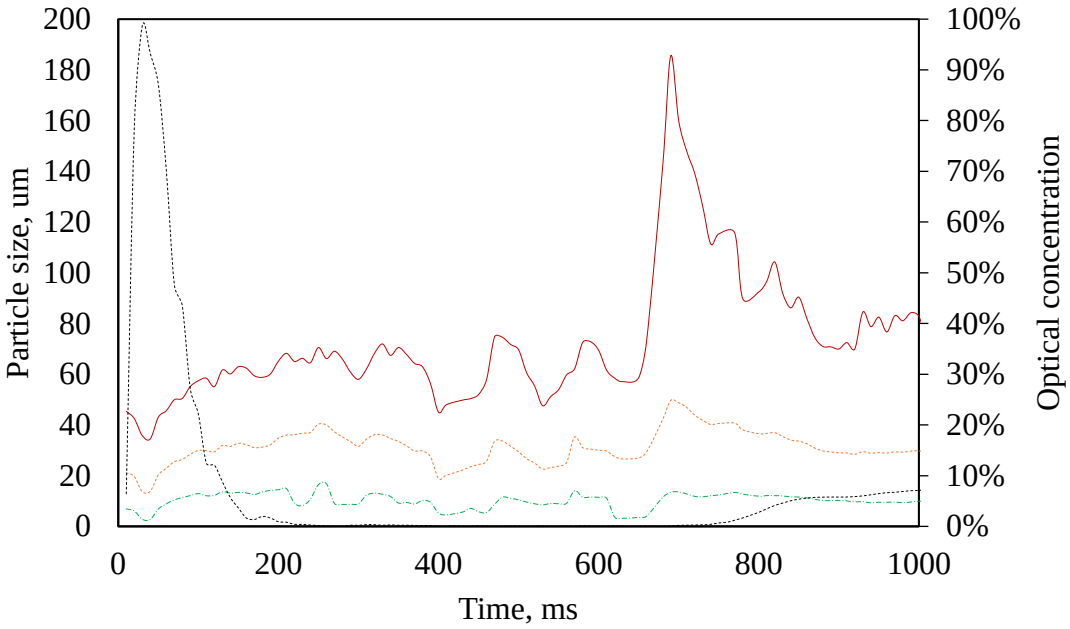

Figure 2-7 - Results of the dispersion tests for Avicel ph 105, before the elbow in the vertical configuration – position 1. The dotted line corresponds to the optical concentration, the three others to D10, D50 and D90.

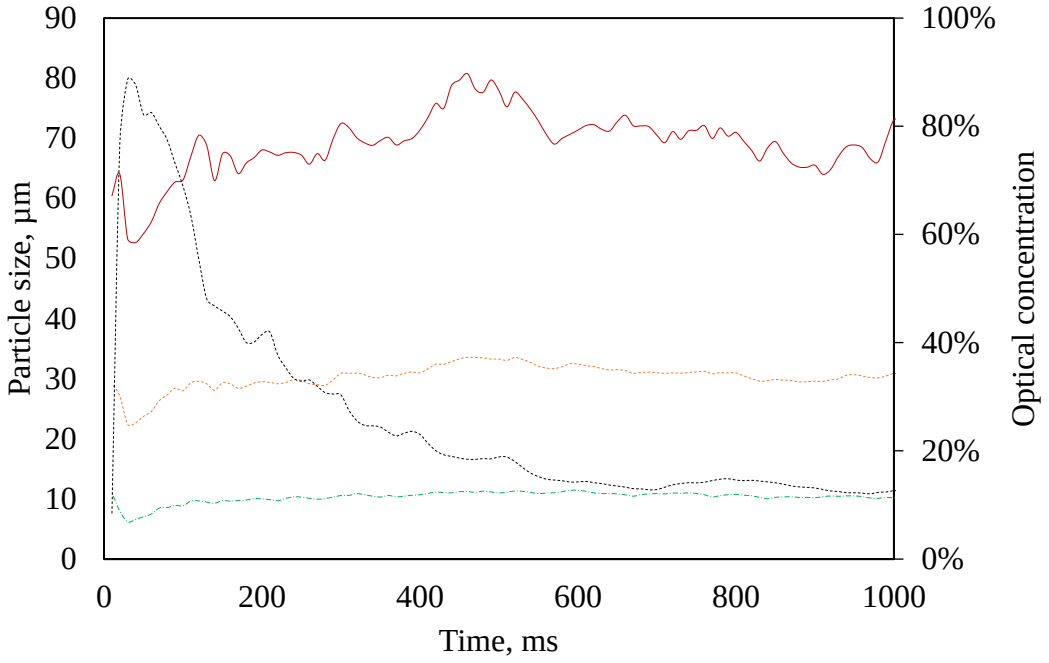

Figure 2-8 - Results of the dispersion tests for Avicel ph 105, after the elbow in the vertical configuration – position 2a. The dotted line corresponds to the optical concentration, the three others to D10, D50 and D90.

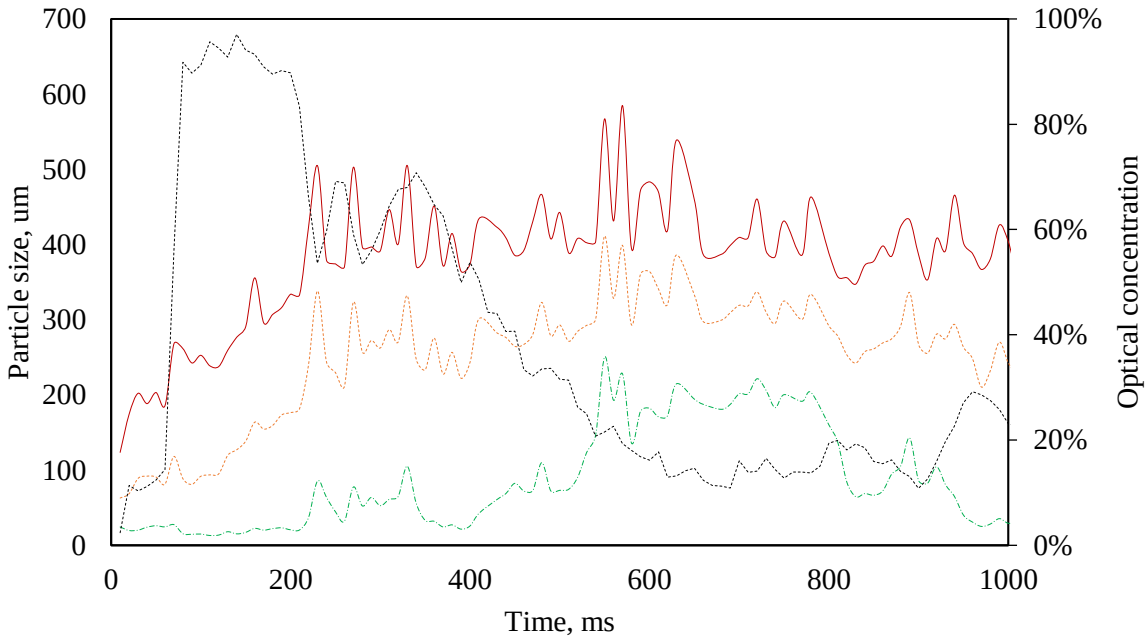

Figure 2-9 - Results of the dispersion tests for Avicel ph 105, after the cylindrical chamber in the vertical configuration – position 3a. The dotted line corresponds to the optical concentration, the three others to D10, D50 and D90.

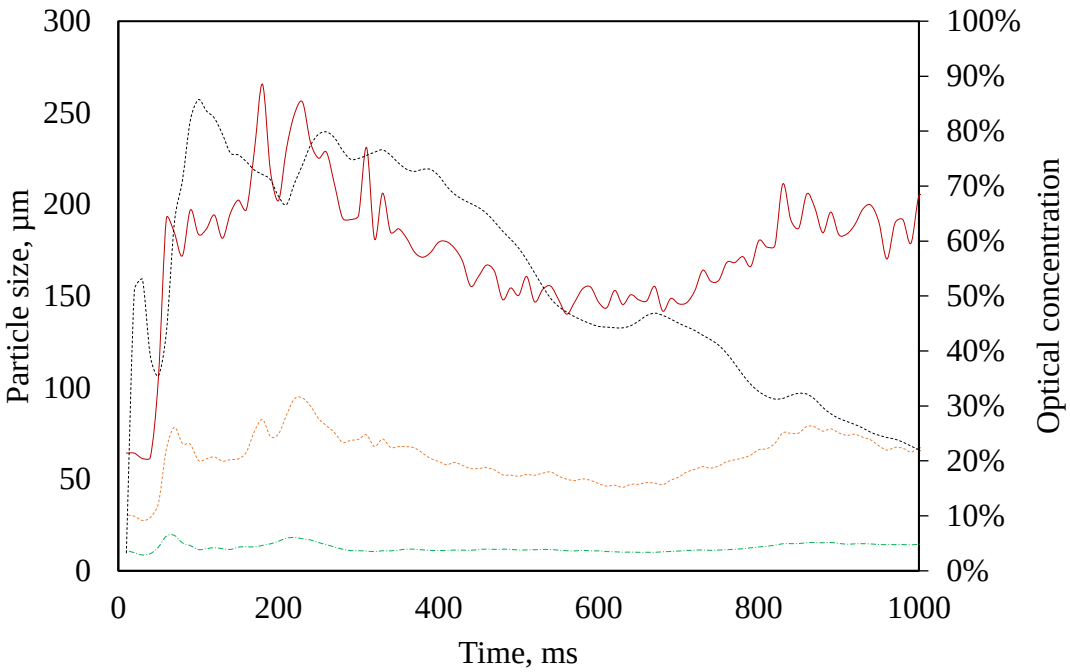

Figure 2-10 - Results of the dispersion tests for Avicel ph 105, after the cylindrical chamber in the horizontal configuration – position 3b. The dotted line corresponds to the optical concentration, the three others to D10, D50 and D90.

This analysis was performed on all samples and in order to compare them, an agglomeration index (AGG) was conceived. It was defined as follows:

$$AGG\ ii = \frac{\sum_{t=0\ ms}^{1000\ ms} Dii\ before,t - Dii\ after,t}{\overline{Dii\ before}} \quad (7)$$

where Dii is the characteristic diameter considered (D10, D50 or D90), *before* and *after* represent the Positions 1 and 3a or 3b respectively, at a given time t, and the denominator is the mean diameter Dii at Position 1. The time range considered was from 0 (the dispersion moment) to 1000 ms. This parameter allows to compare the different tendency to agglomeration, fragmentation or deagglomeration of the powders in the G-G oven. In Figure 2-11, the agglomeration indexes are reported for six samples.

Firstly, wheat starch and Avicel ph 105 showed a profoundly higher tendency to agglomerate than the other samples. Since these powders present a PSD more centred on small sizes (the D50 is 21 µm for Avicel ph 105 and 20 µm for wheat starch), and thus a higher specific area, these agglomerates can be due to more significant surface weak bonds (Van der Waals forces, electrostatic attraction). More generally, it seems that, for a given powder nature, the agglomeration phenomenon is less and less present when D50 increases (Figure 2-11).

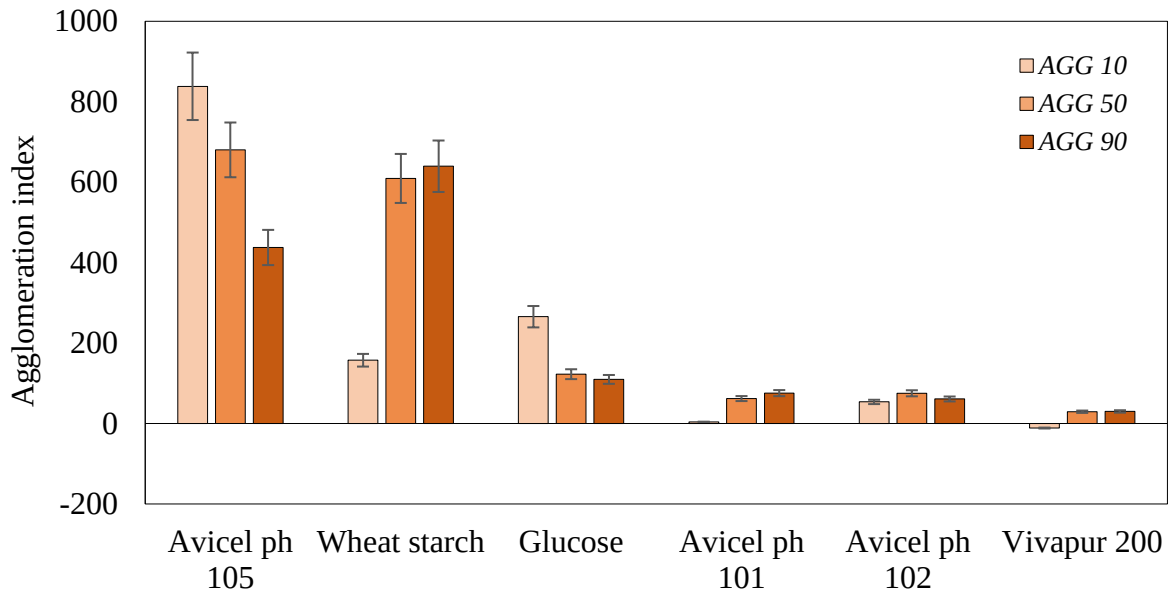

Figure 2-11 - Agglomeration indexes for selected powder samples.

3.2.4 Influence of initial PSD

The sieving step was aimed to point out the contribution and the role of fine, intermediate and coarse fractions to the behaviour of the dust cloud. The sieving yields are reported in Annex 1 (Figure S 2), as well as the characteristic diameters of the sieved fractions (Table S 1). The results of the dispersion tests are represented in Figure 2-12, in terms of agglomeration index AGG90 as a function of the mean D10. As previously predicted, the smaller the D10, the higher the agglomeration index AGG90.

The powders that exhibit a more spherical particle shape and a relatively higher kurtosis, i.e. wheat starch and Avicel ph 105, generated fractions with comparable distribution after the sieving step. The direct consequence is the similar behaviour of these fractions regarding the agglomeration phenomena. The agglomeration index AGG90 of the sieved glucose fractions does not vary neither linearly nor significantly as a function of the D10, which could be related to a change of particle shapes: from large cubic/parallelepiped structures to splinters or flakes.

Celluloses and their fractions exhibited a trend associated with a descending quasi-exponential relationship between the AGG90 and the D10. The finer fraction's role in the agglomeration phenomena occurring in the G-G furnace is thus primary and fundamental, but it is still strongly dependent on the particle nature and shape.

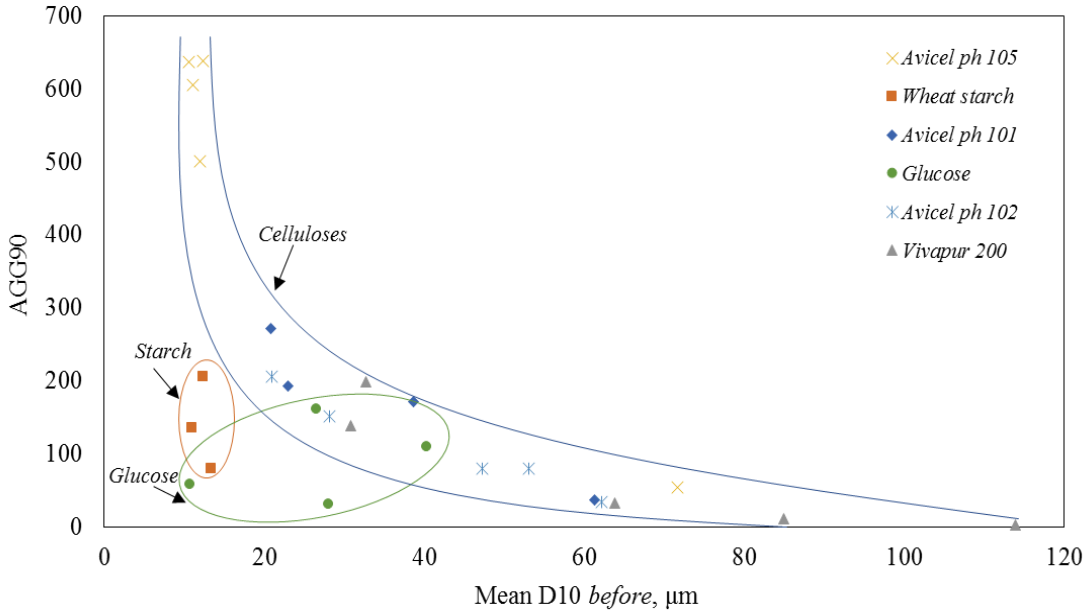

Figure 2-12 - Results of the dispersion tests of the sieved fractions, as a function of the mean D10.

3.2.5 Influence of the dispersion pressure

The influence of the air-pulse pressure on the PSD was studied for the different locations identified in the two configurations. The dispersion tests often showed that 0.1 bar was insufficient to disperse the entire amount of powder in the container, and the dispersion efficiency was too low, preventing the eventual agglomerates already present in the dust container from deagglomerating or fragmentation to occur as stated in 3.2.3. For this reason, in some tests, the lowest value of pulse pressure was set at 0.2 bar. For instance, Figure 2-13 shows the average PSD curves obtained by dispersing the ascorbic acid as a function of the pulse pressure. The curves were obtained by merging all the time-distributions in a single curve (performed with the software Windox 5-Sympatec), obtaining four PSD corresponding to the four values of dispersion pressure considered. Figure 2-14, Figure 2-15 and Figure 2-16 report the characteristic diameters of each average PSD for each position in the G-G furnace, as a function of the dispersion pressure. They refer respectively to ascorbic acid, glucose and Avicel ph 105.

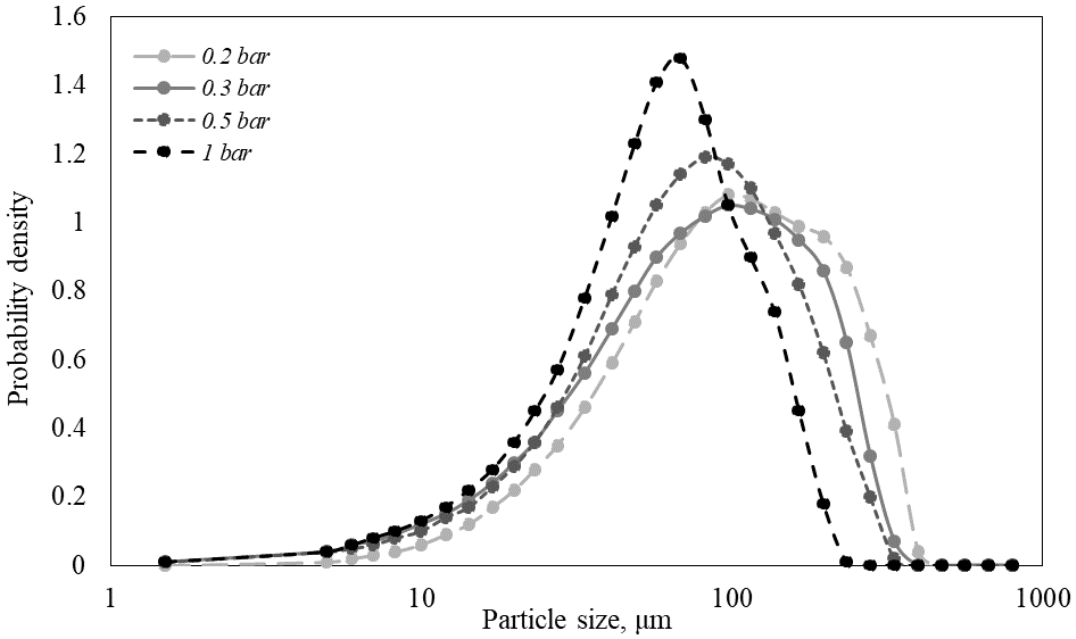

Figure 2-13 - Influence of the pulse pressure on the ascorbic acid dust cloud PSD, after the cylindrical chamber in the horizontal configuration – position 3b

Firstly, as for the results related to ascorbic acid, Figure 2-13 clearly shows that a pressure increase leads to a significant PSD decrease, especially for the particles larger than 100 µm. Considering the D10, i.e. the contribution of the finer particles to the global PSD, it appears that the setup-to-particles and the particle-to-particle interactions are negligibly affected by the dispersion pressure, except in the vertical chamber (Figure 2-14). In fact, in this section of the G-G oven, the double contribution of the increased shear stress (due to the increased pulse pressure) and the increasing particle velocity (and consequently St_p) might be responsible for the deagglomeration of those lumpy structures initially present in the dust container. Considering the data on D50 and D90, it can be assessed that, for the vertical configuration, small and intermediate agglomerates tend to reduce their size as the dispersion pressure increase. On the other hand, larger agglomerates, which are more related to the D90, seemed less affected. It can be related to a deagglomeration mode compatible with the Kendall model (Figure 2-3), where a large structure gradually deagglomerates, which has a substantial impact on the fine fraction (D10) but little consequence on the coarse one (D90). As previously said, it should also be considered that D90 variation is more sensitive to the presence of a limited number of large structures.

As for the horizontal configuration, the pulse pressure seemed to impact the characteristic diameters after the elbow significantly. However, after the heated chamber, its influence appeared to be less pronounced. It could translate into a significant deagglomeration in the first section of the G-G oven (from Position 1 to 2b), which increases the number of isolated particles in the dust cloud, and leads to a less important deagglomeration/fragmentation in the second section (from Position 2b to 3b). It suggests that Rumpf theory (Figure 2-3) can be considered the most suitable one to describe the deagglomeration mode observed in this section of the G-G furnace. As for glucose (Figure 2-15), after the dust container (Position 1), the evolution of the characteristic diameters as a function of the pressure suggests either a marked agglomeration tendency of the particles or a deagglomeration/fragmentation phenomenon depending on the location considered. As indicated in Table 2-1, glucose presented large particles associated with high dispersion inertia (high drag coefficient and powder density). As it appears from Figure

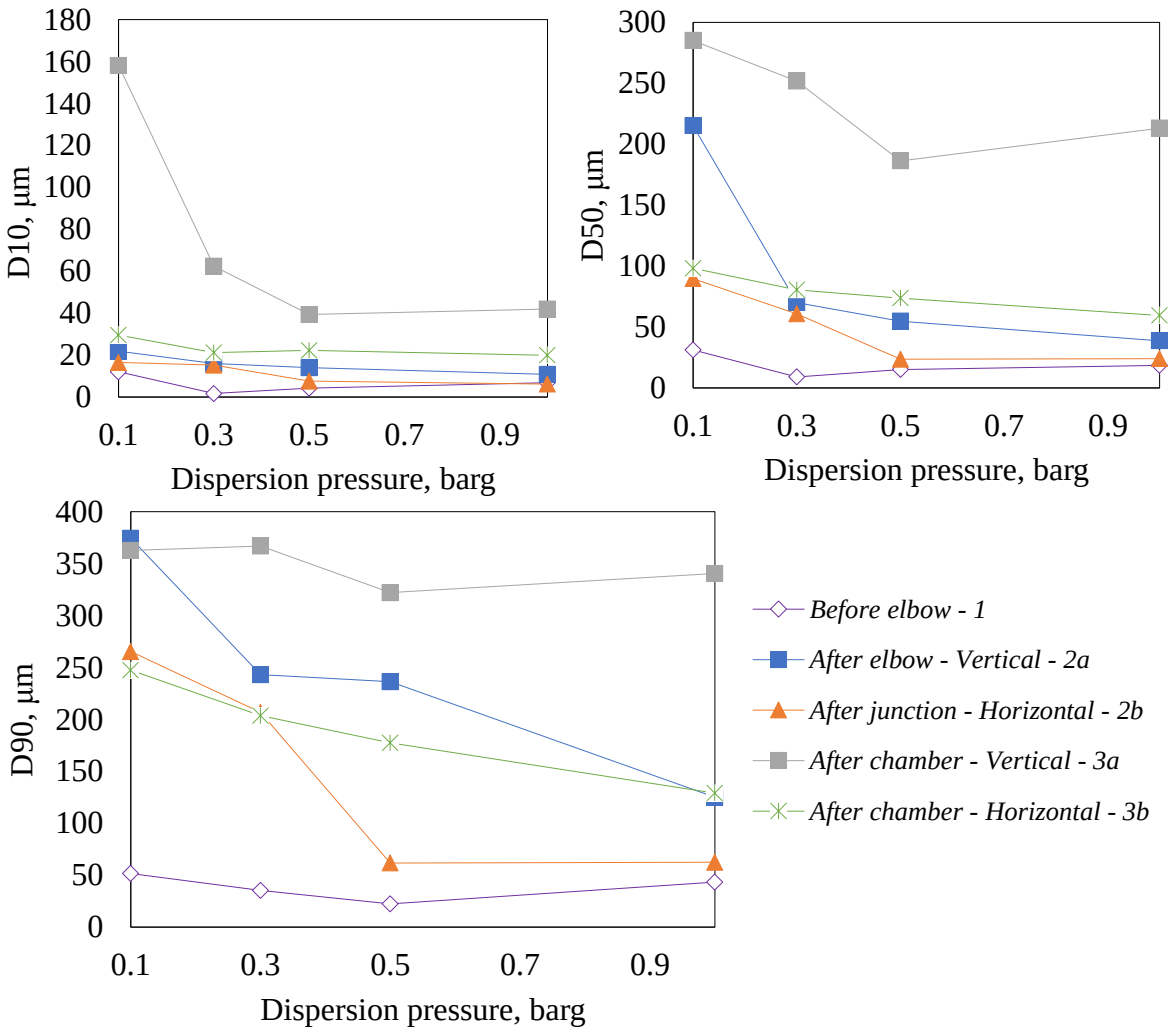

Figure 2-14 - Ascorbic acid cloud characteristic diameters as a function of the dispersion pressure, for different locations in the G-G oven.

2-13, it was thus necessary to increase the pulse pressure to attain a complete dispersion. D10 and D50 recorded at the bottom of the furnace (vertical configuration) were consistently higher than the original values (17 and 119 µm) for dispersion pressures lower than 0.5 bar, whilst these parameters are equal or lower than the characteristics of the raw powder at high dispersion pressures. D90 seemed to stabilise between 250 and 300 µm for higher pressure than 0.3 bar, which is lower than the original D90 (434 µm). It induces that the dispersion is complete as the pulse pressure increases, but at standard dispersion pressures (from 10 kPa to 50 kPa), it not does not necessarily trigger a deagglomeration on a small and intermediate scale.

Between Positions 1 and 2a (after elbow), the trend of D10, D50 and D90 is consistent with the behaviour observed after the dust container. However, several slight differences are noticeable. The setup-to-particle interactions in this section of the G-G oven's vertical configuration have led to a more significant number of fine particles or agglomerates (contributing to an increase in the D10) and a smaller amount of intermediate and larger particles or agglomerates (contributing to a decrease in the D50 and D90). The high shear stress can explain this fragmentation or deagglomeration phenomena due to the significant singular pressure losses in the elbow. Kendall model is the deagglomeration theory that can most accurately explain the results observed and presented so far for glucose.

The horizontal configuration showed significantly lower PSD with regard to the standard configuration: the influence of the elbow on the PSD is unquestionably high. The evolution of D90 should notably be underlined as the D90 observed at the exit of the furnace is greater than after the junction: as these high values are observed for long observation times, the possibility of re-entrainment of large particles having settled in the furnace cannot be excluded.

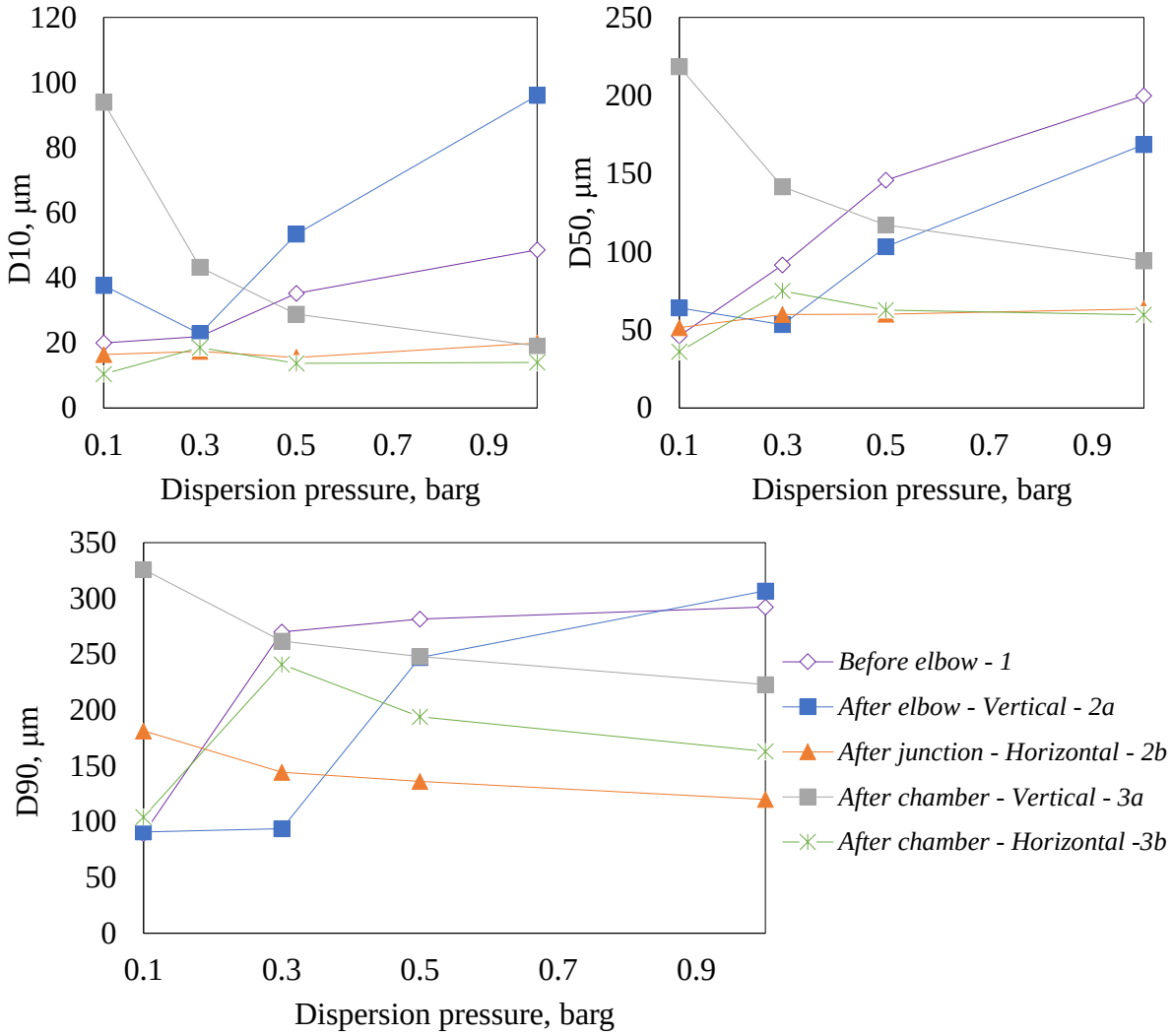

Figure 2-15 - Glucose cloud characteristic diameters as a function of the dispersion pressure, for different locations in the G-G oven

Considering Avicel ph 105 (Figure 2-16), it appears that the D10 changes little throughout the furnace in the horizontal configuration whatever the dispersion pressure, which is not the case in the standard one. However, this parameter approaches the initial D10, i.e. 8 µm (Table 2-1), when the injection pressure is high. Whatever the characteristic diameter considered, it increases after the dust container and before the elbow/junction, when the pressure increases. This trend confirm that entanglement of the cellulose fibres is promoted when the forces applied on the samples increase, leading rapidly to a growth in D90 and more slowly to an increase of D10 and D50: entanglement of large structures is easy compared to the progressive agglomeration of finer fibres. More generally, for the standard configuration, the agglomerates generated before the elbow seem to be broken as soon as the pressure is greater than 30 kPa. However, re-agglomeration takes place within the heated chamber leading to a

global increase of the PSD at the exit of the G-G furnace. Once again, the horizontal configuration appeared not to influence the dust cloud PSD profoundly. As for the D90, since its values remain between 300 and 380 µm at the bottom of the vertical furnace, it might be concluded that the dispersion pressure does not play a significant role in the agglomeration after the vertical chamber. On the contrary, pressure plays a significant role on the D90 in the intermediate stages, but, the agglomeration observed in the cylindrical heater tends to counterbalance the deagglomeration produced in the elbow. The horizontal chamber appears to induce a slight agglomeration at higher pressures, possibly due to increased turbulence or recirculation of larger particles.Once again, the Kendall model is the most appropriate to represent theoretically what is observed experimentally in the vertical configuration. However,

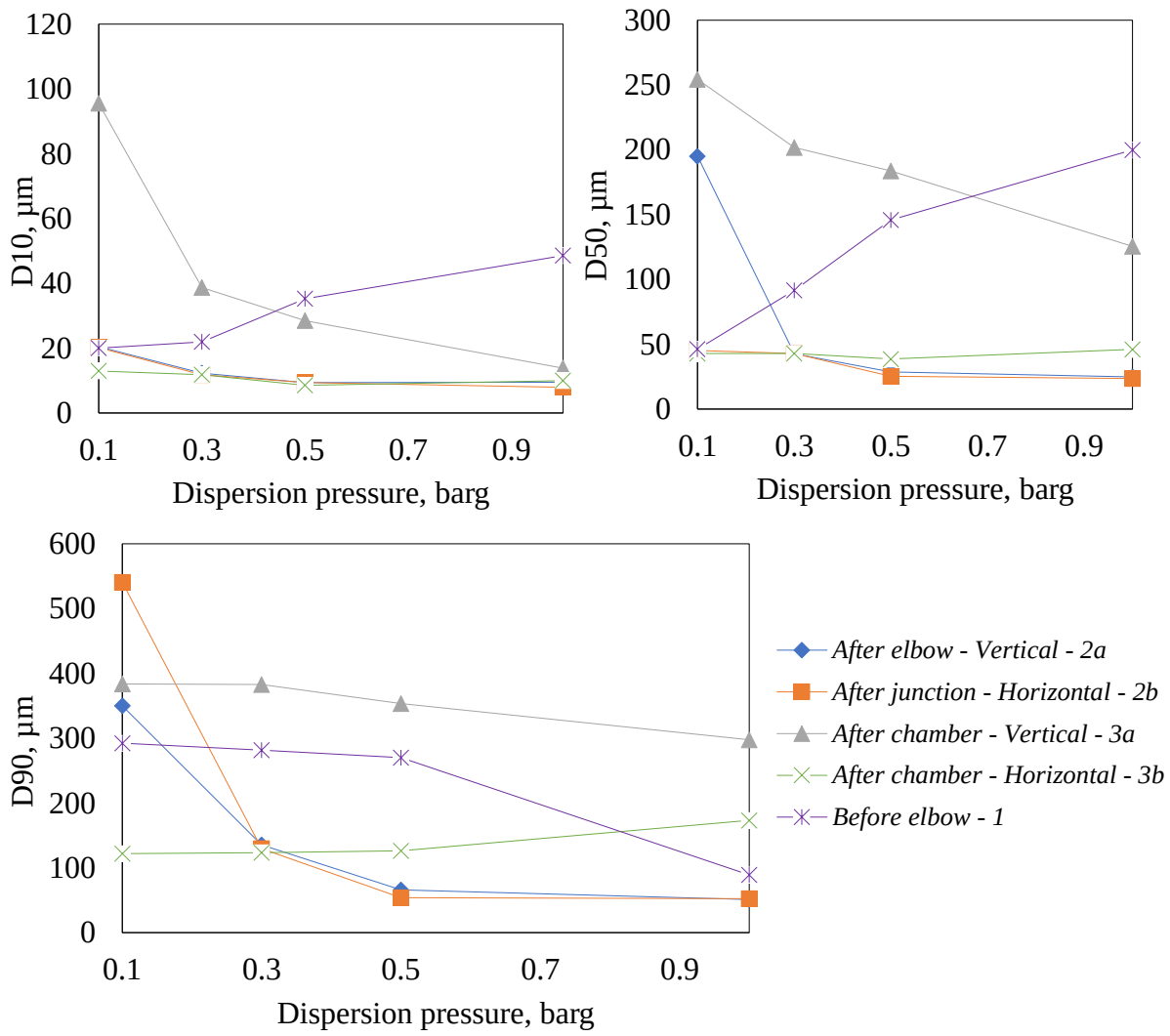

Figure 2-16 - Avicel ph 105 cloud characteristic diameters as a function of the dispersion pressure, for different locations in the G-G oven.

Rumpf's can accurately describe the deagglomeration mode identified in the horizontal layout, in which the D90 is strongly impacted by the dispersion pressure, while the D10 is not.

3.3 Agglomeration and deagglomeration modelling

The method for calculating the inertia, rotary and turbulent stresses as well as the cohesion strength of the agglomerates as defined by Rumpf, Kendall and Weiler was described by Santandrea (Santandrea et al. 2021). A similar approach has been applied here, adapting the properties of the flow (velocity gradient, slip velocity…) and those of the particles (agglomerate porosity…) to glucose. The turbulence dissipation rate at the exit of the dust container has been estimated considering a parabolic velocity profile. Inertia stress is predominant over other contributions. (Santandrea et al. 2021). The inertia stress has been compared to the agglomerate strength using alternatively Rumpf, Kendall and Weiler's theories. The major constraint on such modelling is the choice of the Hamaker constant for glucose, it was then used as a fitting parameter. A satisfactory agreement between Rumpf's model and the stress exerted on glucose particles, i.e. maximum agglomerate diameter of approximately 100 µm at the position 1, was for a Hamaker constant set at 4.10^{-19} J; which is a good order of magnitude for such materials.

3.4 Minimum Ignition Temperature tests

At higher temperatures, the inter-particle interactions described so far may have consequences on the MIT of the dust cloud. Due to the higher accessibility of information concerning its thermal behaviour and the results obtained in the previous part of this work, the study presented hereafter is focused on cellulose. The internal conduction within the particle crucially depends on the particle/agglomerate size, which is determined by the initial PSD and the agglomeration and deagglomeration phenomena. The Biot number (calculated with Equation (8)) allows comparing the resistances to external convection and internal conduction, which considers the particle characteristic length:

$$Bi = \frac{h\,L}{\lambda_s} \tag{8}$$

where h is the external convective heat transfer coefficient, L is the characteristic length and λ is the thermal conductibility. The agglomeration results previously presented for Avicel ph 105 were integrated in this study; hence, hereafter L corresponds to the average D90 of the dust cloud in position 3a. Secondly, the internal heat transfer was compared to pyrolysis, which occurs primarily in the solid phase, through the Pyrolysis (Py) number, i.e. the ratio between

the reaction and the internal heat transfer time scales. The latter is defined in Pyle and Zaror (Pyle and Zaror 1984) as the time necessary to the heating wave to reach the core of the particle and comprehends several heat transfer phenomena. It thus differs from the Biot number, which takes into account only the conductive heat transfer within the particle. Finally, the first Damköhler (DaI) number, which compares the flow and reaction time scales, was used to enlighten the effect of the dispersion pressure on the dust cloud global conversion degree. They are defined by Equations (9) and (10) (Pyle and Zaror 1984):

$$DaI = k\, {C_o}^{n-1} \tau \quad ; \quad Py = \frac{\lambda_s}{k\, \rho_s\, c_{ps}\, L^2} \qquad \text{(9) and (10)}$$

where k is the global kinetic constant of the pyrolysis reaction, C_o is the initial concentration of cellulose, n is the reaction order, τ is the mean residence time of the dust cloud in the heated chamber, ρ_s is the cellulose bulk density and c_{ps} is cellulose heat capacity. The values used for the calculations are reported in Table 2-2. Since pyrolysis represent one of the main focus of this section and its onset temperature is approximately 600K (Piskorz et al. 2000b), the temperatures considered were 600, 700 and 800K.

Table 2-2 - Parameters used in the dimensionless number analysis

Parameter	**Symbol**	**Value**	**Source**
Cellulose density, $kg.m^{-3}$	ρ_s	700	Lédé 2012
Heat capacity, $J.kg^{-1}.K^{-1}$	c_{ps}	1757	Piskorz et al. 2000b
Cellulose thermal conductibility, $W.m^{-1}.K^{-1}$	λ_s	0.048	Piskorz et al. 2000b
Reaction order	n	1	Piskorz et al. 2000b
Pyrolysis activation energy, $J.mol^{-1}$	E_a	197300	Piskorz et al. 2000b
Pyrolysis pre-exponential factor, s^{-1}	A	$1.9 \cdot 10^{16}$	Piskorz et al. 2000b
Air viscosity, Pa.s	μ_g	$1.81 \cdot 10^{-5}$	Engineering toolbox
Mean bulk velocity, $m.s^{-1}$	u	4.6	This work
Average dust cloud residence time, ms	τ	235	This work
Convection heat transfer coefficient, $W.m^{-2}.K^{-1}$	h	44	This work

As shown in Figure 2-17, the particle temperature influences Da I and Py by affecting the kinetic constant. Conversely, supposing that lambda and h are independent of the temperature (or more precisely do not change significantly with temperature), Bi values do not change. Moreover, since Bi < 1 for whatever temperature, which implies that the internal

conduction is significantly faster than the external convection: for these values of particle size, despite the agglomeration phenomena occurring in the setup, the resistance to the internal conduction is negligible. The same results can be deducted considering the original PSD: the agglomeration in the vertical chamber do not affect the Biot number, and, therefore, particles can be considered uniformly isothermal. Da I is slightly affected by the dispersion pressure, which influences the dust cloud residence time in the heated chamber, but it is influenced by the temperature. Initially, at 600K, Da I values are low, which is associated with a low conversion degree. In addition, since Py is associated with high values, pyrolysis is initially the rate-limiting step. Also, the global endothermicity of the pyrolysis process prevents the particle temperature from attaining the reactor temperature. By increasing the particle temperature from 600 to 800K, Da I showed an increase of five orders of magnitude related to the rise of the pyrolysis reaction rate and, thus, the decrease of the reaction time scale. Since Bi < 1 and Py decreases by five orders of magnitude, pyrolysis attained a reaction rate high enough to make the external heat transfers the rate-limiting step of the global phenomenon. Furthermore, the agglomeration observed experimentally has an impactful consequence on the Py, as depicted in Figure 2-17. At 700K, it determines the change of the rate-limiting step from pyrolysis to internal heat transfer, since Py passes from values higher than 1 (approximately 10) to values lower than 1 (approximately 0.1). However, at these temperature levels, higher than cellulose MIT (= 700-800K (IFA)), the concentration of the gaseous pyrolysis product eventually reached the flammability range, triggering the oxidation reactions. Since they are exothermic reactions, a substantial increase in temperature leads to significantly faster reactions and to flame propagation within the dust cloud. To conclude, the pyrolysis can be initially considered the rate limiting step, when the oxidation reactions are not triggered yet. Then, their exothermicity increases the temperature of the chamber, and thus that of the particles, leading to a sensibly higher pyrolysis reaction rate. At this stage of the process, the external convective heat transfer becomes the rate-limiting phenomenon.

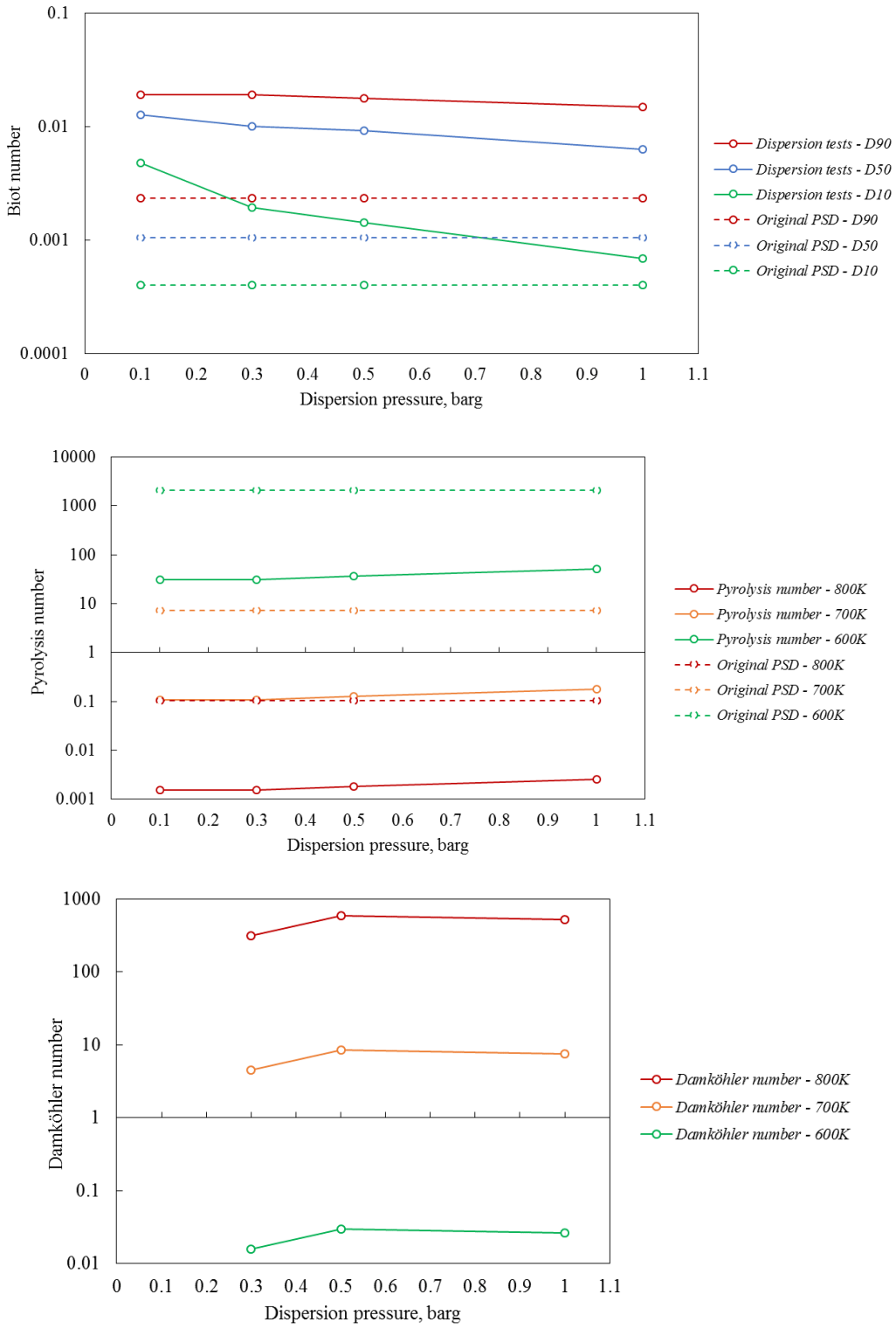

Figure 2-17 - Pyrolysis, Damköhler and Biot numbers as a function of the dispersion pressure

MIT results are reported in Table 2-3 for glucose and cellulose. Tests pointed out the influence of the pulse dispersion pressure on two significant aspects involved in the global phenomenon: the changes of the PSD and the modification of the dust cloud residence time in

the heated chamber. Increasing the dispersion pressure implies reducing the dust cloud residence time, which will limit the heat transfer within the powder. It means that the set temperature needs to be higher to trigger the ignition and sustain the flame propagation so that the MIT will be higher. The same pressure variation can either leads to a fragmentation of the powders or to its agglomeration, as a function of the powder nature and shape. Both effects can then be synergistic or antagonistic with regard to the dust properties.

As for the glucose, the dispersion tests showed its tendency to deagglomerate or fragment in the G-G oven, generating a higher number of finer particles. These last are usually associated with a lower heating characteristic time than the coarser ones, which translates to a higher sensibility to be ignited in a heated chamber or by a hot surface. However, results show the opposite trend as the pressure increases: MIT ranges from 480°C with a 0.2 barg dispersion pulse to 530°C with a 1 barg dispersion pulse. First, as previously said, increasing the pulse pressure means decreasing the dust cloud residence time in the heated chamber. Moreover, the high-temperature effect might also be significant for glucose. Above 150°C, the melting point of glucose and tiny droplets of liquid start to coexist with the solid particles. It can trigger an intense agglomeration process that generates lumpy hybrid structures.

Avicel ph 105 showed a different behaviour, as presented in Table 2-3. MIT varies from 490°C at 0.2 barg to 510°C at 1 barg. However, with an intermediate pressure of 0.5 barg, the dust cloud seemed even more sensible to ignition, being the MIT equal to 470°C. The dispersion tests stressed the overall tendency of Avicel ph 101 to agglomerate, with a slight reduction of the PSD for pulse pressures higher than 0.2 barg. It could explain the initial decrease in MIT. Its subsequent increase might be due to the lower cloud residence time in the heated chamber, as assumed for glucose.

Table 2-3 - The MIT values for glucose and Avicel ph 105, with and without applying the correction provided for the ISO standard.

	0.2 bar	**0.5 bar**	**1 bar**	**ISO 80079-20-2**
Glucose	480	500	530	460 (min - 20°C)
Cellulose	490	470	510	450 (min - 20°C)

4. Conclusions

This work studied the influence of several organic powders' features on the PSD of a dust cloud passing in a G-G furnace. First, the role of their nature was considered by choosing biopolymers (four differently-sized celluloses and wheat starch), monosaccharides (glucose) and more complex organic molecules (ascorbic acid). The chemical structure impacts the particles' shape, mechanical properties and surface behaviours. Cellulose's fibrous conformation was responsible for significant entanglement phenomena, while the branched chain of starch has led to weak-bond surface interactions that generate strong agglomeration. Moreover, the initial PSD profoundly influences the behaviour of the dust cloud. For cellulose, an agglomeration tendency was observed at all dispersion pressures, and it is related to surface cohesion forces and entanglement that characterise the finer and the coarser fractions, respectively. For instance, an increase from 20 to 95 µm was noticed just after the dust contained for both the horizontal and the vertical configuration. Next, the dispersion pressure had a double impact on the dust cloud PSD. First and foremost, at 0.1 and 0.2 barg a lack of dispersion efficiency was often observed, which can be related to the relatively high sedimentation of the particles and, thus, to the low stability of the airborne suspension. For higher pressures (0.3, 0.5 and 1 barg), behaviours stabilised, showing either agglomeration or deagglomeration tendencies. For instance, in both configurations, cellulose's D10 increased from 20 to 95 um. Glucose and ascorbic acid presented a crystalline structure and edgy particle shapes and showed completely different trends. Glucose depicted an agglomeration tendency in the vertical configuration, and a slight deagglomeration in the horizontal one, whereas ascorbic acid seemed to be characterised by a strong deagglomeration in both designs. These results were incorporated in a dimensionless-number analysis to estimate the impact of agglomeration and deagglomeration in an explosion. Biot, Pyrolysis and Damköhler numbers were employed. They allowed us to conclude that, at 600K, the pyrolysis remains the rate-limiting step, despite the agglomeration. On the other hand, it is responsible for changing the regime at 700K: the external heat transfer is likely the rate-limiting step, which would not happen without agglomeration.

References

‘IFA - Institute for Occupational Safety and Health of the German Social Accident Insurance’. (https://staubex.ifa.dguv.de/explosuche.aspx?lang=e).

Bagaria, Pranav, Qiang Li, Ashok Dastidar, and Chad Mashuga. 2019. ‘Classification of Particle Breakage Due to Dust Dispersion’. *Powder Technology* 342:204–13. doi: 10.1016/j.powtec.2018.09.089.

Bu, Yajie, Zepeng Ma, Chang Li, Paul Amyotte, Wenbo Yuan, Chunmiao Yuan, and Gang Li. 2020. ‘Effect of Admixed Solid Inertants on Dispersibility of Combustible Dust Clouds in a Modified Hartmann Tube’. *Process Safety and Environmental Protection* 135:1–11. doi: 10.1016/j.psep.2019.12.017.

Bu, Yajie, Yixiao Yuan, Shaoqian Xue, Paul Amyotte, Chang Li, Wenbo Yuan, Zepeng Ma, Chunmiao Yuan, and Gang Li. 2020. ‘Effect of Admixed Silica on Dispersibility of Combustible Dust Clouds in a Godbert-Greenwald Furnace’. *Powder Technology* 374:496–506. doi: 10.1016/j.powtec.2020.07.071.

Capes, C. E. 1980. ‘Agglomerate Bonding’. Pp. 23–51 in *Handbook of Powder Technology*. Vol. 1. Elsevier.

Di Sarli, Valeria, Enrico Danzi, Roberto Sanchirico, Luca Marmo, and Almerinda Di Benedetto. 2019. ‘Issues of Standard Explosion Tests for Non-Spherical Dusts’. *Chemical Engineering Transactions* 77:691–96. doi: 10.3303/CET1977116.

Dufour, A., P. Girods, E. Masson, Y. Rogaume, and A. Zoulalian. 2009. ‘Synthesis Gas Production by Biomass Pyrolysis: Effect of Reactor Temperature on Product Distribution’. *International Journal of Hydrogen Energy* 34(4):1726–34. doi: 10.1016/j.ijhydene.2008.11.075.

Eckhoff, Rolf K. 1985. ‘Use o f (DPldt)Max from Closed-Bomb Tests for Predicting Violence of Accidental Dust Explosions in Industrial Plants’. 10.

Eckhoff, Rolf K. 2003. ‘Assessment of Ignitability, Explosibility, and Related Properties of Dusts by Laboratory-Scale Tests’. Pp. 473–548 in *Dust Explosions in the Process Industries*. Elsevier.

Eckhoff, Rolf K. 2013. ‘Influence of Dispersibility and Coagulation on the Dust Explosion Risk Presented by Powders Consisting of Nm-Particles’. *Powder Technology* 239:223–30. doi: 10.1016/j.powtec.2013.02.007.

EN 17199-5. 2019. *Workplace Exposure - Measurement of Dustiness of Bulk Materials That Contain or Release Respirabe NOAA or Other Respirable Particles - Part 5: Vortex Shaker Method. p. 37.*

ISO/IEC 80079-20-2. 2016. *Explosive Atmospheres - Part 20-2: Material Characteristics - Combustible Dusts Test Methods*.

Kendall, K. 1988. ‘AGGLOMERATE STRENGTH.’ *Powder Metallurgy* 31(1):28–31.

Klippel, Alexander, Marc Scheid, and Ulrich Krause. 2013. ‘Investigations into the Influence of Dustiness on Dust Explosions’. *Journal of Loss Prevention in the Process Industries* 26(6):1616–26. doi: 10.1016/j.jlp.2013.07.016.

Klippel, Alexander, Martin Schmidt, and Ulrich Krause. 2015. 'Dustiness in Workplace Safety and Explosion Protection – Review and Outlook'. *Journal of Loss Prevention in the Process Industries* 34:22–29. doi: 10.1016/j.jlp.2015.01.011.

Köhler, Ulrich, Thomas Stübinger, and Wolfgang Witt. n.d. 'LASER-DIFFRACTION RESULTS FROM DYNAMIC IMAGE ANALYSIS DATA'. 4.

Lédé, Jacques. 2012. 'Cellulose Pyrolysis Kinetics: An Historical Review on the Existence and Role of Intermediate Active Cellulose'. *Journal of Analytical and Applied Pyrolysis* 94:17–32. doi: 10.1016/j.jaap.2011.12.019.

Marmo, Luca, Roberto Sanchirico, Almerinda Di Benedetto, Valeria Di Sarli, Daniela Riccio, and Enrico Danzi. 2018. 'Study of the Explosible Properties of Textile Dusts'. *Journal of Loss Prevention in the Process Industries* 54:110–22. doi: 10.1016/j.jlp.2018.03.003.

Murillo, Carlos. 2013. 'Experimental and numerical approaches to particles dispersion in a turbulent flow: application to dust explosions'. Université de Lorraine.

Pietraccini, Matteo, Enrico Danzi, Luca Marmo, Pierre-Alexandre Glaude, Anthony Dufour, and Olivier Dufaud. 2022. 'Particle Size Distribution in a Godbert-Greenwald Furnace: Experiments and Modelling'. *Chemical Engineering Transactions* 90:469–74. doi: 10.3303/CET2290079.

Piskorz, J., P. Majerski, D. Radlein, A. Vladars-Usas, and D. S. Scott. 2000. 'Flash Pyrolysis of Cellulose for Production of Anhydro-Oligomers'. *Journal of Analytical and Applied Pyrolysis* 56(2):145–66. doi: 10.1016/S0165-2370(00)00089-9.

Pyle, D. L., and C. A. Zaror. 1984. 'Heat Transfer and Kinetics in the Low Temperature Pyrolysis of Solids'. *Chemical Engineering Science* 39(1):147–58. doi: 10.1016/0009-2509(84)80140-2.

Rumpf, H. 1962. 'The Strength of Granules and Agglomerates'. *Agglomeration*.

Sanchirico, Roberto, Valeria Di Sarli, Paola Russo, and Almerinda Di Benedetto. 2015. 'Effect of the Nozzle Type on the Integrity of Dust Particles in Standard Explosion Tests'. *Powder Technology* 279:203–8. doi: 10.1016/j.powtec.2015.04.003.

Santandrea, Audrey, Stéphanie Pacault, Sébastien Bau, Yohan Oudart, Alexis Vignes, Laurent Perrin, and Olivier Dufaud. 2021. 'Safer and Stronger Together? Effects of the Agglomeration on Nanopowders Explosion'. *Journal of Loss Prevention in the Process Industries* 69:104348. doi: 10.1016/j.jlp.2020.104348.

Tascón, Alberto. 2018. 'Influence of Particle Size Distribution Skewness on Dust Explosibility'. *Powder Technology* 338:438–45. doi: 10.1016/j.powtec.2018.07.044.

Wang, Bing, and Michael Manhart. 2012. 'Two-Phase Micro- and Macro-Time Scales in Particle-Laden Turbulent Channel Flows'. *Acta Mechanica Sinica* 28(3):595–604. doi: 10.1007/s10409-012-0034-6.

Weiler, Claudius, Markus Wolkenhauer, Michael Trunk, and Peter Langguth. 2010. 'New Model Describing the Total Dispersion of Dry Powder Agglomerates'. *Powder Technology* 203(2):248–53. doi: 10.1016/j.powtec.2010.05.015.

Yuan, Zhi, Nima Khakzad, Faisal Khan, and Paul Amyotte. 2015. 'Dust Explosions: A Threat to the Process Industries'. *Process Safety and Environmental Protection* 98:57–71. doi: 10.1016/j.psep.2015.06.008.

CHAPTER 3

Summary

Chapter 2 presented the study of the inter-particle interactions in the Godbert-Greenwald furnace under cold-conditions. Chapter 3 aims to complete chapter with the study of the phenomena under hot conditions. At higher temperatures, the rate of pyrolysis and combustion reactions is faster, and they start to rule out the global process. Several samples of powdered biomass were dispersed in the setup, thus adopting operating conditions comparable to those of a dust explosion (dust cloud formation, small time scale, high heating rates). Reactions products were used to estimate a global conversion degree, and a dust cloud thermal profile was estimated thanks to experimental data and modelling. Furthermore, the versatility of this setup is also underlined by proposing modifications to collect the reaction products.

Resumé

Si le Chapitre 2 présentait une étude in situ des interactions interparticulaires dans le four de Godbert-Greenwald, le Chapitre 3 vise à l'étude des phénomènes à chaud. En effet, à des températures plus élevées, les réactions de pyrolyse et de combustion sont plus rapides, et elles commencent à régir le processus global. Plusieurs échantillons de biomasse en poudre ont été dispersés dans le montage, adoptant ainsi des conditions opératoires comparables à celles d'une explosion de poussière (formation d'un nuage de poussière, petite échelle de temps, vitesses de chauffage élevées). Les produits des réactions ont été utilisés pour estimer un degré de conversion global, et un profil thermique du nuage de poussière a été estimé à partir de données expérimentales et théoriques. De plus, comme dans le Chapitre 2, la versatilité de ce montage est soulignée en proposant des modifications pour collecter les produits de réaction.

Study of flash pyrolysis and combustion of biomass powders using the Godbert-Greenwald furnace: an essential step to better understand organic dust explosions

Matteo Pietraccini[1], Peter Badu[1], Theo Tait[2], Pierre-Alexandre Glaude[1], Anthony Dufour[1], Olivier Dufaud[1,*]

** Corresponding author: olivier.dufaud@univ-lorraine.fr*

[1] *Université de Lorraine, CNRS, LRGP, F-54000 Nancy, France*

[2] *Department of Chemical & Process Engineering, University of Strathclyde, G11XQ Glasgow, Scotland, United-Kingdom*

Abstract

An organic dust explosion is a heterogeneous system on a space and time scale. Predicting the parameters characteristic of its severity needs experimental and theoretical approaches to find the optimal compromise between consistency with reality and modelling time. A hybrid method is proposed to study flash pyrolysis and combustion of several organic powders (cellulose, wheat starch, oak wood, Douglas fir and olive pomace). A Godbert-Greenwald furnace was employed to perform the experiments to mimic the fundamental characteristics of a dust explosion: high particle heating rate, high reaction temperature and short residence times. It appears that, e.g. for cellulose particles greater than 200 µm at 973K, the residence time is too low compared to the pyrolysis characteristic time, leading to a limited conversion. At higher temperatures, secondary reactions of primary tars are evidenced, stressing the influence of the pyrolysis stage and leading to heterogeneous combustion. On the contrary, fine particles devolatilize quickly, generating little tar, which promotes homogeneous gas phase reactions. Therefore, various rate-limiting steps can be observed for the same dust

sample for broad particle size distributions. The gaseous phase's composition varied as a function of the powder nature and furnace temperature. If such influences were expected, differences in composition and reaction mechanisms were highlighted between dust layers or pyrolysis studies on non-powdered materials. Moreover, this study was carried out under conditions relevant to dust explosions. A lumped-kinetic model adapted to dust explosion was developed and validated for cellulose.

Graphical abstract

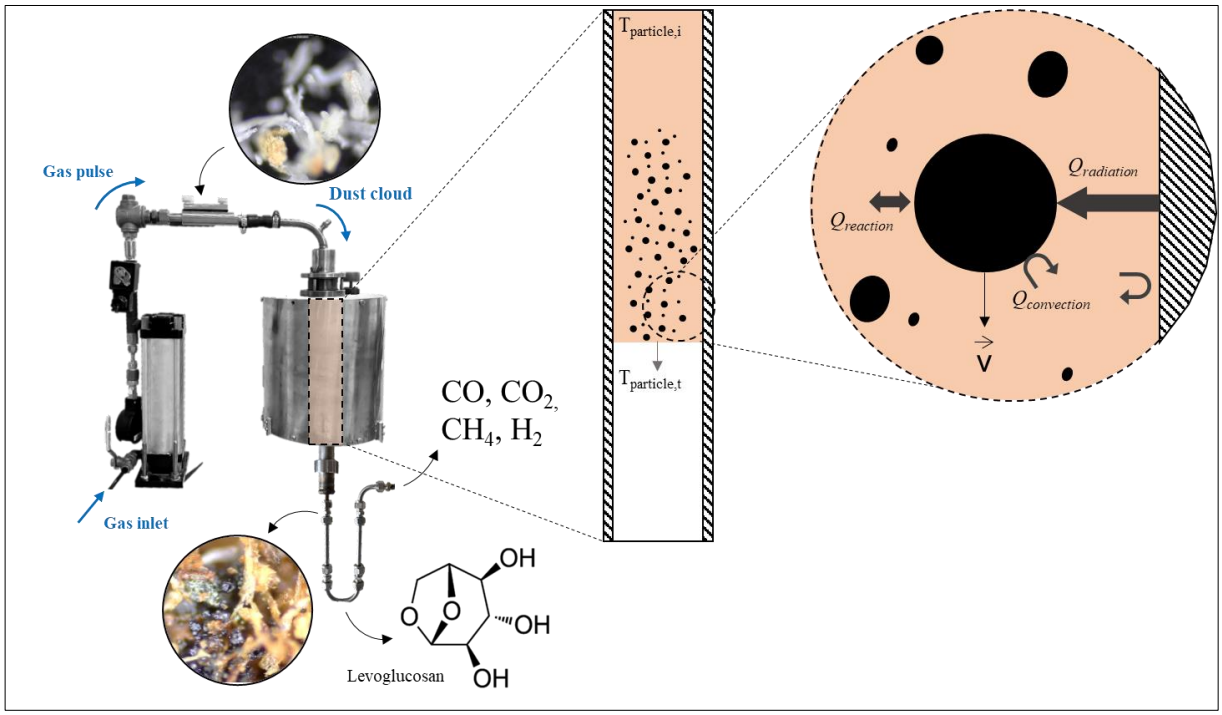

1. Introduction

The answer to the "simple" question asked by an industrialist or a health and safety officer "Can you predict the consequences of an explosion of this specific powder?" is far from obvious. Rephrasing this request, it means to ensure that, under all operating conditions of a process, it is possible to quantitatively evaluate the explosion severity of a product. A response based on a study performed only under standard conditions, although necessary, would not allow the diversity of industrial conditions encountered to be considered and reproduced.

Moreover, an exclusively experimental response would require a costly and time-consuming multiplicity of tests. Similarly, it is clear that the use of modelling, although potentially associated to an appropriate and relevant response, could not be successful without preliminary testing. For instance, Islas (Islas et al. 2022) proposed a three-layer method to study biomass dust explosions: by merging the CFD simulation of the dispersion process, ignition and flame propagation steps, experimental tests and general knowledge of the chemical mechanisms involved, it is possible to deepen the conclusions that may be drawn from an explosion experiment.

However, modelling a dust explosion means considering an impressive number of phenomena, some occurring in parallel, others in series, and all subject to complex interplays. In the case of an organic powder dispersed in air, it is necessary to consider, among others, the preheating of the particles (external radiation and convection, internal conduction), the pyrolysis stage, the mass transfers of gases (air-to-particle and pyrolysis gases-to-ambient gaseous phase), the oxidation reaction, the hydrodynamics of the flame, and the heat transfer from the flame. To study experimentally and independently each of these stages is illusory as they are interdependent. On the other hand, it seems relevant to dissect the explosion into simpler stages: particles heating, pyrolysis and oxidation to better model these three main phenomena. For each of these steps, it is important to estimate their characteristic times, the products involved and to propose global kinetic models.

The operating conditions play an essential role for these three phenomena, and it is therefore required to keep them identical, or at least very close, to what happens during a dust explosion. Therefore, thermogravimetry analysis (TGA), differential thermal analysis (DTA) or differential scanning calorimetry (DSC) are essential resources to study the thermal stability of powders. However, they cannot be used to mimic the reactions of particles dispersed in air, since the heating rate is greatly different. The ideal solution would be to study these explosions on site, under industrial conditions, but this is neither possible nor desirable. At the other end of the spectrum of potential solutions, focusing on the behaviour of a single particle subjected to rapid heat flux, even if this approach offers many advantages, omits all the particle-particle interactions that inevitably occur during an explosion. Finally, a 20 L explosion sphere, a standardised tool accessible in many process safety laboratories (ISO/IEC 80079-20-2 standard), does not, in its original state, allow either the study of the heating and pyrolysis stage or the rapid variation of the initial temperature of the particle cloud over a temperature range consistent with the pyrolysis stage, i.e. more than 300°C. Given these considerations, the use

of the Godbert-Greenwald (G-G) furnace to study the constituent steps of a dust explosion appears to be an interesting alternative, although not unique.

Several works exploited such apparatus for its simplicity and its versatility, for instance, to study complex explosible mixtures, such as coal-rock dust binary mixtures (Azam and Mishra 2019) and carbonaceous dust clouds in presence of CH_4, H_2 and CO (Tan et al. 2020). The influence of the G-G furnace on the cloud particle size distribution was carried out by Bu (Bu, Yuan, et al. 2020b), by identifying and quantifying the modification of characteristic diameters. Nevertheless, scientific literature lacks information regarding both the combustion kinetics and the thermal behaviour of a dust cloud in the G-G oven. For instance, Mittal (Mittal and Guha 1996) worked on the influence of particle size and dust concentration on the MIT of polyethylene fibres. They focused on the identification of the values associated with the worst-case scenario in terms of ignition sensitivity. They later developed a model based on a thermal balance and a single reaction involved in the autoignition of the dust cloud (Mittal and Guha 1997); the activation energy was equal to that of ethylene oxidation and the product of the oxidation enthalpy and reaction rate constant was computed from a single experiment data point. Chen (Chen et al. 2022) compared three models for describing the ignition of a dust cloud in a G-G furnace, detailing the choice of the reaction kinetic parameters used in their work, but without considering the particle heating step. Xu (Xu et al. 2017) focused on the determination of the MIT of coal dust and the kinetics of its combustion. Through thermogravimetry analyses (TGA) and the on-line analysis of the gaseous products, they enlightened that temperature and heating rate have an influence on the reaction rate. The operating conditions used in their work (heating rate, particle final temperature and sweeping gas) are nonetheless far from those typically encountered during an organic dust explosion. Finally, two models were proposed by Addai (Addai et al. 2016) to estimate the MIT of hybrid mixtures. They also showed that the models previously proposed by Krishna, Cassel and Mitsui showed good agreement for pure dust. However, the thermo-kinetic parameters are not made explicit and must be fitted, for each sample, from the MIT experiments.

This work is based on an original approach which consists in identifying the rate-limiting step of the explosion of organic dusts and proposing a simplified mechanism associated to a kinetic law representing this reactional stage, through experiments performed under conditions similar to those of dust explosions. Coupled with heat balances similar to those described in the previous paragraph, this approach aims to develop reaction schemes specific to dust explosions and which would be adaptable to different operating conditions without having to resort to a

systematic adjustment of thermo-kinetic parameters. In addition, this approach assesses the composition of the gases generated during the pyrolysis and combustion phases, which provides valuable information on the gas compounds to be considered for explosion or flame propagation models.

On theoretical and experimental grounds, a model for the particle heating as they fall through the Godbert-Greenwald furnace has been developed. The flash pyrolysis and combustion of five biomass powders were then studied at different temperatures using this apparatus. From the analysis of the collected gases, chars and tars, lumped kinetic mechanisms are proposed to model the constituent steps of the explosions. This study is, to our knowledge, the first report on a Godbert-Greenwald furnace tailored to study both biomass pyrolysis and combustion under relevant conditions for dust explosion.

2. Materials and Methods

2.1 Powder choice and characterisation

The powders chosen were wheat starch, cellulose, oak, Douglas fir and olive pomace. The two first represented pure components. The lignocellulosic materials are known for being chemically complex. Their peculiar behaviour is mainly due to the numerous interactions between the three main components: cellulose, hemicellulose and lignin. Liu (Liu et al. 2021) studied the explosion severity of several binary mixtures of these three and enlightened an overall strong influence of cellulose and lignin on the explosion overpressure. At the same time, hemicellulose seemed to play a more significant role in the rate of pressure rise.

Due to their well-known chemical homogeneity and their abundance, cellulose and starch were chosen as the reference powder samples. The samples used in this study were microcrystalline cellulose from DuPont (Avicel PH-101). Starch is the third most abundant biopolymer, behind only cellulose and chitin. It is broadly classified into three groups based on its origin: type A (from cereals), type B (from tubers, fruits and stem) and type C (from legumes and roots) (Li et al. 2019). In this work, a type A starch (from wheat) was purchased from Sigma Aldrich. Due to the current growing interest in biomass, three lignocellulosic materials were chosen for this study: Douglas fir (softwood), oak (hardwood) and olive pomace. The first two are woody biomasses harvested in the Haut-Beaujolais region (France), while the third one represents an abundant waste product in Mediterranean countries. The wood samples were

initially chunked into small-sized chips, excluding the bark, followed by knife milling (Retsch SM 300) at 1500 rpm. Powdered samples were later sieved for 5 minutes in an AS 200 vibratory shaker with 180 and 56 µm sieves.

The increasing heterogeneity of these five samples was meant to compare the fast oxidation of a pure component (such as cellulose and starch) to that of lignocellulosic materials, by subsequently adding complexity.

The particle appearance of the five powders was characterized by digital (a 5 Mp Dino-lite Pro HR digital microscope) and electronic imaging (JEOL JSM-649-LV Scanning Electronic Microscope or SEM) methods. Photos were also taken with a Canon 2000D to show their macroscopic appearance. The Particle Size Distribution (PSD) of the samples was determined by a Malvern Mastersizer 3000 equipped with an aero-dispersion unit.

Proximate analysis was performed on the five powders, determining their moisture content (MC), volatile matter (VM), fixed carbon (FC) and ash content. The MC was determined with a Mettler Toledo HE53 Moisture Analyzer: approximately 0.5 g of sample was placed in the apparatus and heated at 105°C for 15 minutes by an IR lamp, to determine the water mass loss and thus the humidity of the powder. VM and FC were calculated by thermogravimetric analysis (TGA) in a Mettler Toledo TGA STARe System. The temperature profile was: 105°C for 30 min, then 15 $K.min^{-1}$ up to 900°C, 10 min at 900°C under N_2 and finally 20 min under air at 900°C. This specific temperature profile (reported in Figure S 3 in Annex 2) was used to determine the Volatile Matter (VM) and the Fixed Carbon (FC) of the selected powders. The volatile matter was calculated by subtracting the mass of the sample at 40 min (when the curve reached a plateau after the dehydration step, at 105°C) and 100 min (when the flow gas was switched to air, at 900°C), and normalizing by the mass at 30-40 min. By knowing the Moisture Content (MC), the volatile matter and the ash content, it was possible to calculate the fixed carbon with the following formula:

$$FC = 100 - MC - VM - ash \quad (1)$$

By changing the carrier gas from nitrogen to air, it was possible to differentiate the VM from the FC. Moreover, by exploiting the curves obtained by thermogravimetric analysis, it was also possible to determine the pyrolysis onset temperature T_{onset}. The ash content was assessed with the aid of a Nabertherm B150 oven: samples were weighed, placed in the furnace, heated to 950°C for 4h and then weighted again. The ratio between the residual and the initial mass corresponds to the ash content.

2.2 Modified Godbert-Greenwald furnace

Experiments were carried out in a Godbert-Greenwald furnace, usually employed for the determination of the Minimum Ignition Temperature (MIT) of a dust cloud, according to the ISO/IEC 80079-20-2 standard (ISO/IEC 80079-20-2 2016a). The original G-G furnace was equipped with two coaxial Inconel cylinders to ensure its airtightness, and modified to offer the possibility to collect the products generated by both pyrolysis and combustion, i.e. the solid residues (char), condensable products (tar) and permanent gases. The experimental setup is schematised in Figure 3-1.

The powder was dispersed into the vertical tubular furnace by a gas pulse. Argon was used for the pyrolysis test, whereas air was used for the combustion tests. Before each test, the setup was flushed for approximately five minutes with argon to remove residual air and moisture. To check the airtightness of the apparatus, blank tests were performed without dust.

Oxygen and nitrogen concentrations in the collected gas were analysed by micro-Gas Chromatography (GC), considering the maximum allowable concentrations equal to 0.5 and 2 vol%, respectively. These last were imposed by the air tightness of the experimental setup, which did not allow a 0%-oxygen atmosphere to be reached. Placed just after the heated chamber, a double-layered round metallic 2 mm mesh (10 mm diameter) allowed to sample the solid residues. The condensable fraction was sampled in a U-shaped tube, which was externally cooled by isopropyl alcohol at -30°C (by mixing isopropanol with liquid N_2) in a Dewar. The gaseous products were collected in a collapsible Tedlar bag for analysis. To study the influence of the reactor temperature, experiments were performed at 700, 800 and 900°C. These temperatures (700, 800, 900°C) always refer to the reactor wall temperature and not the particle temperature within the oven, which remains unknown. Several factors came into play to choose these temperatures:

- The MIT of the chosen organic powders (beyond which the combustion can occur);
- The small residence time of the dust cloud in the heated chamber (which must be coupled to temperatures high enough to allow the particles to heat rapidly);
- The exothermicity of the combustion phenomenon (whose contribution to the heating process leads to high flame temperature, which is no longer related to the reactor temperature);
- The maximum temperature that can be reached by the oven (950°C).

For each temperature, 0.2 g of sample was dispersed in the pre-heated chamber, to attain an average dust concentration in the heated chamber of about the stoichiometric value, associated to the combustion of the selected materials. The stoichiometric concentration depends on the powder nature but, since the actual dust concentration varies with time and space as a function of the operating conditions (injection pressure, residence time), it is illusory to adjust "precisely" the nominal concentration (mass of powder divided to the furnace volume) with the theoretical stoichiometric concentration. Previous tests aiming at determining the minimum ignition temperature of the powders showed that the "most vigorous ignition" (ISO/IEC 80079-20-2 2016a) was mainly obtained for the 0.2 g of sample. Moreover, larger amounts of powder would have led to significant deposits of unreacted powder inside the setup. Finally, the dust container was designed to allow the full dispersion of the powder (less than 10 wt% dust remaining in the container after injection).

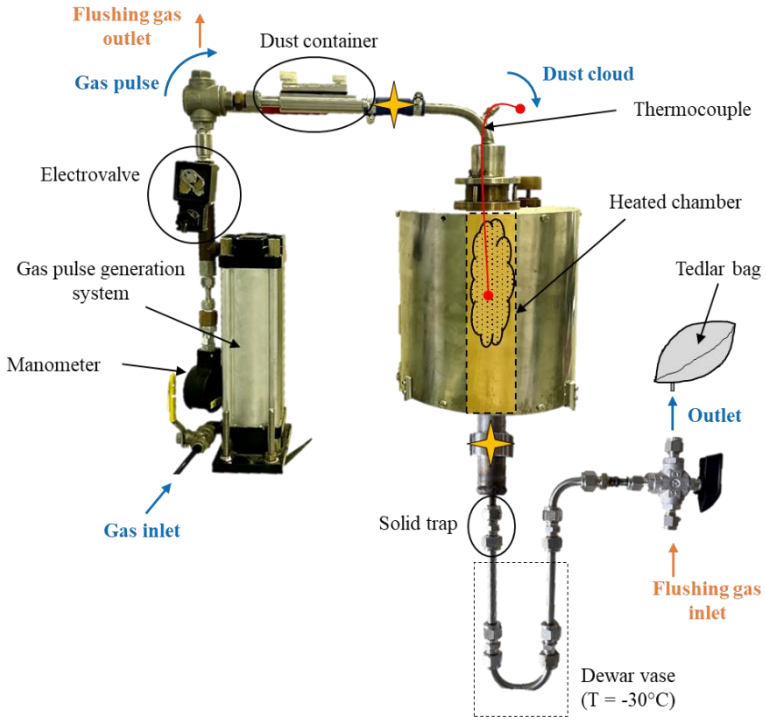

Figure 3-1 - The modified configuration of the Godbert-Greenwald furnace. The yellow stars indicate where the in-situ PSD analysis was performed

The test procedure was repeated fivefold to obtain enough solid and condensable residues for the follow-on analyses. Gaseous products were analysed only for the first dispersion, to avoid contamination by the unreacted powder deposits from the previous dispersions.

The adequate residence time of the dust cloud was obtained by determining the optimum point between an efficient dispersion and enough high degree of conversion. The former is associated with the pressure pulse applied to ensure the dispersion of all of the powder. The latter is associated with the residence time of the particles in the reactor. These two factors are conflicting. A high-speed camera (Mikrotron MotionBLITZ Eo Sens mini, set to an acquisition rate of 200 fps) was employed to find the optimum gas pulse pressure value. It was placed in front of the experimental setup to record the dust cloud's inlet and outlet times, whose difference was used as an estimation of the average residence time of the dust cloud (MotionBLITZ Director2 operator software was used for the high-speed video treatment). By rapidly dispersing the powder samples into the vertical tubular furnace and varying the dispersion pressure (from 1.3 to 1.8 bars), dust residence times within the range of 150 - 200 ms were determined. A dry in-situ dispersion study was also performed with a Helos laser diffraction sensor (Sympatec) at two different levels of the experimental setup (indicated by a yellow star in Figure 3-1). This analysis allowed to monitor the particle size distribution (PSD) of the dust cloud as well as the optical concentration as function of time. This analysis aimed to highlight the agglomeration phenomena of the powders, but also to estimate the residence time range associated to the highest concentration of particles. Analyses were performed thrice for repeatability purposes.

2.3 Thermal study of the dust cloud

After the dispersion, the dust cloud passes through the heated chamber and the temperature of the particles starts to rise. To distinguish and compare the heating and the reaction time, a heat transfer model was developed. Hence, the particle temperature profile along the vertical chamber was determined. Based on the procedure proposed by Piskorz (Piskorz et al. 2000b), the following particle heat balance was built:

$$\frac{1}{4}\pi d_p{}^2 L\,\rho_s C_{ps}\frac{dT_p}{dt} = \dot{q}_{rad} + \dot{q}_{conv} + \dot{q}_{reac} \quad (1)$$

$$\frac{1}{4}\pi d_p{}^2\, L\,\rho_s C_{ps}\frac{dT_p}{dt} = F\varepsilon\sigma\,\pi d_p L\left(T_w{}^4 - T_p{}^4\right) + h\pi d_p L\left(T_w - T_p\right) + \Delta H_p k_r \rho_s \frac{1}{4}\pi d_p L \quad (2)$$

where $\dot{q}_{rad}$ is the radiative heat transfer, $\dot{q}_{reac}$, the reaction heat contribution and $\dot{q}_{conv}$, the convective or conductive heat transfer. The shape of the cellulose particles was approximated with a cylinder to consider its fibrous and elongated structure, associated with a diameter d_p and a length L.

The value of $\dot{q}_{conv}$ can be adjusted as a function of the limiting heat transfer mode. If the Biot number Bi is greater than 1, the internal heat transfer limits the overall heat transfer;

whereas if Bi is lower than unity, the particle conversion is limited by the external heat transfer and the particle is thus deemed "thermally thin". Calculations were done based on the physical properties of the cellulose sample.

$$Bi_{conv} = \frac{h\,d_p}{\lambda} < \frac{d_p}{\lambda}.F\varepsilon\sigma\,\frac{(T_w{}^4 - T_p{}^4)}{(T_w - T_p)} = Bi_{rad} \ll 0.2 \quad (3)$$

Considering a wide range of particle (T_p) and furnace (T_w) temperatures, the convective Biot number is always lower than the radiative Biot number, which is lower than 0.2, as reported in Equation (3). In such a case, the particles are considered to have a uniform temperature, which is consistent with the study of Piskorz (Piskorz et al. 2000b).

According to the shrinking-core theory, the particle size decreases as the pyrolysis processes progress and, assuming a cylindrical particle, the following equation was added to the system:

$$\frac{d(d_p)}{dt} = -k_p\frac{d_p}{2} = -\left\{A.\exp\left(-\frac{E_a}{RT_p}\right)\right\}\frac{d_p}{2} \quad (4)$$

Equations (2) and (4) were solved simultaneously with Matlab (Mathworks), for the three selected wall temperatures. The values used for the calculations are reported in Table 3-1. The emissivity of Al_2O_3 ceramic (G-G furnace wall) is approximately 0.90, varying as a function of the temperature. It is also the case of oxidized Inconel which was used as inner tube: its emissivity exceeds 0.8 as soon as the temperature reaches 600°C and reaches 0.88 at 900°C (Greene et al. 2000). Therefore, the value chosen for the calculation was 0.9.

Table 3-1 - Parameters used for solving the particle heat balance system

Parameter	Value	Unity	Source
d_p	20 – 100 – 200	µm	Determined experimentally
ρ_s	700	$kg.m^{-3}$	Lédé and Authier 2015
C_{ps}	1758	$J.mol^{-1}.K^{-1}$	Piskorz et al. 2000b
F	1	-	Geometrical consideration
ε	0.9	-	Greene et al. 2000
h	30	$W.m^{-2}.K^{-1}$	Dufour et al. 2009b
ΔH_p	335	$J.kg^{-1}$	Piskorz et al. 2000b
E_a	197300	$J.mol^{-1}$	Piskorz et al. 2000b
A	$2.83 \cdot 10^{19}$	s^{-1}	Lédé and Authier 2015

2.4 Product characterization

For all samples, a global mechanism composed of three steps was employed to describe the reactions involved: primary pyrolysis, secondary pyrolysis and oxidation. The products of the pyrolysis and combustion tests were characterized, to collect information concerning the three steps. This lumped multistep reaction scheme is represented in Figure 3-2.

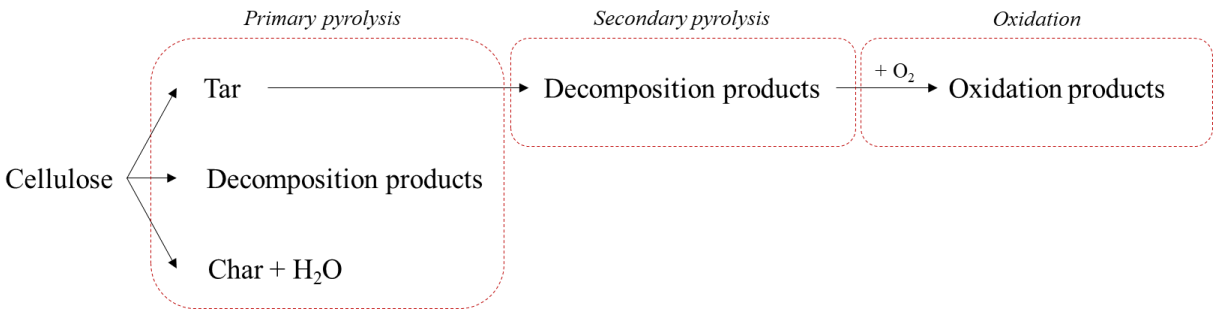

Figure 3-2 - Cellulose lumped combustion multistep mechanism.

2.4.1 Solid products

The solid products (partially converted biomasses) sampled by the trap after the heated chamber were analysed using a 5 Mp Dino-lite Pro HR digital microscope and a JEOL JSM-649-LV Scanning Electronic Microscope. The information obtained was used to characterize their appearance, colour, shape and morphology.

Complementary information about the solid residues was obtained through FT-IR absorbance (Bruker Optics SARL Alpha P) and thermogravimetric analysis (Mettler Toledo, TGA - STARe System thermogravimetric balance). Between 6 and 10 mg of solid residue samples, collected at each temperature were heated from 30° to 950°C at 15°C/min. Experiments were conducted under a nitrogen atmosphere at 1 bar and with a 100 mL/min flowrate.

2.4.2 Condensable product characterization

The condensable fraction collected in the U-shaped tube after the heated chamber was rinsed and solubilized in methanol. 1 µL of 1-tetradecene was added as an internal standard, the solution was filtered with a 0.45 µm pore filter and analysed by a GC-MS, equipped with a FID detector (Agilent 7890A System equipped with a 5975C Triple-Axis detector). Results

were used to determine the most accurate tar-representing molecule in the pyrolysis step for the fast combustion model.

2.4.3 Gaseous product characterization

Pyrolysis and combustion gases were analysed by micro gas chromatography (SRA 3000 µGC equipped with a TCD detector, 3 ways). Permanent gases (CO, CO_2, CH_4, H_2, O_2 and N_2) were measured, as well as some aromatics (benzene, toluene and xylene isomers) and some light hydrocarbons (C_2H_2, C_2H_4 and C_2H_6).

2.4.4 Flash pyrolysis and fast combustion models

The aforementioned multistep reaction system (Figure 3-2) was used to describe the kinetic behaviour of the powders. Results concerning condensable and gaseous products were used to select the most abundant chemical species to be considered in the construction of this mechanism. The main objective of this model is to determine the kinetic parameters (activation energies and pre-exponential factors) of the selected reactions from experimental data.

3. Results and discussion

Figure 3-3 presents the appearance of the powder samples, as well as the colour, shape and surface morphology of the particles. SEM and digital images allowed to underline the importance of two main aspects: the shape of the particles and the heterogeneity of the samples. As for cellulose, oak and Douglas fir, the fibrous character conferred by the cellulose chain results in elongated particles, in which the characteristic length for heat and mass transfer is most probably the thickness, i.e. the smaller dimension (between 20 and 50 µm for cellulose). Oppositely, wheat starch and olive pomace particles are associated with higher sphericity, in which the key length is the diameter. Moreover, from cellulose and starch to olive pomace, an increasing heterogeneity of the particles is noticeable. Table 3-2 reports some characteristic diameters (D10, D50 et D90) and the pyrolysis onset temperature T_{onset} of the powder samples (obtained by the starting point of mass loss from TGA). Except for wheat starch, the PSD characteristic dimensions are in the same order of magnitude. Furthermore, as expected, the chemical nature of the powders seems to influence the pyrolysis onset temperature: as the complexity of the tested material increases (from cellulose to olive pomace), pyrolysis starts at lower temperatures. This can be associated with the higher reactivity of hemicelluloses and lignin compared to cellulose and to mineral catalytic effects. Figure 3-4 shows the proximate

analysis of the samples. Variations in the volatile matter (and thus in the fixed carbon) depend on the composition and content in lignin, cellulose and hemicellulose (Pu et al. 2013; Zoghlami and Paës 2019). Yee Wen Chua (Chua et al. 2021) mentioned a sensible discrepancy between the ratio VM/FC of cellulose and lignin, respectively equal to 10.9 and 1.3. Olive pomace presents a higher ash fraction which is mainly due to the contribution of the olive stone to the overall mineral content of this sample (Salem et al. 2007). It was not possible to determine the volatile matter and fixed carbon fractions of wheat starch due to its tendency to form a foamy structure during the heating process, which was not compatible with the analysis in the thermo-balance.

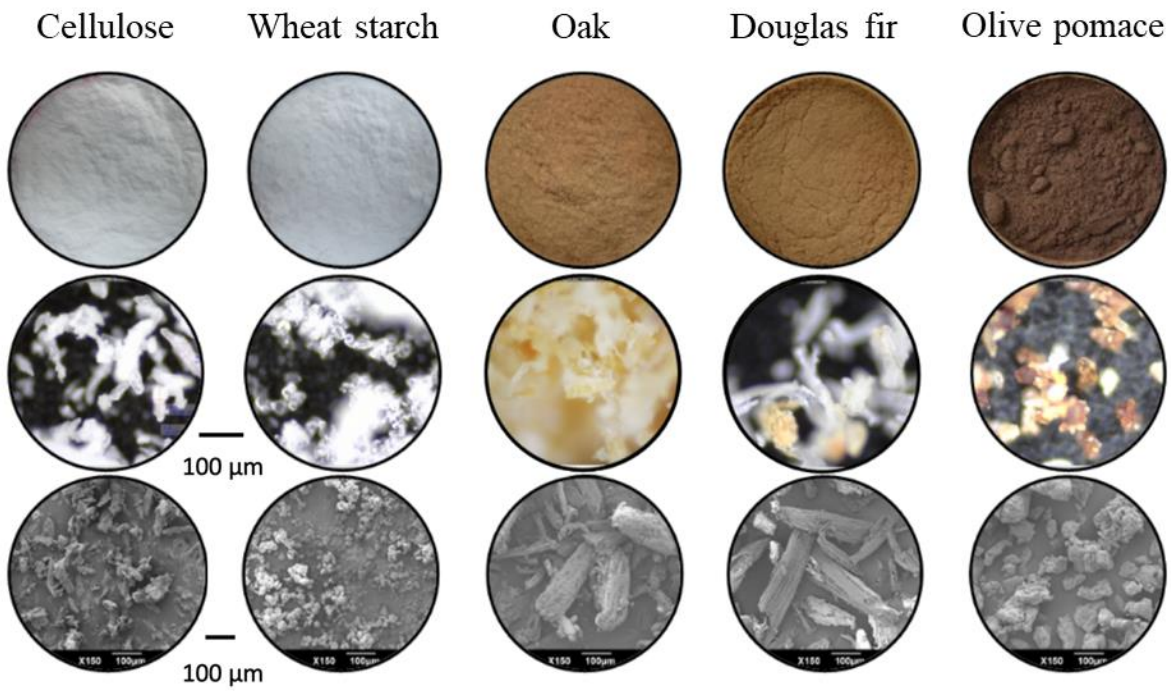

Figure 3-3 - Appearance (top-row), digital (middle-row) and SEM (bottom-row) images of the powder samples.

Table 3-2 - Characteristic PSD diameters and pyrolysis onset temperature of the samples.

Sample	D10 (µm)	D50 (µm)	D90 (µm)	T_{onset} (°C)
Cellulose	21	59	140	305
Wheat starch	12	20	33	-
Oak	20	51	107	264
Douglas fir	19	48	86	292
Olive pomace	24	59	102	176

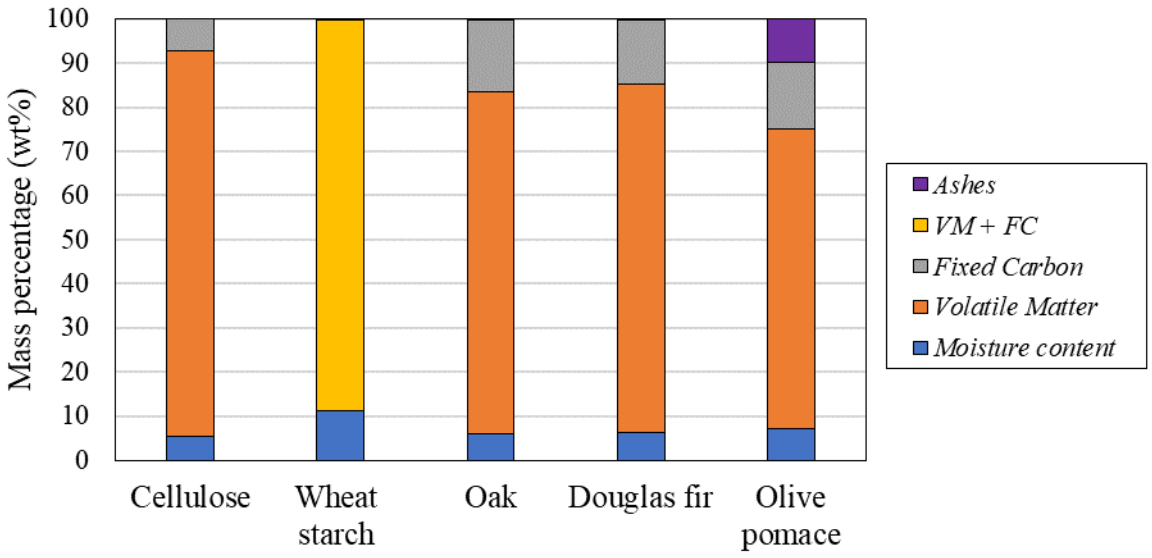

Figure 3-4 - Proximate analysis of the powder samples

3.1 Dust cloud thermal study

The thermal evolution of a cellulose cloud in the G-G furnace was studied. Results are reported in Figure 3-5 and 3-6. The heating of the cellulose fibres is linear in time and then reaches a semi-plateau around 600-700K after triggering pyrolysis reactions. The pyrolysis onset temperature was determined experimentally around 578K for cellulose (as reported in Table 3-2), which is lower than the results obtained with the particle heat balance. Piskorz at al. (Piskorz et al. 2000b) presented a similar particle temperature profile, with a plateau around 700-800K. The discrepancy with their work is likely due to the different reactor temperature (i.e. 1373K) and particle size (two sieved fractions of Avicel ph 102 were used in their work, significantly coarser than the Avicel ph 101 used in this work). The particle then decomposes in a quasi-isothermal way, which leads to the shrinking of the particle. As the fibre thins, its surface-to-volume ratio increases, and both the radiative and convective heat transfer become more significant than pyrolysis. Thus, the particle temperature shows a slight increase.

For the temperature values considered (from 973 to 1173K), the time scale of the pyrolysis step is always higher than the one associated to the particle heating. The initial thickness of the cellulose fibres was set at 20, 100 and 200 µm to enlighten the diversity of the particle size in the dust cloud. A complete conversion of the particles may be attained between 160 and 1400 ms at 973K, and between 70 and 650 ms at 1173K. It clearly shows a considerable heterogeneity of the global conversion degree in space and time, which was expected for a

highly heterogeneous system as a dust cloud. The literature provided scattered values for the pyrolysis reaction enthalpy. Since it is a crucial parameter for the particle heat balance, a sensitivity analysis was carried out to determine its influence on the profiles reported in Figure 3-5 and 3-6. Results are reported in Figures S 7, S 8, S 9 and S 10 in Annex 2.

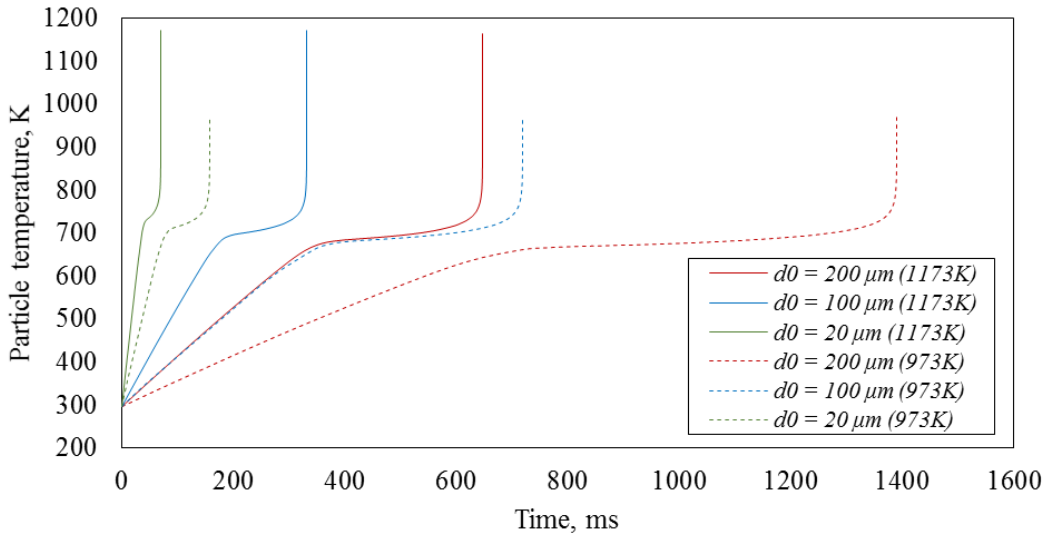

Figure 3-5 - Time-evolution of the particle temperature when exposed to a set temperature in the G-G furnace.

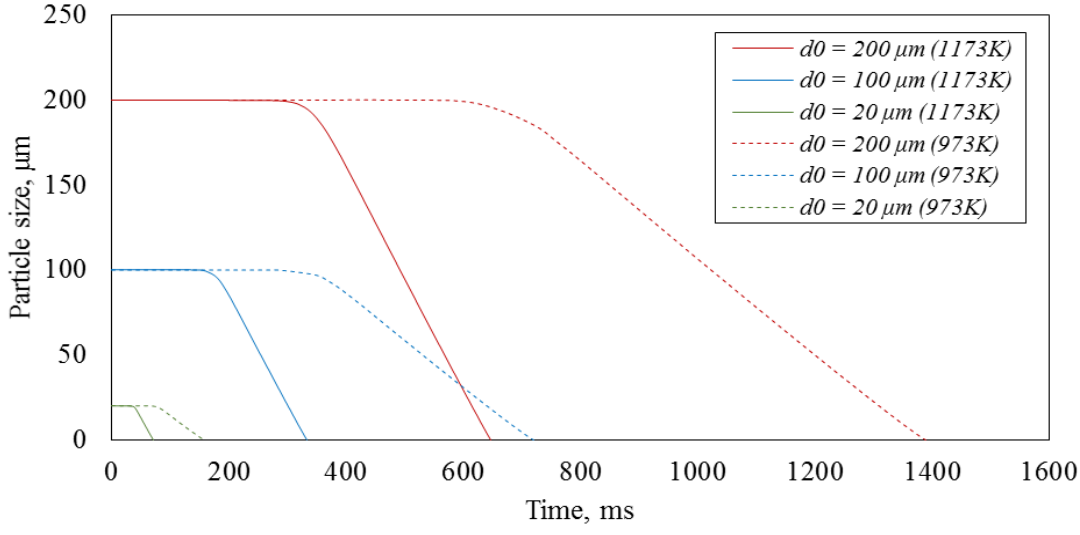

Figure 3-6 - Time-evolution of the particle size when exposed to a set temperature in the G-G furnace

Figure 3-7 reports the time evolution of the particle temperature and the optical concentration associated with the dust cloud passing through the heated chamber. The optical concentration was measured at the heated chamber's inlet and outlet, respectively referred to as "top" and "bottom". A high-particle concentration zone was identified between 0 and 300 ms, approximately. By overlapping the particle temperature profiles (calculated for an intermediate size of 100 µm at 973 and 1173K) and the optical concentration curves, it seemed that, even though particles reached the pyrolysis onset temperature before exiting the furnace, the quasi-isothermal plateau around 700K is attained only after. The second layer of information is associated with the optical concentration, i.e. the extinction level of the laser sensor, which is proportional to the total volume of the particles crossing the laser beam at a given time (GmbH and Pulverhaus). Focusing on the optical concentration associated with the dust cloud exiting the heated chamber (which is considered the most representative of the dust cloud inside the heated chamber), it is then possible to estimate the region where particles react and generate the products subsequently collected and analysed. Figure 3-7 shows that at 1173K, less than 75% of the 100 µm particles have a sufficiently long residence time in the Godbert-Greenwald furnace to reach their pyrolysis temperature. The study of the temporal evolution of the particle size distribution shows that the particles with the shortest residence time are agglomerates or large fibres (see Figure S 4, Figure S 5 and S 6 in Annex 2), mainly due to the inertial effect. These particles being characterized by a higher pyrolysis time scale; hence, they exit the heated chamber only partially pyrolyzed, which will be confirmed by analysing the solid residues in section 3.2. Figure 3-7 also shows that at a temperature of 973K, 100 µm particles would not reach the MIT until 83% of the powder has already left the furnace, which greatly limits the probability of propagation of the potentially created flame core. Previous authors had observed similar behaviours, but without characterising the residence times and particle size distributions. For example, Mishra and Azam (Mishra and Azam 2018) concluded that large coal particles were barely ignitable even at temperature higher than 850 °C due to their low residence time in the G-G furnace. This original experimental approach allows the determining of the actual residence time of each granulometric class and an estimation of the pyrolysis efficiency and thus, of an ignition likelihood. It should also enable to adjust the test parameters to the properties of the powders in a relevant manner for the determination of the MIT.

It must be stressed that this approach has some limitations, especially because the PSD and hydrodynamic analyses were performed on dust clouds at ambient temperature. Moreover, a dust cloud is a heterogeneous entity in space and time, which at high temperature induces a non-homogeneous temperature field, in turn leading to a non-homogeneous conversion degree of the solid phase. Furthermore, the conversion of cellulose at high temperatures forms an intermediate and sticky liquid (Boutin et al. 1998; Dufour et al. 2012) which may induce particle agglomeration.

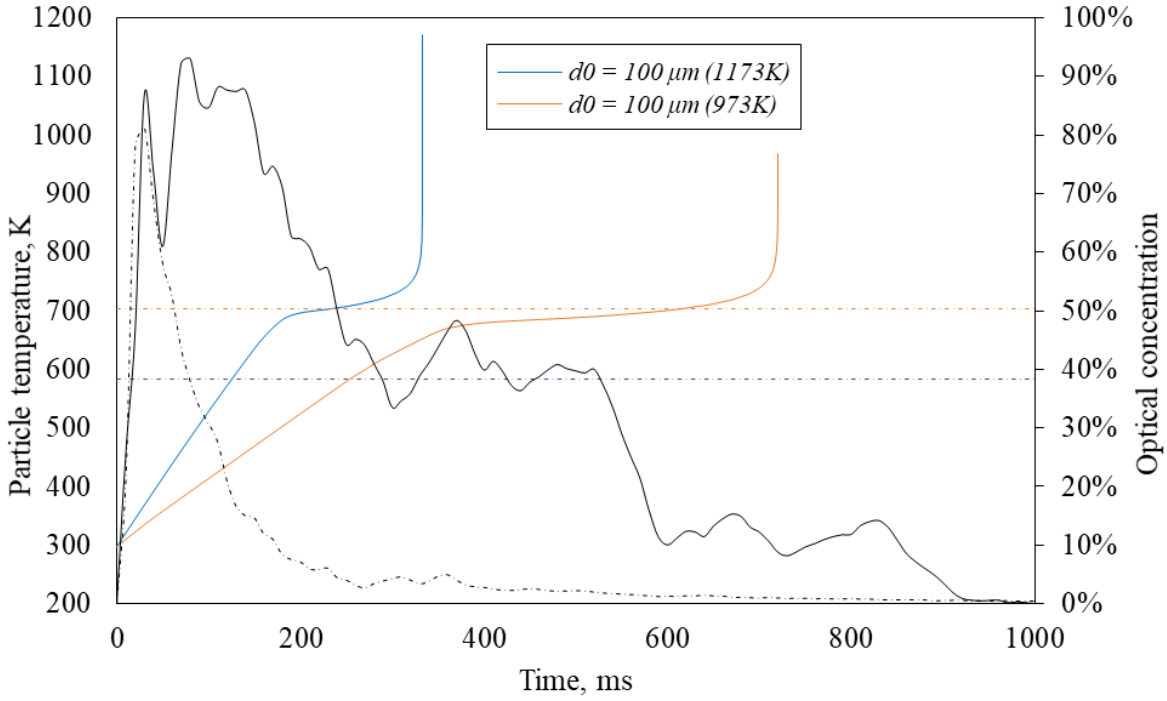

Figure 3-7 - Time-evolution of the particle temperature and the optical concentration obtained before and after the heated chamber (100 µm cellulose).

3.2 Solid products

Figure 3-8 and 3-9 show the digital and SEM images of the solid residues sampled after the heated chamber during pyrolysis tests of cellulose and starch, respectively. They were chosen to be as much representative as possible of the samples collected. As expected, essential changes in the colours of the particles can be noticed in both samples, representing the first qualitative analysis of the global conversion degree of the particles. However, the presence of white or unconverted particles also shows that pyrolysis was not complete for both powders, whatever the temperature. Such a simple and visual analysis allows for example to confirm the value of the pyrolysis onset temperature, approximately 600 K, under the conditions of a dust

explosion (dispersed powder) which are different from those encountered for powder layer (e.g. by TGA).

It is also interesting to notice the high heterogeneity in particle conversion depending on their particle size and their apparent residence time in the G-G furnace. This observation is in good agreement with the modelling and sensitivity results (Figure 3-11), and Figure S 7 and S 9 in Annex 2) showing that particles bigger than 100 µm need a longer residence time to be converted than the dust cloud average value measured in the modified G-G furnace.

A major difference between the thermal behaviour of starch and cellulose dust cloud is clearly perceptible by observing the SEM images. Although cellulose particles tend to form agglomerates as the reactor temperature increases, starch particles show a significantly higher tendency to create even larger clusters. This might be related to a higher formation of the liquid sticky intermediate by starch.

Moreover, the SEM imaging pointed to a modification of the particle surface morphology, as well as an increasing tendency to agglomeration/melting with the reactor temperature, which is related to a higher conversion of cellulose or starch to the intermediate liquid. The high importance of the intermediate liquid formation during cellulose pyrolysis was studied in detail by Dufour (Dufour et al. 2011). This intermediate liquid even controls the global pyrolysis rate of cellulose under fast heating conditions (Boutin et al. 1998; Dufour et al. 2012). SEM images also showed that fine particles react rapidly, even at 700°C. The length of the cellulose fibres is nearly unchanged when the temperature reaches 700°C, whereas it is reduced by approximately 20% and more than 50%, when the temperature rises up to 800 and 900°C, respectively. At the same time, the number of fine particles decreases significantly. Similar tests were performed also with wood powders and olive pomace and show similar trends. For instance, the visual qualitative analysis of the Douglas fir residues, in Figure 3-10, allowed to notice that the presence of char is more and more visible when the temperature increases, especially at 900°C (inducing a higher heat flux brought by the reactor to the surface of the particles). It is worth noting that char is surrounded by a layer of tar, pierced by bubbles. Aerosol release as well as tar cracking of oxygen containing compounds, which occurs from 700 to 850°C, can be responsible for such irregularities; cracking of aromatic compounds occurring at higher temperatures (Vreugdenhil and Zwart 2009). In parallel, the length of the fibres shortens and the residual particles agglomerate.

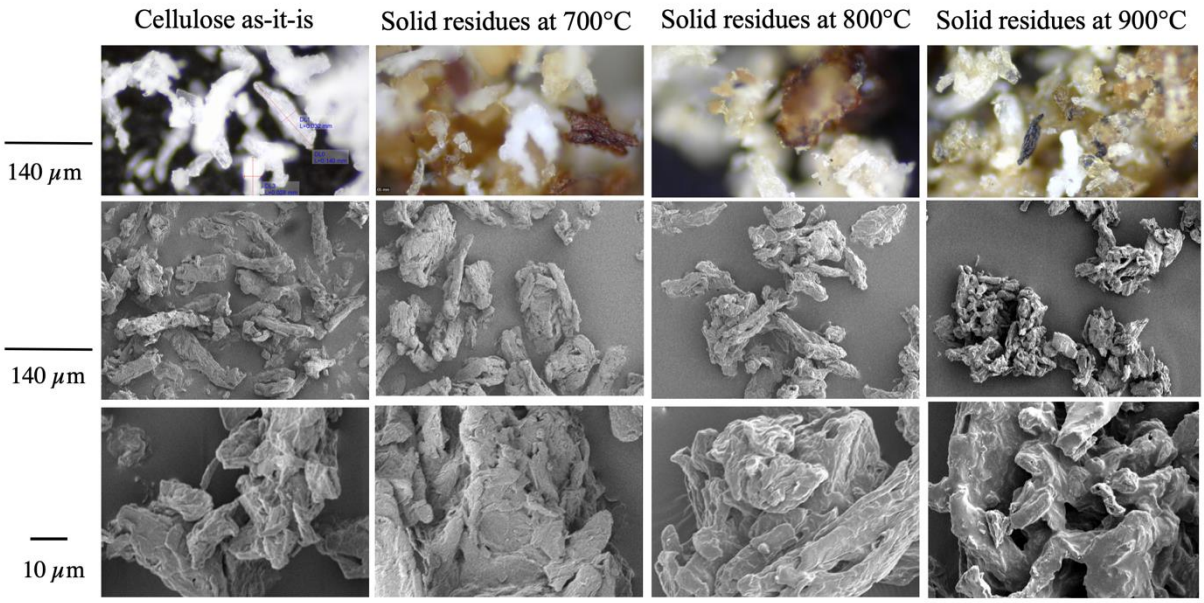

Figure 3-8 - Digital and SEM images of the cellulose sample (as-it-is, to the left) and the pyrolysis solid residues as a function of the furnace temperature.

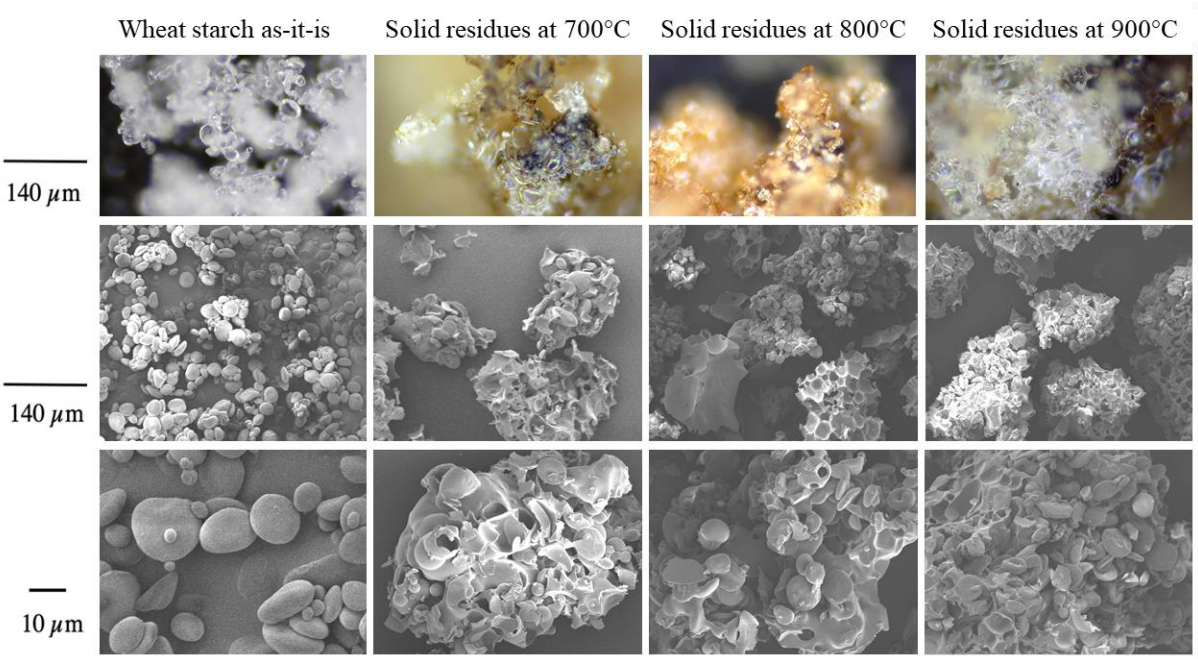

Figure 3-9 - Digital and SEM images of the wheat starch sample (as-it-is, to the left) and the pyrolysis solid residues as a function of the furnace temperature.

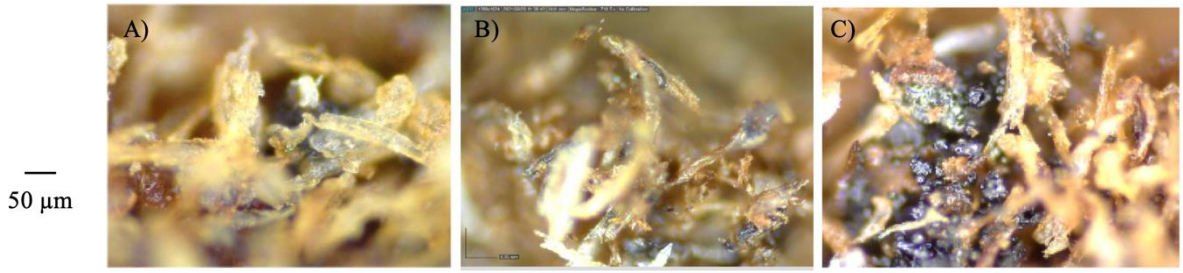

Figure 3-10 - Digital pictures of the solid residues collected for Douglas fir at A) 973K, B) 1073K and C) 1173K.

These results are consistent with the model. In fact, it shows (Figure 3-11) that even a 100 µm thick cellulose fibre would not be completely pyrolyzed after an average residence time of approximately 200 ms in the oven at 1173K (which corresponds to the average residence time determined by the high-speed video approach). Obviously, thicker particles, e.g. 200 µm fibres (i.e. cellulose agglomerates), essentially have time to heat up but not to pyrolyze for residence times below 650 ms. They might represent the white particles noticed in the microscopic observations in Figure 3-8.

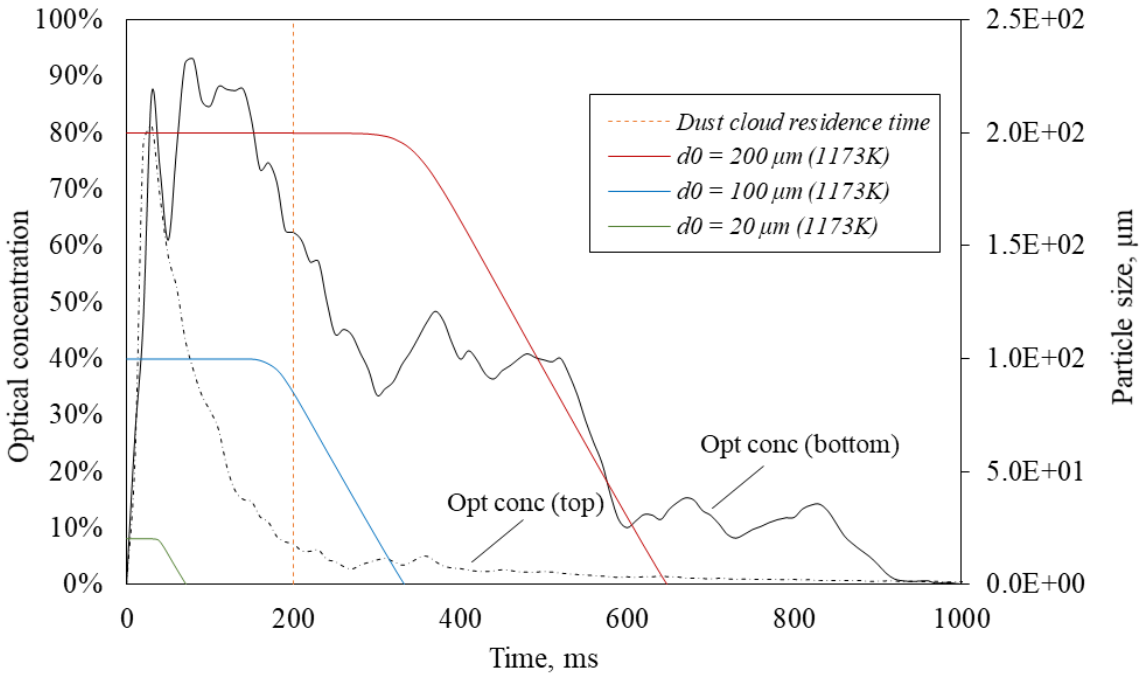

Figure 3-11 - Time-evolution of the particle diameter during their dispersion in the G-G furnace at 1173K, determined for three values of initial particle size (cellulose). The optical concentration was determined experimentally, before and after the heated chamber.

An attempt to quantify the global conversion of cellulose particles collected at the outlet of different reactor temperatures by comparing their volatile content (by TGA) was made. However, tests showed trivial discrepancies (see Annex 2 – Figure S 11 and Figure S 12). Minor differences were noticed in the thermal behaviour of the residues regarding the onset temperatures, the mass loss and the overall trend. At the end of the analysis (at a temperature equal to 950°C), the mass volatilized in the three samples was 89.7%, 94.0% and 92.0% (±0.1%) for respectively the residue collected at 700, 800 and 900°C. The discrepancy between these results is comparable with the sensitivity of the thermo-balance, which leads to the conclusion that there was no significant difference in the volatile matter of the pyrolysis residues. Nevertheless, it should be noted that the onset temperature of the residues appears to be slightly lower than pure cellulose (approximately 305°C), which might demonstrate a partial depolymerization of cellulose. Finally, a major difference between solid residues and raw cellulose is noticeable around 500°C. The rapid pyrolysis of the particles in the vertical chamber of the G-G furnace seems to lead only to a partial conversion of the dust cloud (especially the finer particles), which is in line with the observations given in Figure 3-8 and Figure 3-11.

To better understand the chemical conversion of cellulose as function of reactor temperature, the chemical structure of the different cellulose residues was analysed by FTIR spectroscopy. Figure 3-12 reports the FT-IR absorbance spectra of the cellulose pyrolysis solid residues. Three main regions were considered for the comparison of the samples. The peak around 3300 cm^{-1} corresponds to the O-H stretching associated with H-bonded hydroxyl groups (Janu et al. 2021; Pastorova 1994). The intensity of the signal increased with the reactor temperature, which can be related to the increasing accessibility (i.e. an increasing vibration freedom) of the cellulose-chain OH-groups. The peak around 2900 cm^{-1} is associated with the symmetric aliphatic C-H stretching (Behazin et al. 2016; Janu et al. 2021; Pastorova 1994), whose intensity also increased with the reactor temperature. The last region, between 1600 and 1800 cm^{-1}, is associated with the aromatic C=C and the ketones C=O stretching. This double peak is characteristic of the presence of char, as presented by D'Acierno (D'Acierno 2021), which supports the observations made from Figure 3-8. The increasing bands around 3300, 2900, 1400 and 1040 cm^{-1} were the typical infrared absorption carbohydrate peaks (Wang 2016), which is related to depolymerized cellulose occurring in the primary pyrolysis of cellulose. Pastorova (Pastorova 1994) characterized cellulose biochars obtained at different temperatures (from 250 to 390°C) through their FTIR spectra. Three FTIR characteristic bands proposed in their work can be related to the increasing temperature. The first one is the 2800-

3000 cm^{-1} region. It does not vary from 250 to 310°C but, for a reactor temperature of 390°C, the peak increases significantly, which is consistent with the spectra shown in Figure 3-12. The second band is the double peak between 1600 and 1800 cm^{-1} that was also observed in this work. It steadily increases with temperature, even though the intensity of the signals between this work and Pastorova's is not of the same order of magnitude. Lastly, the peak at 1080 cm^{-1} is related to the pyranose ring skeletal vibrations, which is associated to the integrity of the cellulose. Although it is less intense than the others, in the spectra this peak's intensity decreases with the reactor temperature, showing an increasing conversion degree of the cellulosic chain.

In brief, the analysis of the solid residues allowed to identify key points of the flash pyrolysis of organic powders in suspension:

- The first step of depolymerisation of cellulosic compounds cannot be neglected when proposing reaction mechanisms;
- Flash pyrolysis leads to the production of aerosols and/or non-condensable gases generated from the cracking of tar, which modifies the morphology of particles during the reaction (surface cavities for cellulose, hollow shells for starch);
- The low proportion of char observed in the solid residue, even at 900°C, is a notable difference from low heating rates pyrolysis processes, which lead to high char yield.

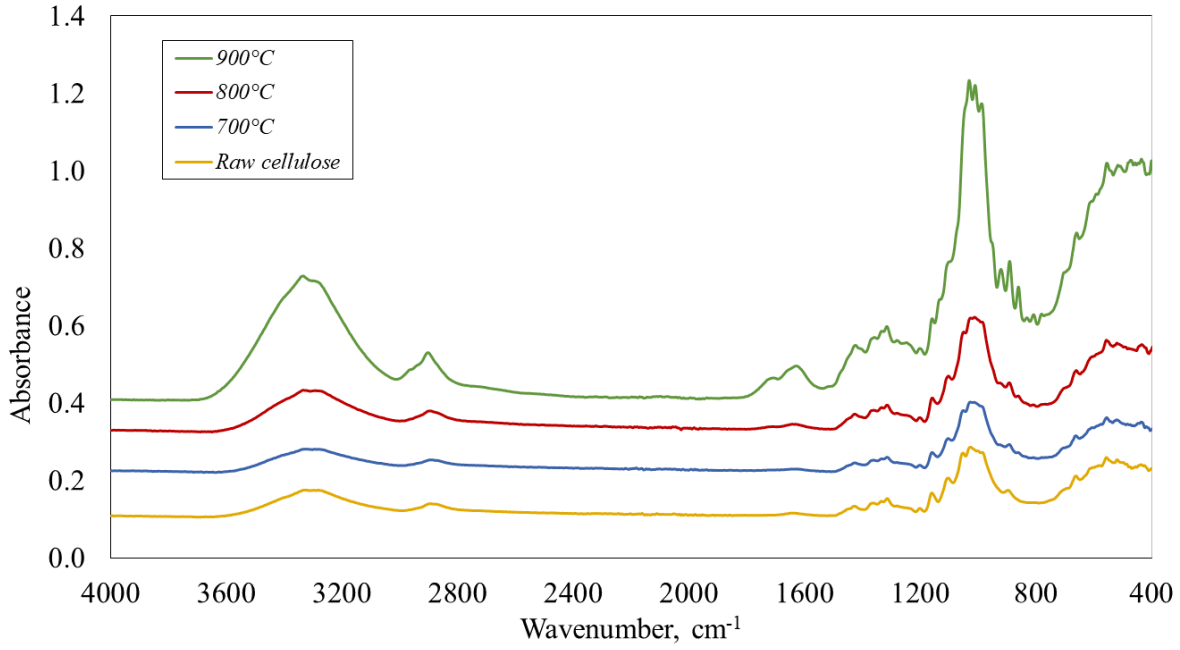

Figure 3-12 - FT-IR absorbance spectra of the solid residues collected after the heated chamber at a different temperature, compared to the pure cellulose.

3.3 Condensable products

Figure 3-13 shows the results of the GC-MS-FID on the condensable fraction. Spectra showed that the most abundant molecule was levoglucosan ($C_6H_{10}O_5$), which comes from the depolymerisation of the cellulose chain during its primary pyrolysis. Other molecules detected were acetic acid, hydroxyacetaldehyde, hydroxyacetone, dihydroxyacetone, cyclopentanepentol and 2-2-dimethoxybutane, but their concentration was much lower than those of levoglucosan. During the pyrolysis tests, the levoglucosan yield showed a peak at 800°C, which can be explained considering two concurrent phenomena: the increasing effect of the primary pyrolysis as the temperature rises and the competing secondary reaction in the gaseous phase as the temperature rises.

The behaviour observed for starch is slightly different since the concentration of hydroxyacetaldehyde was sensibly higher. However, levoglucosan remains the most important compound, and it was considered as the most representative molecule of the primary pyrolysis also for starch. Its yield is lower than the values obtained with cellulose, regardless of the temperature. The maximum yield is reached at 900°C.

Cellulose consists of a monomeric unit ($C_6H_{10}O_5$) formed from anhydrous glucose, held in place by β(1→4) glycosidic bonds (Li et al. 2013). This strong intra-molecular bond and the inter-chain hydrogen bonding result in the formation of a predominantly crystalline structure, leaving little room for amorphous regions. The glucopyranose-units ($C_6H_{10}O_5$) are linked by α(1→4) glycosidic bonds in starch, causing it to generally decompose at slightly lower temperatures than cellulose (Mischnick and Momcilovic 2010), but following the same pyrolytic pathway including glycoside bonds breakage (Fu et al. 2011). Since the devolatilization of starch is easier than that of cellulose (Fu et al. 2011), the lower production of levoglucosan can be explained either by a higher generation of non-condensable gases, or by the presence of glucose-based anhydrosugars containing two or more monomeric units, which are hardly detectable (Moldoveanu 1998). Such analysis thus enables to identify common stages but also some specificities in the pyrolysis process of biomass powders, differences and common features that can be exploited when proposing explosion mechanisms. Under oxidizing conditions, the tar fraction undergoes oxidation reactions and thus the tar yield is lower. For both cellulose and starch, the levoglucosan yields are smaller and they are of the same order of magnitude, although they slightly increased with the temperature.

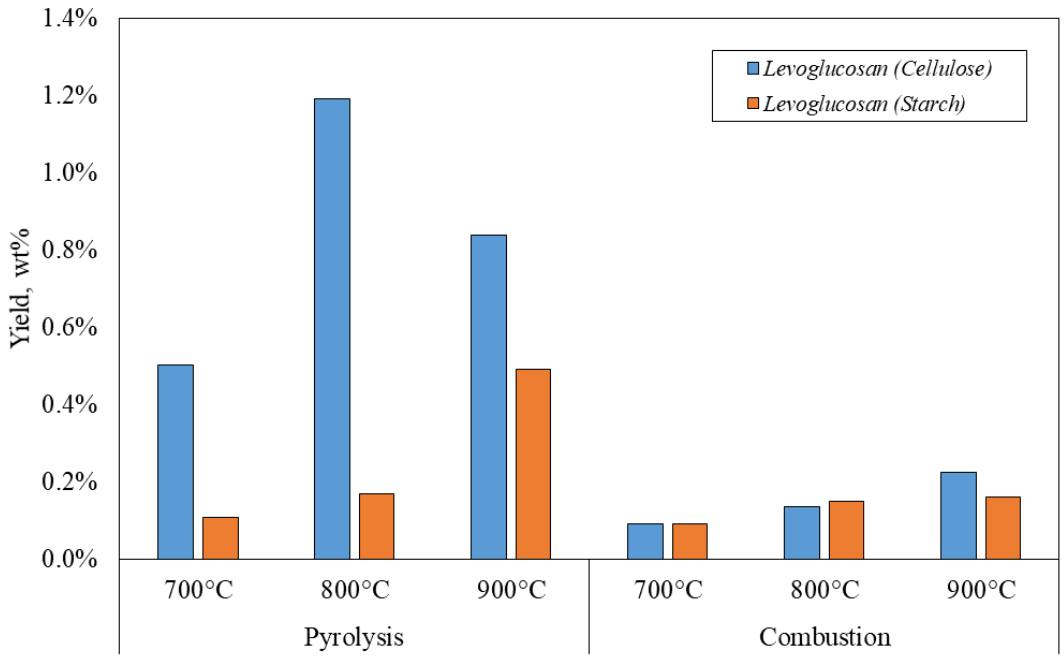

Figure 3-13 - The yield of the most abundant molecule in the condensable fraction, as a function of the reactor temperature, for pyrolysis and combustion tests of cellulose and starch.

3.4 Gaseous products

From the analysis of the pyrolysis gaseous products (Figure 3-14), CO, CO_2, H_2 and CH_4 were the most abundant species generated during the pyrolysis step. Other compounds, such as ethylene, were sometimes present as traces but are neglected here.

H_2, CO, and CH_4 molar fractions globally increase with the reactor temperature, while CO_2 often shows the opposite trend from 700 to 800°C. This trend can be related to:

- The decomposition of the carboxyl groups, which releases CO_2, is triggered at lower temperatures, resulting in lower CO_2 yield at higher reactor temperatures (Fu et al. 2011);
- The secondary reactions on the gas-phase: primary tar conversion, and water gas shift reaction (Sun et al. 2010).

The principal components of syngas (H_2 and CO) generally increased with the temperature, reaching maximum concentration of 70, 75, 59 and 73 mol% regarding the pyrolysis gases, for cellulose, wheat starch, oak and Douglas fir respectively, which is in good agreement with literature (Wei et al. 2006), although the operating conditions were different. Low yields of C_2H_4 (ethylene) and C_6H_6 (benzene - a good indicator of tertiary reactions (Dufour et al. 2011) were identified showing a slight increase as a function of the temperature. The H_2/CO ratio

exhibited a linear increase and a slight reduction at 900°C for wheat starch, oak and Douglas fir, whilst CO/CO_2 ratio increased significantly due to the higher content of CO at elevated reactor temperature (except for cellulose). Olive pomace shows a peculiar behaviour related to the complexity of its composition (Bartocci et al. 2015): the CO_2 content is higher than that of CO. As the chemical composition of olive stone, especially its oxygen content, is consistent with that of other woods (approximately 43 w%), the CO_2 abundance can be explained by the composition of the wet pomace or catalytic effects due to the high mineral content.

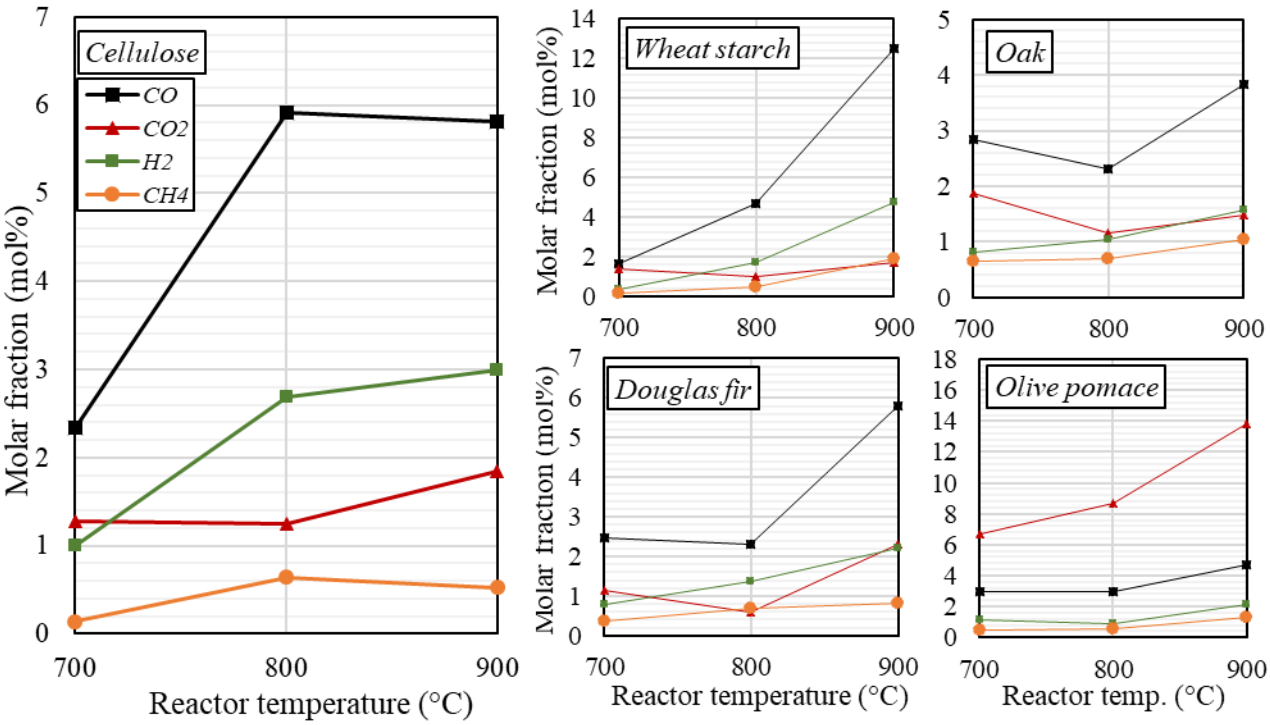

Figure 3-14 - Pyrolysis gases composition as a function of the powder nature and G-G furnace temperature.

Figure 3-15 shows the results obtained during the combustion of the powders in the G-G furnace. The methane concentration is not presented here. Its evolution is similar to hydrogen, but it is always 2 to 4 times lower. The behaviour of cellulose must be analysed independently: the CO_2/CO ratio decreases with temperature until it reaches values close to or even slightly below 1 at 1173K.

For the other organic powders, the CO_2/CO ratio increases from 973K to 1073K and then decreases or remains stable as the temperature reaches 1173K. In parallel, the hydrogen content follows an opposite evolution, with a minimum obtained at 1073K. It should be noted that the high CO_2/CO ratio obtained for oak at 1073K is essentially due to a low carbon

monoxide concentration, equal to 0.4 mol%. To analyse these trends, it must be borne in mind that, unlike the endothermic phenomenon of pyrolysis for which knowledge of the furnace temperature is crucial, the exothermicity of combustion does not allow to determine the exact temperature at which the gaseous products were generated. Indeed, the temperature of the furnace, which conditions the initiation of the pyrolysis and combustion phenomena, must not be confused with the gas-phase temperature, which is unknown here. Another essential point explaining the results shown in Figure 3-15 is the consideration of secondary reactions of primary volatiles (levoglucosan, furans, CO, CO_2, CH_4, H_2, etc.), which can explain both the CO and H_2 increase at a higher temperature.

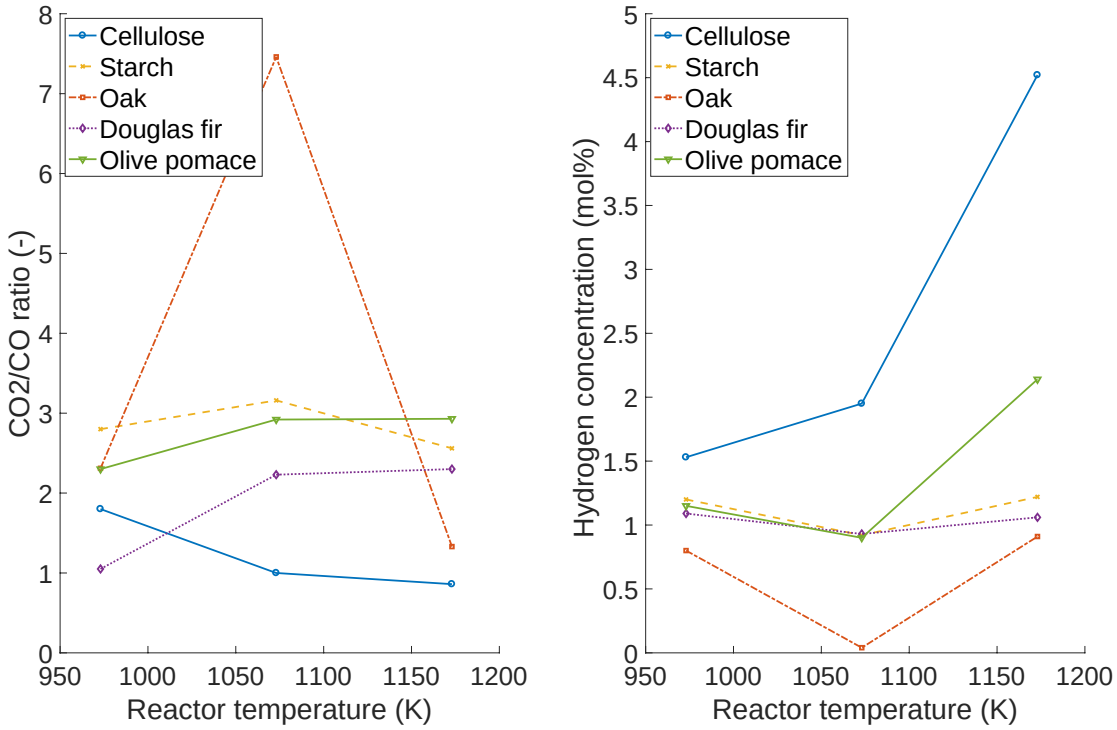

Figure 3-15 - Combustion gases composition (CO_2/CO ratio and hydrogen content) as a function of the powder nature and G-G furnace temperature.

3.5 Pyrolysis and combustion mechanisms for dust explosion modelling

The above analyses, carried out under both pyrolysis and combustion conditions, allow a better understanding of the reaction mechanisms playing a role during an organic dust explosion, and therefore better modelling of these phenomena.

An organic dust explosion can be schematically represented by the following subsequent stages: the heating of the particle, its pyrolysis and the homogeneous oxidation of the pyrolysis gases. Each of these steps can be decomposed into simpler phenomena, such as external and internal heat transfer, diffusive and reaction limitation. The first part of this study has confirmed that the heating step can be limiting at low temperatures for large particles with a short residence time. To be able to compare pyrolysis and oxidation from a kinetic point of view, the following points should be kept in mind:

- Cellulose pyrolysis is an endothermic process, therefore the temperature of the particle during this stage changes only to a limited extent whatever the temperature of the heating source, as demonstrated in Lédé (Lédé 1994);
- The oxidation of pyrolysis products is an exothermic phenomenon, which results in a flame with a temperature sensibly higher than the pyrolysis temperature.

The high complexity of the global explosion phenomenon originates predominantly from the interplay between these two steps. Considering an organic particle that undergoes a pyrolysis process, it is true that the gaseous products encircling the particle can generate a flammable atmosphere, if their concentration is beyond the Lower Flammable Limit (LFL). Assuming that the gaseous mixture ignites, the flame front temperature will influence the heat flux brought to the particles and the apparent pyrolysis rate. Reversely, the volatile composition has an impact on the flame temperature and hence the overall phenomenon strictly depends on this interplay between volatile generation and oxidation. Therefore, pyrolysis and oxidation are coupled during a dust explosion. This approach is exclusively valid when a single-particle combustion is considered. For a group-combustion (low inter-particle distance, high dust concentration), the flame propagates in the direction of the cloud, which leads to the pyrolysis of the particles in the preheating zone (4-zones model: cloud, preheating zone with pyrolysis products, flame, post-combustion zone). In this case, devolatilization/pyrolysis and oxidation, although interdependent, can be more easily distinguished. For small biomass particles, Biot (equation 3) and Damköhler (Da) numbers (Gao et al. 2015) can both be less than unity, which means that the pyrolysis is fast and homogeneous combustion controlled the dust explosion.

Such behaviour has notably be observed for small octadecanol particles (Gao et al. 2015). With regard to our experiments and model (Figure 3-11), Da of large cellulose particles (e.g. greater than 100 µm) would certainly be greater than unity under classical dust explosion conditions: the pyrolysis step should be considered as the rate-limiting step and a heterogeneous combustion is expected (Pang et al. 2021). It is supported by the fact that, when the temperature increases, the oxidation rate increases faster than the pyrolysis rate (Speight 2020).

Therefore, in Figure 3-16, a lumped reaction mechanism is proposed to model the cellulose pyrolysis. The experimental results in the G-G furnace were considered to select the chemical species involved. Classical oxidation reactions of the gaseous products, which are not specific to the heterogeneous reaction mechanisms of biomass (for instance, H_2, CO, C_2H_4, CH_4 oxidation reactions, water gas shift or Boudouard reactions), can then be combined with this mechanism.

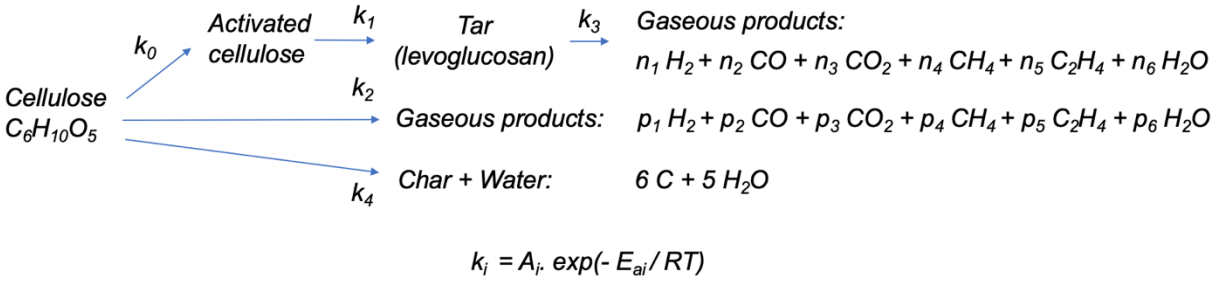

Figure 3-16 - Proposed reaction mechanisms to be considered during an organic dust explosion: example of cellulose.

By focusing only on the pyrolysis step, both the kinetics constants and the stoichiometric coefficients should be determined for reactions from 1 to 4 (Figure 3-16). Reactions corresponding to cellulose activation and tar generation can be represented using the kinetics proposed by Ranzi (Ranzi, Faravelli, and Manenti 2016b). The stoichiometric coefficients of reaction 4 are known (6 and 5 for char and water, respectively, as reported in Ranzi (Ranzi et al. 2016b)). The remaining unknowns of the system are the twelve coefficients of reactions 2 and 3, and the six variables (A_i and $E_{a,i}$) corresponding to the Arrhenius law representing the kinetic constants k_2, k_3 and k_4. Six atomic balances can be deduced by considering the proposed reactions. For instance, considering reaction 3, for carbon, hydrogen and oxygen respectively, it is true that:

$$6 = n_2 + n_3 + n_4 + 2n_5 \qquad (5a)$$

$$10 = 2n_1 + 4n_4 + 4n_5 + 2n_6 \quad (5b)$$

$$5 = n_2 + 2n_3 + n_6 \quad (5c)$$

Furthermore, six equations can be deduced by considering the Godbert-Greenwald furnace a Continuously Stirred Tank Reactor (CSTR). For instance, considering carbon monoxide and hydrogen, it is true that:

$$\frac{[H_2]}{[CO]} = \frac{(\tau \cdot n_1 \cdot k_1 \cdot k_2 + k_4 \cdot p_1)}{(\tau \cdot n_2 \cdot k_1 \cdot k_2 + k_4 \cdot p_2)} \quad (6)$$

where τ is the residence time, determined experimentally and fixed at 200 ms. Ratios were determined experimentally at three different temperatures, while water-to-carbon monoxide and char-to-carbon monoxide ratios are considered unknowns at each temperature (six unknowns in total). The equations system is, hence, made of eighteen balances similar to Equations (5a), (5b) and (5c) and six equations based on atom conservation for reactions 2 and 3; it was solved using a nonlinear least-squares fitting method. Boundaries were set to avoid negative stoichiometric coefficients or unrealistic activation energies. Figure 3-17 describes an example of fitting for cellulose, showing a satisfactory agreement between the model based on the pyrolysis equations in Figure 3-16 and the experimental points in Figure 3-14. The stoichiometric coefficients n_i and p_i were determined, as well as the kinetic constants, providing a pyrolysis model for cellulose under dust explosion conditions. Values are reported in Table 3-3 and Table 3-4. This model is coupled with the oxidation equations globally represented in Figure 3-2. A similar fitting was successfully obtained for the other organic compounds. As can be noticed in Figure 3-17, the code allowed to determine the C- and the H_2O-to-CO ratios, which were not accessible experimentally. Piskorz (Piskorz et al. 2000b) reported the liquid and the insoluble solid yields as a function of the reactor temperature. Water and C follow the same trend as presented in their work, slightly increasing and strongly decreasing with the temperature.

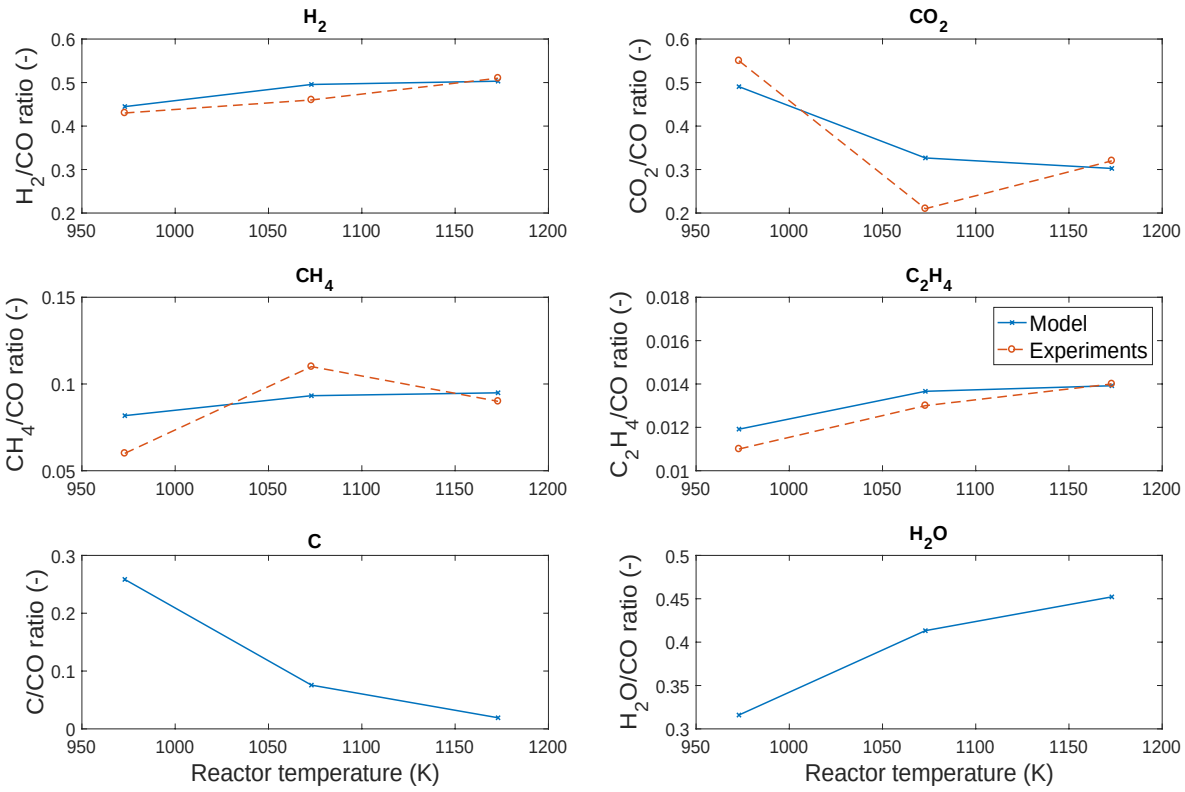

Figure 3-17 - Comparison between the pyrolysis model developed and the experimental gas/CO ratios.

Table 3-3 - Stoichiometric coefficients calculated with the fast cellulose pyrolysis model for cellulose dust explosions.

Reaction	**H_2**	**CO**	**CO_2**	**CH_4**	**C_2H_4**	**H_2O**
Levoglucosan to gaseous products (Reaction 3)	0.93	1.84	0.55	0.17	0.03	0.86
Cellulose to gaseous products (Reaction 2)	0.86	2.38	1.8	0.15	0.02	1.48

Table 3-4 - Activation energies and pre-exponential factors determined with the fast cellulose pyrolysis model for cellulose dust explosions. T is the temperature in K.

Reaction	**E_a, J.mol^{-1}**	**A, s^{-1}**
Cellulose to levoglucosan (Reaction 0 + 1) Ranzi et al. 2016b	$1 \cdot 10^4$	$4 \cdot T$
Levoglucosan to gaseous products (Reaction 3)	$2 \cdot 10^5$	$1 \cdot 10^{16}$
Cellulose to char and water (Reaction 4)	$7 \cdot 10^4$	$4 \cdot 10^{10}$
Cellulose to gaseous products (Reaction 2)	$1 \cdot 10^4$	$1 \cdot 10^8$

Figure 3-18 and Table 3-5 showed a comparison between the kinetic constants determined with the model proposed in this work and with two others frequently used in the literature, also dedicated to cellulose flash pyrolysis (Piskorz et al. 1988a; Ranzi, Debiagi, and Frassoldati 2017). Ranzi (Ranzi et al. 2017) mainly based their model on thermo-gravimetric analysis, while Piskorz (Piskorz et al. 1988a) employed a fluidised bed to study the cellulose flash pyrolysis. Figure 3-18 shows significant differences between the different kinetic constants and demonstrates how an experimental technique's operating conditions influence the kinetic parameters. If the deviations are large over the whole temperature range considered, it is necessary to focus on the range of this study, i.e. from 973 to 1173K, i.e. from 1 to 0.85 for the 1000/T abscissa. The three constants determined are globally higher than those proposed in the literature, in particular for the reactions R3 and R4.

The kinetics of direct generation of non-condensable gases from cellulose (R2) seems to be relatively unaffected by temperature variation. This evolution is consistent with the observations made in this study: small cellulose particles volatilize rapidly, from 700°C, and generate little tar. An increase in temperature hardly modifies the reactivity of the small cellulose particles. However, the direct conversion of larger fibres into non-condensable gas is difficult and becomes the rate-limiting step as the temperature increases. As for the volatilization of tar proposed in this work (R3), it is increasingly favoured by a temperature rise. Specifically, levoglucosan-related secondary reactions are very slow at low temperatures, as known and well documented for low heating rates (Ranzi et al. 2008). Our experimental results confirm the enhancement of this mechanism at high temperatures: the amount of tar decreases, more gases are generated and the presence of bubbles/cracks on the surface of the tar shows the production of gases or aerosols.

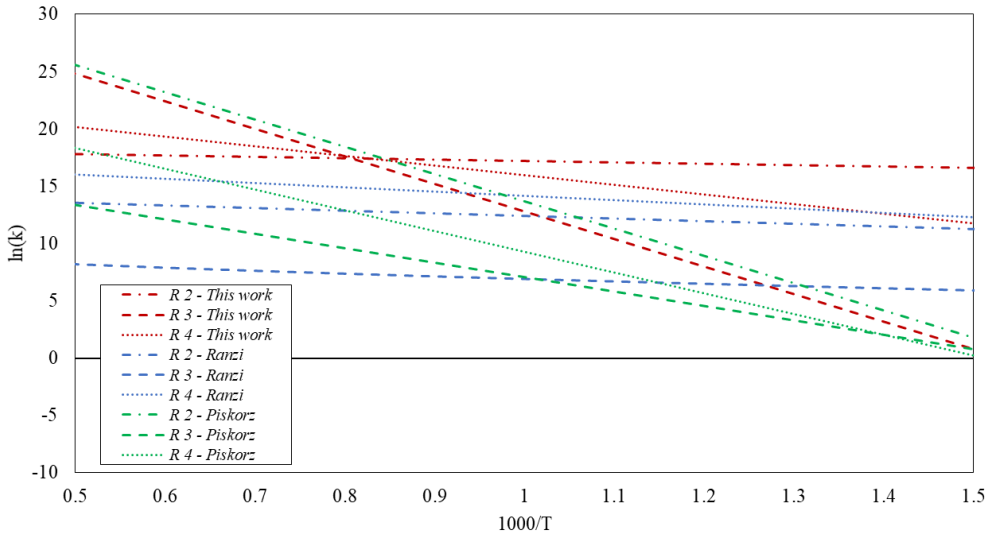

Figure 3-18 - Comparison between the kinetic constants obtained in this work and those reported in Piskorz et al. 1988; Ranzi et al. 2017

Table 3-5 - Lumped flash pyrolysis reactions considered for the comparison in Figure 3-18

References	Reaction R2	Reaction R3	Reaction R4
Ranzi et al. 2017	Activated cellulose → Gases and volatiles	Activated cellulose → Levoglucosan	Cellulose → Char and water
Piskorz et al. 1988	Activated cellulose → Volatiles	Tar and gases → Gases	Activated cellulose → Char and gases
This work	Cellulose → Gases	Levoglucosan → Gases	Cellulose → Char and water

4. Conclusions

The thermal behaviour of six biomass powders, as well as their pyrolysis and combustion mechanisms, were studied using a Godbert-Greenwald furnace. Merging modelling results and experimental data stress that various rate-limiting steps can be observed for the same dust sample, as a function of its particle size distribution: the small particles will heat up and devolatilise rapidly by direct conversion of cellulose to non-condensable gases, giving way to homogeneous phase combustion; the larger particles will either be limited by the heating phase or by the pyrolysis stage, leading to heterogeneous combustion.

Although there are similarities, particularly with regard to the significant influence of the depolymerisation step and the generation of levoglucosan, both the gases and the mechanisms observed differ between this study, carried out under the conditions relevant for dust explosion, and the studies carried out on dust layers or non-powdered materials. The low proportion of char in the solid residue is a notable difference from low heating rates pyrolysis processes, as well as the predominance of levoglucosan-related secondary reactions at high temperatures.

This study, carried out at high heating rates on powders in suspension in a turbulent environment, leads to the development of a lumped-kinetic model adapted to dust explosions. It has been validated for cellulose, but the different behaviours observed for starch (low pyrolysis onset temperature, agglomeration due to tar generation…) or olive pomace (high ash content…) will need its adaptation to more complex materials.

List of symbols

d_p = particle diameter, m

L = particle mean length, m

ρ_s = cellulose density, $kg.m^{-3}$

C_{ps} = specific heat capacity, $J.kg^{-1}.K^{-1}$

T_p = particle temperature, K

λ = thermal conductibility, $W.m^{-1}.K^{-1}$

F = view factor, -

ε = emissivity, -

σ = Stefan-Boltzmann constant, $W.m^{-2}.K^{-4}$

T_w = wall temperature, K

h = convective heat transfer coefficient, $W.m^{-2}.K^{-1}$

ΔH_p = pyrolysis reaction enthalpy, $J.kg^{-1}$

k_r = reaction kinetic constant, s^{-1}

E_a = reaction activation energy, $J.mol^{-1}$

A = reaction pre-exponential factor, s^{-1}

References

Addai, Emmanuel Kwasi, Dieter Gabel, and Ulrich Krause. 2016. 'Models to Estimate the Minimum Ignition Temperature of Dusts and Hybrid Mixtures'. *Journal of Hazardous Materials* 304:73–83. doi: 10.1016/j.jhazmat.2015.10.015.

Azam, Sikandar, and Devi Prasad Mishra. 2019. 'Effects of Particle Size, Dust Concentration and Dust-Dispersion-Air Pressure on Rock Dust Inertant Requirement for Coal Dust Explosion Suppression in Underground Coal Mines'. *Process Safety and Environmental Protection* 126:35–43. doi: 10.1016/j.psep.2019.03.030.

Bartocci, P., M. D'Amico, N. Moriconi, G. Bidini, and F. Fantozzi. 2015. 'Pyrolysis of Olive Stone for Energy Purposes'. *Energy Procedia* 82:374–80. doi: 10.1016/j.egypro.2015.11.808.

Behazin, Ehsan, Emmanuel Ogunsona, Arturo Rodriguez-Uribe, Amar K. Mohanty, Manjusri Misra, and Anthony O. Anyia. 2016. 'Mechanical, Chemical, and Physical Properties of Wood and Perennial Grass Biochars for Possible Composite Application'. 16.

Boutin, O., M. Ferrer, and J. Lédé. 1998. 'Radiant Flash Pyrolysis of Cellulose—Evidence for the Formation of Short Life Time Intermediate Liquid Species'. *Journal of Analytical and Applied Pyrolysis* 47(1):13–31. doi: 10.1016/S0165-2370(98)00088-6.

Boutin, Olivier, Monique Ferrer, and Jacques Lédé. 2002. 'Flash Pyrolysis of Cellulose Pellets Submitted to a Concentrated Radiation: Experiments and Modelling'. *Chemical Engineering Science* 57(1):15–25. doi: 10.1016/S0009-2509(01)00360-8.

Bu, Yajie, Yixiao Yuan, Shaoqian Xue, Paul Amyotte, Chang Li, Wenbo Yuan, Zepeng Ma, Chunmiao Yuan, and Gang Li. 2020. 'Effect of Admixed Silica on Dispersibility of Combustible Dust Clouds in a Godbert-Greenwald Furnace'. *Powder Technology* 374:496–506. doi: 10.1016/j.powtec.2020.07.071.

Chen, Tengfei, Jo Van Caneghem, Jan Degrève, Jan Berghmans, Filip Verplaetsen, and Maarten Vanierschot. 2022. 'Comparison between a Numerical Model and the Classic Thermal Explosion Theories for the Calculation of the Minimum Ignition Temperature of Dust Clouds'. *Process Safety and Environmental Protection* 166:222–31. doi: 10.1016/j.psep.2022.08.022.

Chua, Yee Wen, Hongwei Wu, and Yun Yu. 2021. 'Effect of Cellulose–Lignin Interactions on Char Structural Changes during Fast Pyrolysis at 100–350 °C'. *Proceedings of the Combustion Institute* 38(3):3977–86. doi: 10.1016/j.proci.2020.08.014.

D'Acierno, Francesco. 2021. 'Sustainable Biochars from Carbonization of Cellulose Filaments and Nanocrystals'. 7.

Dufour, A., P. Girods, E. Masson, Y. Rogaume, and A. Zoulalian. 2009. 'Synthesis Gas Production by Biomass Pyrolysis: Effect of Reactor Temperature on Product Distribution'. *International Journal of Hydrogen Energy* 34(4):1726–34. doi: 10.1016/j.ijhydene.2008.11.075.

Dufour, A., E. Masson, P. Girods, Y. Rogaume, and A. Zoulalian. 2011. 'Evolution of Aromatic Tar Composition in Relation to Methane and Ethylene from Biomass Pyrolysis-Gasification'. *Energy & Fuels* 25(9):4182–89. doi: https://doi.org/10.1021/ef200846g.

Dufour, Anthony, Miguel Castro-Diaz, Nicolas Brosse, Roberto Olcese, Mohamed Bouroukba, and Colin Snape. 2012. 'In Situ Analysis of Biomass Pyrolysis by High Temperature Rheology in Relations with H-1 NMR'. *Energy & Fuels* 26(10):6432–41.

Dufour, Anthony, Bajil Ouartassi, Roda Bounaceur, and André Zoulalian. 2011. 'Modelling Intra-Particle Phenomena of Biomass Pyrolysis'. *Chemical Engineering Research and Design* 89(10):2136–46. doi: 10.1016/j.cherd.2011.01.005.

Fu, Peng, Weiming Yi, Xueyuan Bai, Zhihe Li, Song Hu, and Jun Xiang. 2011. 'Effect of Temperature on Gas Composition and Char Structural Features of Pyrolyzed Agricultural Residues'. *Bioresource Technology* 102(17):8211–19. doi: 10.1016/j.biortech.2011.05.083.

Gao, Wei, Toshio Mogi, Jianliang Yu, Xingqing Yan, Jinhua Sun, and Ritsu Dobashi. 2015. 'Flame Propagation Mechanisms in Dust Explosions'. *Journal of Loss Prevention in the Process Industries* 36:186–94. doi: 10.1016/j.jlp.2014.12.021.

GmbH, Sympatec, and Am Pulverhaus. n.d. 'LASER-DIFFRACTION RESULTS FROM DYNAMIC IMAGE ANALYSIS DATA'. 4.

Greene, G. A., C. C. Finfrock, and T. F. Irvine Jr. 2000. 'Total Hemispherical Emissivity of Oxidized Inconel 718 in the Temperature Range 300±1000°C'. *Experimental Thermal and Fluid Science* 9.

Islas, Alain, Andrés Rodríguez Fernández, Covadonga Betegón, Emilio Martínez-Pañeda, and Adrián Pandal. 2022. 'Computational Assessment of Biomass Dust Explosions in the 20L Sphere'. *Process Safety and Environmental Protection* S0957582022006371. doi: 10.1016/j.psep.2022.07.029.

ISO/IEC 80079-20-2. 2016. *Explosive Atmospheres - Part 20-2: Material Characteristics - Combustible Dusts Test Methods*.

Janu, Rainer, Verena Mrlik, Doris Ribitsch, Jakub Hofman, Petr Sedláček, Lucie Bielská, and Gerhard Soja. 2021. 'Biochar Surface Functional Groups as Affected by Biomass Feedstock, Biochar Composition and Pyrolysis Temperature'. *Carbon Resources Conversion* 4:36–46. doi: 10.1016/j.crcon.2021.01.003.

Lédé, J. 1994. 'Reaction Temperature of Solid Particles Undergoing an Endothermal Volatilization. Application to the Fast Pyrolysis of Biomass'. *Biomass and Bioenergy* 7(1–6):49–60. doi: 10.1016/0961-9534(94)00046-V.

Lédé, Jacques, and Olivier Authier. 2015. 'Temperature and Heating Rate of Solid Particles Undergoing a Thermal Decomposition. Which Criteria for Characterizing Fast Pyrolysis?' *Journal of Analytical and Applied Pyrolysis* 113:1–14. doi: 10.1016/j.jaap.2014.11.013.

Li, Li, Jack S. Rowbotham, H. Christopher Greenwell, and Philip W. Dyer. 2013. 'An Introduction to Pyrolysis and Catalytic Pyrolysis: Versatile Techniques for Biomass Conversion'. Pp. 173–208 in *New and Future Developments in Catalysis*. Elsevier.

Li, Qian, Qiu-Yan Wu, Wei Jiang, Jian-Ya Qian, Liang Zhang, Mangang Wu, Sheng-Qi Rao, and Chun-Sen Wu. 2019. 'Effect of Pulsed Electric Field on Structural Properties and Digestibility of Starches with Different Crystalline Type in Solid State'. *Carbohydrate Polymers* 207:362–70. doi: 10.1016/j.carbpol.2018.12.001.

Liu, Aihua, Jieyun Chen, Xiner Lu, Didi Li, and Wenbin Xu. 2021. 'Influence of Components Interaction on Pyrolysis and Explosion of Biomass Dust'. *Process Safety and Environmental Protection* 154:384–92. doi: 10.1016/j.psep.2021.08.032.

Mischnick, Petra, and Dane Momcilovic. 2010. 'Chemical Structure Analysis of Starch and Cellulose Derivatives'. Pp. 117–210 in *Advances in Carbohydrate Chemistry and Biochemistry*. Vol. 64. Elsevier.

Mishra, Devi Prasad, and Sikandar Azam. 2018. 'Experimental Investigation on Effects of Particle Size, Dust Concentration and Dust-Dispersion-Air Pressure on Minimum Ignition Temperature and Combustion Process of Coal Dust Clouds in a G-G Furnace'. *Fuel* 227:424–33. doi: 10.1016/j.fuel.2018.04.122.

Mittal, Manju, and B. K. Guha. 1996. 'Study of Ignition Temperature of a Polyethylene Dust Cloud'. *Fire and Materials* 20(2):97–105. doi: 10.1002/(SICI)1099-1018(199603)20:2<97::AID-FAM568>3.0.CO;2-L.

Mittal, Manju, and B. K. Guha. 1997. 'Minimum Ignition Temperature of Polyethylene Dust: A Theoretical Model'. *Fire and Materials* 21(4):169–77. doi: 10.1002/(SICI)1099-1018(199707/08)21:4<169::AID-FAM604>3.0.CO;2-Y.

Moldoveanu, S. C. 1998. 'Chapter 7. Analytical Pyrolysis of Polymeric Carbohydrates'. Pp. 217–315 in *Techniques and Instrumentation in Analytical Chemistry*. Vol. 20. Elsevier.

Pang, Lei, Jiaojiao Cao, Yu Zhao, Chunmiao Yuan, Kai Yang, and Zhiwen Zhang. 2021. 'Minimum Ignition Energy of LDPE Dust/Ethylene Hybrid Mixture'. *Journal of Loss Prevention in the Process Industries* 72:104546. doi: 10.1016/j.jlp.2021.104546.

Pastorova, Ivana. 1994. 'Cellulose Char Structure : A Combined Analytical Py-GC-MS, F IR, and NMR Study'. *Carbohydrate Research* 21.

Piskorz, J., P. Majerski, D. Radlein, A. Vladars-Usas, and D. S. Scott. 2000. 'Flash Pyrolysis of Cellulose for Production of Anhydro-Oligomers'. *Journal of Analytical and Applied Pyrolysis* 56(2):145–66. doi: 10.1016/S0165-2370(00)00089-9.

Piskorz, Jan, Desmond St. A. G. Radlein, Donald S. Scott, and Stefan Czernik. 1988. 'Liquid Products from the Fast Pyrolysis of Wood and Cellulose'. Pp. 557–71 in *Research in Thermochemical Biomass Conversion*, edited by A. V. Bridgwater and J. L. Kuester. Dordrecht: Springer Netherlands.

Pu, Yunqiao, Fan Hu, Fang Huang, Brian H. Davison, and Arthur J. Ragauskas. 2013. 'Assessing the Molecular Structure Basis for Biomass Recalcitrance during Dilute Acid and Hydrothermal Pretreatments'. *Biotechnology for Biofuels* 6(1):15. doi: 10.1186/1754-6834-6-15.

Ranzi, E., T. Faravelli, and F. Manenti. 2016. 'Pyrolysis, Gasification, and Combustion of Solid Fuels'. Pp. 1–94 in *Advances in Chemical Engineering*. Vol. 49. Elsevier.

Ranzi, Eliseo, Alberto Cuoci, Tiziano Faravelli, Alessio Frassoldati, Gabriele Migliavacca, Sauro Pierucci, and Samuele Sommariva. 2008. 'Chemical Kinetics of Biomass Pyrolysis'. *Energy & Fuels* 22(6):4292–4300. doi: 10.1021/ef800551t.

Ranzi, Eliseo, Paulo Eduardo Amaral Debiagi, and Alessio Frassoldati. 2017. 'Mathematical Modeling of Fast Biomass Pyrolysis and Bio-Oil Formation. Note I: Kinetic Mechanism of Biomass Pyrolysis'. *ACS Sustainable Chemistry & Engineering* 5(4):2867–81. doi: 10.1021/acssuschemeng.6b03096.

Salem, Z., H. Lebik, W. K. Cherafa, and K. Allia. 2007. 'Valorisation of Olive Pits Using Biological Denitrification'. *Desalination* 204(1–3):72–78. doi: 10.1016/j.desal.2006.04.025.

Speight, James G. 2020. ‘Combustion of Hydrocarbons’. Pp. 421–63 in *Handbook of Industrial Hydrocarbon Processes*. Elsevier.

Sun, Shaozeng, Hongming Tian, Yijun Zhao, Rui Sun, and Hao Zhou. 2010. ‘Experimental and Numerical Study of Biomass Flash Pyrolysis in an Entrained Flow Reactor’. *Bioresource Technology* 101(10):3678–84. doi: 10.1016/j.biortech.2009.12.092.

Tan, Xin, Martin Schmidt, Peng Zhao, Aizhu Wei, Weixing Huang, Xinming Qian, and Dejian Wu. 2020. ‘Minimum Ignition Temperature of Carbonaceous Dust Clouds in Air with CH4/H2/CO below the Gas Lower Explosion Limit’. *Fuel* 264:116811. doi: 10.1016/j.fuel.2019.116811.

Vreugdenhil, B. J., and R. W. R. Zwart. n.d. ‘Tar Formation in Pyrolysis and Gasification’. 38.

Wang, Junqi. 2016. ‘Effect of Pyrolysis Conditions on Levoglucosan Yield from Cotton Straw and Optimization of Levoglucosan Extraction from Bio-Oil’. *Journal of Analytical and Applied Pyrolysis* 10.

Wei, Ligang, Shaoping Xu, Li Zhang, Honggang Zhang, Changhou Liu, Hui Zhu, and Shuqin Liu. 2006. ‘Characteristics of Fast Pyrolysis of Biomass in a Free Fall Reactor’. *Fuel Processing Technology* 9.

Xu, Sen, Junfeng Liu, Wei Cao, Yuyan Li, and Weiguo Cao. 2017. ‘Experimental Study on the Minimum Ignition Temperature and Combustion Kinetics of Coal Dust/Air Mixtures’. *Powder Technology* 317:154–61. doi: 10.1016/j.powtec.2017.04.059.

Zoghlami, Aya, and Gabriel Paës. 2019. ‘Lignocellulosic Biomass: Understanding Recalcitrance and Predicting Hydrolysis’. *Frontiers in Chemistry* 7:874. doi: 10.3389/fchem.2019.00874.

CHAPTER 4

Summary

The pyrolysis step was widely studied and described in Chapter 3, and it will continue to be under the spotlight in Chapter 4. The role of the pyrolysis step in a cellulose dust explosion was analysed by studying the influence of each product fraction on the explosion severity. Solid residues, condensable products and gaseous species mimicking the pyrolysis products of cellulose were selected and introduced into the dust cloud, which was subsequently ignited. The behaviour of the dust cloud was thus studied as if the primary pyrolysis step was bypassed. The 20L sphere, a standard apparatus vastly used to recreate a controlled explosive system, was employed as the experimental setup. Results stressed an interesting and non-expected behaviour related to char and tars, which can be associated with a secondary role in the dust explosion. These experiments reminded how complex a dust explosion is, especially when carried out in slightly different operating conditions than usual.

Resumé

L'étape de pyrolyse a été largement étudiée et décrite au Chapitre 3, et elle continuera à être sous les feux de la rampe au Chapitre 4. Le rôle de l'étape de pyrolyse dans une explosion de poussière de cellulose a été analysé en étudiant l'influence de chaque fraction de ses produits sur la sévérité de l'explosion. Des résidus solides, des produits condensables et des espèces gazeuses imitant les produits de pyrolyse de la cellulose ont été sélectionnés et introduits dans le nuage de poussière, qui a ensuite été enflammé. Le comportement du nuage de poussière a ainsi été étudié comme si l'étape primaire de pyrolyse était contournée. La sphère 20L, un appareil standard largement utilisé pour recréer un système explosif contrôlé, a été utilisée comme dispositif expérimental. Les résultats ont mis en évidence un comportement intéressant et non attendu lié au charbon et aux goudrons, qui peut être associé à un rôle secondaire dans l'explosion de poussière. Ces expériences ont rappelé la complexité d'une explosion de poussières, en particulier lorsqu'elle est réalisée dans des conditions de fonctionnement légèrement différentes de celles qui prévalent habituellement.

Making hybrid mixture explosions a common case

Matteo Pietraccini [a], Pierre-Alexandre Glaude [a], Anthony Dufour [a] & Olivier Dufaud [a]

[a] Université de Lorraine, CNRS, LRGP, F-54000 Nancy, France

E-mail: olivier.dufaud@univ-lorraine.fr

Graphical abstract

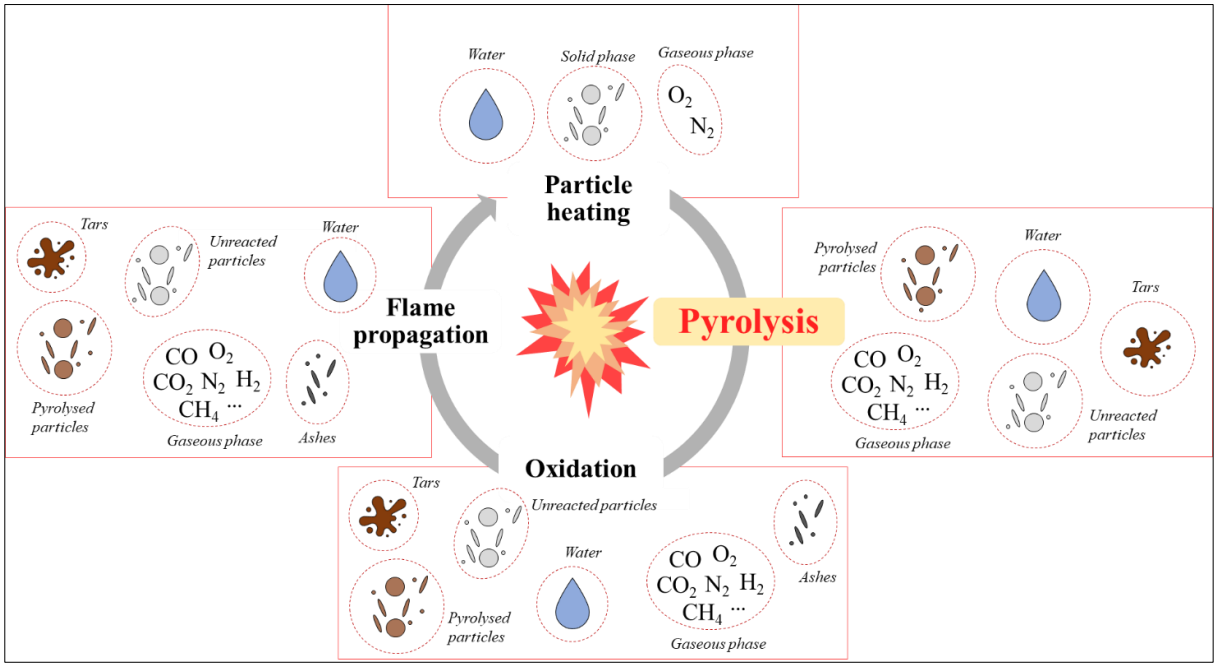

Abstract

Explosions of gas-dust hybrid mixtures have long been considered as particular cases encountered in specific industrial contexts. However, it should be reminded that during the explosion of an organic powder, the presence of a hybrid mixture composed of the dust itself and its pyrolysis gases is compulsory. On these premises, an experimental study to determine the role of cellulose pyrolysis products (gaseous, condensable and solid) on the global phenomenon is presented. Hybrid mixture explosion tests were exploited to carry out the investigation. The G-G furnace and the 20L sphere were employed. Several experimental strategies were chosen to demonstrate the impact of pyrolysis reaction

on the explosion of organic powders: i) the fuel equivalence ratio of the reactive mixture (case 1), or ii) the mass of reactants (case 2) were respectively kept constant, iii) the effects of water vapor, char and tar were tested. They were next compared to identify the most suitable one. The two first experimental approaches lead to significantly different results: only case 2 keeps the maximum explosion pressure almost constant, but maximum rate of pressure rises and deflagration index greatly decrease when the pyrolysis gases concentration decreases, which highlights the importance of the pyrolysis reaction on the explosion kinetics. It should also be stressed that the maximum explosion severity is not obtained for the pure gases but when a small dust content is added. The same evolution is observed when a small amount of char is introduced to pyrolysis gases, which underlines the influence of the radiative transfer. Adding small amounts of tar to cellulose tends to increase its explosion severity. However, this impact is less than that generated by the addition of pyrolysis gases.

Keywords: *dust explosion, pyrolysis, hybrid mixture, cellulose*

1. Introduction

Nowadays, gas and dust explosions are well studied, and determining their characteristic parameters (P_{max}, K_{St} or K_g) is a common procedure. Although some standards may need to be perfected, the global approach of the testing procedures allows responding to industrial needs. However, gas and dust explosion tests may be essential to understand better the phenomenon itself and its fundamental steps (Cloney et al. 2017). Particularly promising is the study of hybrid mixtures explosion, which could potentially represent and simulate complex phenomena involving two combustible phases (Abbas et al. 2022b; Dufaud et al. 2009; Guo et al. 2020; Sanchirico et al. 2015). In this work, hybrid mixtures were exploited to assess the role of pyrolysis during the rapid combustion of an organic powder. When such powders are heated, they undergo a pyrolysis step, generating a gaseous, condensable and solid phase, called char. Subsequently, they react with the oxidiser triggering the oxidation reactions. Each explosion of organic powder is, thus, in reality, a hybrid explosion. The rate of the global phenomenon strictly depends on the slowest step, the rate-limiting one. In this work, hybrid mixtures are used to verify if the pyrolysis step of a cellulose dust explosion can be considered as such and to enlighten the role of the pyrolysis products in this phenomenon.

2. Materials and methods

2.1 Cellulose characterisation

Since its chemical structure and thermal behaviour has been well characterized, the choice of the powder fell on micro-crystalline cellulose (Avicel ph 101), which has an average diameter close to 60 µm. Moreover, the reaction mechanisms of cellulose pyrolysis have been the subject of several detailed studies (Paulsen et al. 2013; Ranzi et al. 2017; Wang et al. 2020), which were used to support the results obtained in this work. A Malvern Mastersizer 3000 equipped with an aero-dispersion unit was employed to determine both samples' Particle Size Distribution (PSD). Images of the samples were taken with a 5 Mp Dino-lite Pro HR digital microscope and a JEOL JSM-649-LV Scanning Electronic Microscope (SEM) (Figure 4-1). The combination of these two imaging tools was exploited to characterise the particles' appearance, shape and surface morphology. In addition to the raw cellulose, the char created during pyrolysis/gasification has also been observed by SEM. No important difference in particle shape is noticeable between the two powders. Nevertheless, it should be noted that the char has a smaller primary size but tend to cluster in agglomerates (Figure 4-1). Proximate analysis was performed on two powder samples: First, the moisture content (MC) was determined with the aid of a Mettler Toledo HE53 Moisture Analyzer. Next, the volatile matter (VM) and the fixed carbon (FC) were determined with a STARe System thermogravimetric balance. Finally, the ash content (ASH) was determined using a Nabertherm B150 oven. Finally, elemental analysis was performed on the powders, employing a Vario MICRO cube CHNOS elemental analyser.

2.1.1 Choice of the pyrolysis products

The products generated during a cellulose fast pyrolysis process constitute three main fractions: gaseous, condensable (tar) and solid (char). The hybrid mixture explosion experiments involved then three product fractions, chosen and determined in three steps:

- Determination of the composition of two gaseous mixtures, representing the gaseous products;
- Choice of the sample representing solid products;
- Synthesis of the condensable products;

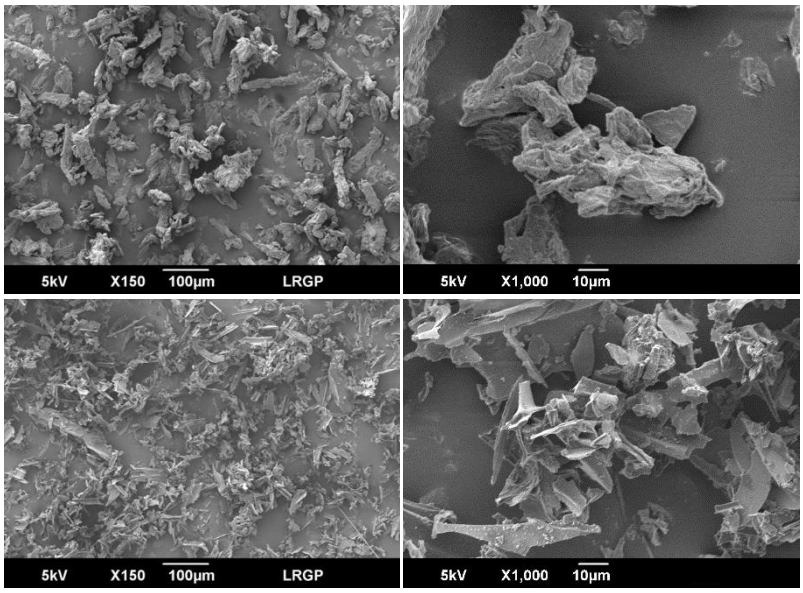

Figure 4-1 - SEM photos of the cellulose (top) and the char sample (bottom)

2.1.2 Pyrolysis gaseous products

The first stage of the study was carried out in a modified Godbert-Greenwald furnace, as in Pietraccini (Pietraccini et al. 2021). This apparatus was chosen because it allows the reproduction of the features of a dust explosion: short time scale, transient system, and dust suspension. The influence of the heated chamber temperature was studied. Two experiment series were performed at 700 and 900 °C, for each of which the gaseous product composition was measured. 0.2 g of cellulose was dispersed in each test with an argon gas pulse, and each was performed thrice for accuracy. The main measurable components were H_2, CO, CO_2 and CH_4 (traces of ethylene, benzene and toluene have been neglected), and two gas bottles were prepared according to the experimental results. For clarity purposes, from this point on, the gaseous mixture obtained at 700 °C will be called mix A, while the gaseous mixture obtained at 900 °C will be called mix B. It should be remembered that water vapor is also generated during the pyrolysis step. Since it was difficult to determine the water concentration experimentally, it was extracted from Piskorz (Piskorz et al. 2000b), whose work has been carried out in a similar experimental setup for cellulose pyrolysis with comparable operating conditions. It should be underlined that the effect of the temperature does not influence only the composition of the gaseous pyrolysis products but their yield as well. An increase in the temperature usually translates into an increase in pyrolysis gaseous product yield. This aspect was not directly considered in this work, which means that only the compositions of the gases

will be compared, they will not be combined with simultaneous changes in concentrations, expected when the temperature varies. Such evolutions will be the subject of future work.

2.1.3 Pyrolysis solid products

The large amount of powder needed for an explosion severity test series made it difficult to experimentally produce a large amount of cellulose char, needed for the hybrid mixture explosion experiments. Hence, to represent the solid pyrolysis products, an already available sample of char was employed. It was collected in a bag filter system of a biomass gasification plant. The char was characterised with the same techniques employed for the cellulose powder.

2.1.4 Pyrolysis condensable products

Considering solid and gaseous factions as the only products of the cellulose flash pyrolysis would mean considering a non-complete process. The condensable fraction (tar) generated during such a phenomenon can account for up to 20wt% of the cellulose feeding (Graham et al. 1984; Piskorz et al. 2000b), and its composition includes monosaccharides (levoglucosan, furanoses), disaccharides (cellobiosan principally) and several lighter molecules (hydroxyacetaldehyde, acetic acid, acetol, formaldehyde, formic acid).

A micro-fluidized bed, especially designed for this study, was employed to synthesize it (a schematic representation is reported in Figure S 14 in Annex 3). A sand bed constituted the reactive volume, which allowed obtaining a reactive volume homogeneous in temperature (from 300 to 500°C) and composition through the fluidization. Tars were collected at the outlet of the reactor in two bubbling condensers, cooled with isopropanol at -30°C, and filled with water and glass beads. Then, the liquid fraction was dehydrated in a lyophilizer for 48h to remove any trace of water and subsequently weighted to calculate the proper tar-to-cellulose ratio for the coating test.

To determine their chemical composition, a sample of the tar was solubilized in methanol and 1 µL of 1-tetradecene was added as an internal standard. Next, the solution was filtered with a 0.45 µm pore filter and analysed by a gas chromatography GC-MS (Agilent 7890A System equipped with a 5975C Triple-Axis detector).

It should be underlined that this fraction's high viscosity and stickiness represent a non-negligible drawback, which is incompatible with an injection in the 20L sphere. It was then mixed with the cellulose powder to coat the particles and simulate a partially pyrolysed solid phase. Ethanol was employed to facilitate the dispersion of the viscous condensable fraction

and guarantee a homogeneous coating. Ethanol was subsequently removed by drying. The detailed experimental procedure and the results are reported in Section 3 in Annex 3.

2.2 Explosion experiments

2.2.1 Pyrolysis step experimental study

In Figure 4-2, the scheme globally resumes the approach followed during the hybrid mixture explosibility tests. Series 1 was carried out considering only the volatilization process occurring in cellulose pyrolysis and without considering the water as a product. In series 2, the water was accounted for among the pyrolysis products. Finally, in series 3, both the volatilization and charring processes were considered. To include the char in the tests means to consider a complete pyrolysis process, as well as to enlighten the role of the radiative heat transfer in the dust cloud (Torrado 2017). In fact, a higher emissivity than cellulose characterises char; thus, adding a small amount in the cellulose powder might result in a more crucial radiative heat flux from the flame front to the pre-heating zone. The choice of the amount of char added to the cellulose powder in the explosion experiments was made considering the yield values commonly encountered in a cellulose flash pyrolysis phenomenon. According to Commandré at al. (Commandré et al. 2011) and Zanzi (Zanzi, Sjöström, and Björnbom 1996), whose works were carried out in similar free-fall reactors for flash pyrolysis of biomass, the char yield lies between 7 and 10 wt%. For the hybrid mixture explosion tests with char, the amount of char chosen was 10 wt% of the cellulose injected in the 20L sphere.

The explosion experiments were carried out in a standard 20L spherical vessel equipped with a rebound nozzle and two 100 J chemical igniters as ignition sources. This energy was chosen as it is both sufficiently high to ignite the pure dust (MIE cellulose and char) and sufficiently low to limit overdriving effect (Taveau et al. 2017). As no standard procedure exists (yet) to determine the explosion severity of hybrid mixtures (Spitzer et al. 2020), the procedure used for powders (EN 14034) has been adapted to such mixtures (Dufaud et al. 2009). The sphere was partially vacuumed to pressures as low as 50 mbar (punctually 30 mbar). The corresponding amount of gas is introduced into the vessel by recording the partial pressure. Next, the air is introduced to set the absolute pressure at 0.4 bar. Next, a specific amount of liquid water was introduced into the system before ignition to include it among the pyrolysis products. As aforementioned, the information about the water yield was taken from Piskorz (Piskorz et al. 2000b), corresponding to 8wt% of the amount of cellulose introduced. The low

pressure in the 20L vessel allowed its complete vaporisation. Finally, the test is performed "classically", and the powder, stored in the dust container at 20 bar, is injected through the rebound nozzle at the bottom of the vessel. The temperature is kept constant at 25 °C using the water jacket. The explosion overpressure P_m and the rate of pressure rise $(dP/dt)_m$ were determined for each test. K_{St} (or K_g for gases) were then calculated applying the cube-root law.

Nevertheless, the procedure developed to simulate and study the role of pyrolysis in an organic dust explosion has two critical limits. First, the experimental protocol to characterize the gaseous products in the G-G furnace provided for pyrolysis performed in an inert atmosphere, while the pyrolysis step of a dust explosion occurs in an oxidative atmosphere. The kinetics and thermicity of the two processes may thus present some significant differences. Moreover, during the hybrid mixture tests in the 20L sphere, the pyrolysis mixture is already present in the gaseous phase, whilst in a "classic" dust explosion test, they are generated and mixed with the air in a second moment. Nevertheless, the approach proposed in this article is original and allows the contribution of each type of intermediate products generated during the explosion (tar, pyrolysis gases or char and water) to be assessed separately.

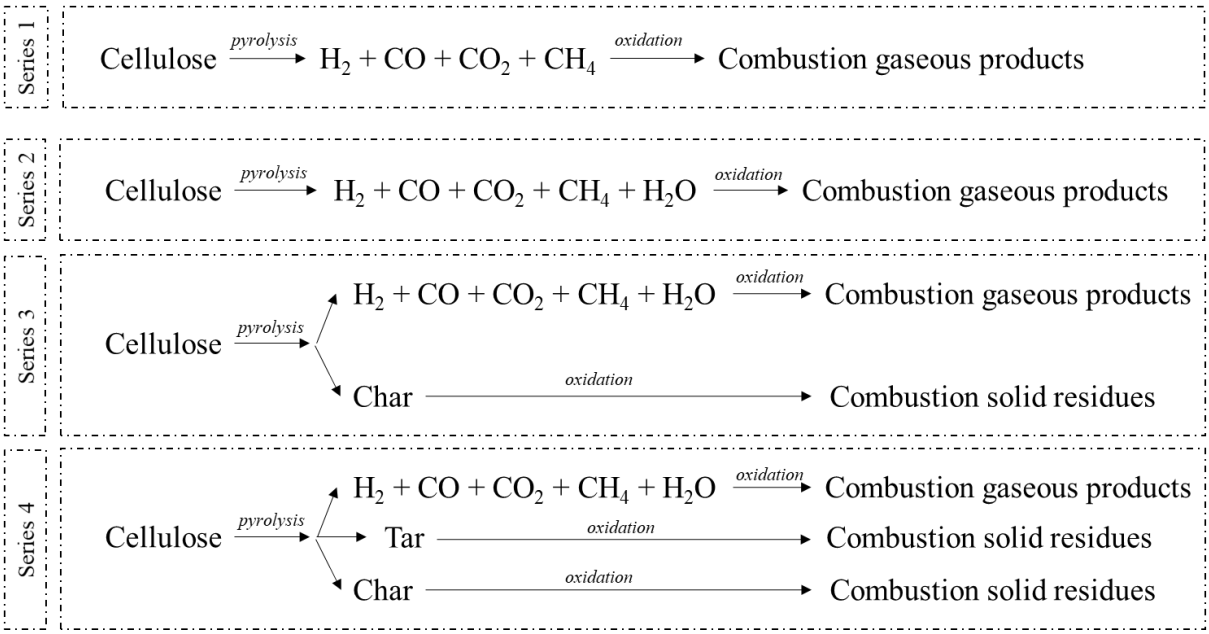

Figure 4-2 - A schematic representation of the procedure adopted for the cellulose pyrolysis experimental simulation

2.2.2 Constant ER approach

The first approach adopted for the hybrid mixture explosion tests consisted of keeping the reacting system's equivalence ratio (ER) constant. By imposing the amount of pyrolysis gaseous mixture (mix A or B) and knowing the amount of oxygen introduced in the 20L vessel (following the EN 14034 standard procedure), it was possible to adjust the cellulose amount to obtain a specific ER. 0.7, 0.9 and 1.1 were chosen as ER values. It should be stressed that the calculation of an equivalence ratio was related to the definition of a set of independent oxidation reactions for each combustible compound, independence which is only theoretical.

2.2.3 Constant reacting mass approach

The second approach keeps the initial total mass of cellulose and pyrolysis products constant. By subsequently replacing a fixed amount of cellulose powder with mix A and B, it was possible to determine the explosion severity characteristics of several systems representing several conversion degrees of cellulose. An experimental simulation of the pyrolysis step in an organic dust explosion was thus carried out. The total mass was fixed at 10 g to avoid excessively high dust concentrations in the sphere, but mainly to avoid requiring a large amount of gas mixture in the 20L vessel. In fact, as aforementioned, the procedure followed for the hybrid mixture explosion tests was inspired by the standard one. Since it was impossible to decrease the internal pressure below 0.15 bara, introducing a large amount of gas mixture in the chamber would have meant changing the initial pressure (above 0.4 bara). The maximum concentration attainable was then approximately 38vol% (at such concentration the sphere was vacuumed at 30 mbar).

3. Results and discussion

3.1 Product characterisation

3.1.1 Cellulose and char characterisation

Table 4-1 reports the characteristic diameters of cellulose and char and their proximate and elemental analysis. Cellulose presents a narrower Particle Size Distribution (PSD) than char, which is slightly finer than cellulose. Since an organic particle tends to shrink when it undergoes pyrolysis, this last characteristic allowed the char to represent such a phenomenon better. Concerning the proximate analysis, it can be noticed that the higher value of fixed carbon (FC)

in the char sample is due to the organic matter that did not entirely volatilise but converted into a porous structure richer in carbon, as confirmed by the elemental analysis. This fraction is also characterised by a much higher ash content than cellulose. The slightly higher nitrogen content might be due to the biomass feedstock that generates the char.

Table 4-1 - Characteristic diameters, proximate and elemental analysis of the powder samples

Sample	**Cellulose**	**Char**
Particle Size Distribution		
D10, µm	22	8
D50, µm	68	25
D90, µm	146	120
Proximate analysis		
MC, %wt	5.3	2.9
VM, %wt	87.4	28.8
FC, %wt	7.2	48.6
Ash, %wt	0.10	19.6
Elemental analysis		
C	46.3	52.6
H	6.5	1.8
O	47.0	45.1
N	0.1	0.4
S	0.1	0.1

3.1.2 Pyrolysis gaseous mixes

The composition of mix A and B are reported in *Table 4-2*. Amongst the hundreds of products of fast cellulose pyrolysis, the most abundant species in the gaseous phase are CO, CO_2, H_2, CH_4, H_2O, light hydrocarbons such as C_2H_4 and C_2H_6, acetic acid and other light organics (Piskorz et al., 2000). Considering only the so-called “permanent gases” (CO, CO_2, CH_4 and H_2) and neglecting the other molecules, whose concentrations were negligible, one of the main effects of the temperature is the increment of the yield of the gaseous products. The two gaseous mixes globally present a composition similar to that presented in other works (Funazukuri, Hudgins, and Silveston 1986; Graham et al. 1984; Paulsen et al. 2013) performed

in similar experimental setups, temperatures and residence times. CO and CO_2 are always the most abundant ones among the permanent gases. As in Funazukuri (Funazukuri et al. 1986), hydrogen molar fraction increases with the temperature (from mix A to mix B), while methane concentration is similar to that presented in Graham (Graham et al. 1984). Furthermore, the CO molar fraction decreases from 700 to 900°C, whereas it shows the opposite behaviour in Funazukuri (Funazukuri et al. 1986) and Paulsen (Paulsen et al. 2013). CO_2 concentration does not seem to be significantly affected by the temperature in Funazukuri's and Graham's works, but it is reduced by almost half in this work. These differences may be due to the significant increase of the hydrogen fraction, which modifies the proportions between the chemical species and the differences in the phenomena between this work and theirs.

Table 4-2 - Composition of the pyrolysis gaseous mixes A and B

Species	**Composition, %mol**	
	Mix A (obtained at 700°C)	**Mix B (obtained at 900°C)**
H_2	3	24
CO	61	51
CO_2	33	18
CH_4	3	7

3.2 Pure compounds explosion

3.2.1 Cellulose explosion severity

The explosion severity of cellulose (Avicel ph 101) was studied by determining P_{max} and K_{St}. Figure 4-3 shows the classical evolution of the explosion severity of cellulose as a function of the dust concentration. The powder sample is associated with an approximate minimum explosible concentration of 60 g/m^3, a P_{max} of 7.1 bar and a K_{St} of 77 bar.m/s, which is consistent with the values of the literature, especially those of the Gestis-Dust database (IFA). Nevertheless, it should be noted that, whereas the deflagration index K_{st} is in the range of values identified in the database (from 30 to 130 bar.m/s for particles of similar sizes), the maximum explosion overpressure is slightly lower than expected (from 7.5 to 9.5 bar).

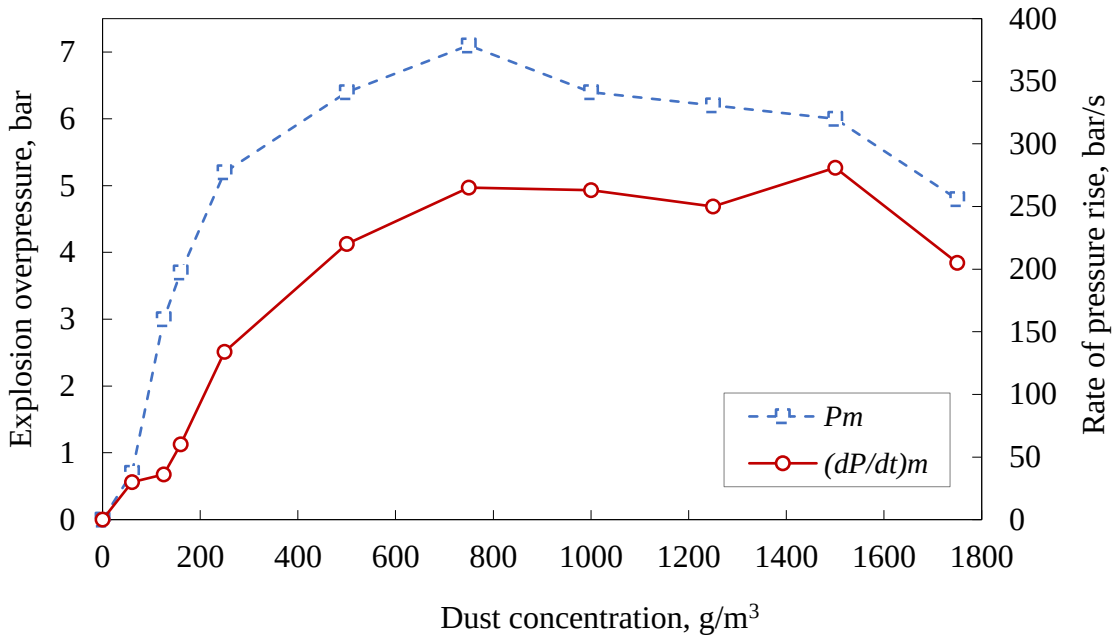

Figure 4-3 - Explosion severity of pure cellulose (d50: 68 µm)

3.2.2 Gaseous mixtures explosion severity

The maximum explosion overpressure obtained with the pyrolysis gases are of the same order of magnitude as for cellulose, i.e. 6.2 and 6.5 bar for mix A (700 °C) and mix B (900 °C), respectively. However, they differ consistently in terms of deflagration index K_g with 242 and 587 bar.m.s^{-1} for mix A and mix B, respectively. The small difference of the P_{max} values is related to the small difference of composition between the two mixtures. In fact, their energetic content (in terms of enthalpy of combustion) is 208 kJ/mol for mix A and 278 kJ/mol for mix B. It should also be stressed that the maximum explosion overpressure of pyrolysis gases and dust are close.

Table 4-1 shows that the hydrogen content dramatically affects the molar composition. Therefore, the higher fraction of hydrogen in the pyrolysis gases obtained at 900 °C leads to a higher combustion reaction rate and, consequently, to a higher Kg. Moreover, the presence of a larger amount of hydrogen significantly lowers the Lower Explosible Limit (LEL) of the gases, from 10.8 vol% (mix A) to 7.1 vol% (mix B) using Le Chatelier's law, which is also enlightened in . Due to the presence of carbon dioxide in the mixture, the experimental LEL are higher than the theoretical values. As expected, both the ignition sensitivity and explosion severity appear to depend on the temperature at which the organic powder is exposed. By

affecting the particle heating rate, it defines the average temperature of the dust cloud and, as a consequence, the global conversion degree of the particles.

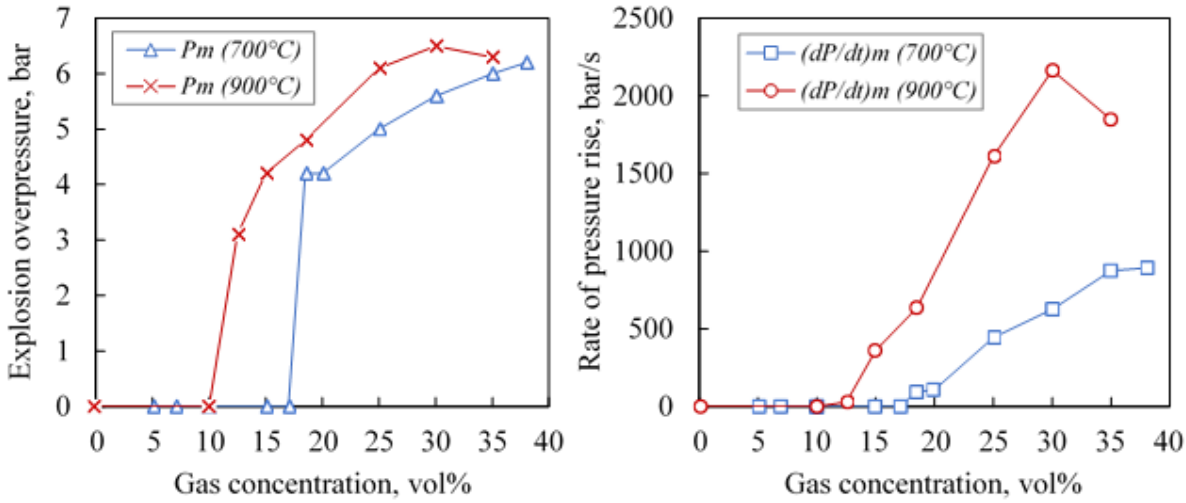

Figure 4-4 - Explosion overpressure (to the left) and rate of pressure rise (to the right) of the pyrolysis gases generated at 700°C (Mix A) and 900°C (Mix B)

3.3 Time scale analysis

As abovementioned, a cellulose dust explosion can be seen as a combination of four fundamental bricks: particle heating, pyrolysis, oxidation and flame propagation. To identify the rate-limiting one, a time scale analysis was carried out. Each step was associated with a characteristic time to compare one phase to another. The variability of the data found in the literature and due to the heterogeneity (mainly in temperature and particle size) of the system was considered by introducing variability bars, as presented in Figure 4-5.

The particle heating phenomenon was associated with the pyrotechnical igniters (energy delivered of 100 J). They are composed of barium nitrate (30wt%), barium dioxide (30%wt) and Zirconium (40%wt) (EN 14034-1 2004; EN 14034-2 2006), the last having the role of combusting and generating the spark cloud for the ignition. Zirconium combustion reached approximately 4930K (Doyle, Conway, and Grosse 1958), which will -locally- be considered to estimate the characteristic time of the radiative heat transfer. The convection and the conduction modes will be neglected due to the high temperature of the burning Zr particles. Particle temperature also increases due to the radiative heat transfers from the flame front to the pre-heating zone. This contribution will be taken into account in the flame propagation step.

The pyrolysis characteristic times were calculated from the kinetic constants proposed by several works focused on cellulose flash pyrolysis (Lédé 2012; Miller and Bellan 1996; Piskorz et al. 1988b, 2000b; Ranzi et al. 2017). It must be underlined that the comparison between different works is not straightforward because the reactions proposed sometimes involve "lumped species", such as "volatiles", "gases", and "tars". Moreover, the number of reactions considered strictly depends on the work's objectives, and it varies between one and five in the considered mechanisms. Nonetheless, the reactions chosen to be compared were selected to reduce the data divergence. The slowest parallel reactions proposed in each mechanism were neglected, and only the fastest were thus considered. As for the serial reactions, all the reactions were considered and a global characteristic time was determined.

The oxidation step was represented by the reaction between the main products of the pyrolysis and oxygen. CO, CO_2, H_2, CH_4, H_2O, levoglucosan (LVG) and O_2 were selected as species involved in the reactions, and the time scale associated with their oxidation was calculated. Data were taken from Wang (Wang et al. 2012) and Peterson and Brown (Peterson and Brown 2021).

The next step that was analysed was the flame propagation in the gaseous phase, constituted solely by cellulose pyrolysis products and no dust. Considering the cellulose flash pyrolysis experiments carried out by Piskorz (Piskorz et al. 2000b) and Graham (Graham et al. 1984), an average composition was determined, and the flame speed was calculated on Chemkin (Ansys).

Finally, the speed of a flame propagating in a cellulose dust cloud was estimated using the results of this work and the Silverstrini's relationship (Silvestrini et al. 2008) modified as proposed by Santandrea (Santandrea et al. 2020). A space of 16.1 cm (distance between the centre of the 20L vessel and the inner wall) was considered in the calculation.

Section 4 in Annex 3 provides further details and resumes formulas and data used in the time scale analysis.

As depicted in Figure 4-5, the first four phenomena represent four fundamental bricks of the global phenomenon, while flame propagation is a 1D phenomenon involving all the previous ones. Pyrolysis requires more time to occur, while the particle heating and the gaseous product oxidation steps are significantly lower. The oxidation of LVG is also faster than pyrolysis, but their reaction rate is nonetheless comparable. It should be noticed that LVG oxidation occurs at sensibly higher temperatures than cellulose pyrolysis, whose endothermicity limits the increase of the particle temperature (Boutin et al. 2002b; Piskorz et al. 2000b). Once the enthalpy of oxidation is released, the temperature suddenly increases, and so do the reaction

rates. These results constitute the reason that convinced the authors to build this work, which focused on the role of pyrolysis and its products in organic dust explosions.

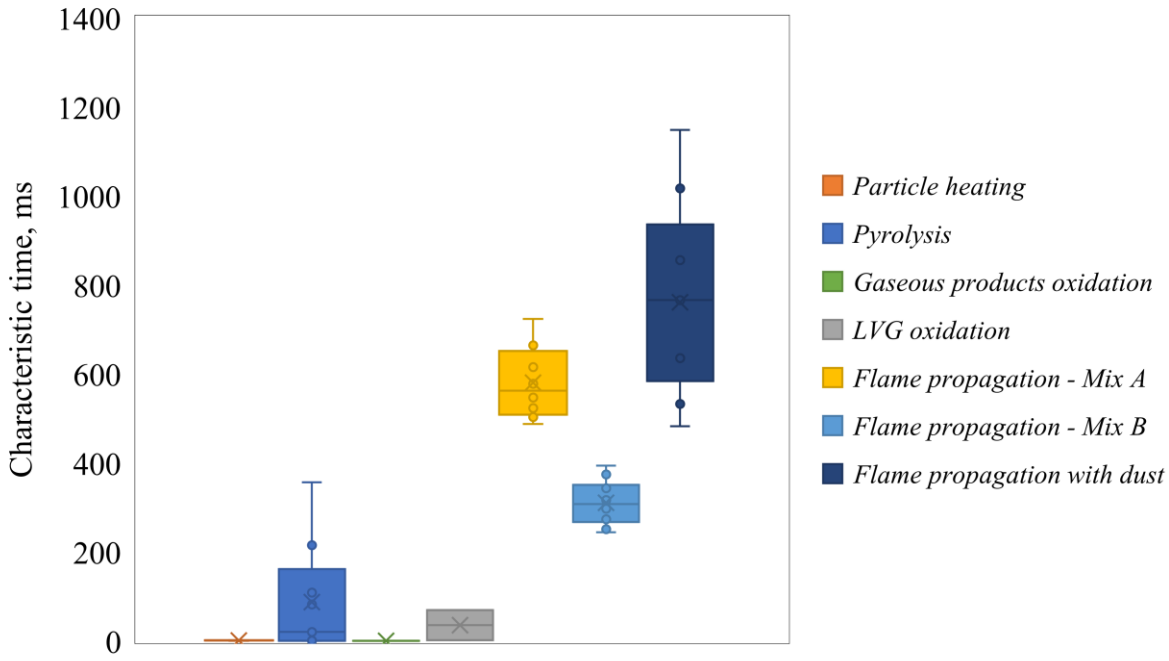

Figure 4-5 - Characteristic times of the steps considered in the time scale analysis

3.4 Hybrid mixture explosion

3.4.1 Constant ER experiments

To highlight the effect of the pyrolysis step on cellulose explosion, tests were performed on cellulose/pyrolysis gas mixtures in the 20L sphere using the procedure previously described. The evolution of the rate of pressure rise and explosion overpressure are shown in Figure 4-7 and Figure 4-6. At least three series of experiments were performed by keeping the equivalence ratio constant, as represented by the dotted lines in Figure 4-7. It appears clearly that the explosion overpressure varies slightly at constant ER (Figure 4-6). Over the concentration range, the highest explosion pressures were obtained for gas concentrations comprised between 19 and 35 vol% and dust concentrations lower than 300 g/m^3.

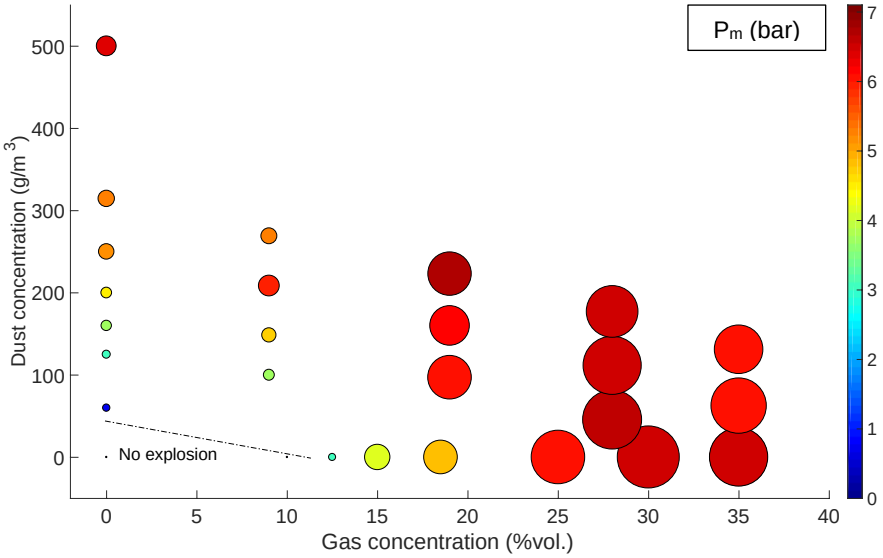

Figure 4-6 - Explosion overpressure of cellulose/pyrolysis gases (900°C). The presence of water vapor is considered for hybrid mixtures; no char. Both size and colour of the circle are related to P_m

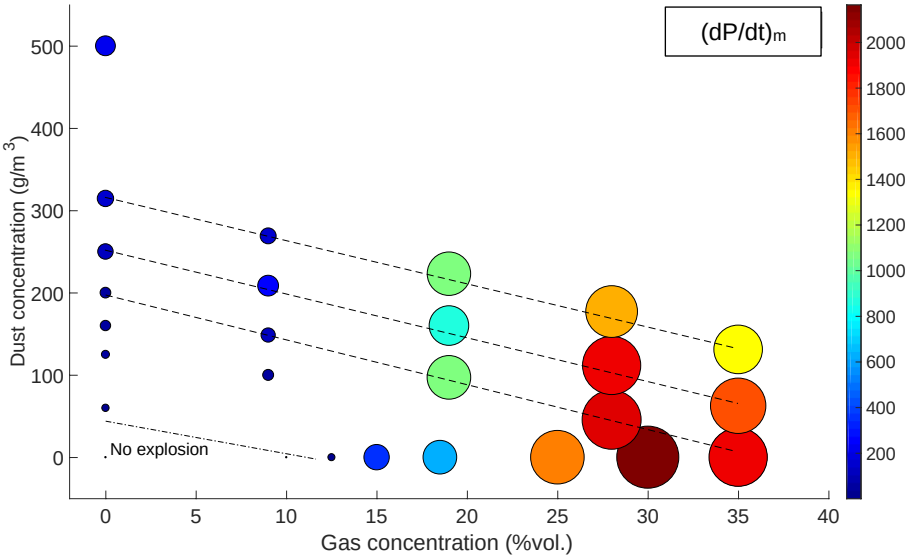

Figure 4-7 - Rate of pressure rise of cellulose/pyrolysis gases (900°C). The presence of water vapor is considered for hybrid mixtures; no char. Both size and color of the circle are related to dP/dt_m

The impact of the pyrolysis step on the explosion kinetics is obvious in Figure 4-6. At a constant ER, the rate of pressure rise can vary by a factor of 30 depending on the composition of the hybrid mixture. At low ER, the highest rates of pressure rise are obtained for hybrid mixtures and not for pure gas, e.g. 1955 bar/s for a mixture of 28 vol% gas and 0.91 g cellulose compared to 1910 bar/s for 35 vol% pure gas. Although the increase described here is small and remains questionable due to experimental errors, similar trends were obtained for mixtures

made from gases generated at 700°C (from 900 bar/s to 1315 bar/s by adding 1 g of cellulose to 38 vol% gases – Figure 4-6). On the other hand, increasing slightly the gas content from a pure dust-air cloud (left-hand side of Figure 4-6) does not change significantly its explosion severity. In this specific case, the effect of pyrolysis gas addition on the explosion kinetics is clearly visible for gas concentrations greater than the lower explosible limit. As soon as the local concentration of pyrolysis gases is higher than the LEL, the rate-limiting step of the explosion is no longer the particle pyrolysis but becomes related to the oxidation of the pyrolysis products in homogeneous phase. However, as previously mentioned, this does not mean that the solid particles present in the mixture do not play a specific role in the explosion. This will be particularly highlighted when studying the influence of char.

3.4.2 Constant reactant mass experiments

Tests were also carried out on hybrid mixtures by keeping the reactant mass constant at 10 g, i.e. by testing 10 g of pyrolysis gases, 10 g of cellulose or any combination of x grams of cellulose and y grams of gases (with x + y = 10 g). Results are shown in Figure 4-8 for both gas mixtures. At first, it appears that, whatever the gas mixture, the explosion overpressure remains nearly constant and unaffected by the hybrid mixture composition, which validates this approach.

These results also confirm that the maximum value of $(dP/dt)_m$ is not necessarily obtained for pure gases and that the addition of a slight amount of dust can significantly increase the rate of pressure rise. Moreover, it is confirmed that for high dust concentrations, a gas concentration increases up to 8 vol% does not modify significantly the explosion severity. This assertion is especially true when dealing with the gas generated at 700 °C. For the mix B (900 °C), the high content of hydrogen leads to an increase of the maximum rate of pressure rise, from approximately 1000 $bar.s^{-1}$ for a mixture of 2 g cellulose and 8 g of mix A to 2080 $bar.s^{-1}$ with mix B. Again, the impact of both the pyrolysis step and the gas composition on explosion kinetics is then clearly stressed. It should be noted that the influence of particle heating has been neglected due to the small PSD.

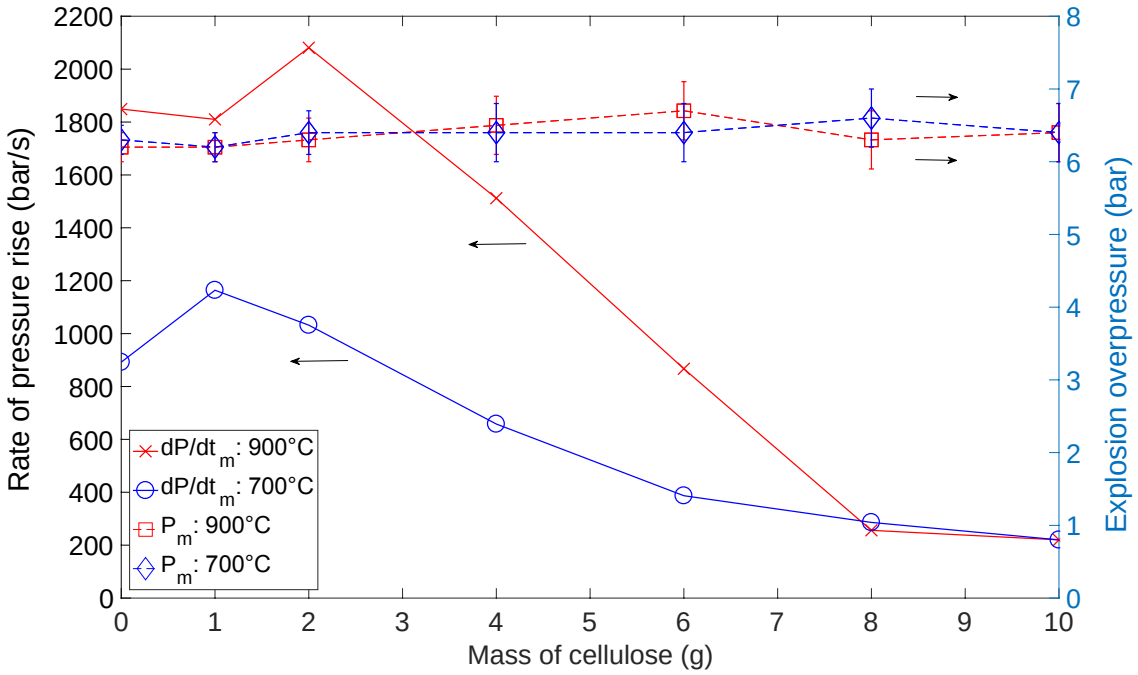

Figure 4-8 - Explosion severity of cellulose/pyrolysis gases (generated at 900 and 700°C) for a constant reactant mass of 10 g and considering water vapor; no char

3.4.3 Influence of water vapor

The previous experiments were performed by adding water vapor up to 8 wt% of the gas composition, in order to take the water generated by pyrolysis into account. Figure 4-9 shows a set of tests realized at constant equivalence ratio (ER = 0.7) with or without adding water vapor. A slight pressure decrease is observed when water vapor is added to the reactive mixture; however, this effect should be examined with caution due to experimental uncertainties and can even be considered negligible.

The influence of water vapor on the combustion kinetics appears to be more pronounced, while remaining moderate. Tests performed with hybrid mixtures of mix A (700 °C) and cellulose confirmed that the deflagration index slightly decreases (less than 7 %) when water vapor is added to the reactive mixture. Such effect is especially well known and used in hydrocarbons combustion to reduce the flame temperature and, therefore, decrease the NO_x emission.

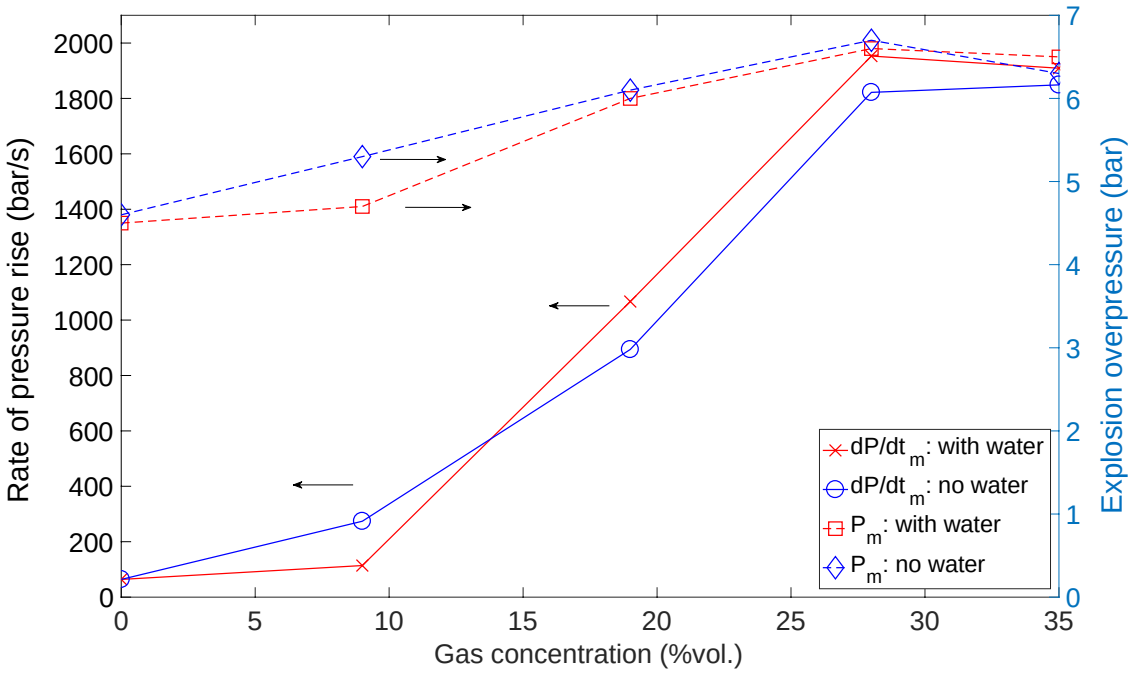

Figure 4-9 - Influence of water vapor generated during pyrolysis on the explosion severity of cellulose/pyrolysis gases (generated at 900 °C) for a theoretical fuel equivalence ratio of 0.7; no char

3.4.4 Influence of char

As described in Figure 4-2, the products generated by the pyrolysis of an organic particle are mainly permanent gases, water vapor, tars, which can be gasified at high temperatures, and also char. Even if the char quantity is usually low, especially during a flash pyrolysis (between 5 and 10 wt%), it is legitimate to ask if its impact is negligible or not on the dust explosion kinetics. 'Kinetics', as from a thermodynamic point of view, the char contribution can be regarded as negligible, which seems to be confirmed by the evolution of the explosion overpressure in Figure 4-10 (parameter which still can be affected by heat transfer modification).

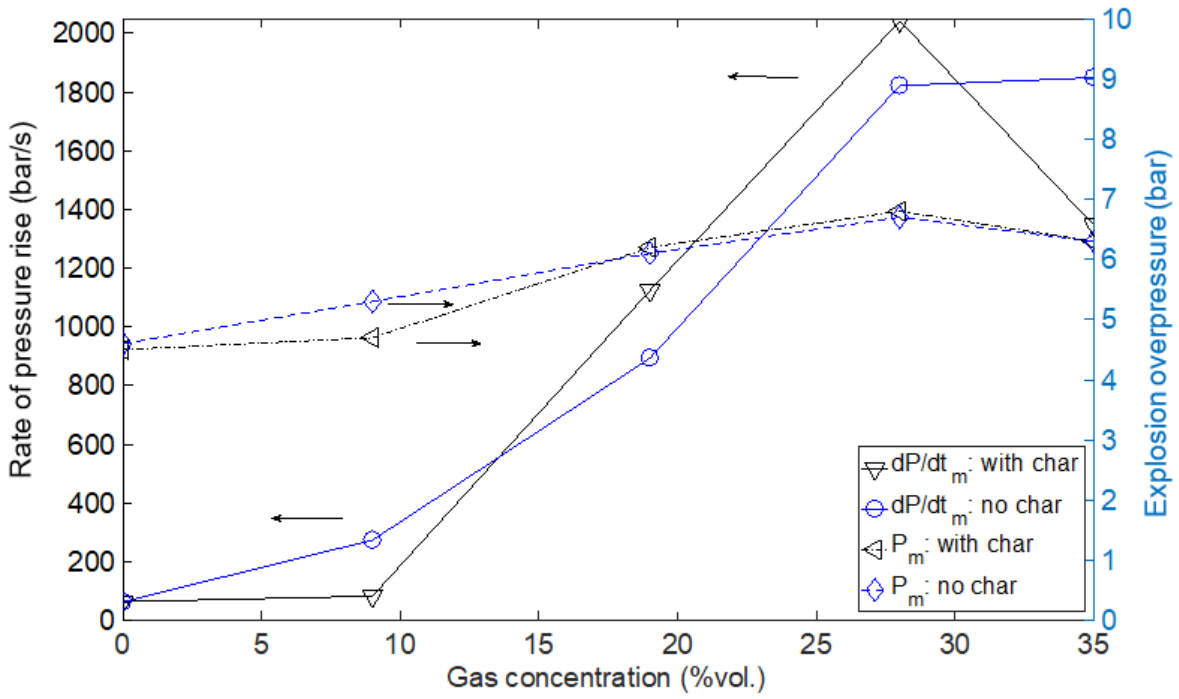

Figure 4-10 - Effect of char generated during pyrolysis on the explosion severity of cellulose/pyrolysis gases (generated at 900 °C) for a theoretical fuel equivalence ratio of 0.7; no water vapor

On the contrary, the rate of pressure rise appears to be influenced by the presence of char, even for very low quantities added (here, only 50 mg). At 28 vol% gas concentration and 0.91 g of cellulose, the addition of char leads to the augmentation of the $(dP/dt)_m$ from 1855 to 2045 bar/s. Similar tests were performed on mix A and demonstrated a significant increase of the maximum rate of pressure rise from less than 900 bar/s to 1315 bar/s when 100 mg of char was added to pure gases. Such evolution confirms the positive effect already noticed when a small amount of cellulose is combined to pure gases. The origins of the explosion severity enhancement of these hybrid mixtures can notably be found in the essential role of the powders on the radiative transfer (Torrado, 2017). Nevertheless, their effect on the flame stretching but also the fact that they can act as solid kernels for soot nucleation should also be considered.

3.4.5 Influence of tars

Figure 4-11 shows the results of the explosion severity tests performed with the tar-coated cellulose at 200 g/m^3. In Annex 3, further details are provided concerning the four tar-cellulose mixes. As can be seen, the condensable fraction concentration influences both the explosion overpressure and the rate of pressure rise. Increasing the availability of these pyrolysis products means skipping several steps of the global kinetic mechanisms and thus simulating partial

pyrolysis. Among the reaction bypassed, the cellulose activation, the main chain's depolymerisation, and the generation of levoglucosan, volatiles, and gaseous species can be found. Moreover, the char that would be produced in an actual pyrolysis process is not present in the initial system, which has consequences on the radiative heat transfers during the flame propagation. Tars can thus participate in secondary pyrolysis reactions or directly react with oxygen. However, they are in a liquid/solid state at the beginning of the tests and absorbed onto the cellulose particles' surface, meaning they need to vaporise to react, which can change the thermal equilibrium of the global process (compared to pure cellulose). The most abundant compound in the condensable products collected was levoglucosan ($C_6H_{10}O_5$), which corresponds to the monomer of cellulose. It is typically considered a non-volatile species and usually degrades before vaporisation. However, forming an intermediate ("metaplast") liquid is possible at high particle heating rates, whose vaporisation is associated with a non-negligible vaporisation enthalpy (Dufour et al. 2011; Oja and Suuberg 1999; Suuberg et al. 1996). It can be related to the low increase of P_m and $(dP/dt)_m$ noticeable in Figure 4-11. It also appears that a plateau was rapidly attained as a small amount of tar was added to the powder. The increase in explosion severity is not as great as when pyrolysis gases are added, because by substituting tar for cellulose, the permanent gases generated during primary pyrolysis are not taken into account. This difference illustrates the importance of the latter in the dust explosion process. With the exception of the point corresponding to 15.6% of tar (sample apparently less homogeneous), almost no variation between the four tar contents is noticeable, likely related to faster gaseous product generation. Consequently, the LEL is attained more rapidly than pure cellulose, triggering the oxidation reactions sooner. In a further step, the explosion severity of cellulose will be compared to that of a mixture of char, tar, water vapour and permanent pyrolysis gases at constant mass.

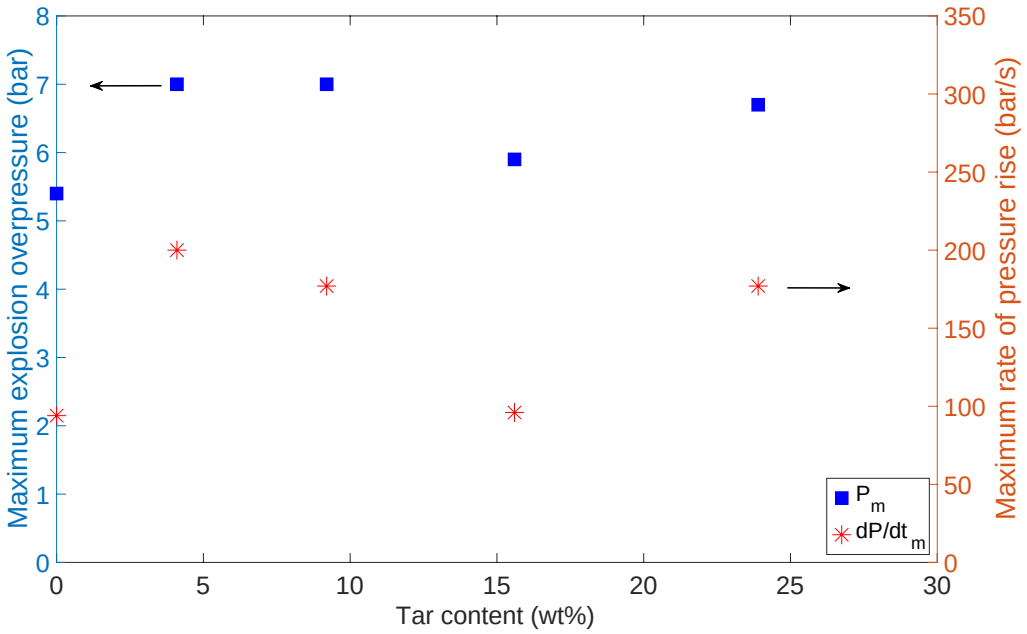

Figure 4-11 - The explosion severity parameters as a function of the tar content for cellulose/tar mixture at 200 g/m^3

4. Conclusions

The role of pyrolysis in an organic dust explosion phenomenon was studied. The influence of the gaseous products, the char, tar and the water vapour was also analysed. Moreover, by the means of the modified configuration of the Godbert-Greenwald furnace, it was possible to underline the role of the temperature of the pyrolysis step in a dust explosion; or, to be more precise, the role of the thermal gradient applied to the organic powder cloud, as the pyrolysis temperature is usually limited by the endothermicity of this process. The main conclusions are:

- A constant mass experimental approach allows to obtain the same explosion pressure for a cellulose cloud and a hybrid cellulose/pyrolysis gas mixture, which validates the relevance of this method in order to identify the rate-limiting steps;
- Keeping both the fuel equivalence ratio or the reactive mass content constant is not sufficient to obtain the same rate of pressure rise for hybrid mixtures of cellulose and pyrolysis gases. Pyrolysis reaction is then the main rate-limiting step during an organic dust explosion, as long as the particle heating is very fast (e.g. a powder with a wide PSD can exhibit both reaction-, heating- and diffusion-limitation according to the diameter of its particles);

- The presence of a sufficient amount of pyrolysis gases around the particles enhances the explosion kinetics, but replacing all or part of an organic powder by its pyrolysis gases modifies very little the energetic content of the hybrid mixture and thus the explosion thermodynamics;
- The hydrogen fraction in the gaseous mixtures, and therefore, the temperature at which the pyrolysis takes place, upstream of the flame front, had a strong influence on the explosion sensitivity as well as on the combustion kinetics. During the development of an organic dust explosion, the flame temperature evolves as well as the pyrolysis gases composition, which impacts the flame propagation dynamics;
- The amount of solid particle, char or unburnt cellulose, present ahead of the flame front, has no or little impact on the reactivity of the powders. Nevertheless, it plays an important role on the flame propagation, as it increases significantly the radiative heat transfer towards the pre-heating zone;
- The water vapor produced during the pyrolysis does not affect greatly the thermodynamic of the combustion reaction, but it seems to slightly influence the kinetics by modifying the flame temperature;
- The condensable fraction had a non-negligible influence on the explosion severity, likely due to their direct reaction with oxygen, which increases both P_m and $(dP/dt)_m$, and their volatilisation, which limits the global process rate.

In conclusion, studying hybrid mixtures reveals several aspects of organic dust explosion and appears to be essential to better understand and model this phenomenon (Pico et al., 2020). More than a particular case, this makes hybrid mixtures explosion “a common case”.

References

Abbas, Zaheer, Dieter Gabel, Arne Krietsch, and Ulrich Krause. 2022. 'Quasi-Static Dispersion of Dusts for the Determination of Lower Explosion Limits of Hybrid Mixtures'. *Journal of Loss Prevention in the Process Industries* 74:104640-. doi: 10.1016/j.jlp.2021.104640.

Boutin, Olivier, Monique Ferrer, and Jacques Lédé. 2002. 'Flash Pyrolysis of Cellulose Pellets Submitted to a Concentrated Radiation: Experiments and Modelling'. *Chemical Engineering Science* 57(1):15–25. doi: 10.1016/S0009-2509(01)00360-8.

Cloney, Chris T., Robert C. Ripley, Michael J. Pegg, and Paul R. Amyotte. 2017. 'Evaluating Regime Diagrams for Closed Volume Hybrid Explosions'. *Journal of Loss Prevention in the Process Industries* 49:912–18. doi: 10.1016/j.jlp.2017.03.004.

Commandré, J. M., H. Lahmidi, S. Salvador, and N. Dupassieux. 2011. 'Pyrolysis of Wood at High Temperature: The Influence of Experimental Parameters on Gaseous Products'. *Fuel Processing Technology* 92(5):837–44. doi: 10.1016/j.fuproc.2010.07.009.

Doyle, W. L., J. B. Conway, and A. V. Grosse. 1958. 'The Combustion of Zirconium in Oxygen'. *Journal of Inorganic and Nuclear Chemistry* 6(2):138–44. doi: 10.1016/0022-1902(58)80059-7.

Dufaud, O., L. Perrin, M. Traore, S. Chazelet, and D. Thomas. 2009. 'Explosions of Vapour/Dust Hybrid Mixtures: A Particular Class'. *Powder Technology* 190(1–2):269–73. doi: 10.1016/j.powtec.2008.04.046.

Dufour, Anthony, Bajil Ouartassi, Roda Bounaceur, and André Zoulalian. 2011. 'Modelling Intra-Particle Phenomena of Biomass Pyrolysis'. *Chemical Engineering Research and Design* 89(10):2136–46. doi: 10.1016/j.cherd.2011.01.005.

EN 14034-1. 2004. *Determination of Explosion Characteristics of Dust Clouds - Part 1: Determination of the Maximum Explosion Pressure Pmax of Dust Clouds*.

EN 14034-2. 2006. *Determination of Explosion Characteristics of Dust Clouds - Part 2: Determination of the Maximum Rate of Explosion Pressure Rise (Dp/Dt)Max of Dust Clouds*.

Funazukuri, T., R. R. Hudgins, and P. L. Silveston. 1986. 'Product Distribution in Pyrolysis of Cellulose in a Microfluidized Bed'. *Journal of Analytical and Applied Pyrolysis* 9(2):139–58. doi: 10.1016/0165-2370(86)85004-5.

Graham, R. G., L. K. Mok, M. A. Bergougnou, H. I. De Lasa, and B. A. Freel. 1984. 'Fast Pyrolysis (Ultrapyrolysis) of Cellulose'. *Journal of Analytical and Applied Pyrolysis* 6(4):363–74. doi: 10.1016/0165-2370(84)80030-3.

Guo, Chaowei, Hao Shao, Shuguang Jiang, Yajun Wang, Kai Wang, and Zhengyan Wu. 2020. 'Effect of Low-Concentration Coal Dust on Gas Explosion Propagation Law'. *Powder Technology* 367:243–52. doi: 10.1016/j.powtec.2020.03.045.

Lédé, Jacques. 2012. 'Cellulose Pyrolysis Kinetics: An Historical Review on the Existence and Role of Intermediate Active Cellulose'. *Journal of Analytical and Applied Pyrolysis* 94:17–32. doi: 10.1016/j.jaap.2011.12.019.

Miller, R. S., and J. Bellan. 1996. 'Analysis of Reaction Products and Conversion Time in the Pyrolysis of Cellulose and Wood Particles'. *Combustion Science and Technology* 119(1–6):331–73. doi: 10.1080/00102209608952004.

Oja, V., and E. M. Suuberg. 1999. 'Vapor Pressures and Enthalpies of Sublimation of D -Glucose, D -Xylose, Cellobiose, and Levoglucosan'. *Journal of Chemical & Engineering Data* 44(1):26–29. doi: 10.1021/je980119b.

Paulsen, Alex D., Matthew S. Mettler, and Paul J. Dauenhauer. 2013. 'The Role of Sample Dimension and Temperature in Cellulose Pyrolysis'. *Energy & Fuels* 27(4):2126–34. doi: 10.1021/ef302117j.

Peterson, Chad A., and Robert C. Brown. 2021. 'Global Gas-Phase Oxidation Rates of Select Products from the Fast Pyrolysis of Lignocellulose'. *Energy & Fuels* 35(21):17103–13. doi: 10.1021/acs.energyfuels.1c01207.

Pietraccini, Matteo, Eloise Delon, Audrey Santandrea, Stéphanie Pacault, Pierre-Alexandre Glaude, Anthony Dufour, and Olivier Dufaud. 2021. 'Determination of Heterogeneous Reaction Mechanisms: A Key Milestone in Dust Explosion Modelling'. *Journal of Loss Prevention in the Process Industries* 73:104589. doi: 10.1016/j.jlp.2021.104589.

Piskorz, J., P. Majerski, D. Radlein, A. Vladars-Usas, and D. S. Scott. 2000. 'Flash Pyrolysis of Cellulose for Production of Anhydro-Oligomers'. *Journal of Analytical and Applied Pyrolysis* 56(2):145–66. doi: 10.1016/S0165-2370(00)00089-9.

Piskorz, Jan, Desmond St. A. G. Radlein, Donald S. Scott, and Stefan Czernik. 1988. 'Liquid Products from the Fast Pyrolysis of Wood and Cellulose'. Pp. 557–71 in *Research in Thermochemical Biomass Conversion*, edited by A. V. Bridgwater and J. L. Kuester. Dordrecht: Springer Netherlands.

Ranzi, Eliseo, Paulo Eduardo Amaral Debiagi, and Alessio Frassoldati. 2017. 'Mathematical Modeling of Fast Biomass Pyrolysis and Bio-Oil Formation. Note I: Kinetic Mechanism of Biomass Pyrolysis'. *ACS Sustainable Chemistry & Engineering* 5(4):2867–81. doi: 10.1021/acssuschemeng.6b03096.

Sanchirico, Roberto, Paola Russo, Anna Saliva, Aurelie Doussot, Valeria Di Sarli, and Almerinda Di Benedetto. 2015. 'Explosion of Lycopodium-Nicotinic Acid–Methane Complex Hybrid Mixtures'. *Journal of Loss Prevention in the Process Industries* 36:505–8. doi: 10.1016/j.jlp.2014.12.008.

Santandrea, Audrey, Marine Gavard, Stéphanie Pacault, Alexis Vignes, Laurent Perrin, and Olivier Dufaud. 2020. '"Knock on Nanocellulose": Approaching the Laminar Burning Velocity of Powder-Air Flames'. *Process Safety and Environmental Protection* 134:247–59. doi: 10.1016/j.psep.2019.12.018.

Silvestrini, M., B. Genova, and F. J. Leon Trujillo. 2008. 'Correlations for FLame Speed and Explosion Overpressure of Dust Clouds inside Industrial Enclosures'. *Journal of Loss Prevention in the Process Industries* 19.

Spitzer, S., Krietsch, A., Askar, E., and Schröder, V. 2020. *Developments on determination procedures for safety parameters of explosion protection for hybrid mixtures [Entwicklungen zu bestimmungsverfahren für sicherheitstechnische kenngrößen des explosionsschutzes für hybride gemische]*. 2376. VDI.

Suuberg, Eric M., Ivan Milosavljevic, and Vahur Oja. 1996. 'Two-Regime Global Kinetics of Cellulose Pyrolysis: The Role of Tar Evaporation'. *Symposium (International) on Combustion* 26(1):1515–21. doi: 10.1016/S0082-0784(96)80373-0.

Taveau, J. R., J. E. Going, S. Hochgreb, S. M. Lemkowitz, and D. J. E. M. Roekaerts. 2017. 'Igniter-Induced Hybrids in the 20-l Sphere'. *Journal of Loss Prevention in the Process Industries* 49:348–56. doi: 10.1016/j.jlp.2017.07.014.

Torrado, David. n.d. 'Effet de Nanoparticules de Noir de Carbone Sur La Sévérité d'explosions de Mélanges Des Gaz'.

Wang, Lin, Zhaohui Liu, Sheng Chen, and Chuguang Zheng. 2012. 'Comparison of Different Global Combustion Mechanisms Under Hot and Diluted Oxidation Conditions'. *Combustion Science and Technology* 184(2):259–76. doi: 10.1080/00102202.2011.635612.

Wang, Qing, Hao Song, Shuo Pan, Nanhang Dong, Xinmin Wang, and Shipeng Sun. 2020. 'Initial Pyrolysis Mechanism and Product Formation of Cellulose: An Experimental and Density Functional Theory(DFT) Study'. *Scientific Reports* 10(1):3626. doi: 10.1038/s41598-020-60095-2.

Zanzi, Rolando, Krister Sjöström, and Emilia Björnbom. 1996. 'Rapid High-Temperature Pyrolysis of Biomass in a Free-Fall Reactor'. *Fuel (Guildford)* 75(5):545–50. doi: 10.1016/0016-2361(95)00304-5.

CHAPTER 5

Summary

Chapter 5 relates to an experimental setup that does not belong to the usual dust explosion testing domain: a micro-fluidised bed. This reactor allows to attain a permanent-regime flash pyrolysis process and to control the temperature of the reactive volume, contrarily to 20L sphere and G-G furnace. It allowed, thus, to decouple the pyrolysis step from the oxidation of the gaseous products, usually intimately linked during the fast combustion of an organic powder. A deep understanding of the fluidisation regimes and a comprehension of the influence of the temperature are vital for optimising the reactor operating conditions. Cellulose and oak wood were selected as powder samples, and their thermal degradation was observed through a visualisation window during the pyrolysis. This work exploits an in-situ high-speed video recording system to follow the modifications in the fluidisation regimes as the thermal conversion proceeds. Agglomeration and bed compaction were analyzed in real-time during the pyrolysis of biomass powders. Based on these analyses, the conditions (biomass flow rate, temperature, etc.) for a stable operation of the micro-fluidized bed were defined.

Resumé

Le Chapitre 5 porte sur un dispositif expérimental qui n'appartient pas au domaine habituel des explosions de poussières : un lit micro-fluidisé. Ce réacteur permet de créer un processus de pyrolyse flash en régime permanent et de contrôler la température du volume réactif, contrairement à la sphère de 20L et au four G-G. Il a permis, donc, de découpler l'étape de pyrolyse de l'oxydation des produits gazeux, habituellement intimement liée lors de la combustion rapide d'une poudre organique. Une connaissance approfondie des régimes de fluidisation et une compréhension de l'influence de la température sont essentielles pour optimiser les conditions de fonctionnement du réacteur. La cellulose et le bois de chêne ont été sélectionnés comme échantillons de poudre, et leur dégradation thermique a été observée à travers une fenêtre de visualisation pendant la pyrolyse. Ce travail exploite un système d'enregistrement vidéo à haute vitesse in-situ pour suivre les modifications des régimes de fluidisation au fur et à mesure que la conversion de la biomasse avance. L'agglomération et la compaction du lit ont été analysés en temps réel pendant la pyrolyse des poudres de biomasse. Sur la base de ces analyses, les conditions (débit de biomasse, température, etc.) pour un fonctionnement stable du lit micro-fluidisé ont été définies.

Effect of air on the operability of biomass pyrolysis in a micro-fluidized bed

Matteo Pietraccini [1], Olivier Dufaud [1], Pierre-Alexandre Glaude [1], Anthony Dufour [1,*]

[1] *Université de Lorraine, CNRS, LRGP, F-54000 Nancy, France*

* *corresponding author: anthony.dufour@univ-lorraine.fr*

Abstract

Biomass autothermal pyrolysis is a promising approach for reducing the bottleneck effect of heat transfer in pyrolysis reactors notably in fluidized beds. However, including oxygen in the reactor results in modifications of the products and of the fluidisation regime. In this work, the influence of oxygen on a biomass (cellulose and oak wood) oxidative pyrolysis process is studied in a micro-fluidized bed, especially by focusing on the sand bed agglomeration tendency. The fluidization behaviour of the sand bed was recorded in operando, during the pyrolysis, by a high-speed camera through a quartz window. We have characterized by the high-speed videos the bed height and the surface bubbling line trend over biomass feeding time. At 400 and 500°C, under nitrogen, cellulose led to critical compaction of the sand bed, changing the fluidisation regime and enhancing the surface bubbling, due to an agglomeration of the bed with sticky intermediate liquid. Contrarily, stable fluidisation was observed for cellulose under air. Oxygen reduces the agglomeration due to the intermediate liquid. Concerning oak wood, the bubbling of the splash zone decreased under nitrogen at 400 and 500°C due to some agglomeration. Oxygen presents a lower improvement of the fluidization stability than for cellulose.

Graphical abstract

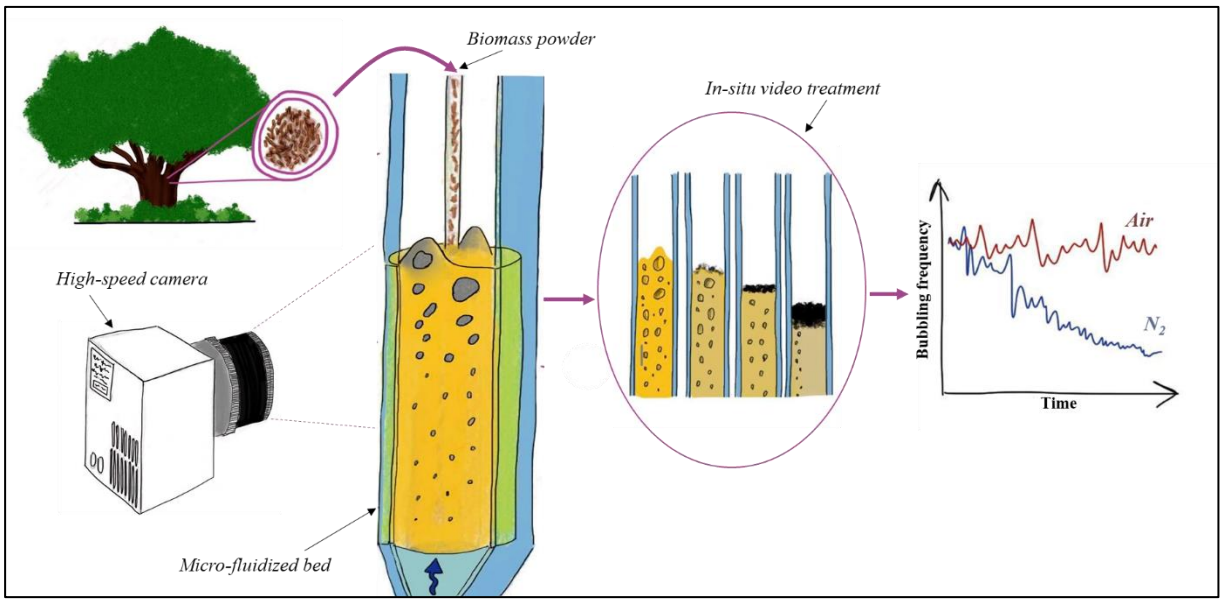

1. Introduction

Pyrolysis is conventionally considered as a thermal degradation process that allows for transforming a carbonaceous material into solid, liquid and gaseous products. Numerous operating conditions influence the final result and product yields: the reactor temperature, the heating rate, and the sweep gas composition are only a few. By choosing a low heating rate (order of magnitude of hundreds of Kelvins per hour, approximately), the process can be classified into "slow pyrolysis", favouring solid residues (char) formation. On the other hand, by selecting a high heating rate (in the range of more than 10K/s), the formation of bio-oil can be promoted and the pyrolysis can be defined as "fast pyrolysis".

According to Bridgwater (Bridgwater 2003), fast pyrolysis has gained interest in the beginning of the XXIth century. Several reactors can be exploited to perform fast pyrolysis, accordingly to the purpose of a study. The choice may fall on (Boutin et al. 2002b; Kim et al. 2014; Le Brech et al. 2016; Venderbosch and Prins 2010): bubbling fluidized and circulating beds; entrained downflow and freefall reactors; ablative reactors; moving-grate vacuum reactors; rotating-cone pyrolysers; image or solar furnace. Small particles of biomass are required for fast pyrolysis in order to reduce intra-particle heat transfer. As described in Polin (Polin et al. 2019), one of the main challenges when using such a finely subdivided material is

improving the heat transfer efficiency between the reactor and the external surface of the powder.

Fluidised beds promote the heat transfers from the hot sand to the external surface of particles. The fluidization promotes the temperature homogeneity in the sand, as well as the external gas-to-particle diffusion (X. Liu, Xu, and Gao 2008). In 2005, Potic (Potic et al. 2005) proposed to employ a micro fluidised bed (MFB) for studying the kinetics of thermal degradation of biomass. Furthermore, Wang (Wang 2011) have defined the operability of Micro Fluidised Bed Reaction Analysis (MFBRA), which exploits the micro fluidised beds to determine complex reaction mechanisms in kinetically-controlled systems. Biomass thermal conversion processes are widely studied in MFB (Kim et al. 2014; Le Brech et al. 2016; Polin et al. 2019). However, the global endothermicity of fast pyrolysis may impact its operability and reduce the temperature of the bed. The oxidative pyrolysis (or autothermal pyrolysis) is catching the scientific community's attention. Introducing oxygen into the system triggers exothermic oxidation reactions, providing the heat necessary for the pyrolysis reactions. Several works (Amutio et al. 2012; Bilbao et al. 1997; Kim et al. 2014; Polin et al. 2019; Shen et al. 2011) already showed the potential interest in oxidative pyrolysis to intensify the fluidized bed reactor, without profoundly impacting the quality of the products (especially the bio-oil). The introduction of oxygen in the pyrolysis fluidized bed reduces considerably the complexity of the pyrolysis process. Indeed, in complex dual fluidized bed reactors, the sand is heated by char combustion in a separate fluidized bed and the hot sand is looped back to pyrolyser.

This work proposes a characterization method to analyse and quantify the operability of biomass oxidative pyrolysis in a micro-fluidized bed. It focuses on the sand bed's agglomeration and on the influence of the atmosphere (air/nitrogen) on the fluidization behaviour. The paper completes previous studies (Jia et al. 2017a; 2017b; 2015, 2016) with a different biomass injection system (continuous vs step-wise in previous studies) and by studying the effect of air as fluidisation gas. To the best of our knowledge, we present for the first time the visualization of a micro-fluidized bed in operando conditions, with a fast camera, in real-time during the pyrolysis of biomass.

2. Materials and Methods

2.1 Powder characterization

Cellulose (Vivapur 200) and oak wood were chosen as feedstock powder samples. They represent two different complexity levels of biomass feedstock. Cellulose was used as it is. The bark was removed from oak, which was then reduced in chips and ground in a knife mill, using subsequently a 5-, 2- and 1-mm screen. Finally, the wood powder was sieved with 50- and 200-μm sieves to reduce the finest and the coarsest particle fraction. Fines might hinder the powder flow in the feeding system by decreasing the flowability, while coarser might geometrically obstacle the particles inlet flow. Furthermore, fine particles may be rapidly elutriated from the reactor. The particle size distribution (PSD) of the two samples was determined by a Malvern Mastersizer 3000 equipped with an aero-dispersion unit. Results are shown in Table 5-1. Particle shape and morphology were characterised by a Scanning Electronic Microscope (JEOL JSM-649-LV) and by a digital microscope (5 Mp Dino-lite Pro HR digital microscope). Proximate and elemental analyses were performed to determine the moisture content (MC), volatile matter (VM), fixed carbon (FC) and ash content of the samples. A Mettler Toledo HE53 Moisture Analyzer was used to determine the MC. VM and FC were calculated by thermogravimetric analysis (TGA) in a Mettler Toledo TGA STARe System. Finally, the ash content was assessed by using a Nabertherm B150 oven. The C, H, O, N and S contents were determined by a Vario MICRO cube CHNOS elemental analyser. Results are reported in Table 5-2.

Table 5-1 - Characteristic diameters of the powders (μm)

	D10	**D50**	**D90**	**Sauter diameter**	**De Brouckere diameter**
Cellulose	65	219	463	134	246
Oak	70	155	318	101	177
Sand	189	264	371	256	273

Table 5-2 - Proximate and elemental analysis of cellulose and oak wood

	Cellulose	**Oak wood**	
Proximate analysis			
MC	5.3	6.1	wt%
VM	87.4	77.5	wt%
FC	7.2	16.2	wt%
Ash	0.1	0.3	wt%
Elemental analysis			
C	44.4	46.3	wt%
H	6.2	6.5	wt%
O	49.4	47.0	wt%
N	-	0.1	wt%
S	-	0.1	wt%

2.2 Experimental setup

Our experimental device is mainly composed of a home-made microfluidized bed with a quartz window and a high-speed camera allowing operando imaging of the fluidization during the pyrolysis of biomass.

2.2.1 Micro-fluidized bed reactor

Figure 5-1 shows a schematic diagram of the reactor. Its design is based on the study of Liu (X. Liu et al. 2008), by choosing the correct reactor internal diameter and bed sand particle size as the ones proposed by Liu (Liu et al. 2008). According to Liu, fluidised beds with an inner diameter of less than 20 mm is significantly more sensitive to bed wall effects than larger reactors. The reactor was composed of a quartz cylindrical tube of 20 mm of internal diameter, a 4-mm (I.D.) inlet gas, and a sintered silica plate for promoting a homogeneous gas distribution in the fluidised bed. The bed was 20 g of Fontainebleau silica sand (3 cm static bed height), whose PSD and particle morphology were characterised by a Malvern Mastersizer 3000 equipped with an aero-dispersion unit and by a 5 Mp Dino-lite Pro HR digital microscope, respectively. Particle sizes of the sand are reported in Table 5-1. The sand belongs to the group

B (sand-like class) according to the Geldart classification, both at 20 and 500°C (see Figure S 19 in Annex 4). The particle size and the amount of the sand are consistent with the values provided by Liu (Liu et al. 2008). It presents a stable and homogeneous fluidisation. The outlet line is an 8 mm inner diameter glass-quartz tube placed approximately 150 mm above the sintered plate to ensure the outlet flow. The freeboard represents a volume of 38 cm^3, which corresponds to a residence time of the gas/vapour phase of around 1 s in this section.

The heating system was developed at CNRS Nancy and it is composed of a Thermocoax® heating element set into a quartz tube in order to visualise the fluidisation during the operation (see Figure 5-3). This in-situ visualisation of the fluidized bed at pyrolysis temperatures allows to capture in real-time the evolution of the fluidisation characteristics. The temperature profile along the reactor was measured for set sand temperatures of 400 and 500°C and they are reported in Figure S 20 in Annex 4.

2.2.2 Feeding system

The feeding system was conceived to ensure a continuous powder flow in the fluidised bed. It is a homemade system constituted by an electric motor, a powder reservoir and a connection to the reactor. The motor allows to convey the powder in a 150 mm glass tube ending into the sand bed. Its rotation speed can be changed to have the desired powder flow rate in the bed. The reservoir is a polycarbonate cylinder with a conic end that avoids significant dead volumes. Its capacity is approximately 5 g of biomass powder. A gas flow on the internal upper part counterbalances the pressure from above and guarantees a good flowability of the powder. Similarly as Piskorz (Scott and Piskorz 1982), this flow rate of carrier gas (N_2 or air) entrains the biomass powders through an injection tube into the dense bubbling bed (at about 5mm from the bed surface). Another flow rate of gas was included in the reactor head freeboard to avoid tar deposits and dead volume in this zone. Flow rates were controlled by Brooks electronic flowmeters. The minimal fluidisation velocity of the sand (u_{mf}) was measured with the same method as in Liu (Liu et al. 2008), and it was 4 cm/s. This result is in excellent agreement with their work. All the experiments were conducted at u/u_{mf} equal to 2, therefore with a gas velocity of approximately 8 cm/s. The three gas flows were determined by optimising the biomass/air ratio to have a constant sand bed temperature upon the operation time.

2.2.3 High-speed video analysis

Through the visualisation window (see Figure 5-1 and Figure 5-2), it was possible to assess and better quantify in-situ the peculiar characteristics of the fluidised bed during the pyrolysis processes. Three features were chosen for this purpose:

- Fluidisation flow regimes;
- Bed expansion and height;
- Splash zone deformation.

The different regions of fluidisation were determined by a qualitative visual observation of the flow regimes, similarly to the work of McDonough et al. [226] and Wang et al. [217]. Bed expansion rate and bubbling frequency were chosen to represent and characterize the influence of the agglomeration tendency of the sand bed on the pyrolysis process.

The different regions of fluidisation were determined by a qualitative visual observation of the flow regimes, similarly to the work of McDonough (McDonough et al. 2019) and Wang (Wang 2011). Bed expansion rate and bubbling frequency were chosen to represent and characterize the influence of the agglomeration tendency of the sand bed on the pyrolysis process. All experiments were recorded with a Mikrotron MotionBLITZ Eo Sens mini high-speed camera, set to an acquisition rate of 70 fps. The shutter speed varied between 50 and 300 µs according to the brightness of the surrounding environment. MotionBLITZ Director2 operator software was used for treating high-speed videos. The video duration ranged between 1 and 2 s, and they were recorded approximately each 30 s from the beginning of each experiment. The first 100 frames were extracted from each video to be treated.

A first MATLAB code was developed to calculate the bed height. The frames from each high-speed video were binarized to maximise the contrast between the different zones of the image. The intensity threshold value for the binarisation ranged between 60 and 150. Next, the *Bounding box* function was used to calculate the height of the sand bed. Finally, the *Image batch processor* toolbox was employed to treat all the selected frames simultaneously. The application of the code is represented in Figure 5-2.

A second MATLAB code was built to determine the surface bubbling magnitude. The same binarisation function was adopted to enhance the differences between the sand and the rest of the setup. The background was removed, and a third filter enlightened the edges of the binarized zones. The length of the line corresponding to the sand bed surface was then used to

quantify the bubbling fluidization. Furthermore, the standard deviation of each series allowed appreciating the bed surface fluctuation. Tests were performed at room temperature, 400 and 500°C. An example of the procedure is reported in Figure 5-3.

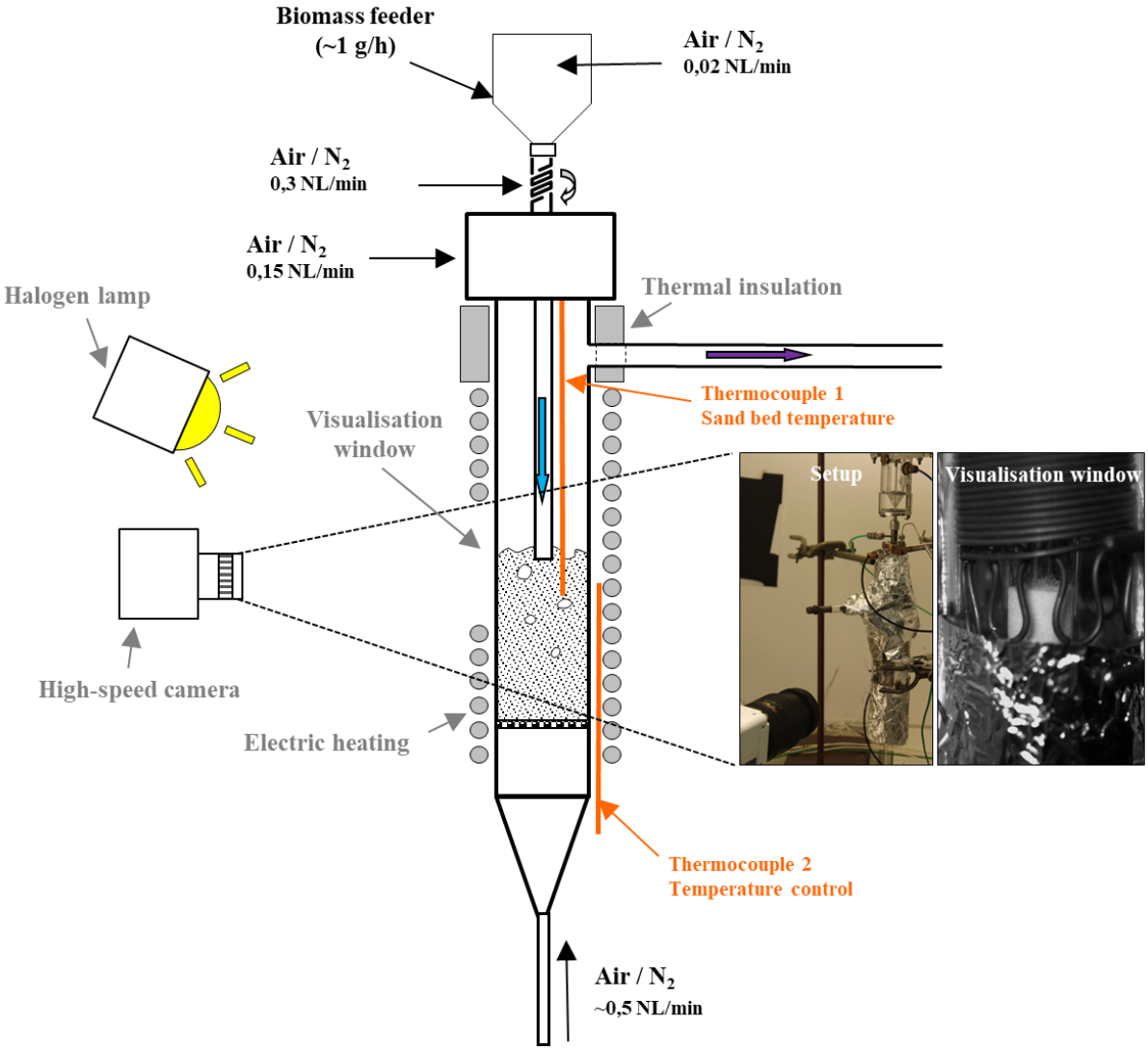

Figure 5-1 - The simplified global scheme of the experimental setup

2.3 Agglomeration characterization

To better characterise the sand bed's agglomeration and add an information layer to the high-speed video analysis, physical characterisation of the sand bed after each test was carried out. The appearance of the char agglomerates, the colour of the residues and the structure of the

sand-char-tar lumpy structures will be fundamental for understanding the mechanisms of agglomeration and compaction. A 5 Mp Dino-lite Pro HR digital microscope was employed.

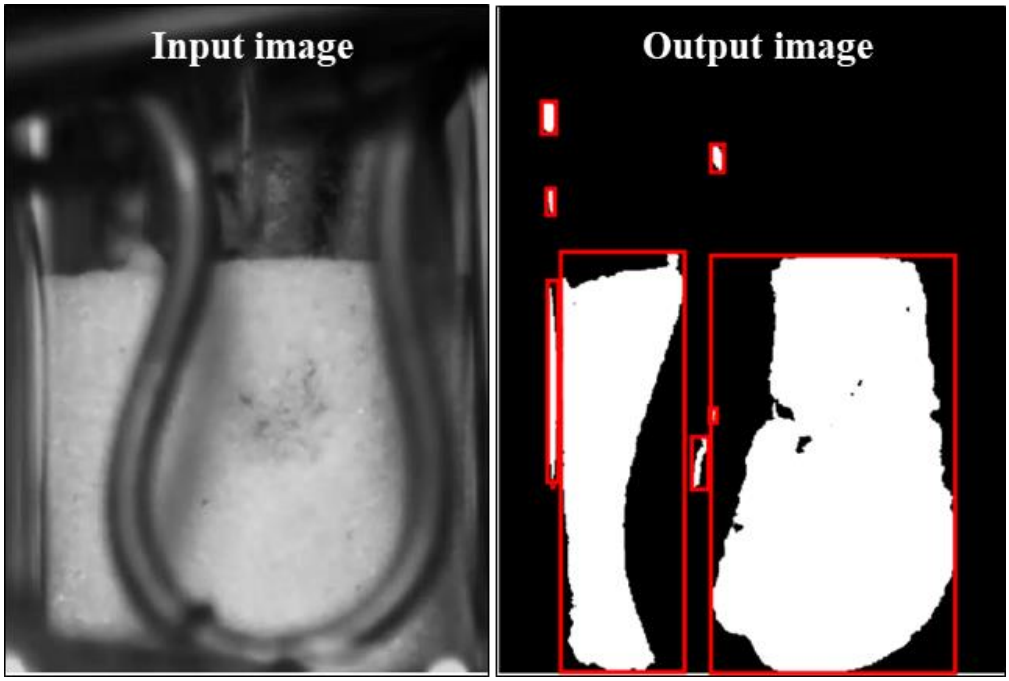

Figure 5-2 - Representation of the in-situ high-speed video treatment to determine the bed height

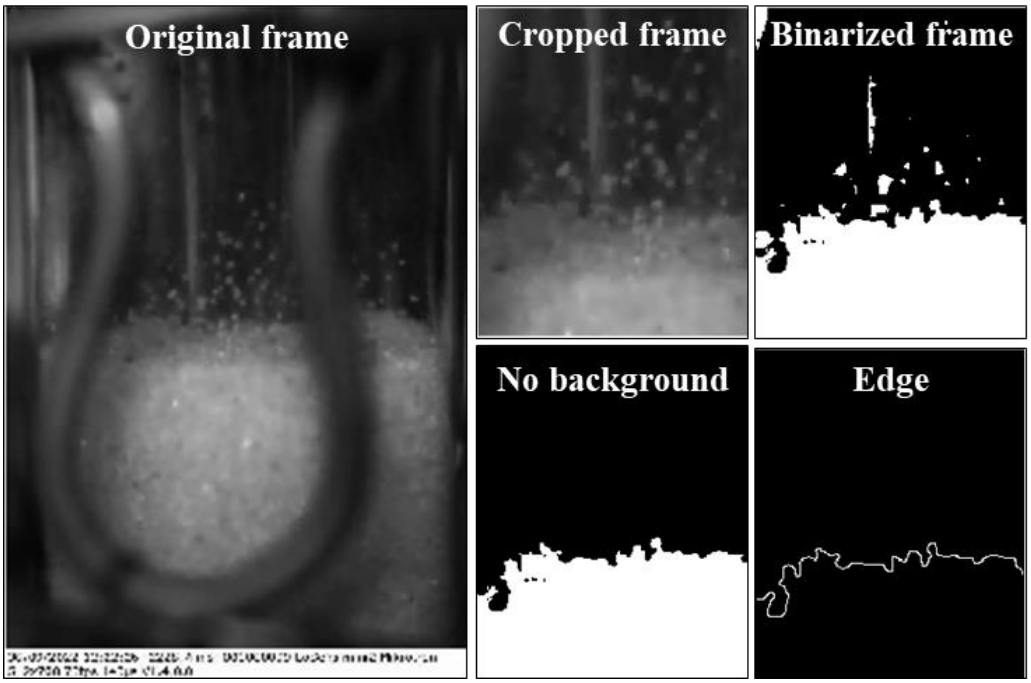

Figure 5-3 - Representation of the high-speed video treatment to determine the surface bubbling line, which translates the bubbling magnitude

3. Results and Discussion

3.1 Sand bed expansion

3.1.1 Test with no feeding

Figure 5-4 reports the relative bed height as a function of the u/u_{mf} ratio for sand temperatures of 20, 400 and 500°C. Moreover, the standard deviation associated with each point is related to the bed height fluctuations, which translates to the sand bed bubbling magnitude. The expansion due to the fluidisation is more gradual for a sand bed at room temperature than at higher temperatures. At 20°C, the minimal fluidisation condition was observed at 750 $NmL.min^{-1}$ or 3.98 cm/s. A fully developed bubbling regime was attained around 1100 $NmL.min^{-1}$ ($u/-u_{mf}$ ratio = 1.46), which can be appreciated in Figure 5-4 through increased uncertainty bars. The rise of the sand bed in relative terms (Figure 5-4) shows that the effect of the sand temperature is crucial. Minimal fluidisation velocities lay between 270 and 310 $NmL.min^{-1}$, respectively, at 500 and 400°C. A fully developed bubbling regime was observed between 350 and 450 $NmL.min^{-1}$ for the three temperature levels, which correspond to a u-to-u_{mf} ratio ranging from 1.31 to 1.47, respectively.

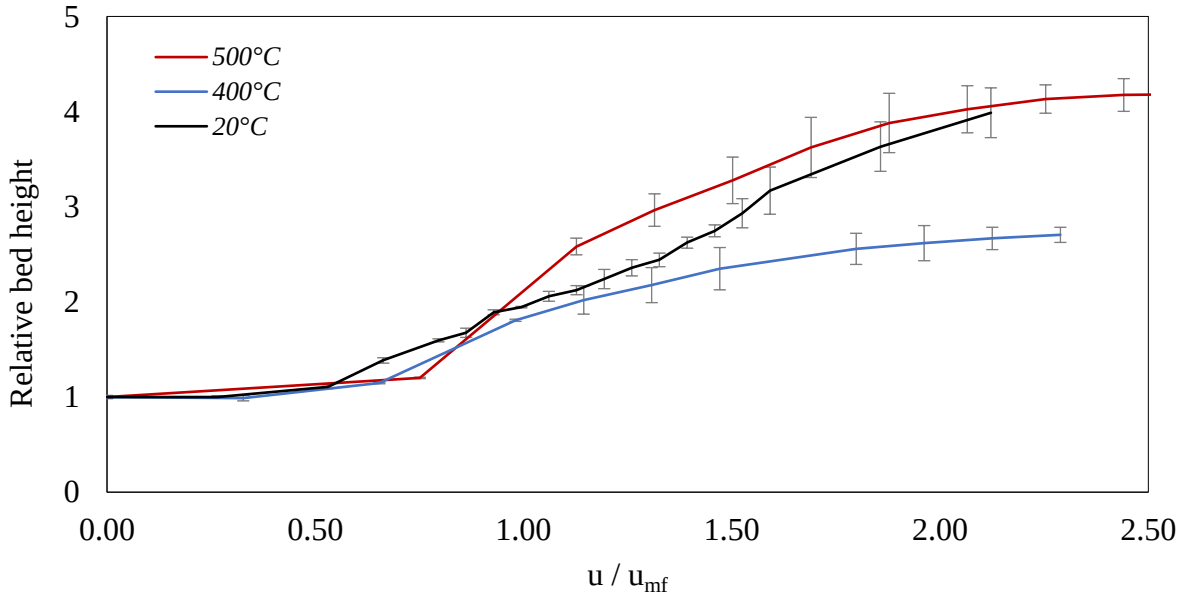

Figure 5-4 - Sand bed relative height as a function of the u-to-u_{mf} ratio, at different temperatures and without feeding of the biomass

3.1.2 Test with cellulose

Figure 5-5 shows the fluidised bed height as a function of the time while feeding cellulose powder. As expected, a significant difference is noticeable when oxygen is introduced into the system. Moreover, this difference is profoundly enhanced by the temperature.

Under air, at 400°C in the fluidized bed, the endothermicity of the pyrolysis takes over the global process in the first part of the test, causing a temperature decrease in the sand bed (a delta of approximately 10°C, see Section 3 in Annex 4), which in turn causes a reduction in the bubbling magnitude and the bed height. This is likely due to a sudden generation of pyrolysis products, which reduce the bubbles' size, and to slight compaction of the bed. At 500°C, the initial diminution of the bed height is slightly visible. Oxygen allowed gas-phase oxidation reactions to occur. They had two main consequences on the sand bed: oxygen provides heat to the system, increasing slightly the temperature of the bed (see Figure S 21 in Annex 4). Furthermore, oxygen enhances the stabilization of the fluidisation regime (constant bed height), as represented in Figure 5-5.

Under nitrogen, the fluidisation regime shows a more changing character. At 400°C, the bed height does not vary significantly, while at 500°C, a strong agglomeration tendency is obvious and induces compaction of the sand bed and a complete defluidization after about 4 minutes of cellulose injection, corresponding to 0.07 g of cellulose injected. Since the maximum temperature variation observed corresponds only to 14°C (see Figure S 22 in Annex 4), the decrease of the bed height can be attributable to the pyrolysis products. At 500°C, it is well known that cellulose forms an intermediate liquid (Boutin et al. 1998; Dufour et al. 2011). This intermediate sticky liquid promotes the agglomeration of the cellulose char and sand grains. It is interesting to notice that air reduces the agglomeration probably by reducing the life-time of this reactive intermediate liquid.

Fine particles of char were sampled during the tests under nitrogen, while a smaller amount was recovered after the test with air (the temperature profiles are reported in Annex 4). This difference can be related to the oxidation of char.

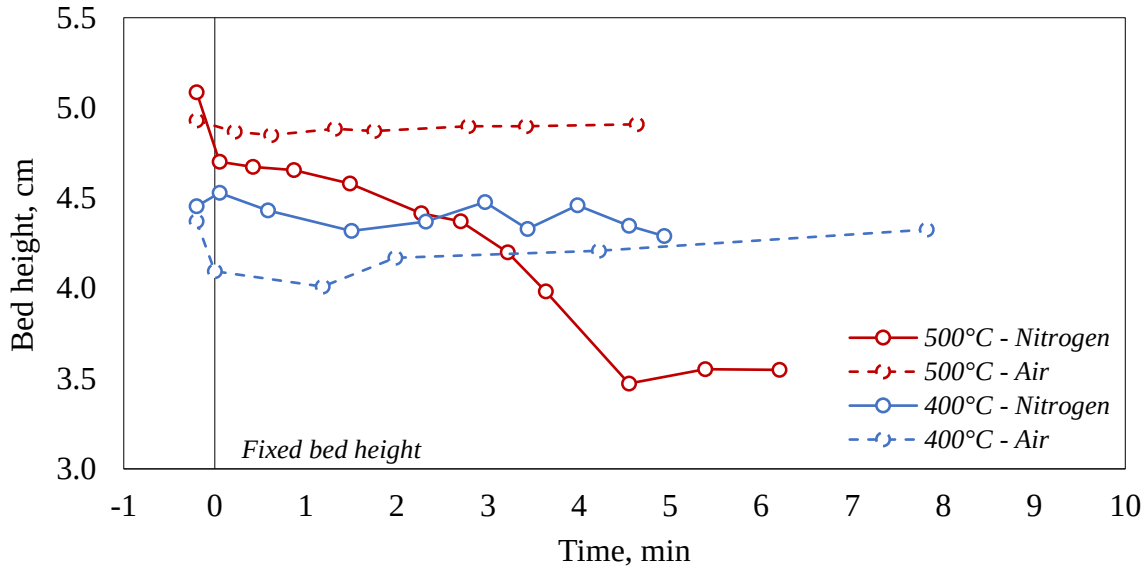

Figure 5-5 - Sand bed height as a function of the time, for cellulose fast pyrolysis

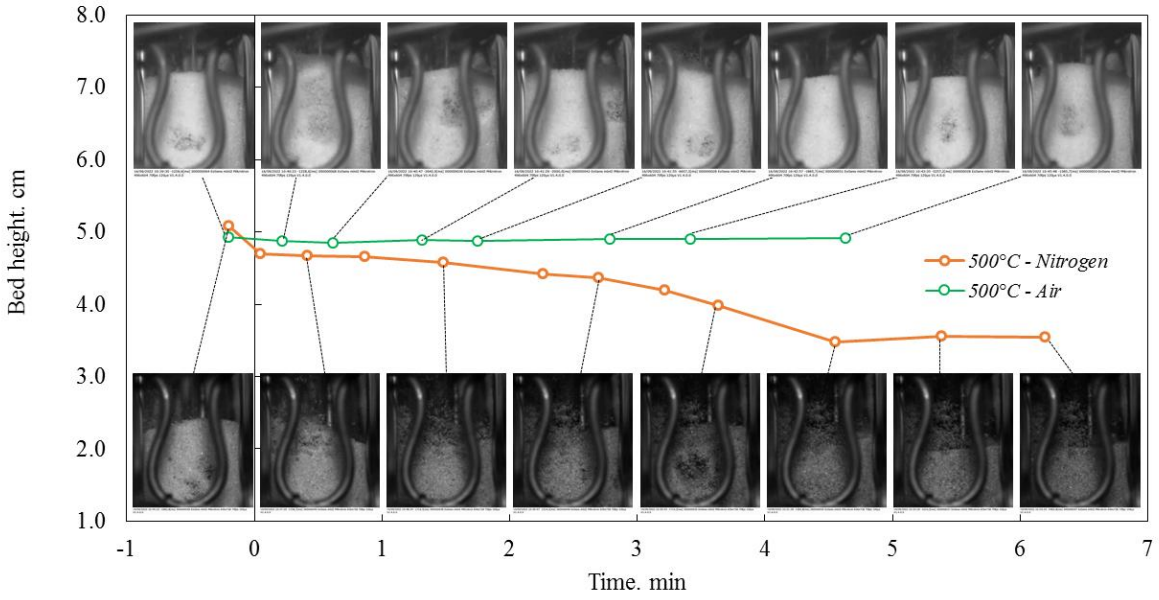

Figure 5-6 - In-situ high-speed frames relative to the tests under nitrogen and air at 500°C, for cellulose, as a function of feeding time

3.1.3 Tests with oak wood

The sand bed height showed a behaviour similar to cellulose when oak wood is fed, as resumed in Figure 5-7 - *Sand bed height as a function of the time, for oak wood*. Under nitrogen, an agglomeration tendency is noticeable at both 400 and 500°C, while a relatively stable trend is associated with the tests under air. Again, at 400°C in the presence of oxygen, a slight decrease of temperature in the first part of the experiment is the direct consequence of pyrolysis endothermicity. Oak, as a ligno-cellulosic biomass, presents a more complex behaviour to form an intermediate liquid than cellulose (Dufour et al. 2012). Oak, as a lingo-cellulosic biomass, presents a more complex behaviour to form an intermediate liquid than cellulose [163]. It presents a lower agglomeration tendency than cellulose. Cellulose forms more intermediate liquid which is more cohesive on the sand bed than for oak. As can be seen in Figure 5-8, the wood particles convert to char, which is well stirred in the bed by the fluidised sand.

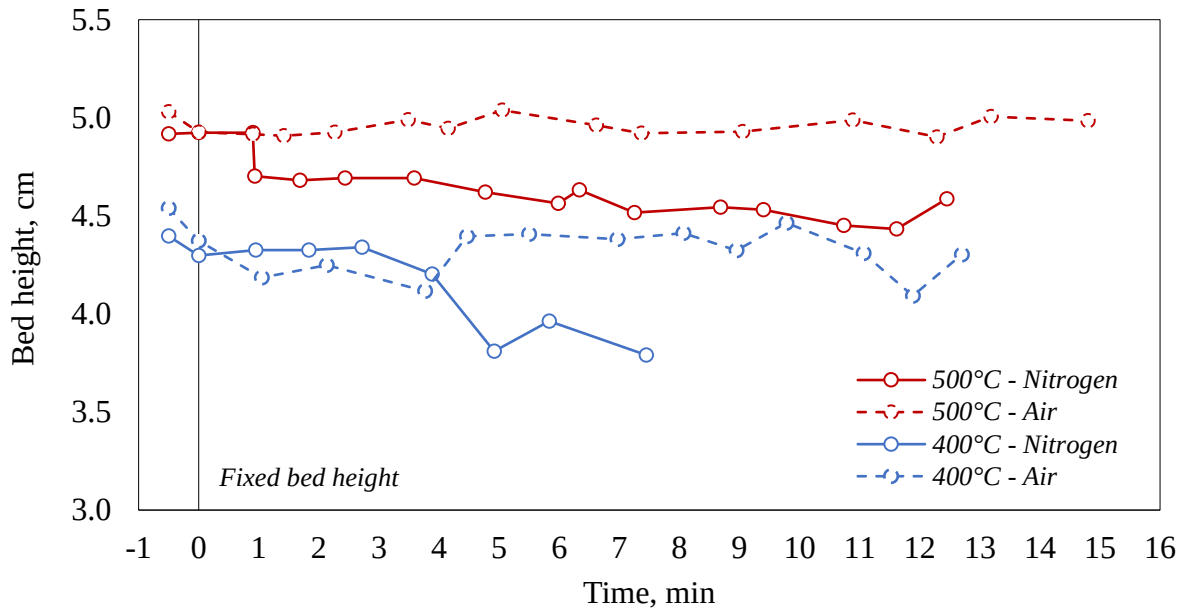

Figure 5-7 - Sand bed height as a function of the time, for oak wood

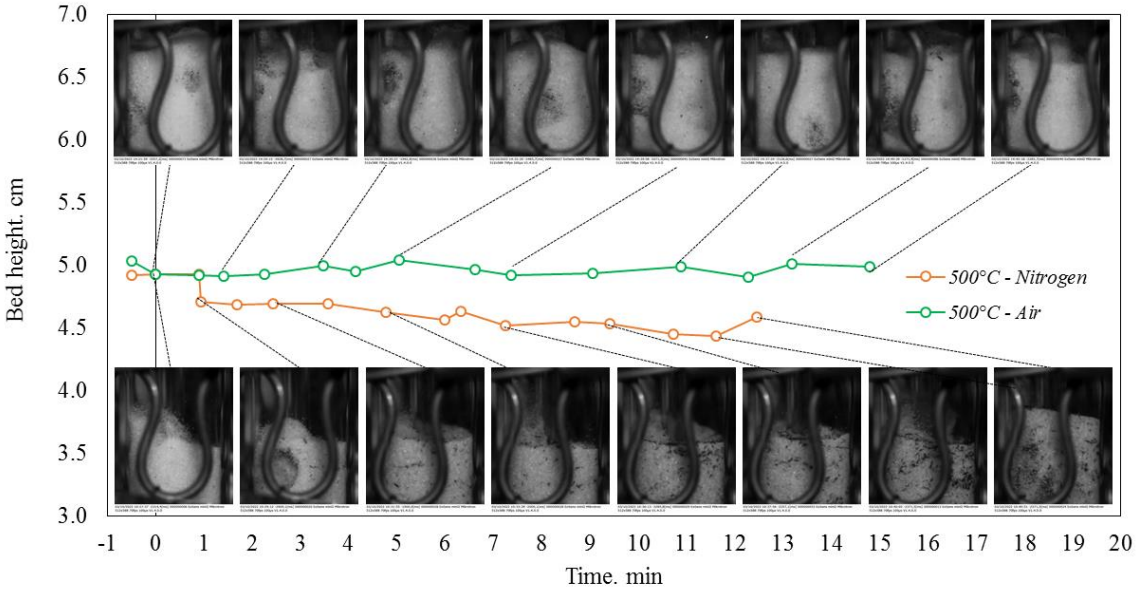

Figure 5-8 - In-situ high-speed frames relative to the tests under nitrogen and air at 500°C, for oak wood, as a function of the feeding time

3.2 Surface bubbling

3.2.1 Tests with no feeding

The dependency of the bed surface bubbling line as a function of the u-to-u_{mf} ratio revealed unexpected aspects of the fluidisation regimes. As reported in Figure 5-9, at room temperature, its length peaks around 1, corresponding to the minimal fluidisation regime, a decreasing section until approximately u/umf = 1.4, and then it rises again. These three behaviours are consistent with what was observed experimentally: a gradual expansion of the bed, slight fluidisation, an increase in the bubble dimension and, finally, a fully developed bubbling regime. Since the bubbling line length reflects the fluctuations of the bed surface, the rising section before the minimal fluidisation corresponds to a slight wrinkling. Between 1 and 1.5 u/umf, the movements in the sand bed start to settle, and when the bubbling reaches a fully developed condition, the surface line length increases again. At 400 and 500°C, a rising step followed by a decreasing one was observed. Although trends are similar, they are associated with a lower magnitude.

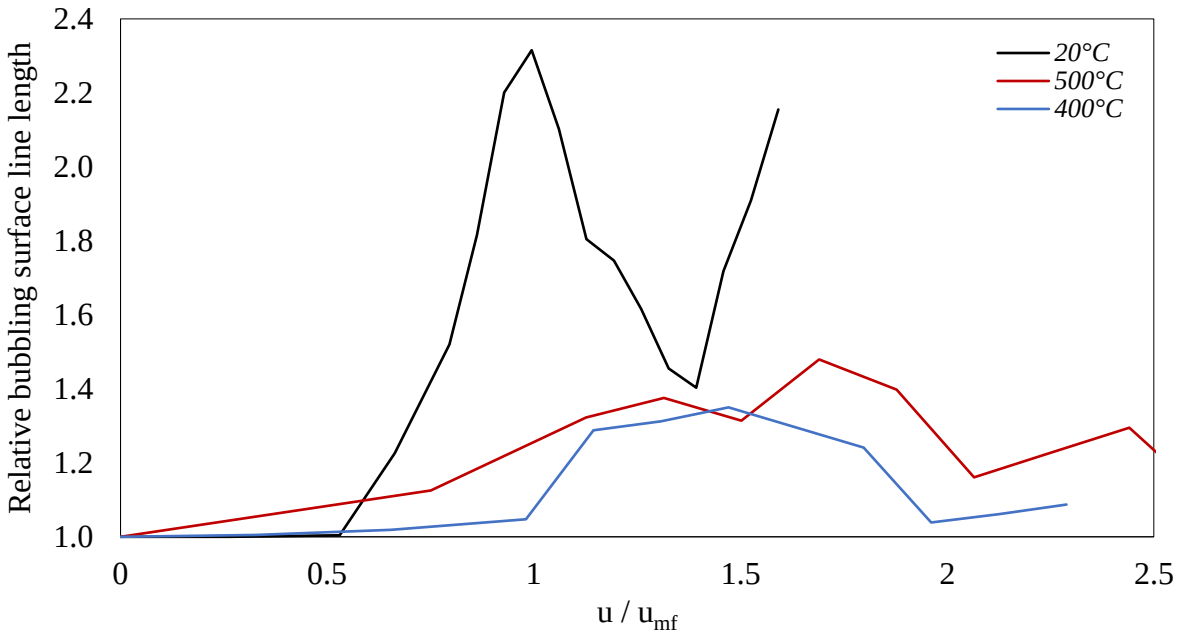

Figure 5-9 - Relative bubbling surface line length determined in the test with no feeding

3.2.2 Tests with cellulose

Figure 5-11 shows the relative bubbling surface line as a function of the time during the tests with cellulose. The length of the bubbling line was normalized by the average length of the bed surface before starting to feed cellulose. Again, a crucial difference between the curves under nitrogen and air is noticeable. In nitrogen, the bubbling line globally increases for the 2 temperatures. In air, it stays globally stable (with a slight increase at 400°C), confirming the interest of air feeding to maintain a stable operation of the bed.

The abovementioned agglomeration observed at 500°C under nitrogen results in an increment of the bubbling surface magnitude. By observing the high-speed in-situ videos, a global decrease in bubble size was noticed. Higher dynamic viscosity and density of the gaseous phase due to the generation of the pyrolysis products can be related to smaller average bubble size. Nonetheless, the agglomeration of the sand bed is undoubtedly accompanied by the formation of preferential paths, which can be connected to an increase in the bubbling surface line. The velocity of the bubbles is consequently higher, and it generates a more critical fluctuation of the bubbling line attaining the bed surface. This can explain the trends of the curves under nitrogen in Figure 5-10. A similar phenomenon was noticed at 400°C under nitrogen, but its global magnitude is less pronounced than at 500°C.

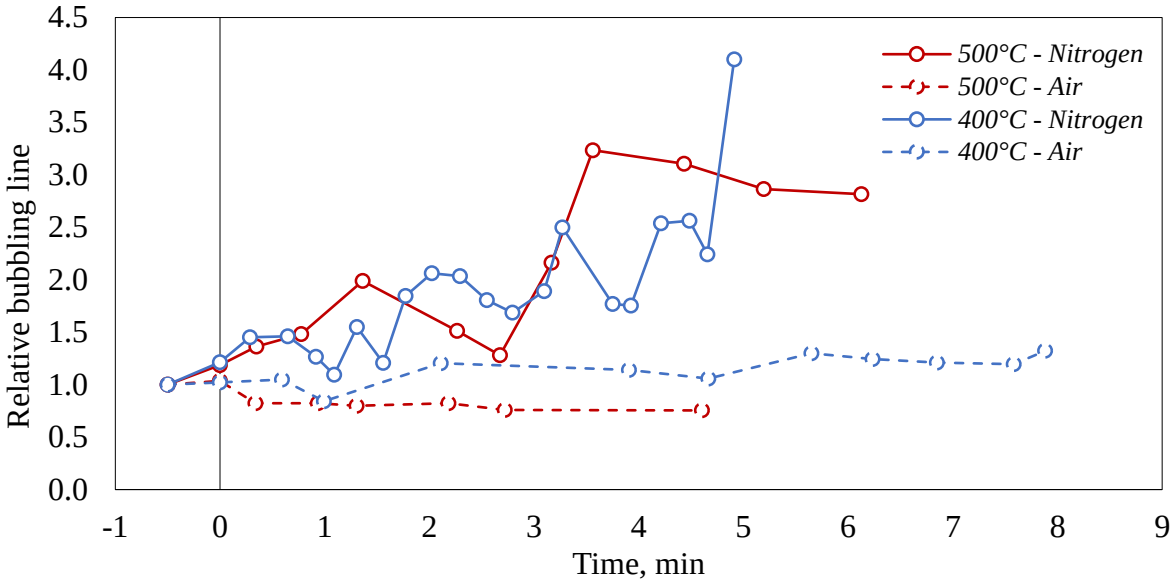

Figure 5-10 – Relative bubbling line length as a function of the time, for cellulose

3.2.3 Tests with oak wood

With oak wood, the surface bubbling line showed a different behaviour than cellulose, as stated in Figure 5-11. Globally, no increase in the bubbling magnitude was noticed for oak Furthermore, the effect of oxygen is significant solely at 500°C, maybe because the oxidation reactions are slower at 400°C. The agglomeration tendency is nonetheless present. Consequently, the bubbles at the surface induce lower fluctuations of the bubbling line, whose length does not vary much during the experiments.

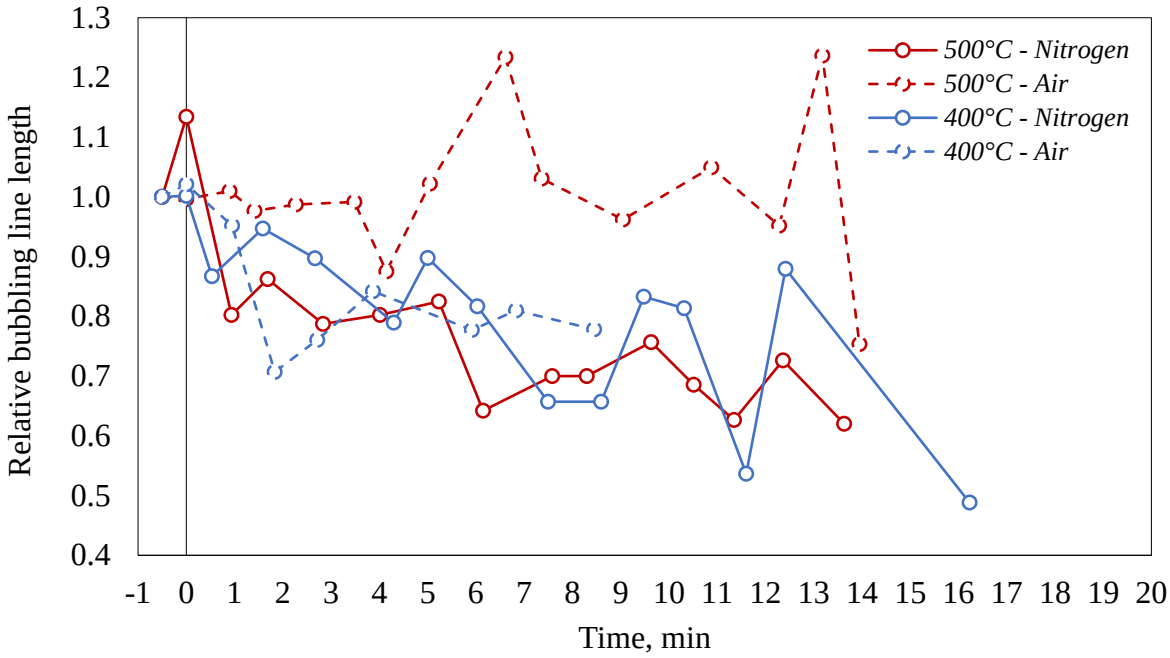

Figure 5-11 – Relative bubbling line length as a function of the time, for oak wood

3.3 Identification of the fluidisation regimes

The in-situ high-speed video recording allowed for characterising the fluidisation regimes associated with a specific temperature and u-to-u_{mf} ratio (see Figure 5-13). A visual and qualitative analysis of the bed behaviour was carried out following the fluidisation features characteristic of each regime, as reported in several works in literature (McDonough et al. 2019; Milacic et al. 2022; Soria-Verdugo et al. 2011). The results of the study previously presented applied to the tests without feeding were used to define the borders of the following regions:

- Packed bed (linear rise of the pressure drop as a function of the gas velocity, no movement of the particles, flat bed surface, no bubbles, eventual slight bed expansion)
- Minimal fluidisation (maximum pressure drop, bed expansion as the gas velocity increase, flat bed surface with noticeable wrinkling, no bubbles)
- Particulate fluidisation (little movement of the particles across the bed, tiny bubbles to the walls, no more bed expansion, visible wrinkling of the bed surface)
- Bubbling (important fluidization of the sand, large bubbles over the bed section, considerable fluctuations of the bed surface)

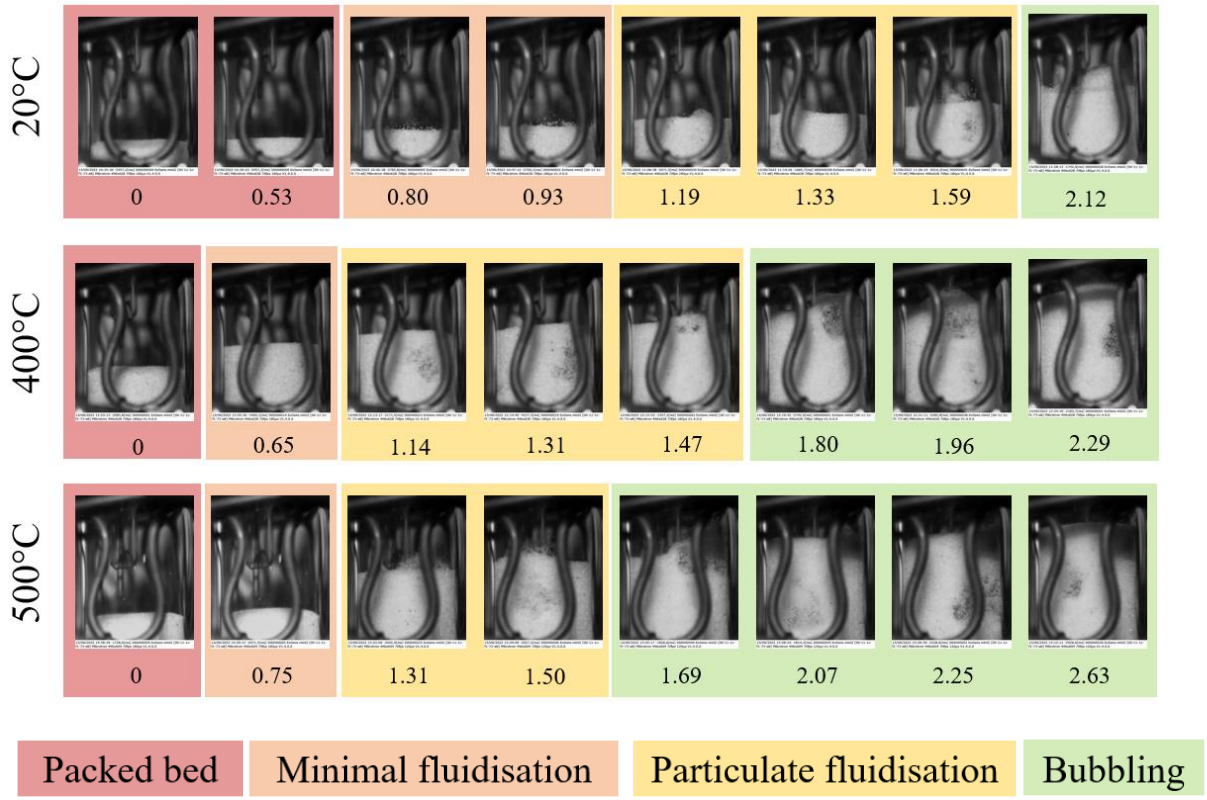

Figure 5-13 - In-situ high-speed visualisation of the fluidisation regimes as a function of U/Umf

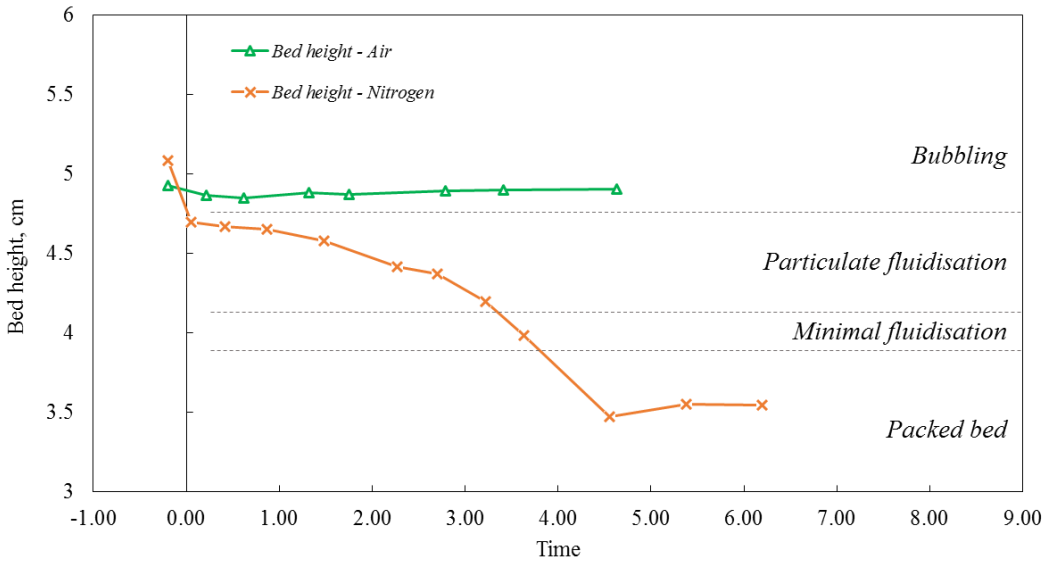

Figure 5-12 - Definition of the fluidisation regimes for the tests with cellulose at 500°C

3.4 Solid residue characterization

After each test, the sand bed was cooled down as quickly as possible in order to preserve it to the maximum extent by switching to nitrogen, increasing its flow and moving down the heating system. The characteristic sand particle agglomerates and char residues were thus minimally modified. The digital microscope imaging enlightened the sand bed's different agglomeration and compaction behaviours. The images are reported in Figure 5-14 and Figure 5-15, and they were chosen to be as representative as possible of the whole sand bed. Cellulose induced more significant compaction of the bed, as previously presented, and it is consistent with the visual observations of the sand. The formation of the intermediate liquid (e.g. as cellobiosan) generates large agglomerates from partially-pyrolysed cellulose particles (with a brown colour) and sand grains, which are noticeable at 400°C but not at 500°C. A higher char content was produced in the test under nitrogen at 400 and 500°C. Moreover, at 500°C, no residue is present under air, and some char particles are visible under nitrogen. This result can be combined with the relative bed height presented in Figure 5-5. By increasing the sand temperature to 500°C, the life time of the intermediate liquid is reduced and the agglomeration of the bed is reduced. Oak presents very different char particles: not agglomerated and keeping the overall wood fibres macro-structure. The magnitude of agglomeration is different with oak wood. In fact, it forms a lower intermediate liquid than cellulose.

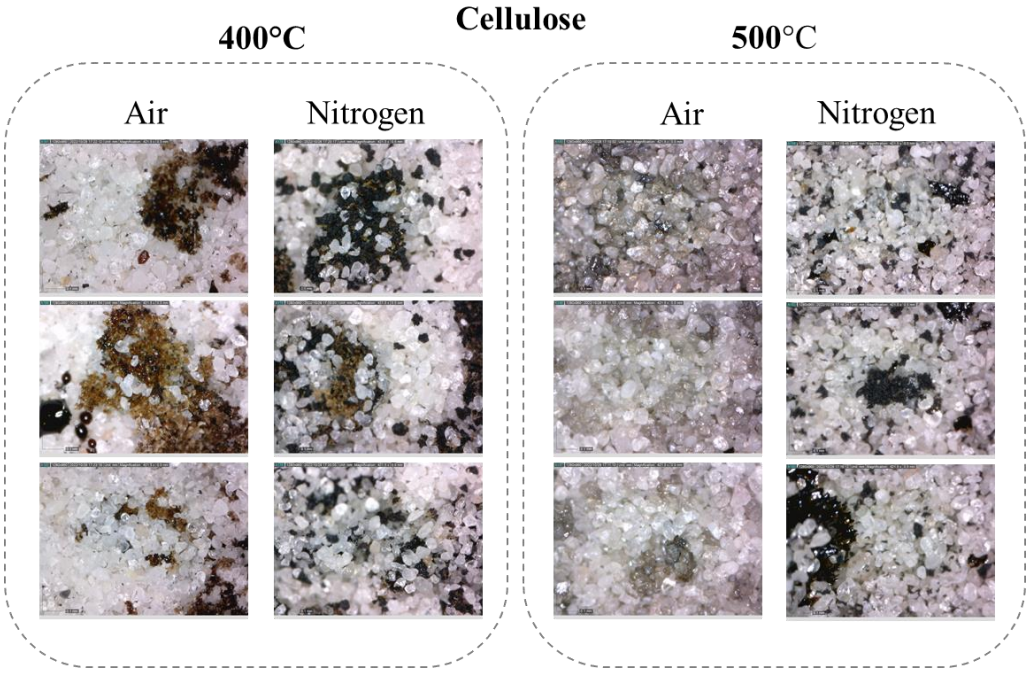

Figure 5-14 - Digital images of the sand bed after each pyrolysis test with cellulose

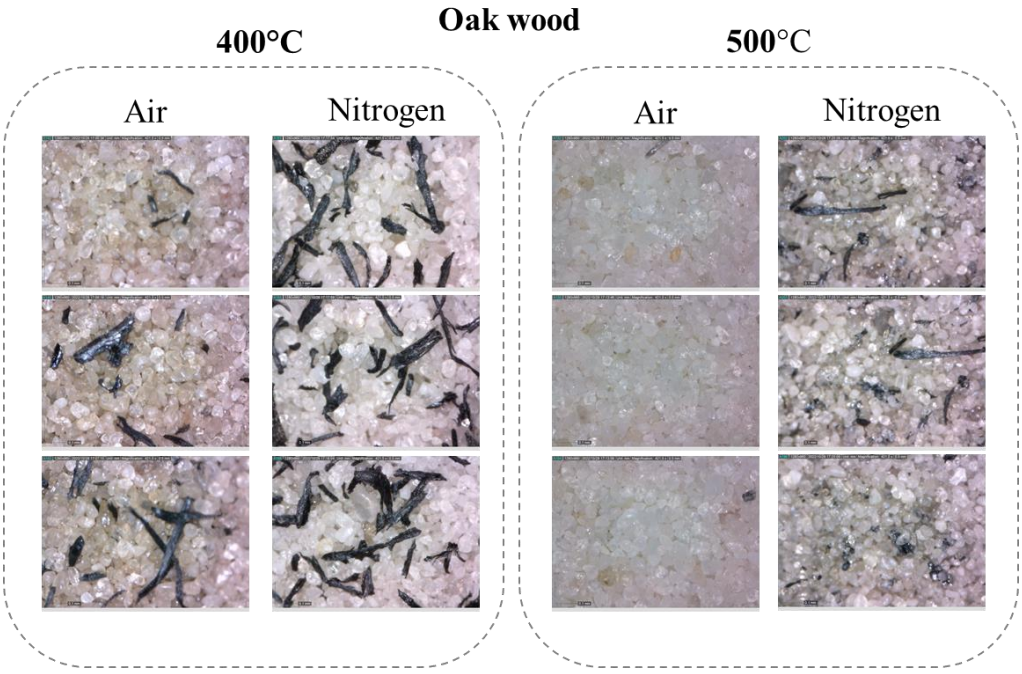

Figure 5-15 - Digital images of the sand bed after each pyrolysis test with oak wood

4. Conclusions

The study of the operability of biomass oxidative pyrolysis was carried out in a micro-fluidised bed. A novel methodology to quantify the fluidisation behaviour in operando was set. A high-speed in-situ video recording system has been conceived and optimised for fulfilling the task. Tests have shown that cellulose is more prone to bed agglomeration than oak. Air significantly improves the bed's stability, notably for cellulose, by oxidising the reactive intermediate liquid formed during cellulose pyrolysis. This intermediary is likely responsible for the compaction, acting like a cohesive force between the sand grains. Oak leads to lower agglomeration than cellulose, and char particles globally kept the fibrous macro-structure of wood. This work will be extended to quantify operability criteria (biomass flow rate/sand mass) as a function of pyrolysis conditions.

References

Amutio, Maider, Gartzen Lopez, Roberto Aguado, Maite Artetxe, Javier Bilbao, and Martin Olazar. 2012. 'Kinetic Study of Lignocellulosic Biomass Oxidative Pyrolysis'. *Fuel* 95:305–11. doi: 10.1016/j.fuel.2011.10.008.

Bilbao, R., J. F. Mastral, M. E. Aldea, and J. Ceamanos. 1997. 'The Influence of the Percentage of Oxygen in the Atmosphere on the Thermal Decomposition of Lignocellulosic Materials'. *Journal of Analytical and Applied Pyrolysis* 42(2):189–202. doi: 10.1016/S0165-2370(97)00050-8.

Boutin, O., M. Ferrer, and J. Lédé. 1998. 'Radiant Flash Pyrolysis of Cellulose—Evidence for the Formation of Short Life Time Intermediate Liquid Species'. *Journal of Analytical and Applied Pyrolysis* 47(1):13–31. doi: 10.1016/S0165-2370(98)00088-6.

Boutin, Olivier, Monique Ferrer, and Jacques Lédé. 2002. 'Flash Pyrolysis of Cellulose Pellets Submitted to a Concentrated Radiation: Experiments and Modelling'. *Chemical Engineering Science* 57(1):15–25. doi: 10.1016/S0009-2509(01)00360-8.

Bridgwater, A. V. 2003. 'Renewable Fuels and Chemicals by Thermal Processing of Biomass'. *Chemical Engineering Journal* 91(2–3):87–102. doi: 10.1016/S1385-8947(02)00142-0.

Dufour, Anthony, Miguel Castro-Diaz, Nicolas Brosse, Roberto Olcese, Mohamed Bouroukba, and Colin Snape. 2012. 'In Situ Analysis of Biomass Pyrolysis by High Temperature Rheology in Relations with H-1 NMR'. *Energy & Fuels* 26(10):6432–41.

Dufour, Anthony, Bajil Ouartassi, Roda Bounaceur, and André Zoulalian. 2011. 'Modelling Intra-Particle Phenomena of Biomass Pyrolysis'. *Chemical Engineering Research and Design* 89(10):2136–46. doi: 10.1016/j.cherd.2011.01.005.

Jia, Liangyuan, Felipe Buendia-Kandia, Stéphane Dumarcay, Hélène Poirot, Guillain Mauviel, Philippe Gérardin, and Anthony Dufour. 2017. 'Fast Pyrolysis of Heartwood, Sapwood, and Bark: A Complementary Application of Online Photoionization Mass Spectrometry and Conventional Pyrolysis Gas Chromatography/Mass Spectrometry'. *Energy & Fuels* 31(4):4078–89. doi: 10.1021/acs.energyfuels.7b00110.

Jia, Liangyuan, Anthony Dufour, Yann Le Brech, Olivier Authier, and Guillain Mauviel. 2017. 'On-Line Analysis of Primary Tars from Biomass Pyrolysis by Single Photoionization Mass Spectrometry: Experiments and Detailed Modelling'. *Chemical Engineering Journal* 313:270–82. doi: 10.1016/j.cej.2016.12.021.

Jia, Liangyuan, Yann Le Brech, Guillain Mauviel, Fei Qi, Matthias Bente-von Frowein, Sven Ehlert, Ralf Zimmermann, and Anthony Dufour. 2016. 'Online Analysis of Biomass Pyrolysis Tar by Photoionization Mass Spectrometry'. *Energy & Fuels* 30(3):1555–63. doi: 10.1021/acs.energyfuels.5b02274.

Jia, Liangyuan, Yann Le-Brech, Binod Shrestha, Matthias Bente-von Frowein, Sven Ehlert, Guillain Mauviel, Ralf Zimmermann, and Anthony Dufour. 2015. 'Fast Pyrolysis in a Microfluidized Bed Reactor: Effect of Biomass Properties and Operating Conditions on Volatiles Composition as Analyzed by Online Single Photoionization Mass Spectrometry'. *Energy & Fuels* 29(11):7364–74. doi: 10.1021/acs.energyfuels.5b01803.

Kim, Kwang Ho, Xianglan Bai, Marjorie Rover, and Robert C. Brown. 2014. 'The Effect of Low-Concentration Oxygen in Sweep Gas during Pyrolysis of Red Oak Using a Fluidized Bed Reactor'. *Fuel* 124:49–56. doi: 10.1016/j.fuel.2014.01.086.

Le Brech, Yann, Liangyuan Jia, Sadio Cissé, Guillain Mauviel, Nicolas Brosse, and Anthony Dufour. 2016. 'Mechanisms of Biomass Pyrolysis Studied by Combining a Fixed Bed Reactor with Advanced Gas Analysis'. *Journal of Analytical and Applied Pyrolysis* 117:334–46. doi: 10.1016/j.jaap.2015.10.013.

Liu, Xinhua, Guangwen Xu, and Shiqiu Gao. 2008. 'Micro FLuidized Beds: Wall Effect and Operability'. *Chemical Engineering Journal* 6.

McDonough, J. R., R. Law, D. A. Reay, and V. Zivkovic. 2019. 'Fluidization in Small-Scale Gas-Solid 3D-Printed Fluidized Beds'. *Chemical Engineering Science* 200:294–309. doi: 10.1016/j.ces.2019.01.048.

Milacic, E., M. Nunez Manzano, S. Madanikashani, G. J. Heynderickx, K. M. van Geem, A. A. M. van de Greef, A. Richter, S. H. L. Kriebitzsch, K. A. Buist, M. W. Baltussen, and J. A. M. Kuipers. 2022. 'Experimental Study on the Temperature Distribution in Fluidised Beds'. *Chemical Engineering Science* 248:117062. doi: 10.1016/j.ces.2021.117062.

Polin, Joseph P., Chad A. Peterson, Lysle E. Whitmer, Ryan G. Smith, and Robert C. Brown. 2019. 'Process Intensification of Biomass Fast Pyrolysis through Autothermal Operation of a Fluidized Bed Reactor'. *Applied Energy* 249:276–85. doi: 10.1016/j.apenergy.2019.04.154.

Potic, B., S. R. A. Kersten, M. Ye, M. A. van der Hoef, J. A. M. Kuipers, and W. P. M. van Swaaij. 2005. 'Fluidization with Hot Compressed Water in Micro-Reactors'. *Chemical Engineering Science* 60(22):5982–90. doi: 10.1016/j.ces.2005.04.047.

Scott, D. S., and J. Piskorz. 1982. 'The Flash Pyrolysis of Aspen-Poplar Wood'. *The Canadian Journal of Chemical Engineering* 60(5):666–74. doi: 10.1002/cjce.5450600514.

Shen, D. K., S. Gu, Baosheng Jin, and M. X. Fang. 2011. 'Thermal Degradation Mechanisms of Wood under Inert and Oxidative Environments Using DAEM Methods'. *Bioresource Technology* 102(2):2047–52. doi: 10.1016/j.biortech.2010.09.081.

Soria-Verdugo, A., L. M. Garcia-Gutierrez, S. Sanchez-Delgado, and U. Ruiz-Rivas. 2011. 'Circulation of an Object Immersed in a Bubbling Fluidized Bed'. *Chemical Engineering Science* 66(1):78–87. doi: 10.1016/j.ces.2010.10.006.

Venderbosch, R. H., and W. Prins. 2010. 'Fast Pyrolysis Technology Development'. *Biofuels, Bioproducts and Biorefining* 4(2):178–208. doi: 10.1002/bbb.205.

Wang, Junwu. 2011. 'From Bubbling to Turbulent Fluidization Advanced Onset of Regime Transition in Micro-Fluidized Beds'. *Chemical Engineering Science* 7.

CHAPTER 6

Summary

Chapter 6 completes the work. The propagation of a flame within a dust cloud is studied from three different points of view. The first one comes from Chapter 5, where a micro-fluidised bed was used to study the operability of a biomass oxidative pyrolysis process. In the work presented hereafter, the same reactor was used to create and stabilise a flame directly fuelled with the products of oxidative pyrolysis. It allowed the decoupling of the pyrolysis step from the oxidation of the pyrolysis vapours. The laminar flame speed was determined via a high-speed recording system. The second and third systems were focused on flame propagation within the dust cloud. A vertical tube and a sphere were employed to follow the process and to estimate its rate. Finally, these results were compared to enlighten the strengths and drawbacks of the experimental apparatuses.

Resumé

Chapitre 6 complète le travail. La propagation d'une flamme dans un nuage de poussière est étudiée de trois points de vue différents. Le premier provient du Chapitre 5, où un micro-lit fluidisé a été utilisé pour étudier l'opérabilité d'un procédé de pyrolyse oxydative de la biomasse. Dans le travail présenté ci-après, le même réacteur a été utilisé pour créer et stabiliser une flamme directement alimentée par les produits de la pyrolyse oxydative. Cela a permis de découpler l'étape de pyrolyse de celle de l'oxydation. La vitesse de la flamme laminaire a été déterminée par un système d'enregistrement à haute vitesse. Les deuxième et troisième systèmes se sont concentrés sur la propagation de la flamme à l'intérieur du nuage de poussière. Un tube vertical et une sphère ont été utilisés pour suivre le processus et estimer sa vitesse. Enfin, ces résultats ont été comparés pour mettre en évidence les forces et les faiblesses des appareils expérimentaux.

A three-way experimental method to determine the laminar flame speed of organic powders

Matteo Pietraccini [1], Olivier Dufaud [1], Pierre-Alexandre Glaude [1], Anthony Dufour [1,*]

[1] *Université de Lorraine, CNRS, LRGP, F-54000 Nancy, France*

* *corresponding author: anthony.dufour@univ-lorraine.fr*

Graphical abstract

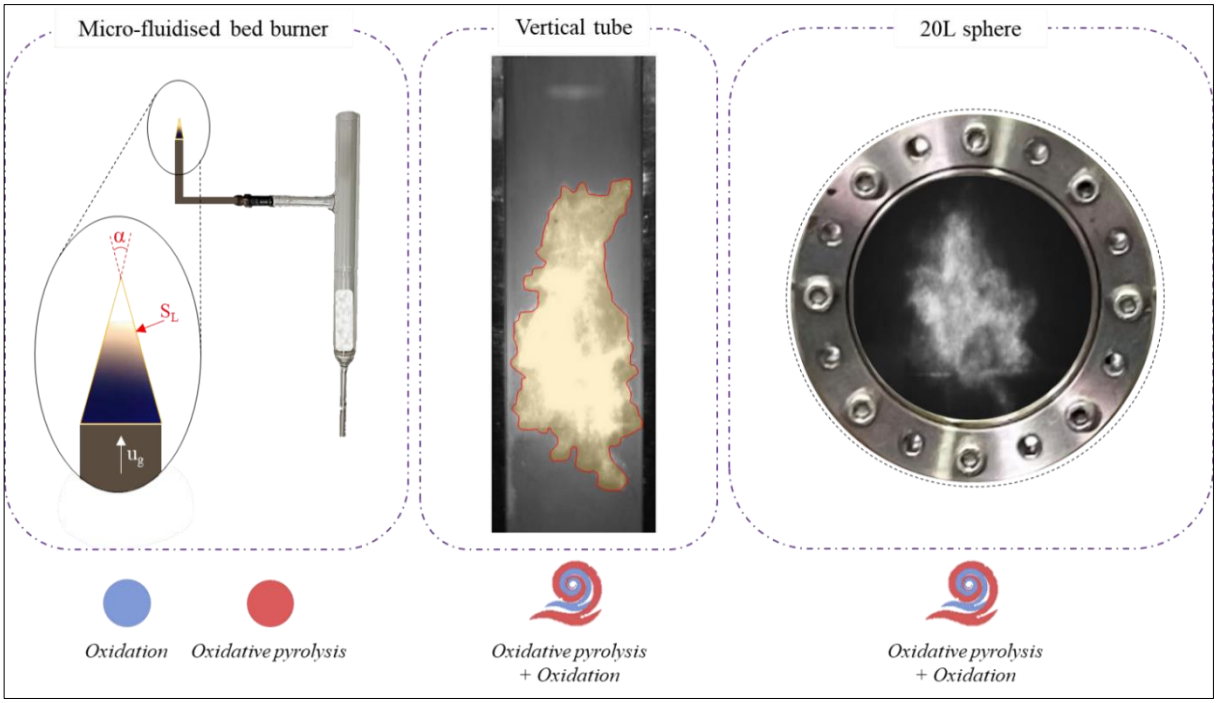

Abstract

Determining the laminar flame speed of dusts is far from straightforward. A strong dependency on the experimental setup and the data treatment's high complexity make it a true challenge. At the same time, the information in the flame speed is complete, as it concerns the ensemble of the phenomena occurring in a dust explosion phenomenon. This work compares

three complementary experimental setups: a modified Hartmann tube, a 20L sphere and a micro-fluidised bed (MFB) burner. The first two consider the flame propagation phenomenon in its globality, which means that numerous elemental steps are involved simultaneously (particle heating, pyrolysis, oxidation, radiative heat transfer, flame stretching), while the third one decomposes pyrolysis and combustion, to focus mainly on the oxidation rate. It was conceived to generate pyrolysis products (in a micro-fluidised bed) and burn them in a laminar flame. The flame speed values determined with the first two setups were consistent and equal to 22.0 and 26.6 cm/s, respectively. Silvestrini's equation was also employed to compare the results: values ranging between 14.0 and 33.4 cm/s, according to the dust concentration in the 20L sphere, were obtained. With the MFB burner, the flame speed was much higher (135-155 cm/s), due to the higher temperature of the fresh mixture and the fact that only the oxidation of the pyrolysis gases is considered. In this case, a numerical simulation (Chemkin) confirmed the reliability of these values since the range 133.2 - 230.7 cm/s was obtained for ER of 0.6 and 1.2, respectively. The discrepancy between the laminar flame speed determined in the sphere or in the tube and that obtained in the MFB highlights the significant influence of pyrolysis during a dust explosion.

1. Introduction

More than two hundred years separate today from the first ever documented dust explosion, which occurred in a bakery in Turin (Italy) in 1785 and was reported by Count Morozzo later in 1788. Deep knowledge of this phenomenon has been built over the years, but unfortunately, the industry's risk associated with dust explosions cannot be neglected yet. According to the 2020 mid-year Combustible Dust Incident Report (Cloney 2020), 244 dust explosions were registered between 2016 and 2019, which globally caused 417 injuries and 47 fatalities. Organic powders always account for more than 60% of the total accidents. These numbers must activate the intention to better comprehend these common yet ‘apparently mysterious’ and complex phenomena. Nonetheless, as stated by Skjold (Skjold 2022), building a bridge from the combustion properties of a powder to its behaviour in an explosion is not a simple task. These systems are reacting, transient, turbulent and particle-laden. Moreover, low repeatability between duplicated tests and high sensitivity to minor parameter variations add a level of complexity. Laminar flame speed is crucial to characterise a dust cloud's explosibility. It corresponds to the flame front velocity that propagates in a non-turbulent system. In addition,

it resumes precious information related to the dust cloud itself, such as the reaction kinetics, which can be significantly elaborate for organic dusts, the diffusivity of the species and the thermal features of the different processes that constitute the global (Munajat et al. 2012). This single parameter can thus represent a dust explosion's complexity straightforwardly. Moreover, it is an intrinsic parameter, i.e. its value only depends on the reactive mixture. Combining the laminar speed velocity to classical equations relating it to the spatial flame velocity and the root mean square velocity, is the classical approach used in Computational Fluid Dynamics in order to predict the consequences of such explosion in complex structures. [229]. This single parameter can thus represent a dust explosion's complexity straightforwardly. Moreover, it is an intrinsic parameter, i.e. its value only depends on the reactive mixture. Combining the laminar speed velocity to classical equations relating it to the spatial flame velocity and the root mean square velocity, is the classical approach used in Computational Fluid Dynamics in order to predict the consequences of such explosion in complex structures.

There are two crucial drawbacks of experimentally measuring the laminar flame speed of a powder:

- The intricacy of developing an experimental setup to accomplish the task, due to the presence of two phases and a high turbulence level;
- The low repeatability of the experiments due to the large number of parameters involved having a primary role in the global process, related to the numerous and chaotic inter-particles interactions during the dispersion and the resulting turbulence.

In this work, three experimental methods to measure the laminar flame speed of an organic dust will be considered, studied and compared. The first one is a modified Hartmann tube, i.e. a square-section vertical tube equipped with two electrodes that ensure the presence of an ignition source (an electrical spark). The second is an open-20L vessel, with a visualisation window and a relief disc valve to ensure propagation at atmospheric pressure. As for these two systems, the flame front propagates directly in the dust cloud and is recorded by a high-speed camera. The third one is a burner coupled to a micro-fluidised bed. The flammable gases, responsible for propagating the flame in the dust cloud, are produced in the fluidised bed and sent to the flame, whose burning velocity was also measured through a high-speed camera. In the first two approaches, the pyrolysis and the oxidation steps are merged together, while the third system provides for decoupling these two steps.

2. Material and Methods

2.1 Sample choice and characterisation

Since cellulose pyrolysis mechanism is well-characterised, and the scientific literature is rich in information and data, the organic powder chosen for this study was micro-crystalline cellulose. Two samples were considered: Avicel ph 101 and Vivapur 200. The first one was chosen for the propagation test in dust clouds for its finer PSD, which facilitates the experimental procedure by increasing the ignition probability and reducing the sedimentation due to coarser particles. The second one was chosen for the MFB burner for its higher flowability, which reduced the likelihood of clogging the inlet powder flow. The particle size distribution was measured with a Malvern Mastersizer 3000 equipped with an aero-dispersion unit working with 2-bar pressurised air. A 5 Mp Dino-lite Pro HR digital microscope and a JEOL JSM-649-LV Scanning Electronic Microscope (SEM) were used to characterise particle shape and morphology. Proximate analysis was performed to determine the moisture content (MC), volatile matter (VM), fixed carbon (FC) and ash content of the samples. The parameters were determined with a Mettler Toledo HE53 Moisture Analyzer, a Mettler Toledo TGA STARe System and a Nabertherm B150 oven, respectively. Results are reported in Table 6-1 and in Figure 6-1.

Table 6-1 - Particle Size Distribution and proximate analysis of the cellulose powder

Particle Size Distribution			
	Avicel ph 101	*Vivapur 200*	
D10	21	65	µm
D50	59	219	µm
D90	140	463	µm
Proximate analysis			
MC		5.3	wt%
VM		87.4	wt%
FC		7.2	wt%
Ash		0.1	wt%

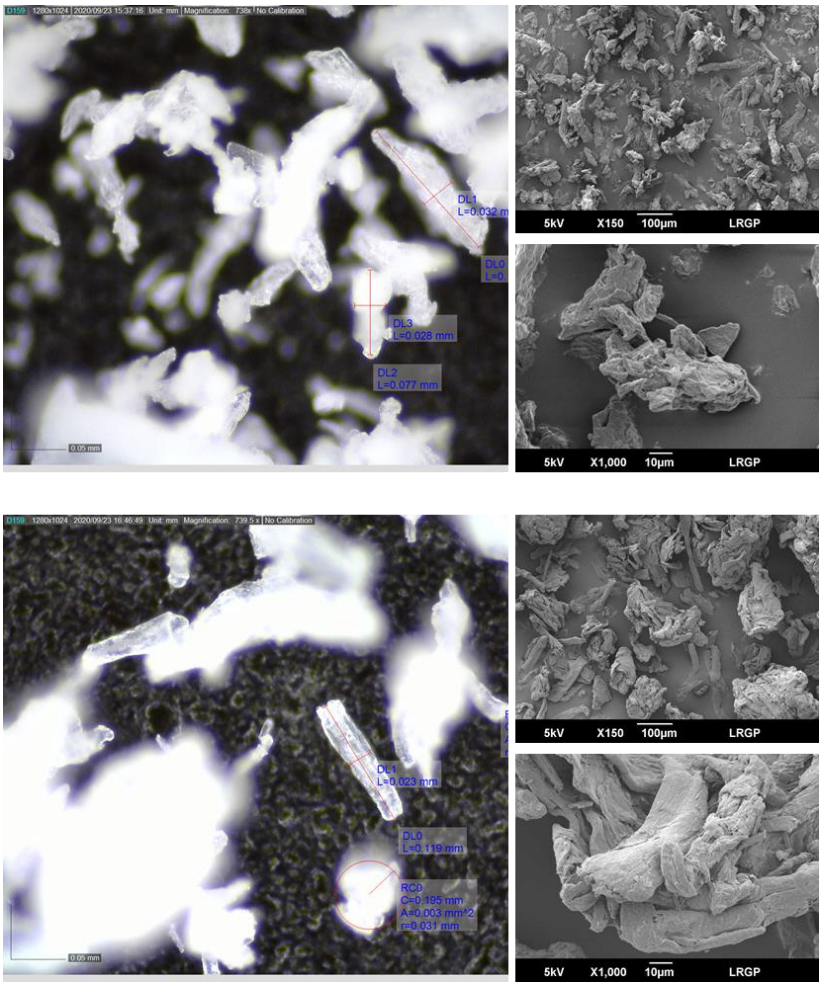

Figure 6-1 - Digital and electronic miscroscope images of the celluloses used in this work: Avicel ph 101 (top), Vivapur 200 (bottom).

2.2 Experimental setups

2.2.1 Flame propagation tube

The flame propagation tube consists of a semi-open tube of 1 m long and a square section of 49 cm^2. Its graphical representation is shown in Figure 6-2. The powder dispersion is ensured by a 7-bar compressed air pulse, passing through a mushroom nozzle at the bottom of the tube (Cuervo et al. 2017). 1 g of powder was used for the tests. Two electrodes are placed 9 cm above it and generate the electric spark necessary for igniting the dust cloud. The powder dispersion is ensured by a 7-bar compressed air pulse, passing through a mushroom nozzle at the bottom of the tube. 1 g of powder was used for the tests. Two electrodes are placed 9 cm above it and generate the electric spark necessary for igniting the dust cloud. A modified Hartmann tube was connected to the electrodes and the ignition energy chosen for this study

was set at 1 J as it is both greater than the Minimum Ignition Energy of cellulose and it is not likely to generate overdriving. A critical parameter is the delay time (t_v) between the dispersion and the spark generation: a value of 180 ms represented a good compromise between too high t_v, which corresponds to high segregation of the particles but low turbulence, and too low t_v, which on the other hand corresponds to increased turbulence and small segregation.

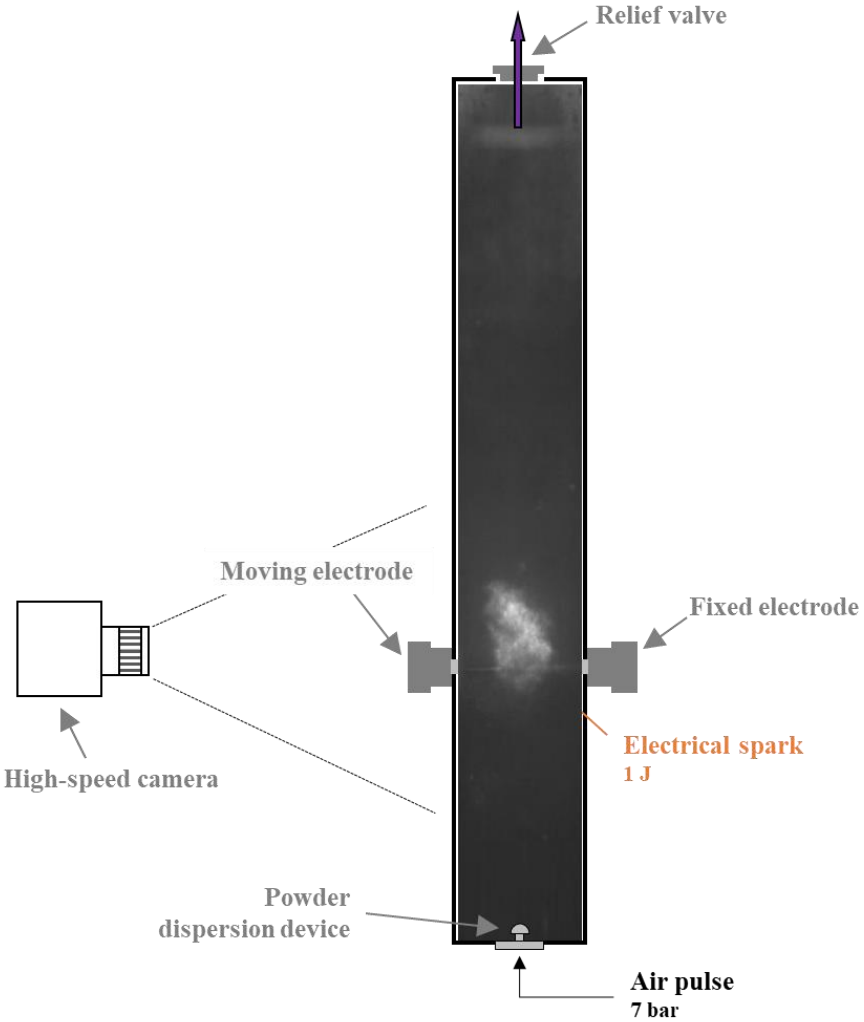

Figure 6-2 - Modified Hartmann tube employed for the vertical flame propagation analysis

2.2.2 20L vessel

A spherically propagating dust-air flame was studied in two ways. The first approach uses a standard 20L vessel, usually employed to determine the explosion parameters according to the (EN 14034-1 2004:14) standard procedure. Here it was used to estimate the parameters necessary to calculate the unstretched flame velocity S_u^0. 100 J pyrotechnical igniters (i.e. igniters with the lowest available energy) were used as the ignition source, and a delay time t_v of 60 ms (i.e. the standard one) was set for the explosion tests.

Based on the explosion severity parameters P_{max} and $(dP/dt)_{max}$, the relationship developed by Silvestrini (Silvestrini et al. 2008) allows the calculation of S_u^0 as follows:

$$S_u{}^0 = 0.11 \frac{K_{St}}{P_{max} \left(\frac{P_{max}}{P_0}\right)^{0.14} \left(\frac{P_{max}}{P_0}\right)^{\frac{1}{\gamma}}} \quad (1)$$

where P_0 is the atmospheric pressure and γ is the heat capacity ratio (c_p / c_v). It must be underlined that several assumptions accompany this equation, such as a spherical expansion of the flame, negligible turbulent length scales, laminar flow and expanding burnt gases segregated in the post-reaction zone (they do not diffuse in the pre-heating zone). Supposing that these assumptions introduce a small error in the procedure, the modification proposed by Santandrea (Santandrea et al. 2020) was adopted. It consisted in considering the explosion overpressure (P_m) and the rate of pressure rise ($(dP/dt)_m$) in place of P_{max} and $(dP/dt)_{max}$, thus relating each dust concentration to a flame speed. It was then used to determine the unstretched flame speed over a wide range of dust concentrations. Equation (1) changes as follows:

$$S_u{}^0 = 0.11 \frac{\left(\frac{dP}{dt}\right)_m V^{\frac{1}{3}}}{P_m \left(\frac{P_m}{P_0}\right)^{0.14} \left(\frac{P_m}{P_0}\right)^{\frac{1}{\gamma}}} \quad (2)$$

The second approach is based on a vented-20L sphere equipped with 4 windows (Figure 6-3) allowing the visualisation of the flame propagation. This work was performed for cellulose (more precisely for nanocellulose) with the framework of Audrey Santandrea's PhD thesis (Santandrea et al. 2020). This work was performed for cellulose (more precisely for nanocellulose) with the framework of Audrey Santandrea's PhD thesis (Santandrea et al. 2020). The author experimentally determined the unstretched flame speed of a nanocellulose-air mixture, because such powder has a low sedimentation rate and can be tested at rather low turbulence levels (approaching the 'unstretched flame' velocity). A dust concentration of 500 $g.m^{-3}$ was selected for the tests, and a permanent spark constituted the ignition source to avoid overdriving phenomena and too high brightness interfering with the video recording. Videos were automatically analysed using Matlab's image toolbox and an homemade software developed to extract the flame position, flame surface and flame expansion rate.

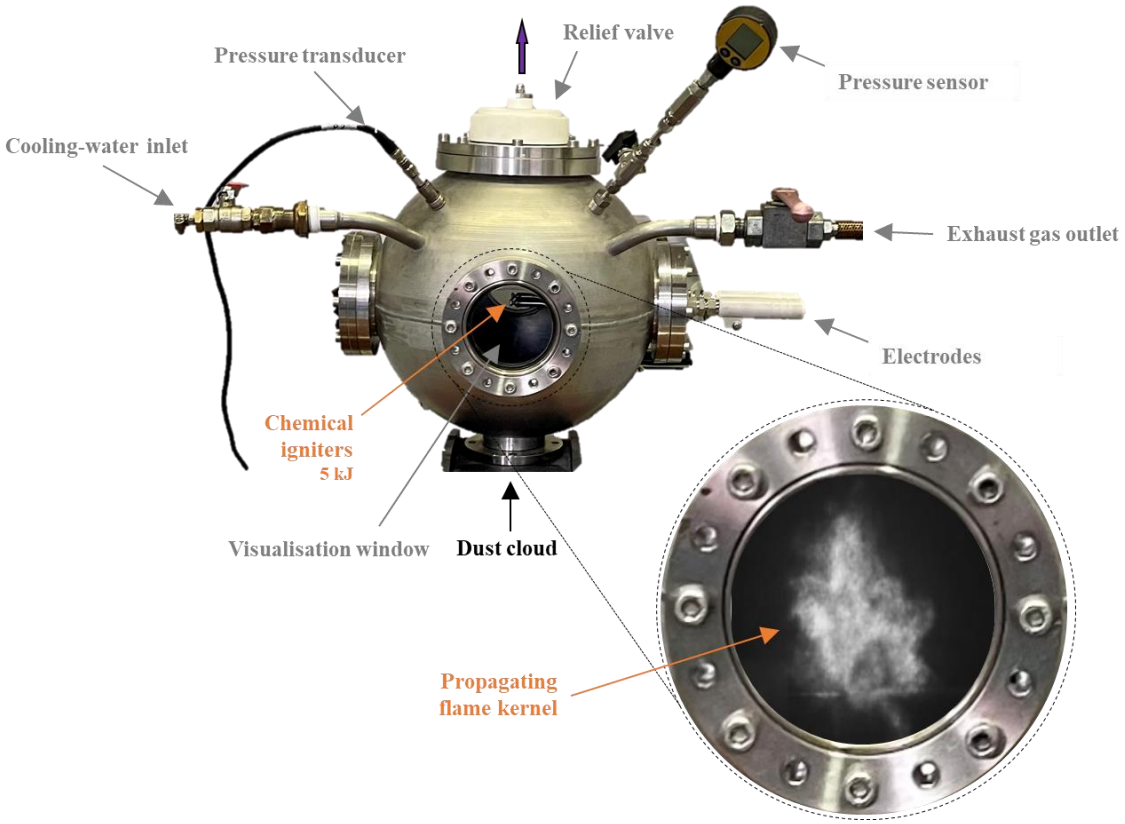

Figure 6-3 - 20L vessel equipped with visualisation windows for studying the flame propagation

2.2.3 Micro-fluidised bed burner

A micro-fluidised bed burner (MFB burner, see Figure 6-4) was conceived to decouple an organic dust explosion's (oxidative) pyrolysis and oxidation steps, as well as to remove the effect of the turbulence and the mass transfer, which are present in the vertical tube and in the 20L sphere. The objective is to enlighten the contribution of the pyrolysis products to flame propagation within the dust cloud by removing the "interference" of the solid particles. The setup comprises two main parts: the pyrolysis of the solid particles in a fluidised sand bed and a pyrolysis products-air burner. A scheme of the design is presented in Figure 6-4. A cylindrical quartz tube of 20 mm of inner diameter constituted the reactor. A sintered silica plate assured a correct distribution of the gas in the entirety of the section. Air was used to fluidise the sand bed, constituted by Fontainebleau sand (see Figure S 24 in Annex 5 for its characteristics). Two gas flows in the upper part of the system (Reservoir and Dusty flows, see Figure 6-4) ensure a stable powder flow and prevent it from clogging the glass stem. A third gas flow sweeps the reactor head (Head flow in Figure 6-4) to facilitate the pyrolysis products exiting the reactor

and to reduce the tar deposits in this zone. Finally, pyrolysis gases and vapours flow to the burner. Its temperature is controlled and set at 350°C to avoid tar condensation and clogging the tube. An inox tube also maintained at 350°C leads the mixture to the burner.

Calculations started by imposing the fluidisation gas velocity: previous studies (Jia et al. 2017a; 2017b; 2015; 2016) revealed a minimum fluidisation velocity of 4 cm/s, and a u-to-u_{mf} ratio of 2 was adopted to reach a fully bubbling fluidisation. In order to reach approximately an equivalence ratio of 1, the cellulose feed rate to the reactor was approximately 20 g/h. It was set by imposing the rotation velocity of the electric motor that constituted the feeding system. The results presented in Chapter 5 allowed to set the temperature of the fluidised sand bed at 400°C to obtain an isothermal process and thus pyrolysis gases with a constant average composition. The inner diameter of the burner was calculated to obtain a laminar flame speed in the range of 10-15 $cm.s^{-1}$. To determine the pyrolysis product flow to the flame, and thus to set the airflow to reach an equivalence ratio of approximately 1, the results proposed by Piskorz (Piskorz et al. 2000b) were considered. They consisted in the product yields obtained for a cellulose flash pyrolysis process in a free-fall reactor, with similar temperature and residence time as this work. The detailed calculation is reported in Annex 5.

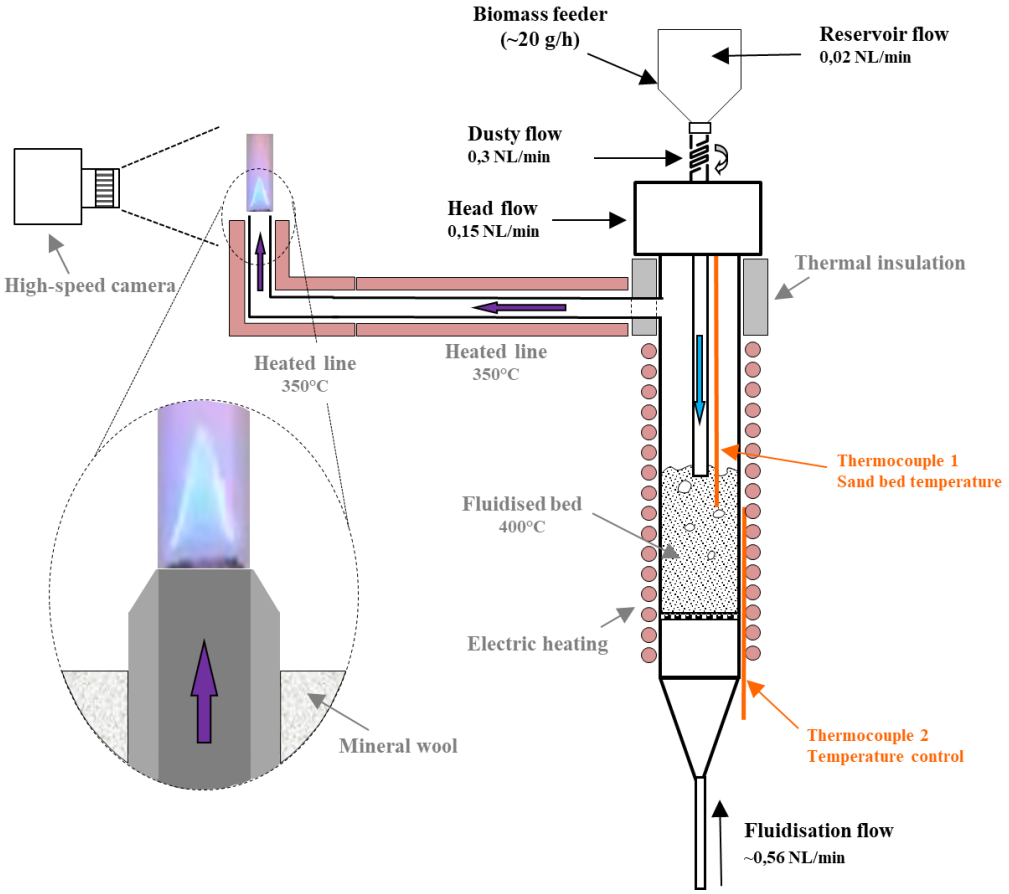

Figure 6-4 - Global scheme of the fluidised bed burner used to measure the laminar flame speed of the pyrolysis products

2.3 Flame speed determination

2.3.1 Spherically-propagating flame video analysis

A high-speed video camera (MotionBlitz EoSens mini 2) was used to record the flame propagation in the tube. The frame acquisition rate and the shutter speed set were 2000 fps and 300 µs. MotionBLITZ Director2 operator software was used for treating high-speed videos. The video treatment procedure was inspired by the model presented by Cuervo (Cuervo et al. 2017). First, each frame is extracted from the flame propagation video. Next, the flame kernel is identified in the frames. The analysis starting point was the ignition instant (more precisely, as soon as the high brightness due to the spark/ignition source allows the visualization of the flame kernel), and the ending point corresponded to when the flame front touched the walls. In fact, since the laminar flame speed must be independent of the apparatus shape, size and geometry, the flame-to-wall interactions must be reduced as much as possible. Hence, only the interval from 0 to approximately 30-35 ms was considered. Three characteristics are determined

for each frame: the cross-section A_s (the kernel projection on a plane perpendicular to the vertical axis), the estimated 3D flame surface A_f (assuming a spherical or an ellipsoidal shape of the flame kernel, depending on the frame), and the vertical position z of the apex of the flame front. Knowing the position z over time means knowing the spatial velocity S_s, which allows calculating the flame burning velocity S_u using the formula proposed by Andrews and Bradley (Andrews, Bradley, and Lwakabamba 1975)::Knowing the position z over time means knowing the spatial velocity S_s, which allows calculating the flame burning velocity S_u using the formula proposed by Andrews and Bradley [231]:

$$S_u = S_s \frac{A_s}{A_f} \tag{3}$$

The following three conditions must be satisfied to employ this equation:

- A constant burning velocity, which can be associated with a constant local equivalence ratio during the propagation;
- A flame thickness smaller than its curvature;
- A spatial velocity Ss constant over the entire flame surface.

The turbulence and intrinsic heterogeneity of the dust cloud are the primary responsible for the deviation from these conditions that may be present in the system studied. Hence, a fraction of the incertitude associated with the final results likely comes from these assumptions. An expansion factor χ was adopted to correct the previous formula to consider the contribution of the hot gas thermal expansion in the S_u. It corresponds to the ratio between the temperature of the hot burnt gases (determined as the adiabatic flame temperature using the NASA Glenn's computer code CEA - Chemical Equilibrium with Applications (McBride, B.J. and Gordon, S.) and that of the fresh mixture. It corresponds to the ratio between the temperature of the hot burnt gases (determined as the adiabatic flame temperature using the NASA Glenn's computer code CEA - Chemical Equilibrium with Applications [232]) and that of the fresh mixture. Equation (3) was modified as follows:

$$S_u = \frac{1}{\chi} S_s \frac{A_s}{A_f} \tag{4}$$

A characteristic feature of flames propagating within dust clouds is their shape and surface irregularities, and their influence must be carved out in order to be able to calculate a laminar flame speed. Karlovitz (Karlovitz, Denniston, and Wells 1951) proposed a factor K, the Karlovitz factor, that can be employed to do so: Karlovitz et al. [233] proposed a factor K, the Karlovitz factor, that can be employed to do so:

$$K = \frac{1}{A_f} \frac{dA_f}{dt} \tag{5}$$

Several relationships can be found in the literature to link K and flame speed. Santandrea (Santandrea et al. 2020) compared linear and non-linear relations and concluded that a 4% discrepancy existed between the two for cellulose powders. For simplicity reasons, the following linear equation will be used in this work:

$$S_u = -\delta_M K + {S_u}^0 \quad (6)$$

where S_u^0 is the unstretched flame speed, and δ_M is the Markstein length. Its validity range comprehends low K and a Lewis number (i.e. the ratio of thermal diffusivity to mass diffusivity) close to 1 (Clavin 1985; Markstein 1964). where S_u^0 is the unstretched flame speed, and δ_M is the Markstein length. Its validity range comprehends low K and a Lewis number (i.e. the ratio of thermal diffusivity to mass diffusivity) close to 1 [234,235].

2.3.2 Conic laminar flame video analysis

The same recording system was used for the MFB burner (MotionBlitz EoSens mini 2 high-speed camera). The shutter speed and the frame acquisition rate were set at 10000 µs and 30 fps, respectively. MotionBLITZ Director2 operator software was used for treating high-speed videos. A Matlab code was developed to subsequently analyse the videos. As represented in Figure 6-5, the simplified procedure adopted to calculate the burning velocity associated with the MFB burner flame provided for determining the alfa angle and the fresh mixture velocity at the flame v_u. First, a MATLAB code was developed to calculate the flame height, exploiting the BoundingBox function (see Figure 6-5). Next, knowing the nozzle diameter made it possible to determine alfa. As for the mixture velocity at the flame, a manual bubble flowmeter was employed to estimate the flow rate of the hot gases arriving at the flame. Since their temperature decreased the surface tension of the water-soap bubbles in the flowmeter, and their velocity led to high bubble growing rates, v_u can be considered the first source of uncertainty affecting the final result of S_u. Furthermore, it should be added that the burner is obviously not adiabatic and that heat losses are inevitable at the outlet.

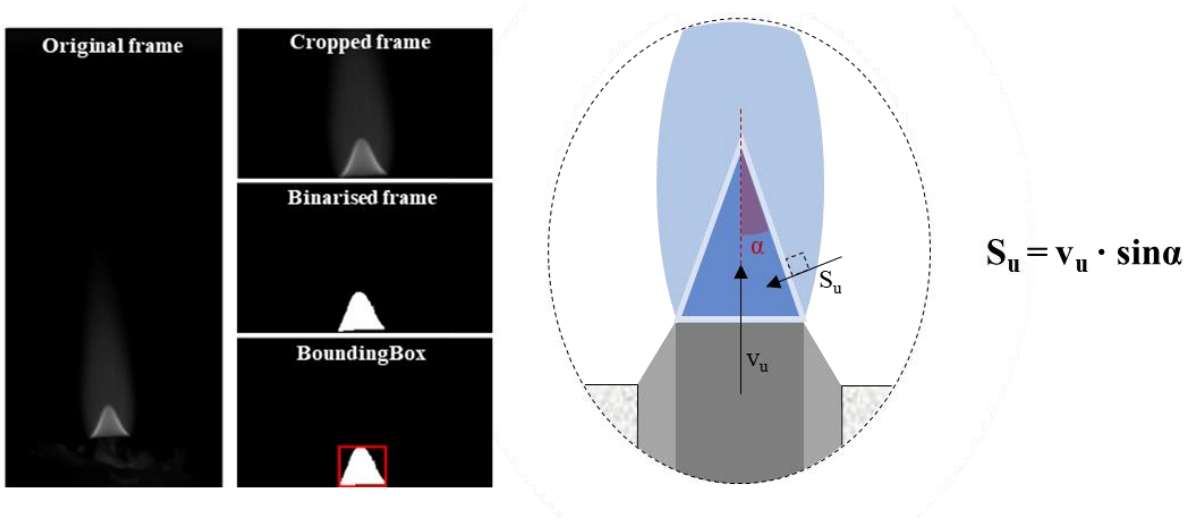

Figure 6-5 - Procedure adopted to calculate the burning velocity of the flame created with the MFB burner

2.3.3 Numerical calculation

To support the experimental results, a numerical simulation was carried out on Chemkin (Kee, R. J., Rupley, F. M., and Miller, J. A. 1989) to estimate the laminar flame speed of the pyrolysis products-air mixture.[236] to estimate the laminar flame speed of the pyrolysis products-air mixture. The objective was to compare the speed of the flame front propagating within the dust cloud and in a homogeneous system (without dust). The pyrolysis products considered in this calculation and their relative concentration were taken from Graham (Graham et al. 1984), whose work focused on cellulose flash pyrolysis in an entrained bed, characterised by small residence time (200-400 ms) and a high reactor temperature (750-900°C). In their work, high heat transfer was accomplished with a solid-solid interaction in the reaction volume, which assured a high heat flux to the particles, comparable to that encountered in a dust explosion test in the 20L sphere. The calculation was based on a detailed kinetic model developed for dimethylfuran (DMF) oxidation and adapted to include levoglucosan, which is the main tar product from cellulose primary pyrolysis. A 1D free propagating adiabatic flame was chosen as the simulation system. Rate constant of each reaction is assumed to follow the Arrhenius equation (7):

$$k = A\ T^n \exp\left(-\frac{E}{RT}\right) \tag{7}$$

and is associated with three parameters (A, n and E). Finally, the transport coefficients of each species necessary to take into account the axial mass diffusivity were employed to calculate a mixture-averaged global transport coefficient. It has been shown that the cellulose flash pyrolysis process is related to an endothermicity that leads to a plateau of the particle

temperature around 773K (Piskorz et al. 2000b), as also stated in Chapter 3. The products released in this stage are likely responsible for creating the flammable atmosphere necessary to trigger the oxidation reactions and, thus, the flame propagation. For this reason, 773K was chosen as the fresh mixture's initial temperature. Further details of the Chemkin simulation are reported in the Annex 5.

3. Results and Discussion

3.1 Flame propagation tube

Figure 6-7 - Frames extracted from the video considered for the analysis of the flame propagation (cellulose injected = 1 g, tv = 180 ms, ignition energy = 1 J shows seven frames extracted from a video recorded for cellulose (Avicel ph 101), from 1 to 51 ms after the ignition. Tests were repeated until the flame kernel propagation was visible and not hidden by excessive light diffraction within the dust cloud. As can be seen, the flame presented corrugated and wrinkled contours, which increased the complexity of the video treatment. This was also underlined by Skjold (Skjold, Olsen, and Castellanos 2013).This was also underlined by Skjold et al. [237]. By performing free-expanding Lycopodium explosion tests inside a balloon (it expands and eventually ruptures, allowing the explosion to be quasi-isobaric), they assessed the intricacy of following the flame contour within the dust cloud because of diffraction and high brightness of the hot combustion products. Testing also propane and comparing the results with Lycopodium tests, they proved that the presence of particles generates higher turbulence in the mixture through temperature variations, pyrolysis gas flow fluctuations and particle movements, which increase the instability of the flame propagation. But, above all, the probability of introducing errors in the flame front recognition step increases. This is because the 2D frames recorded by the high-speed camera represent only the projection of the flame, whose morphology along the third coordinate is not considered. Moreover, the shape and structure of a flame propagating in a (microsized) dust cloud resent the system's heterogeneity. Zhang (Zhang et al. 2017) pointed out the role of solid particles in forming flame clusters in the flame. Zhang et al. [238] pointed out the role of solid particles in forming flame clusters in the flame. According to their study on micrometric PMMA powder explosions, these clusters are responsible for locally destabilising the flame propagation, introducing turbulence and increasing, even more, the heterogeneity of the system. Nonetheless, the incertitude due to these considerations was partially compensated by manually checking the code's automatic flame

contouring. Around 30-35 ms, the flame-to-wall interactions, due to the compression of the gases between them and the quenching effect due to the contact, are no more negligible. Moreover, the brightness of the hot products became too high to allow accurate flame contouring. Hence, the high-speed video analysis stopped at this moment. Figure 6-6 reports the results concerning the flame speed as a function of the Karlovitz factor. An unstretched flame speed of 22.0 cm/s was obtained with the procedure previously described. The value is consistent with those of similar works (Proust 2017; Silvestrini et al. 2008).The value is consistent with those of similar works [206,239].

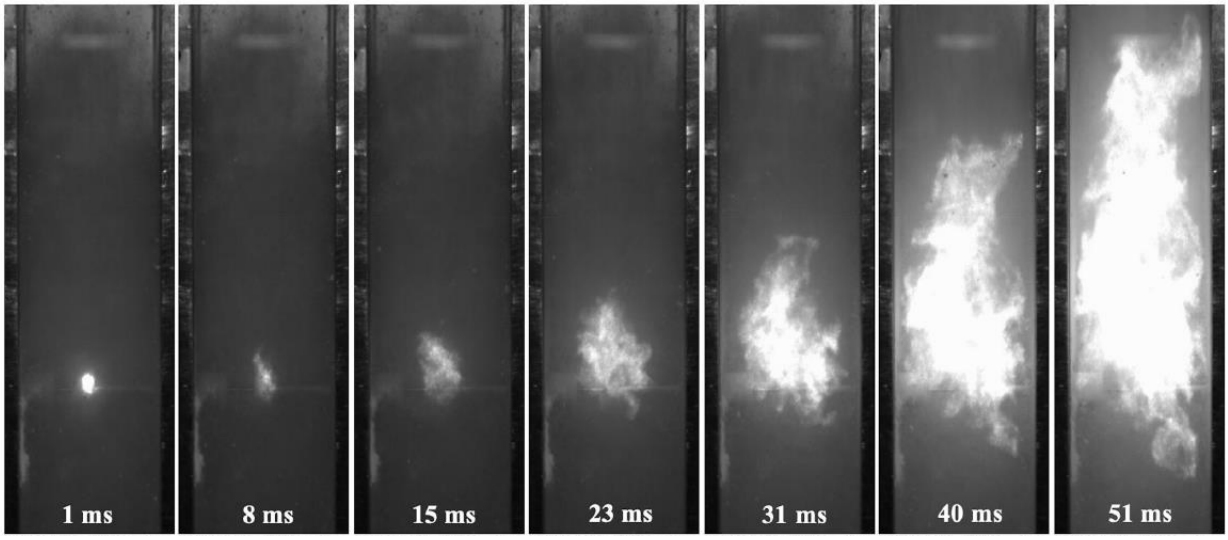

Figure 6-7 - Frames extracted from the video considered for the analysis of the flame propagation (cellulose injected = 1 g, tv = 180 ms, ignition energy = 1 J)

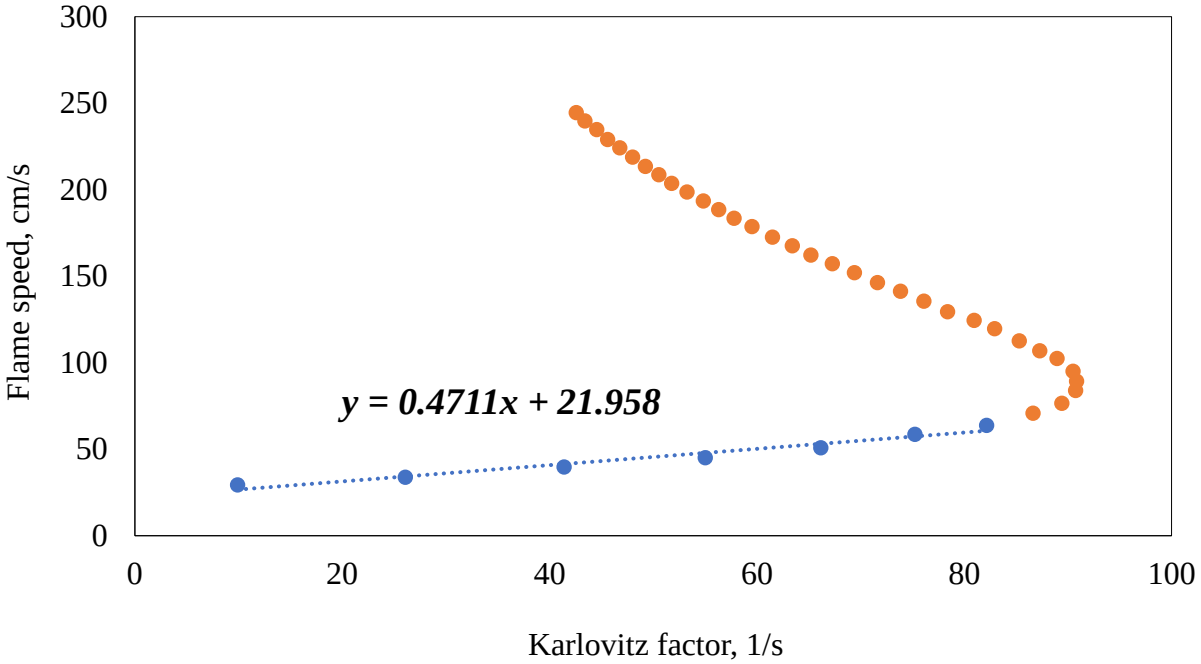

Figure 6-6 - Cellulose flame speed as a function of the Karlovitz factor

3.2 20L vessel

Figure 6-9 shows the explosion severity test results obtained by Santandrea (Santandrea et al. 2020) with micro-crystalline cellulose as a function of the dust concentration. They obtained an unstretched flame speed of 26.6 cm/s. As can be noticed, values are consistent with those found in the semi-opened vertical tube. The slight discrepancy is likely related to the different particle sizes of the cellulose and the setups used. The spherical propagating flame tests were carried out with cellulose nanocrystals powder (primary fibre dimensions: 3 nm of width and 70 nm of length), whilst in the semi-open tube, micro-crystalline cellulose (Avicel ph 101) was employed. The higher specific surface area and the more regular propagation of the flame front in a nano-dust cloud (Zhang et al. 2017). If this trend is not limited by the formation of agglomerates due to Van der Waals forces, it can be related to a higher flame speed value. The higher specific surface area and the more regular propagation of the flame front in a nano-dust cloud. If this trend is not limited by the formation of agglomerates due to Van der Waals forces, it can be related to a higher flame speed value. Figure 6-10 - Unstretched flame speed for cellulose, calculated with the Silvestrini's equation (Silvestrini et al. 2008) with the modification proposed by Santandrea (Santandrea et al. 2020 reports the flame speed results after using the Silvestrini formula, modified according to Santandrea (Santandrea et al. 2020), on the explosion parameters obtained in this work. The increasing trend and the absence of a maximum point could have been related to lean mixtures, but it is not the case, as proven by the maximum associated with $(dP/dt)_m$, corresponding to an ER = 1 comprised between 650 and 700 g/m^3. However, it should be stressed that the maximum explosion pressure is recorded at 1500 g/m^3. Considering the value of flame speed individuated by these concentrations, i.e. approximately 20 cm/s, it can be concluded that the experimental methods presented so far are consistent. However, attention should be paid when comparing the flame speed obtained in the vertical tube and that obtained in the 20L sphere. As stated in Murillo (Murillo et al. 2015), numerous parameters must be correctly set to improve the reproducibility of the data obtained in the vertical tube. The delay between dispersion and ignition, the position of the ignition source, and the dispersion pressure play a primary role in imposing the dust cloud's turbulence level. Still, the heterogeneous (nominal) dust concentration field along the tube makes it complex to associate the flame speed value with a specific ER. In the 20L sphere, changing the dust concentration allows for studying the influence of the (nominal) dust concentration, enlightening a maximum point likely associated with ER around the unity.

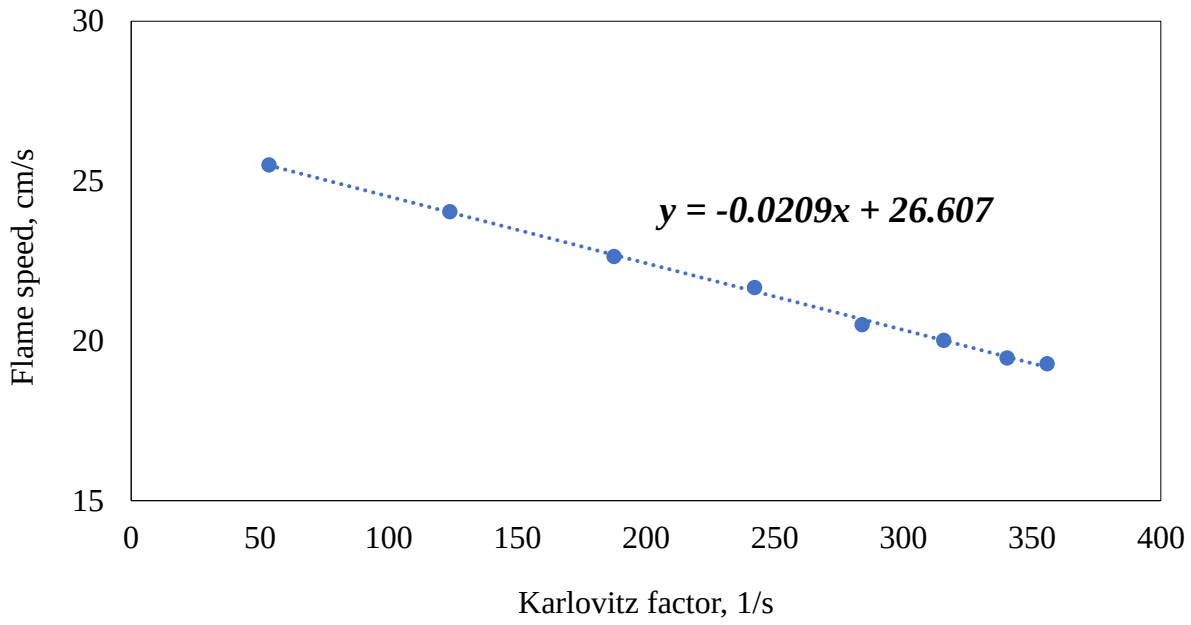

Figure 6-8 - Flame speed as a function of the Karlovitz number, relative to the test reported in Santandrea et al. 2020

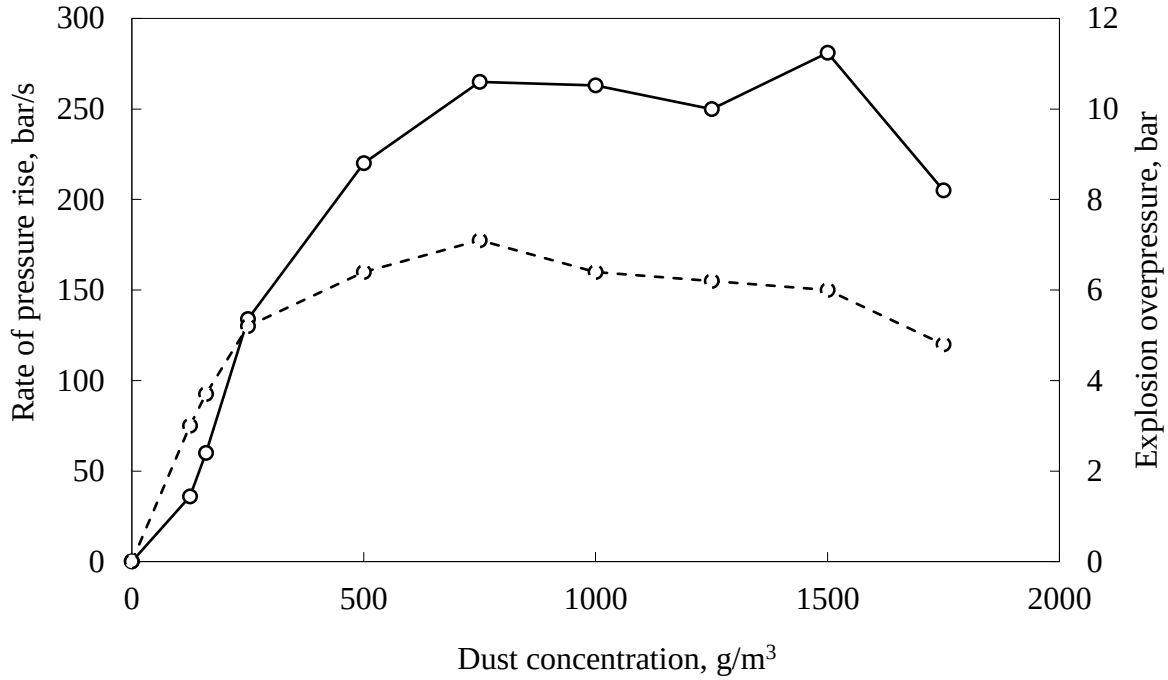

Figure 6-9 - Explosion severity parameters as a function of the cellulose (Avicel ph 101) concentration

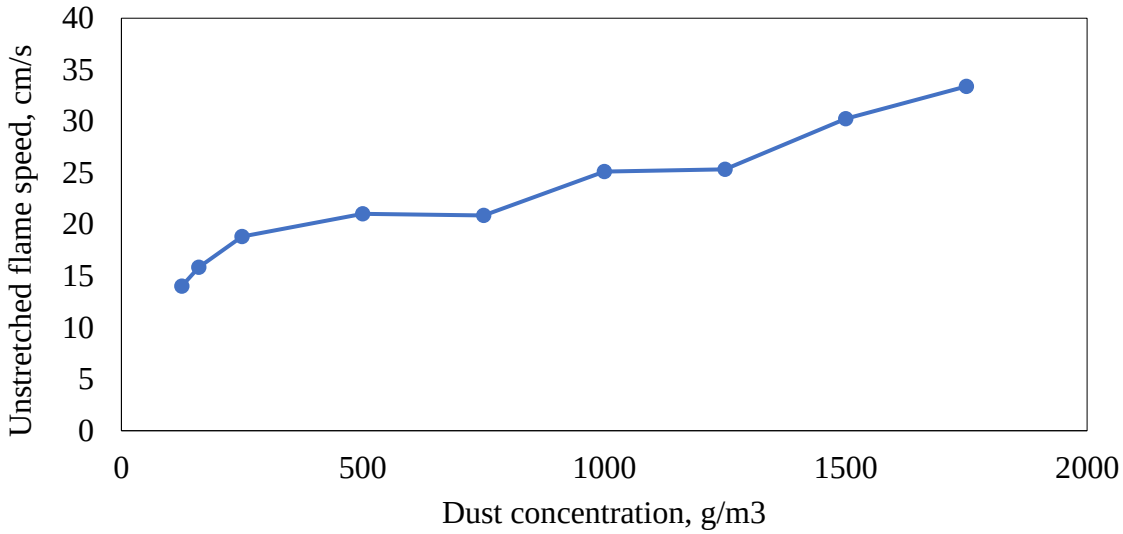

Figure 6-10 - Unstretched flame speed for cellulose, calculated with the Silvestrini's equation (Silvestrini et al. 2008) with the modification proposed by Santandrea (Santandrea et al. 2020)

3.3 MFB burner

An instance of the results is reported in Figure 6-12. The flame was lit with a match since no pilot flame or ignition devices were included in the setup. The instabilities partially shown in Figure 6-12 resulted from oscillations in the pyrolysis gas generation system, i.e. in the micro-fluidised bed. In particular, the feeding system did not ensure a perfectly stable powder flow, which generated slight changes in flow and composition. Variations in the equivalence ratio were thus present during the experiments and can be considered responsible for the flame instabilities. As reported in Wu (Wu 2016), the observed stretching combined with the tip opening are symptoms of a lean mixture. As reported in Wu [241], the observed stretching combined with the tip opening are symptoms of a lean mixture. Nonetheless, the fluidised bed contributed to smoothing them, increasing the stability of the gas mixture flowing to the burner. Despite these variations, the flame was stabilised for 8 seconds. Tip opening was observed in the first part of the test until approximately 6 s from the starting point, while after 15 s, the flame backfired and disappeared. The height of the flame was relatively low, which can be related to a low turbulence level of the flow arriving at the flame {Citation}. The flame angle was determined for each frame as illustrated by Figure 6-11. Due to the flame instabilities and uncertainties related to gas flow fluctuations, the analysis lead to a flame speed range of approximately 135-155 cm/s, which is consistent with the results relative to the numerical simulation on Chemkin of the flame propagation in a pyrolysis product-air mixture at 500°C.

The composition of the pyrolysis gases considered in the numerical simulation are reported in Annex 5. Numerical results are reported in Figure 6-13, as a function of the equivalence ratio (ER). Values are comparable to those obtained experimentally and allow identification of the ER range associated with the results. As the flame speed determined with the MFB burner was between 135 and 155 cm/s, it corresponds to a theoretical ER between 0.6 and 0.7. It also supports the visual results showing an open tip flame, associated with a lean mixture. As abovementioned, the main advantage of this setup is the possibility of decoupling the (oxidative) pyrolysis and the oxidation steps usually occurring in a fast combustion process of organic materials. Studying the laminar flame speed with the MFB burner is comparable to studying the flame propagation within a dust cloud and carving out the "interference" due to the presence of the solid particles. They can be seen as punctual obstacles that increase the turbulence by locally changing the temperature field of the dust cloud, generating pyrolysis gases that locally change the composition field, and directly and indirectly interacting with other particles (interparticle shocks, agglomeration, fragmentation, radiative heat transfers, etc.). As stated by Eckhoff (Eckhoff 2003), a burning dust cloud can be described as an ensemble of Nusselt flames, characterised by heterogeneous combustion maintained by the oxygen diffusion toward the particle's surface, conducting to premixed combustion on a macroscopic scale, but local diffusion flames. Skjold (Skjold 2022) defined it as a "premixed combustible system with non-premixed substructures". Remove the presence of the particles allowed then to remove a potential source of turbulence and to study a flame of solely the hot pyrolysis gases freshly generated, without the interference of mass and heat transfers.

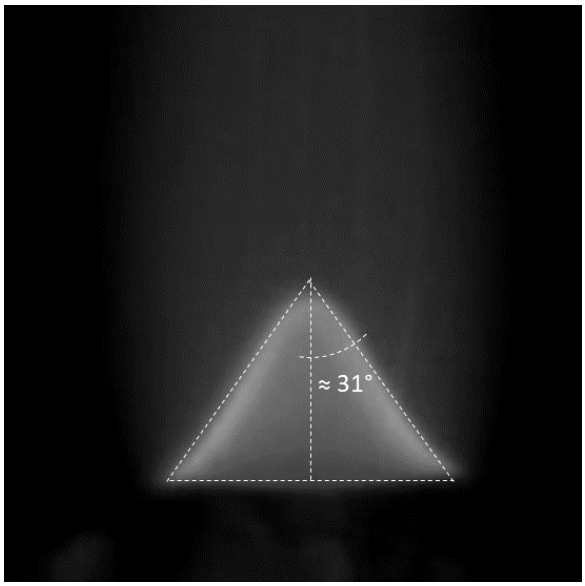

Figure 6-11 - Example of the determination of the flame angle

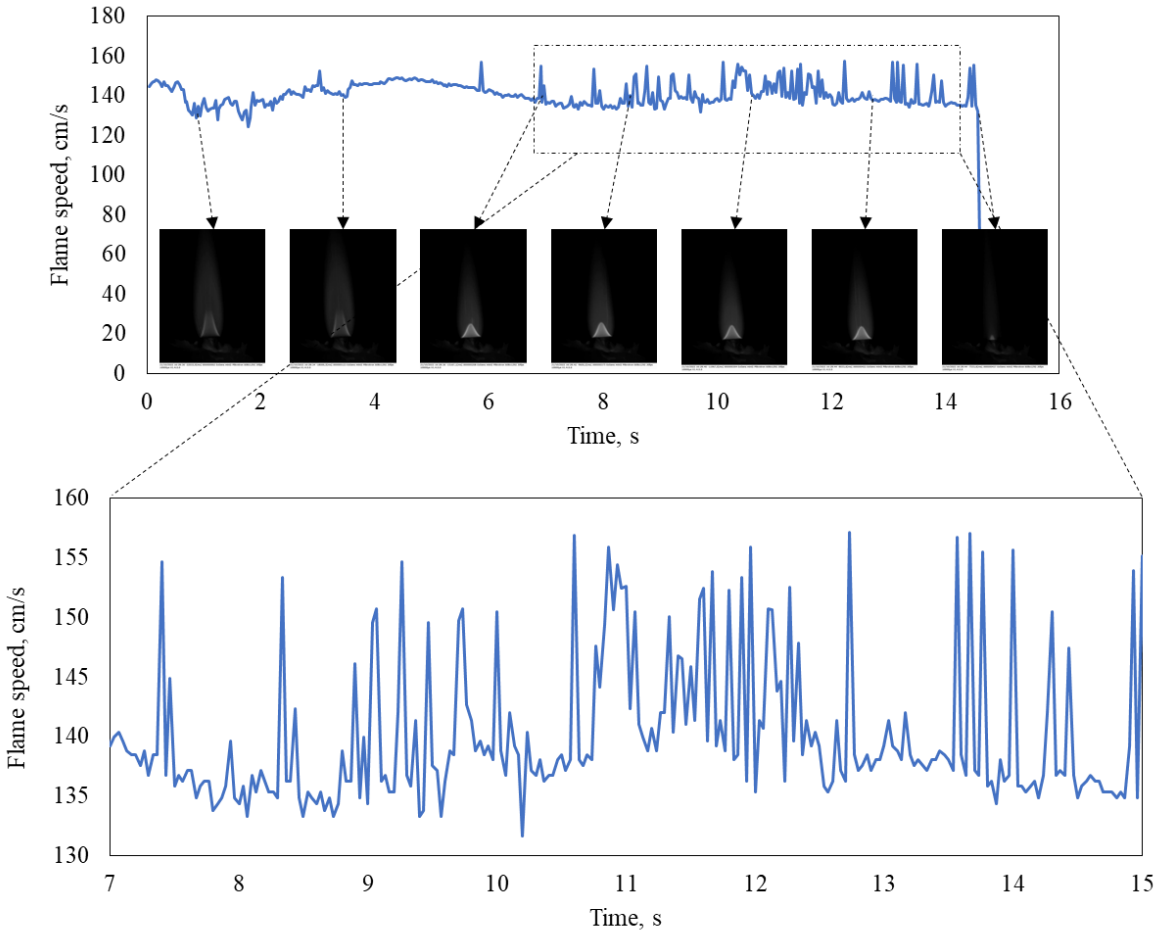

Figure 6-12 - Flame speed as a function of the experiment duration time

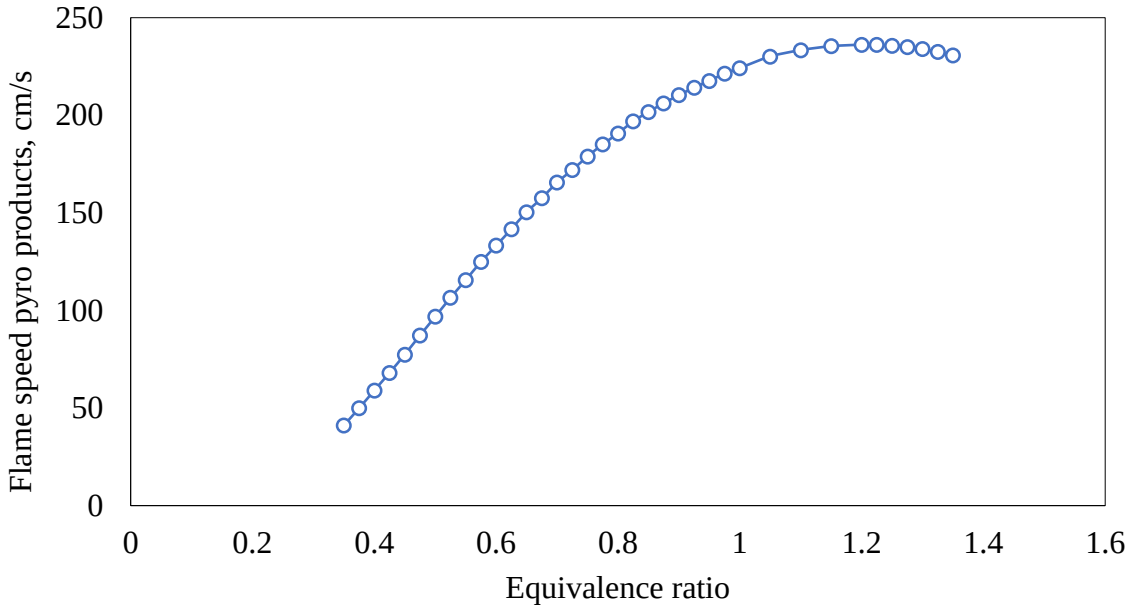

Figure 6-13 - Flame speed associated with the pyrolysis product-air mixture, calculated with Chemkin

4. Conclusions

This work allowed the laminar speed of a flame propagating in a dust cloud to be assessed. In order to do so, three experimental setups were compared and analysed: a modified Hartmann tube, a 20L sphere and a micro-fluidised bed (MFB) burner. Each flame propagation device has drawbacks and advantages, and often they are related to the complexity of the video treatment step. Results obtained with the first two apparatuses were consistent (22.0 and 26.6 cm/s, respectively). They were also compared to those obtained with a widely used semi-empirical non-linear relationship, which led to values ranging between 14.0 and 33.4 cm/s, according to the dust concentration in the 20L sphere. With the MFB burner, the flame speed was much higher (135-155 cm/s), due to the higher temperature of the fresh mixture. Still, the numerical simulation confirmed the reliability of these values since the range 133.2 - 230.7 cm/s was obtained for ER of 0.6 and 1.2, respectively. The discrepancy between the laminar flame speed determined in the sphere or in the tube and that obtained in the MFB highlights the significant influence of pyrolysis during a dust explosion. These results support the hypothesis of a rate-limiting step consisting mainly of the phenomenon of pyrolysis of the biomass (or of its heating rate, for large particles) during its explosion.

However, it should be underlined that some limitations characterised the third setup due to its complexity, such as a stable mixture, in terms of composition and flow, entering the flame. Moreover, measuring the pyrolysis product-air mixture flow rate entering the flame was not straightforward. It led to values affected by high uncertainty, which might have introduced some non-negligible errors in the final value of the flame speed.

References

Andrews, G. E., D. Bradley, and S. B. Lwakabamba. 1975. 'Turbulence and Turbulent Flame Propagation—A Critical Appraisal'. *Combustion and Flame* 24:285–304. doi: 10.1016/0010-2180(75)90163-7.

Clavin, Paul. 1985. 'Dynamic Behavior of Premixed Flame Fronts in Laminar and Turbulent Flows'. *Progress in Energy and Combustion Science* 11(1):1–59. doi: 10.1016/0360-1285(85)90012-7.

Cloney, Chris. 2020. *2020-Mid-Year-Combustible-Dust-Incident-Report-v5.Pdf*. Dust Safety Science.

Cuervo, Nicolas, Olivier Dufaud, and Laurent Perrin. 2017. 'Determination of the Burning Velocity of Gas/Dust Hybrid Mixtures'. *Process Safety and Environmental Protection* 109:704–15. doi: 10.1016/j.psep.2017.06.009.

Eckhoff, Rolf Kristian. 2003. 'Dust Explosions - Origin, Propagation, Prevention, and Mitigation: An Overview'. in *Dust explosions in the process industries*.

EN 14034-1. 2004. *Determination of Explosion Characteristics of Dust Clouds - Part 1: Determination of the Maximum Explosion Pressure Pmax of Dust Clouds*.

Graham, R. G., L. K. Mok, M. A. Bergougnou, H. I. De Lasa, and B. A. Freel. 1984. 'Fast Pyrolysis (Ultrapyrolysis) of Cellulose'. *Journal of Analytical and Applied Pyrolysis* 6(4):363–74. doi: 10.1016/0165-2370(84)80030-3.

Jia, Liangyuan, Felipe Buendia-Kandia, Stéphane Dumarcay, Hélène Poirot, Guillain Mauviel, Philippe Gérardin, and Anthony Dufour. 2017. 'Fast Pyrolysis of Heartwood, Sapwood, and Bark: A Complementary Application of Online Photoionization Mass Spectrometry and Conventional Pyrolysis Gas Chromatography/Mass Spectrometry'. *Energy & Fuels* 31(4):4078–89. doi: 10.1021/acs.energyfuels.7b00110.

Jia, Liangyuan, Anthony Dufour, Yann Le Brech, Olivier Authier, and Guillain Mauviel. 2017. 'On-Line Analysis of Primary Tars from Biomass Pyrolysis by Single Photoionization Mass Spectrometry: Experiments and Detailed Modelling'. *Chemical Engineering Journal* 313:270–82. doi: 10.1016/j.cej.2016.12.021.

Jia, Liangyuan, Yann Le Brech, Guillain Mauviel, Fei Qi, Matthias Bente-von Frowein, Sven Ehlert, Ralf Zimmermann, and Anthony Dufour. 2016. 'Online Analysis of Biomass Pyrolysis Tar by Photoionization Mass Spectrometry'. *Energy & Fuels* 30(3):1555–63. doi: 10.1021/acs.energyfuels.5b02274.

Jia, Liangyuan, Yann Le-Brech, Binod Shrestha, Matthias Bente-von Frowein, Sven Ehlert, Guillain Mauviel, Ralf Zimmermann, and Anthony Dufour. 2015. 'Fast Pyrolysis in a Microfluidized Bed Reactor: Effect of Biomass Properties and Operating Conditions on Volatiles Composition as Analyzed by Online Single Photoionization Mass Spectrometry'. *Energy & Fuels* 29(11):7364–74. doi: 10.1021/acs.energyfuels.5b01803.

Karlovitz, Béla, D. W. Denniston, and F. E. Wells. 1951. 'Investigation of Turbulent Flames'. *The Journal of Chemical Physics* 19(5):541–47. doi: 10.1063/1.1748289.

Kee, R. J., Rupley, F. M., and Miller, J. A. 1989. *Chemkin-II: A Fortran Chemical Kinetics Package for the Analysis of Gas-Phase Chemical Kinetics*. SAND-89-8009 ON: DE90000917. Sandia National Lab. (SNL-CA), Livermore, CA (United States).

Markstein, Geroge H. 1964. *Nonsteady Flame Propagation*. Vol. 75. AGARDograph.

McBride, B.J. and Gordon, S. n.d. *Computer Program for Calculation of Complex Chemical Equilibrium Compositions and Applications II. Users Manual and Program Description*. NASA.

Munajat, Nur Farizan, Catharina Erlich, Reza Fakhrai, and Torsten H. Fransson. 2012. 'Influence of Water Vapour and Tar Compound on Laminar Flame Speed of Gasified Biomass Gas'. *Applied Energy* 98:114–21. doi: 10.1016/j.apenergy.2012.03.010.

Murillo, Carlos, Nathalie Bardin-Monnier, Felipe Muñoz, and Olivier Dufaud. 2015. 'Application of CFD on the Sensitivity Analyses of Some Parameters of the Modified Hartmann Tube'. *Journal of Loss Prevention in the Process Industries* 36:296–307. doi: 10.1016/j.jlp.2014.12.023.

Piskorz, J., P. Majerski, D. Radlein, A. Vladars-Usas, and D. S. Scott. 2000. 'Flash Pyrolysis of Cellulose for Production of Anhydro-Oligomers'. *Journal of Analytical and Applied Pyrolysis* 56(2):145–66. doi: 10.1016/S0165-2370(00)00089-9.

Proust, Christophe. 2017. 'Turbulent Flame Propagation in Large Dust Clouds'. *Journal of Loss Prevention in the Process Industries* 49:859–69. doi: 10.1016/j.jlp.2017.05.011.

Santandrea, Audrey, Marine Gavard, Stéphanie Pacault, Alexis Vignes, Laurent Perrin, and Olivier Dufaud. 2020. '"Knock on Nanocellulose": Approaching the Laminar Burning Velocity of Powder-Air Flames'. *Process Safety and Environmental Protection* 134:247–59. doi: 10.1016/j.psep.2019.12.018.

Silvestrini, M., B. Genova, and F. J. Leon Trujillo. 2008. 'Correlations for FLame Speed and Explosion Overpressure of Dust Clouds inside Industrial Enclosures'. *Journal of Loss Prevention in the Process Industries* 19.

Skjold, Trygve. 2022.'Dust Explosion Modelling: Challenges and Limitations'. Presented at the DUST EXPLOSION SAFETY FOR THE PROCESS INDUSTRY Online workshop organised by RISE, January 21, Online edition.

Skjold, Trygve, Kjetil L. Olsen, and Diana Castellanos. 2013. 'A Constant Pressure Dust Explosion Experiment'. *Journal of Loss Prevention in the Process Industries* 26(3):562–70. doi: 10.1016/j.jlp.2012.08.003.

Wu, Yi. 2016. 'Experimental Investigation of Laminar Flame Speeds of Kerosene Fuel and Second Generation Biofuels in Elevated Conditions of Pressure and Preheat Temperature'. INSA Rouen and CORIA lab, Rouen.

Zhang, Xinyan, Jianliang Yu, Wei Gao, Dawei Zhang, Jinhua Sun, Song Guo, and Ritsu Dobashi. 2017. 'Effects of Particle Size Distributions on PMMA Dust Flame Propagation Behaviors'. *Powder Technology* 317:197–208. doi: 10.1016/j.powtec.2017.05.001.

CHAPTER 7

General conclusions

The main objective of this thesis was to analyse major phenomena involved in organic dust explosions and propose experimental procedures to quantify characteristic parameters. Organic dust explosion can be divided into 3 main steps: particle heating, pyrolysis and gas oxidation. Studying the reaction kinetics, especially related to the pyrolysis step, was the subject of a focus. Figure 7-1 shows schematic representation of the global structure of the studies presented in this thesis and the fundamental interconnections enlightened in this work.

In Chapter 2, several organic powders' agglomeration and deagglomeration tendency was analysed through an in-situ experimental analysis of the dust cloud generated in the Godbert-Greenwald furnace. The first aspect enlightened is heterogeneity that characterises a dust cloud in terms of the nature of the powder, particle shape, morphology and size. Hence, the inter-particle interactions are uncountable; thus, an organic dust cloud in the G-G oven is inevitably subjected to significant modifications of its PSD. Therefore, an agglomeration index was proposed to quantify them, and it was conceived considering the in-situ analyses performed in the G-G oven. It enlightened the primary contribution of the finer fraction (approximately < 50 µm) to the agglomeration phenomena and a less significant role of the coarser one (> 150 µm). Moreover, studying the influence of the dispersion pressure was fundamental for understanding how the dust cloud PSD change on its path. Finally, consequences on the thermal behaviour of the dust cloud were estimated via three dimensionless numbers: Py, Da and Bi. Agglomeration can have a non-negligible impact on the Py (the ratio between the pyrolysis reaction and the internal heat transfer characteristic times), according to the temperature of the particle.

Numerous aspects can be improved and deepened. First and foremost, more refined and precise modelling would sustain the experimental data, which cannot beneficiate from literature data support to be compared. However, the modelling approach presented in Chapter 2 needs specific agglomerate parameters (Hamaker constant, porosity, bulk density, shape factor, etc.) that are not easy to find or calculate. An experimental approach adapted to the powder considered would allow determining them and reducing the uncertainty of the final results.

At higher temperatures (from 700 to 900°C), other phenomena intervened. Pyrolysis is one of them, and it was widely studied via experimental and modelling approaches. The modification applied to the G-G oven and the development of a new experimental protocol was

the key to a complete characterisation of the flash pyrolysis occurring in the vertical heated chamber. Solid residues showed an important heterogeneity of the particle conversion degree, but an overall low conversion degree varying from 10 to 15%. The qualitative analysis of the condensable fraction revealed that the most abundant product was the levoglucosan, an essential index for comparison to other similar works in literature. Gaseous product compositions were exploited to elaborate and validate a model that calculates the kinetic parameters of lumped pyrolysis reactions occurring in conditions relevant to dust explosions. The model shows a good agreement with the experimental data, but also discrepancies with the kinetic parameters determined by other authors using TGA or fluidized bed. These deviations highlight the role of the analytical technique employed to determine them, and the importance of determining these parameters under the same conditions as a dust explosion and with the same material (powders). Another level of information was layered for a better understanding of the kinetics of an organic dust explosion. A dust cloud thermal analysis supported the experimental results and enriched the knowledge thus obtained.

As for the previous work, since the physicochemical parameters of the selected organic powders were used in the thermal analysis (density, specific heat, thermal conductibility, pyrolysis heat of reaction), determining them experimentally would increase the accuracy of the global study. Furthermore, the oxidation step of the model is currently being elaborated based on the obtained results.

The composition of the pyrolysis products determined in Chapter 3 was fundamental for developing the study presented in Chapter 4. Hybrid mixture explosion tests were employed to study the influence of the pyrolysis step in an organic dust explosion. In particular, the role of the primary products on cellulose dust explosions was analysed in the 20L sphere, a standard apparatus commonly used to determine ignition sensitivity and explosion severity parameters. Char, tars and pyrolysis gases were mixed with pure cellulose, and their explosion severity was determined. The effect of the pyrolysis gases was straightforward: in the dust-pyrolysis gas mixture, as the gas concentration increased, the rate of pressure rise increased as well, while the explosion overpressure showed a less significant augmentation. This suggested that the oxidation reactions occurring in the gaseous phase and involving the gaseous pyrolysis products can accelerate the process by bypassing the pyrolysis step. Evidence that the latter was the slowest among the fundamental steps in a cellulose dust explosion was furnished in the work. Tar and char showed secondary yet non-negligible roles: a slight and constant augmentation of both P_m and $(dP/dt)_m$ was observed for the tar-coated cellulose, while a moderate increase of

the explosion parameters was noticed by adding char to the system, evolution which could be related to strong modification of the radiative heat transfer. Water vapour showed little impact on explosion severity parameters, comparable with the experimental uncertainty.

Several more combinations of pyrolysis products were already considered to improve the work and highlight the role of hydrogen of the ignition sensitivity and combustion kinetics. By considering the yield of char, tar and gaseous products typical of a flash pyrolysis phenomenon, a classification of the role of each in a cellulose dust explosion can be elaborated.

Chapter 5 aimed to assess the operability region of a biomass oxidative pyrolysis process conducted in a micro-fluidised bed. The visualisation of the fluidisation was converted into a quantitative analysis through a high-speed in-situ video recording system. A Matlab code allowed for determining the evolution of bed height and splash zone fluctuation over time as the biomass was fed. In addition, the effects of the temperature (400 and 500°C) and the atmosphere (air and nitrogen) were studied. At 500°C, tar-generating reactions are faster and lead to a more significant agglomeration, especially for cellulose. Under air, on the other hand, oxidation reactions consume the liquid-intermediary of cellulose pyrolysis, leading to a stable fluidisation regime. The regions were the operability of the biomass oxidative pyrolysis were identified by means of the in-situ investigation tool developed. Digital imaging allowed to complete the study by characterising the agglomerates' morphology, the sand bed's colour and the char's presence. They confirmed what observed in the high-speed videos.

The high-speed videos of the fluidised bed realised while feeding the biomass are still full of information to exploit. The path of the char particles in the fluidised bed and their content, the bubble size and their evolution over time and the formation of preferential paths are only a few aspects that can be exploited for deepening the study. Further analysis will also be performed on the sand bed to determine the composition of the products responsible for the agglomeration (via methanol rinsing and GC-MS-FID analysis) and those adsorbed or trapped in the char structures (via LDI-FTMS).

Finally, Chapter 6 employed the information obtained in the previous one to generate a stable flow of cellulose pyrolysis products in a micro-fluidised bed and to design a burner to study the flame speed of the same gaseous products. The objective was to decouple the pyrolysis step from the oxidation step, typically occurring almost simultaneously in an organic dust explosion, to characterise the role of the pyrolysis gases in the flame propagation within a dust

cloud. Results were compared to those obtained in a vertical semi-open flame propagation tube and a 20L sphere. Some discrepancies were observed between the values (21 cm/s obtained with the propagation tube, 26 cm/s obtained with the 20L sphere, compared to 145 cm/s obtained with the MFB burner for pyrolysis gases), but their complementarity was exploited to underline the role of pyrolysis gases in the flame propagation within a dust cloud.

The main objective that is envisaged is, first and foremost, a longer stabilisation of the flame, which will enable to obtain of more accurate data. Next, a more precise measure of the mixture pyrolysis product-air flow entering the flame will increase the reliability of the flame speed value obtained. Finally, a parametric study will be carried out by changing the diameter of the nozzle and the air-to-biomass ratio. The latter will influence the burning mixture's fuel equivalence ratio and, thus, the flame speed.

This thesis proposed experimental and modelling tools to study phenomena involved in organic dust explosions. The quantitative analysis carried out allowed to determine precious parameters that can be used as a basis for further research applications. For instance, the procedures presented in Chapters 2 and 3 could be merged to conceive a vertical downward flame propagation system from the G-G furnace. Characterising the dust cloud PSD (and thus the actual diameters of the particle/agglomerates reacting) and knowing the behaviour of the particles as a function of the temperature would mean deeply understanding the response of the dust cloud. On these premises, this well-characterised system would be an interesting setup for generating pyrolysis gases in conditions very similar to those of a dust explosion. The subsequent ignition of the gases thus generated would allow studying the flame propagation of the same gas phase generated during an organic dust explosion. The other main aspect enlightened by this study is the predominance of particle structure over chemical formula. It demonstrates that predictive dust explosion models must be adapted to the powder specificities, and not only to its chemical composition. Results presented in Chapter 3, enriched of the experimental tools proposed in Chapter 2 and 4, will be extended to starch and cellulose-starch mixtures. The reaction mechanisms thus obtained will be integrated in another existing model (Torrado et al., 2018) to estimate the laminar flame velocity of organic powders and, in a second time, to predict their maximum rate of pressure rise in a 20L sphere. A comparison with the MFB burner will allow to validate the results.

To conclude, avoiding the so-called "black-box approach" enables adapting the study to a specific case, obtaining reliable and precise information about a chaotic, transient, turbulent

and heterogeneous system such as an organic dust explosion. Results presented in this work are meant to deepen the knowledge around dust explosions. They are applicable to industry to make biomass gasification, pyrolysis and combustion processes intrinsically safer by including a deeper understanding of the risks related to biomass powders.

Conclusions générales

L'objectif principal de cette thèse était d'analyser les principaux phénomènes impliqués dans les explosions de poussières organiques et de proposer des procédures expérimentales pour quantifier les paramètres caractéristiques. L'explosion de poussières organiques peut être divisée en 3 étapes principales : le chauffage des particules, la pyrolyse et l'oxydation des gaz. L'étude de la cinétique de réaction, notamment liée à l'étape de pyrolyse, a fait l'objet d'un focus. La Figure 7-1 montre une représentation schématique de la structure globale des études présentées dans cette thèse et des interconnexions fondamentales éclairées dans ce travail.

Dans le Chapitre 2, la tendance à l'agglomération et à la désagglomération de plusieurs poudres organiques a été analysée par une analyse expérimentale in-situ du nuage de poussière généré dans le four Godbert-Greenwald. Le premier aspect mis en lumière est l'hétérogénéité qui caractérise un nuage de poussière en termes de nature de la poudre, de forme, de morphologie et de taille des particules. Ainsi, les interactions inter-particules sont innombrables ; par conséquent, un nuage de poussière organique dans le four G-G est inévitablement soumis à des modifications importantes de sa PSD. C'est pourquoi un indice d'agglomération a été proposé pour les quantifier, et il a été conçu en tenant compte des analyses in-situ effectuées dans le four G-G. Il a mis en évidence la contribution de la fraction la plus fine (environ < 50 µm) aux phénomènes d'agglomération et un rôle moins important de la fraction la plus grossière (> 150 µm). De plus, l'étude de l'influence de la pression de dispersion a été fondamentale pour comprendre comment la PSD du nuage change sur son chemin. Enfin, les conséquences sur le comportement thermique du nuage ont été estimées via trois nombres sans dimension : Py, Da et Bi. L'agglomération peut avoir un impact non négligeable sur le Py (le rapport entre le temps caractéristique de la réaction de pyrolyse et celui du transfert de chaleur interne), en fonction de la température de la particule. De nombreux aspects peuvent être améliorés et approfondis. Tout d'abord, une modélisation plus fine et précise permettrait de soutenir les données expérimentales, qui ne peuvent bénéficier d'un support de données bibliographiques pour être comparées. Cependant, l'approche de modélisation présentée dans le Chapitre 2 nécessite des paramètres spécifiques de l'agglomérat (constante de Hamaker, porosité, densité apparente, facteur de forme, etc.) Une approche expérimentale adaptée à la poudre considérée permettrait de les déterminer et de réduire l'incertitude des résultats finaux.

A des températures plus élevées (de 700 à 900°C), d'autres phénomènes interviennent. La pyrolyse est l'un d'entre eux, et elle a été largement étudiée via des approches expérimentales et de modélisation. La modification appliquée au four G-G et le développement d'un nouveau protocole expérimental ont été la clé d'une caractérisation complète de la pyrolyse flash se produisant dans la chambre chauffée verticale. Les résidus solides ont montré une hétérogénéité importante du degré de conversion des particules, et un faible degré de conversion global variant de 10 à 15%. L'analyse qualitative de la fraction condensable a révélé que le produit le plus abondant était le lévoglucosan, un indice essentiel pour la comparaison avec d'autres travaux similaires dans la littérature. Les compositions des produits gazeux ont été exploitées pour élaborer et valider un modèle qui calcule les paramètres cinétiques des réactions de pyrolyse se produisant dans des conditions pertinentes pour les explosions de poussières. Le modèle montre un bon accord avec les données expérimentales, mais aussi des divergences avec les paramètres cinétiques déterminés par d'autres auteurs utilisant la TGA ou le lit fluidisé. Ces écarts soulignent le rôle de la technique analytique employée pour les déterminer, et l'importance de déterminer ces paramètres dans les mêmes conditions qu'une explosion de poussières et avec le même matériau (poudres). Un autre niveau d'information a été ajouté pour une meilleure compréhension de la cinétique d'une explosion de poussières organiques. Une analyse thermique du nuage de poussière a permis de soutenir les résultats expérimentaux et d'enrichir les connaissances ainsi obtenues. Comme pour les travaux précédents, les paramètres physico-chimiques des poudres organiques sélectionnées ayant été utilisés dans l'analyse thermique (densité, chaleur spécifique, conductibilité thermique, chaleur de réaction de pyrolyse), leur détermination expérimentale augmenterait la précision de l'étude globale. Par ailleurs, l'étape d'oxydation du modèle est en cours d'élaboration sur la base des résultats obtenus.

La composition des produits de pyrolyse déterminée au Chapitre 3 a été fondamentale pour développer l'étude présentée au Chapitre 4. Des tests d'explosion de mélanges hybrides ont été employés pour étudier l'influence de l'étape de pyrolyse dans une explosion de poussière organique. En particulier, le rôle des produits primaires sur les explosions de poussières de cellulose a été analysé dans la sphère de 20L, un appareil standard couramment utilisé pour déterminer les paramètres de sensibilité à l'allumage et de gravité des explosions. Du char, des goudrons et des gaz de pyrolyse ont été mélangés à de la cellulose pure, et leur sévérité d'explosion a été déterminée. L'effet des gaz de pyrolyse était direct : dans le mélange poussière-gaz de pyrolyse, la vitesse d'augmentation de la pression augmentait avec la concentration de

gaz, tandis que la surpression d'explosion montrait une augmentation moins significative. Cela suggère que les réactions d'oxydation se produisant dans la phase gazeuse et impliquant les produits de pyrolyse gazeux peuvent accélérer le processus en contournant l'étape de pyrolyse. La preuve que cette dernière était la plus lente des étapes fondamentales dans une explosion de poussière de cellulose a été fournie dans le travail. Le goudron et le charbon ont joué des rôles secondaires mais non négligeables : une augmentation légère et constante de P_m et de $(dP/dt)_m$ a été observée pour la cellulose recouverte de goudron, tandis qu'une augmentation modérée des paramètres d'explosion a été constatée en ajoutant du char au système, évolution qui pourrait être liée à une forte modification du transfert thermique radiatif. La vapeur d'eau a montré un faible impact sur les paramètres de gravité de l'explosion, comparable à l'incertitude expérimentale. Plusieurs autres combinaisons de produits de pyrolyse ont déjà été considérées pour améliorer le travail et mettre en évidence le rôle de l'hydrogène sur la sensibilité à l'allumage et la cinétique de combustion. En considérant le rendement en char, goudrons et produits gazeux typiques d'un phénomène de pyrolyse flash, une classification du rôle de chacun dans une explosion de poussière de cellulose peut être élaborée.

Le Chapitre 5 visait à évaluer la région d'opérabilité d'un procédé de pyrolyse oxydative de la biomasse réalisé dans un lit micro-fluidisé. La visualisation de la fluidisation a été convertie en une analyse quantitative grâce à un système d'enregistrement vidéo in-situ à grande vitesse. Un code Matlab a permis de déterminer l'évolution de la hauteur du lit et la fluctuation de la zone de *splashing* au cours du temps, en alimentant la biomasse. En outre, les effets de la température (400 et 500°C) et de l'atmosphère (air et azote) ont été étudiés. A 500°C, les réactions génératrices de goudrons sont plus rapides et conduisent à une agglomération plus importante, notamment pour la cellulose. Sous air, en revanche, les réactions d'oxydation consomment le liquide-intermédiaire de la pyrolyse de la cellulose, conduisant à un régime de fluidisation stable. Les régions où l'opérabilité de la pyrolyse oxydative de la biomasse ont été identifiées grâce à l'outil d'investigation in-situ développé. L'imagerie numérique a permis de compléter l'étude en caractérisant la morphologie des agglomérats, la couleur du lit de sable et la présence de charbon. Elles ont confirmé ce qui a été observé dans les vidéos à haute vitesse. Les vidéos à haute vitesse du lit fluidisé réalisé lors de l'alimentation de la biomasse sont encore riches d'informations à exploiter. Le parcours des particules de charbon dans le lit fluidisé et leur pourcentage par rapport au sable, la taille des bulles et leur évolution dans le temps, la formation de chemins préférentiels ne sont que quelques aspects qui peuvent être exploités pour approfondir l'étude. Des analyses complémentaires seront également réalisées sur le lit de sable

afin de déterminer la composition des produits responsables de l'agglomération (via un rinçage au méthanol et une analyse GC-MS-FID) et ceux adsorbés ou piégés dans les structures du char (via LDI-FTMS).

Enfin, le Chapitre 6 a utilisé les informations obtenues dans le précédent pour générer un flux stable de produits de pyrolyse de la cellulose dans un lit micro-fluidisé et pour concevoir un brûleur afin d'étudier la vitesse de flamme de ces mêmes produits gazeux. L'objectif était de découpler l'étape de pyrolyse de l'étape d'oxydation, se produisant typiquement presque simultanément dans une explosion de poussières organiques, afin de caractériser le rôle des gaz de pyrolyse dans la propagation de la flamme au sein d'un nuage de poussière. Les résultats ont été comparés à ceux obtenus dans un tube vertical semi-ouvert de propagation de flamme et dans une sphère de 20L. Quelques écarts ont été observés entre les valeurs (21 cm/s obtenus avec le tube de propagation, 26 cm/s obtenus avec la sphère 20L, par rapport aux 145 cm/s obtenus avec le brûleur MFB pour les gaz de pyrolyse), mais leur complémentarité a été exploitée pour souligner le rôle des gaz de pyrolyse dans la propagation de la flamme au sein d'un nuage de poussière. L'objectif principal envisagé est, tout d'abord, une stabilisation plus longue de la flamme, ce qui permettra d'obtenir des données plus précises. Ensuite, une mesure plus précise du débit du mélange produit de pyrolyse entrant dans la flamme permettra d'augmenter la fiabilité de la valeur de vitesse de flamme obtenue. Enfin, une étude paramétrique sera réalisée en modifiant le diamètre de la buse et le ratio air-biomasse. Ce dernier influencera le rapport d'équivalence combustible du mélange en combustion et donc la vitesse de flamme.

Cette thèse a proposé des outils expérimentaux et de modélisation pour étudier les phénomènes impliqués dans les explosions de poussières organiques. L'analyse quantitative réalisée a permis de déterminer des paramètres précieux qui peuvent servir de base à des applications de recherche ultérieures. Par exemple, les procédures présentées dans les Chapitres 2 et 3 pourraient être fusionnées pour concevoir un système de propagation verticale descendante de la flamme à partir du four G-G. Caractériser le PSD du nuage de poussière (et donc les diamètres réels des particules/agglomérats qui réagissent) et connaître le comportement des particules en fonction de la température signifierait comprendre en profondeur la réponse du nuage de poussière. Sur ces bases, ce système bien caractérisé serait une configuration intéressante pour générer des gaz de pyrolyse dans des conditions très similaires à celles d'une explosion de poussière. L'allumage ultérieur des gaz ainsi générés permettrait d'étudier la propagation de la flamme de la même phase gazeuse générée lors d'une

explosion de poussière organique. L'autre aspect principal éclairé par cette étude est la prédominance de la structure des particules sur la formule chimique. Elle démontre que les modèles prédictifs d'explosion de poussières doivent être adaptés aux spécificités de la poudre, et pas seulement à sa composition chimique. Les résultats présentés dans le Chapitre 3, enrichis des outils expérimentaux proposés dans les Chapitres 2 et 4, seront étendus aux mélanges amidon et cellulose-amidon. Les mécanismes réactionnels ainsi obtenus seront intégrés dans un autre modèle existant (Torrado et al., 2018) pour estimer la vitesse de flamme laminaire des poudres organiques et, dans un second temps, pour prédire leur vitesse maximale de montée en pression dans une sphère de 20L. Une comparaison avec le brûleur MFB permettra de valider les résultats.

En conclusion, éviter l'approche dite "boîte noire" permet d'adapter l'étude à un cas spécifique, en obtenant des informations fiables et précises sur un système chaotique, transitoire, turbulent et hétérogène tel qu'une explosion de poussières organiques. Les résultats présentés dans ce travail sont destinés à approfondir les connaissances autour des explosions de poussières. Ils sont applicables à l'industrie pour rendre les processus de gazéification, de pyrolyse et de combustion de la biomasse intrinsèquement plus sûrs en incluant une compréhension plus profonde des risques liés aux poudres de biomasse.

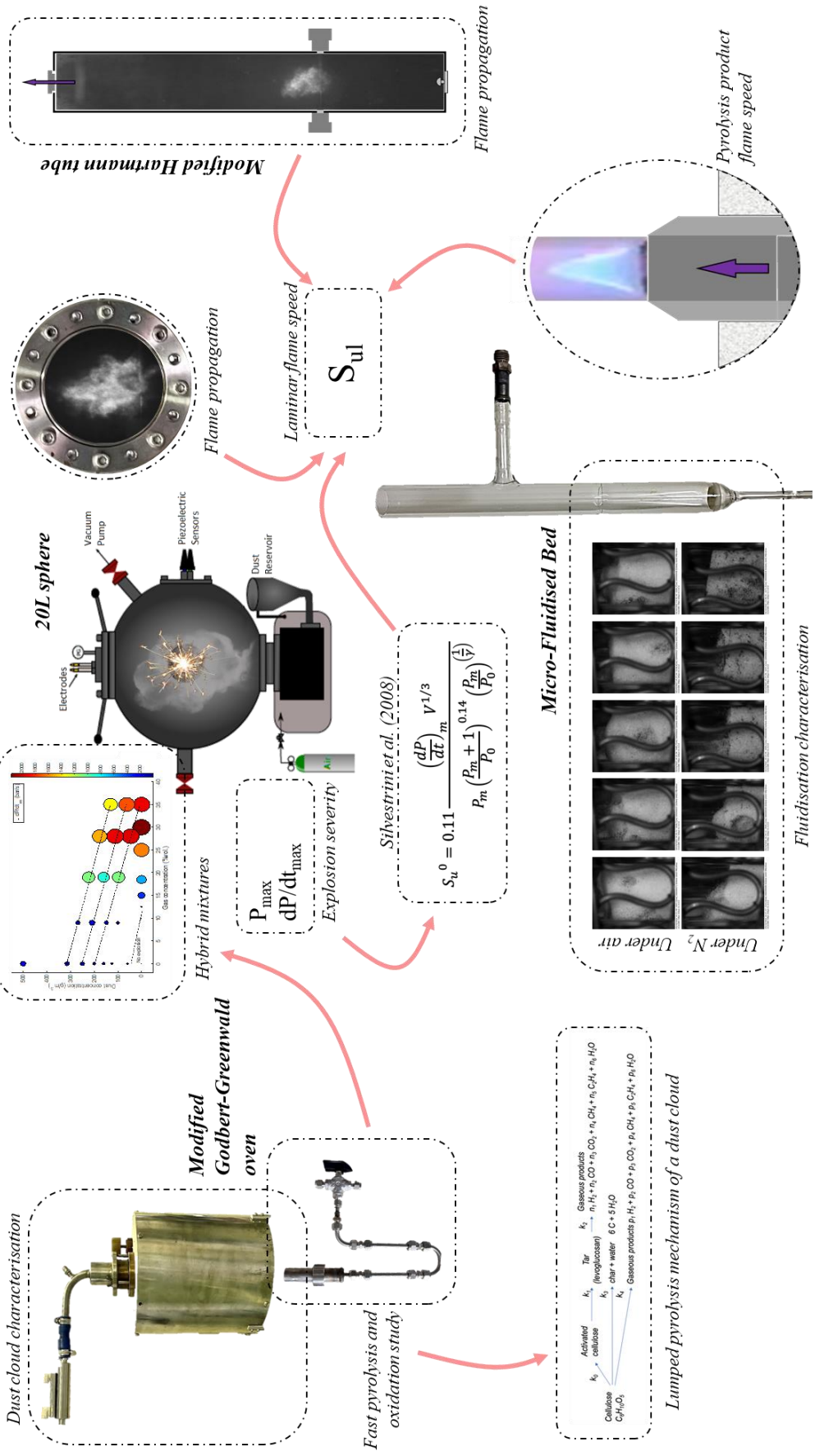

Figure 7-1 - Schematic representation of the global structure of this work

ANNEXES

Annex 1

A travel through space and time in the Godbert-Greenwald furnace: the evolution of a dust cloud particle size distribution

Matteo Pietraccini [1], Pierre-Alexandre Glaude [1], Anthony Dufour [1], Luca Marmo [2], Enrico Danzi [2], Olivier Dufaud[1,]*

** Corresponding author: olivier.dufaud@univ-lorraine.fr*

[1] Université de Lorraine, CNRS, LRGP, F-54000 Nancy, France

[2] Politecnico di Torino, Dipartimento di Scienza Applicata e Tecnologia, Torino, Italy

Supporting information

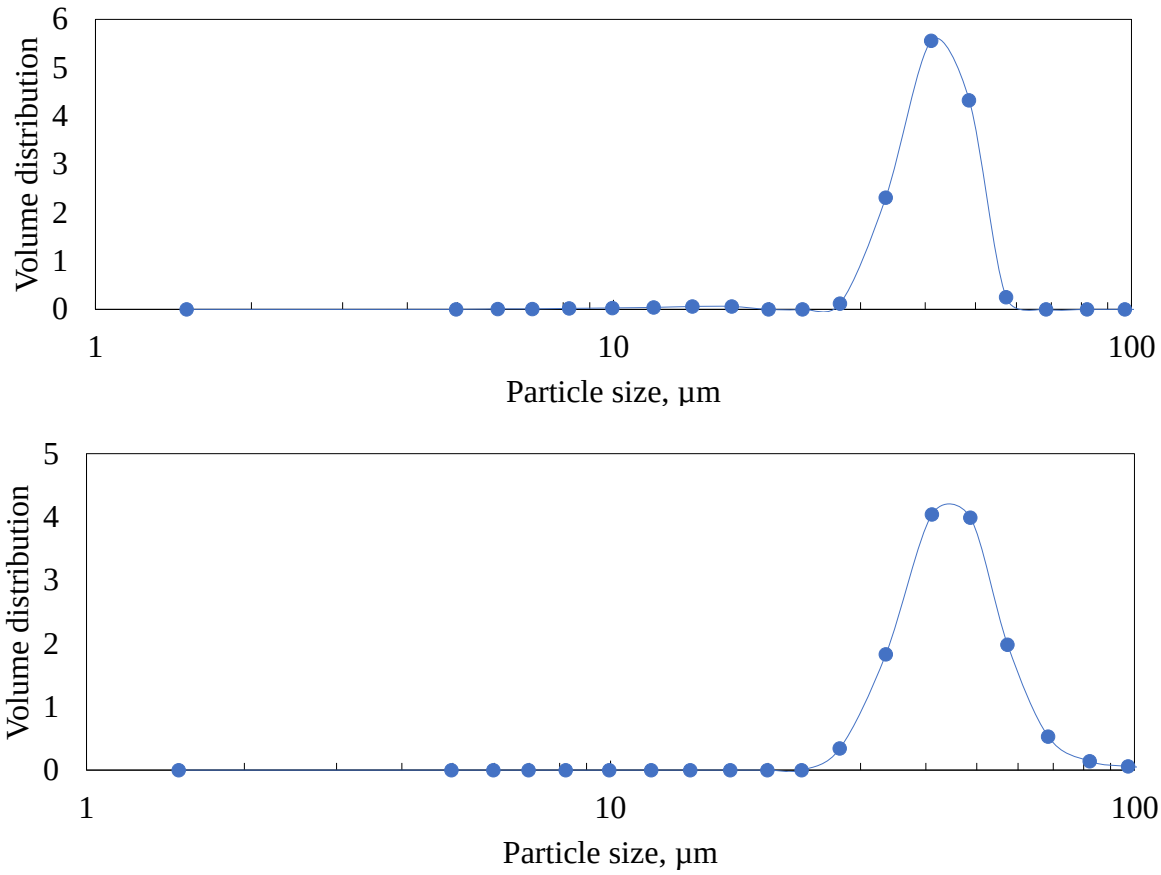

Figure S 1 - Reference dispersion measure with glass beads, performed at 0.5 barg in Position 1 and 3a

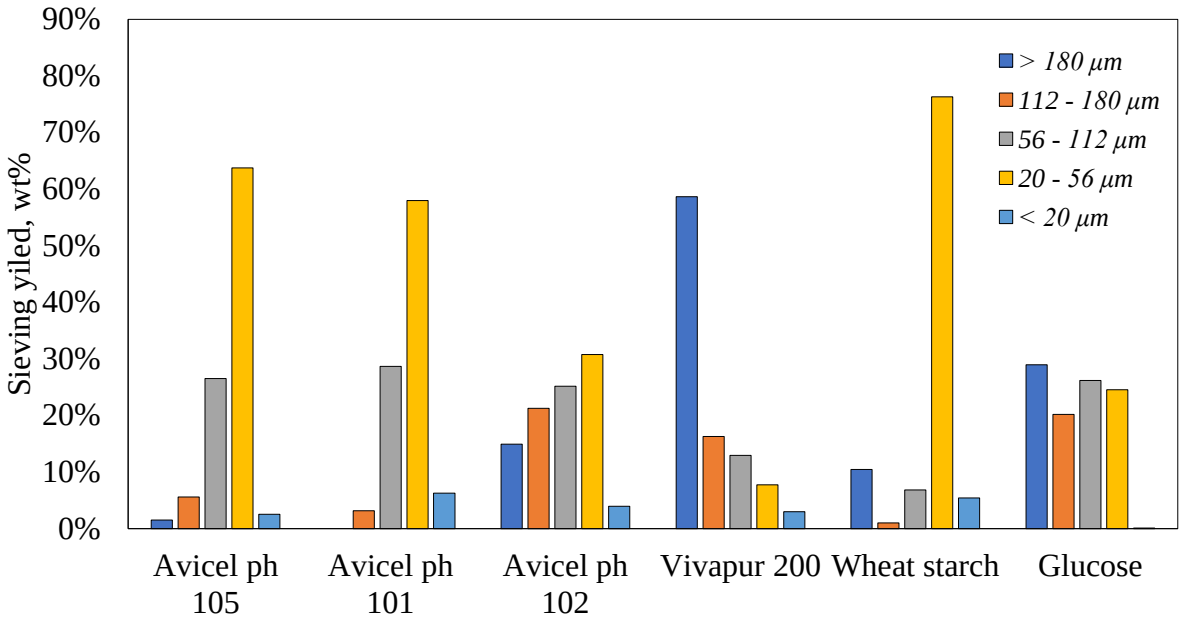

Figure S 2 - Sieving yield of the sieved powder samples.

Table S 1 - PSD of the fractions obtained after the sieving test

Avicel ph 101

Fraction, µm	D10, µm	D50, µm	D90, µm
< 20 µm	20,8	45,4	86,4
20 - 56 µm	23,0	50,8	98,9
56 - 112 µm	61,2	102,6	163,2
112 - 180 µm	38,6	89,9	173,6
> 180 µm	-	-	-

Wheat starch

Fraction, µm	D10, µm	D50, µm	D90, µm
< 20 µm	10,6	18,8	32,5
20 - 56 µm	11,7	19,7	32,4
56 - 112 µm	15,4	64,0	125,0
112 - 180 µm	15,1	106,0	200,0
> 180 µm	11,6	20,2	34,4

Glucose

Fraction, µm	D10, µm	D50, µm	D90, µm
< 20 µm	3,4	19,1	50,3
20 - 56 µm	3,5	21,1	51,8
56 - 112 µm	6,5	59,5	117,0
112 - 180 µm	4,7	43,1	168,0
> 180 µm	5,5	68,3	270,0

Avicel ph 102

Fraction, µm	D10, µm	D50, µm	D90, µm
< 20 µm	20,9	47,3	97,6
20 - 56 µm	28,2	57,0	110,8
56 - 112 µm	62,2	104,4	165,6
112 - 180 µm	47,2	92,9	164,1
> 180 µm	53,0	118,6	193,0

Avicel ph 105

Fraction, µm	D10, µm	D50, µm	D90, µm
< 20 µm	71,7	189,8	278,4
20 - 56 µm	10,6	29,0	60,6
56 - 112 µm	12,3	27,9	57,7
112 - 180 µm	12,0	30,5	66,6
> 180 µm	11,1	28,2	57,9

Vivapur 200

Fraction, µm	D10, µm	D50, µm	D90, µm
< 20 µm	32,7	189,8	278,4
20 - 56 µm	30,8	29,0	60,6
56 - 112 µm	63,9	27,9	57,7
112 - 180 µm	84,9	30,5	66,6
> 180 µm	113,9	28,2	57,9

Annex 2

Study of flash pyrolysis and combustion of biomass powders using the Godbert-Greenwald furnace: an essential step to better understand organic dust explosions

Matteo Pietraccini[1], Peter Badu[1], Theo Tait[2], Pierre-Alexandre Glaude[1], Anthony Dufour[1], Olivier Dufaud[1,*]

** Corresponding author: olivier.dufaud@univ-lorraine.fr*

[1] Université de Lorraine, CNRS, LRGP, F-54000 Nancy, France

[2] Department of Chemical & Process Engineering, University of Strathclyde, G11XQ Glasgow, Scotland, United-Kingdom

Supporting information

1. Proximate analysis

The temperature profile reported in Figure S 1 was used to determine the Volatile Matter (VM) and the Fixed Carbon (FC) of the selected powders. The VM was calculated by subtracting the mass of the sample at 40 min (when the curve reached a plateau after the dehydration step, at 105°C) and 100 min (when the flow gas was switched to air, at 900°C), and normalizing by the mass at 30-40 min. By knowing the Moisture Content (MC), the VM and the ash content, it was possible to calculate the FC with the following formula:

$$FC = 100 - MC - VM - ash$$

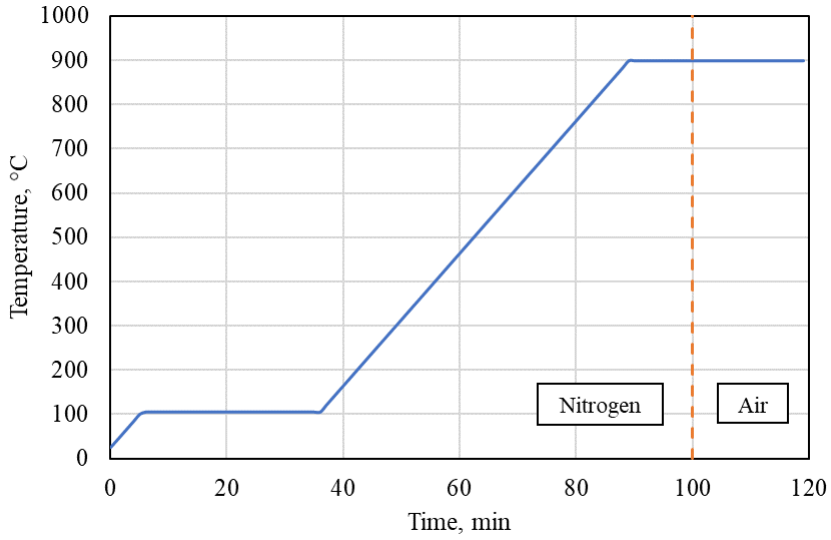

Figure S 3 - Temperature profile used during the thermo-gravimetric analysis, to estimate the Volatile Matter (VM) and the Fixed Carbon (FC).

2. In- situ PSD analysis

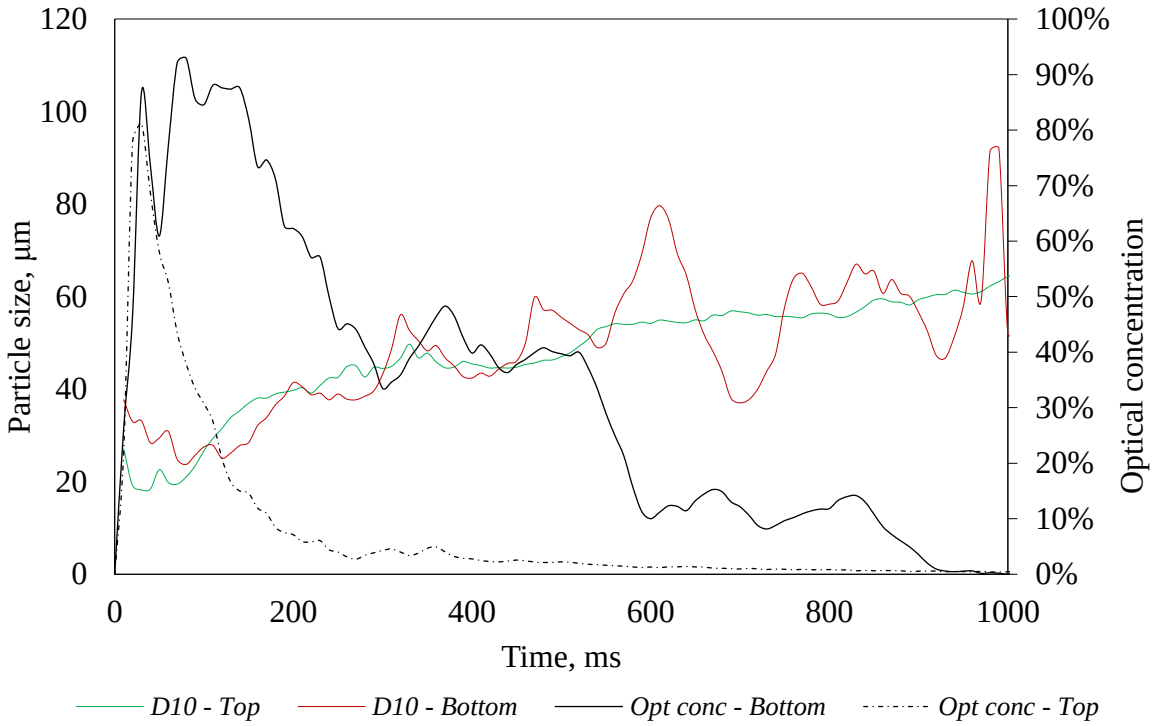

Figure S 4 - D10 characteristic diameter and optical concentration measured at the top and the bottom of the heated chamber.

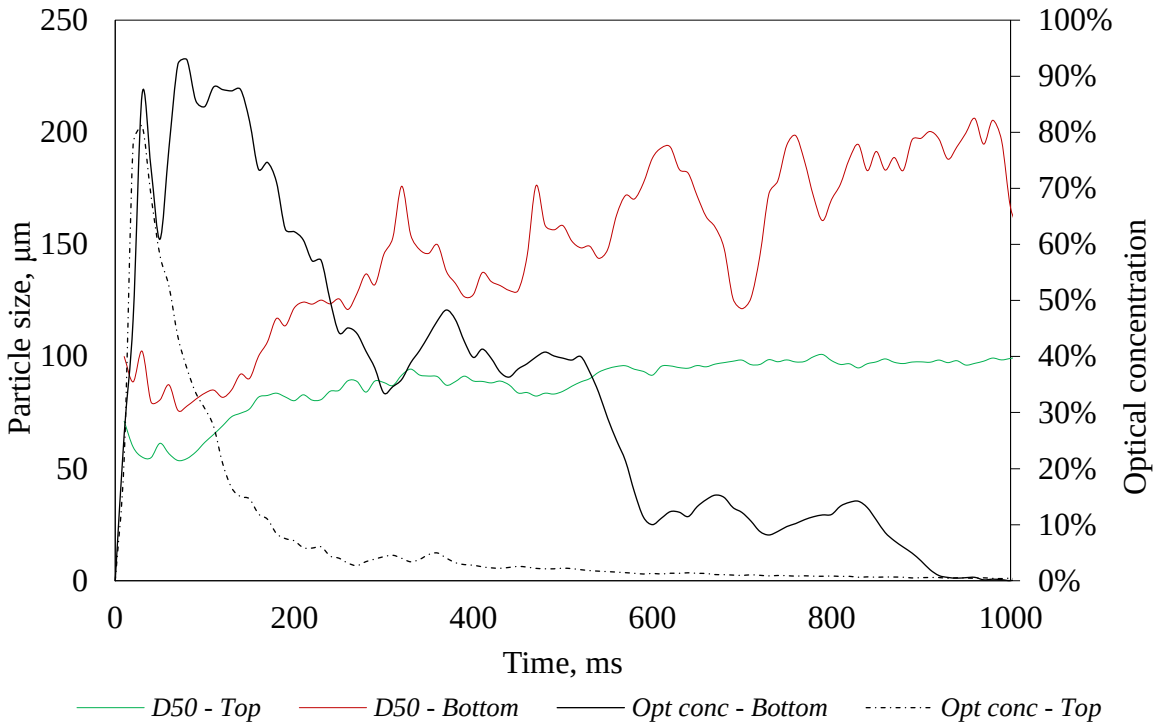

Figure S 5 - D50 characteristic diameter and optical concentration measured at the top and the bottom of the heated chamber.

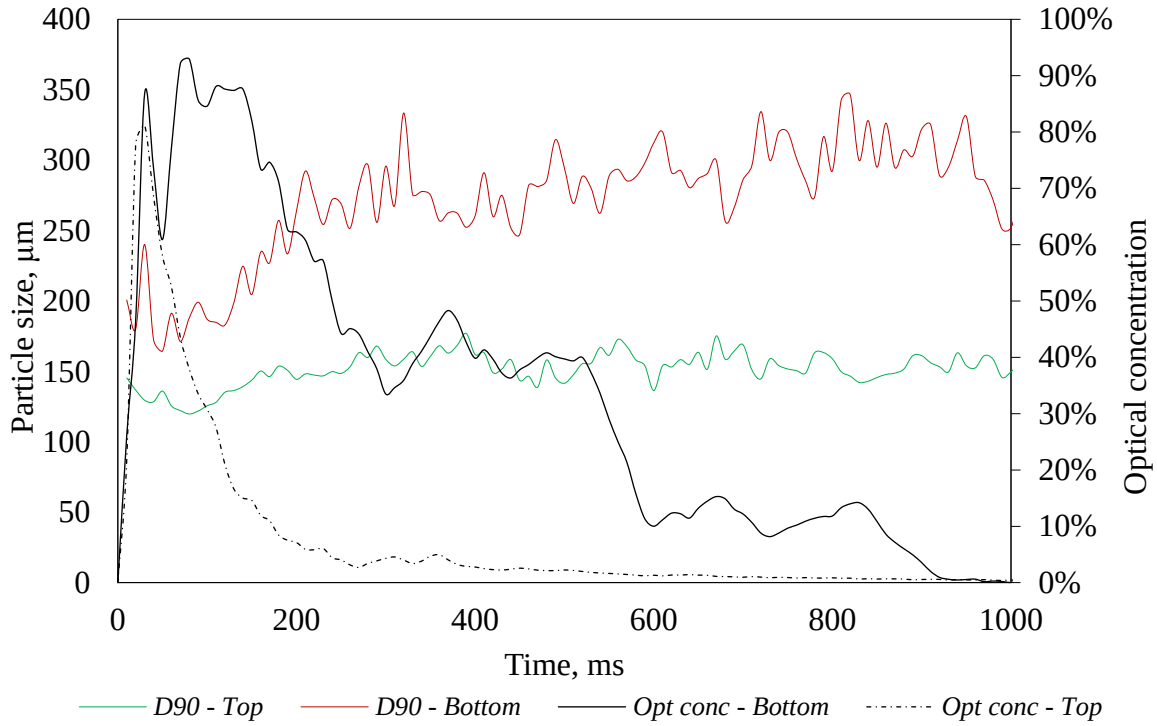

Figure S 6 - D90 characteristic diameter and optical concentration measured at the top and the bottom of the heated chamber.

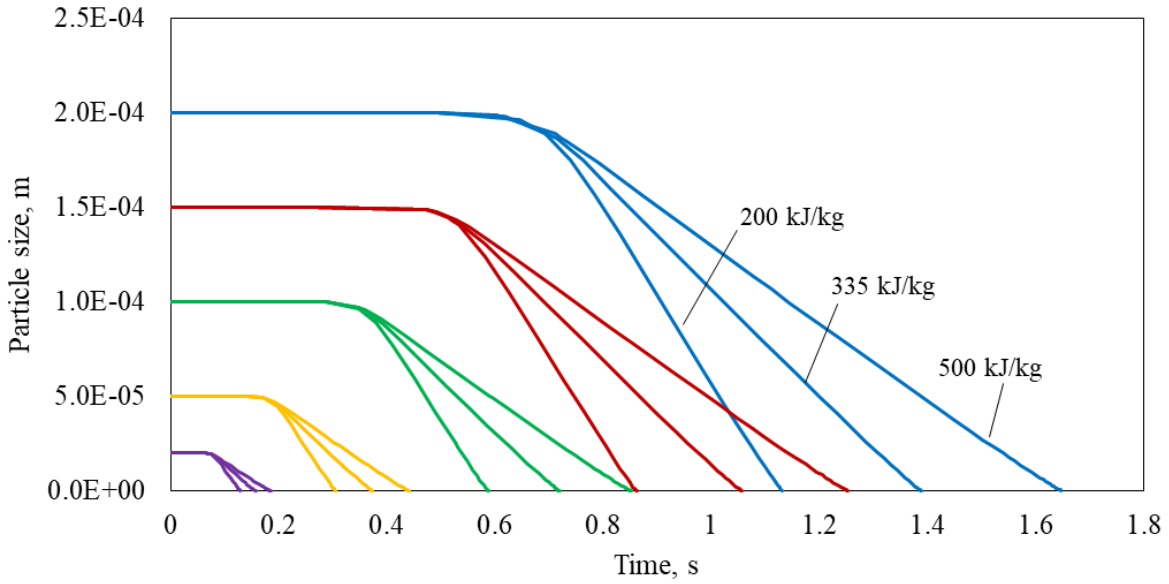

Figure S 7 - Study of the influence of the pyrolysis reaction enthalpy on the particle size profile over time, for five different initial particle sizes at 973K.

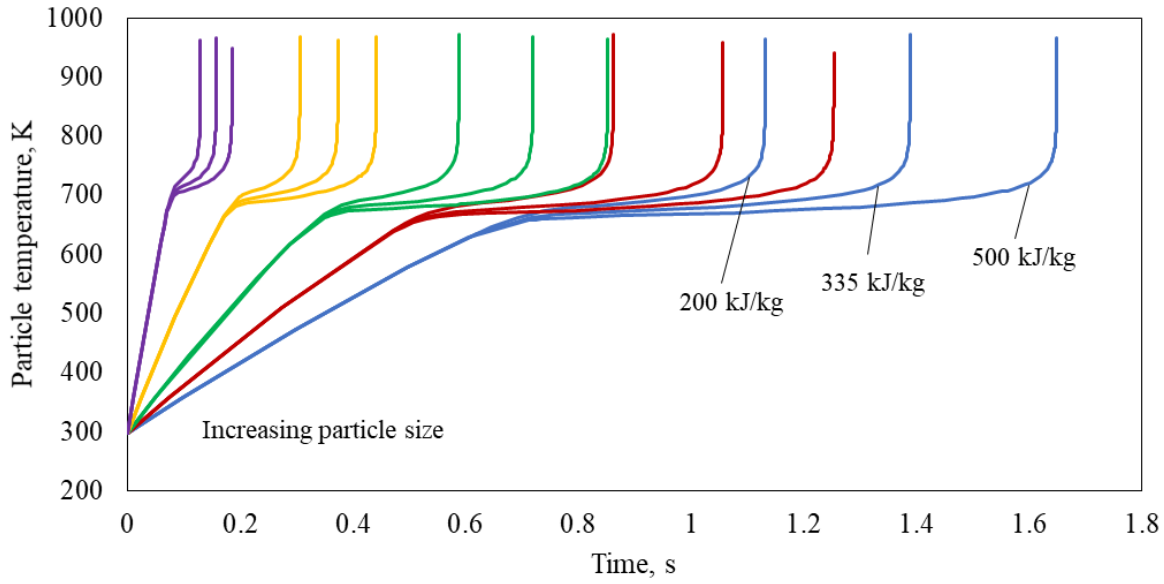

Figure S 8 - Study of the influence of the pyrolysis reaction enthalpy on the particle temperature profile over time, for five different initial particle sizes at 973 K.

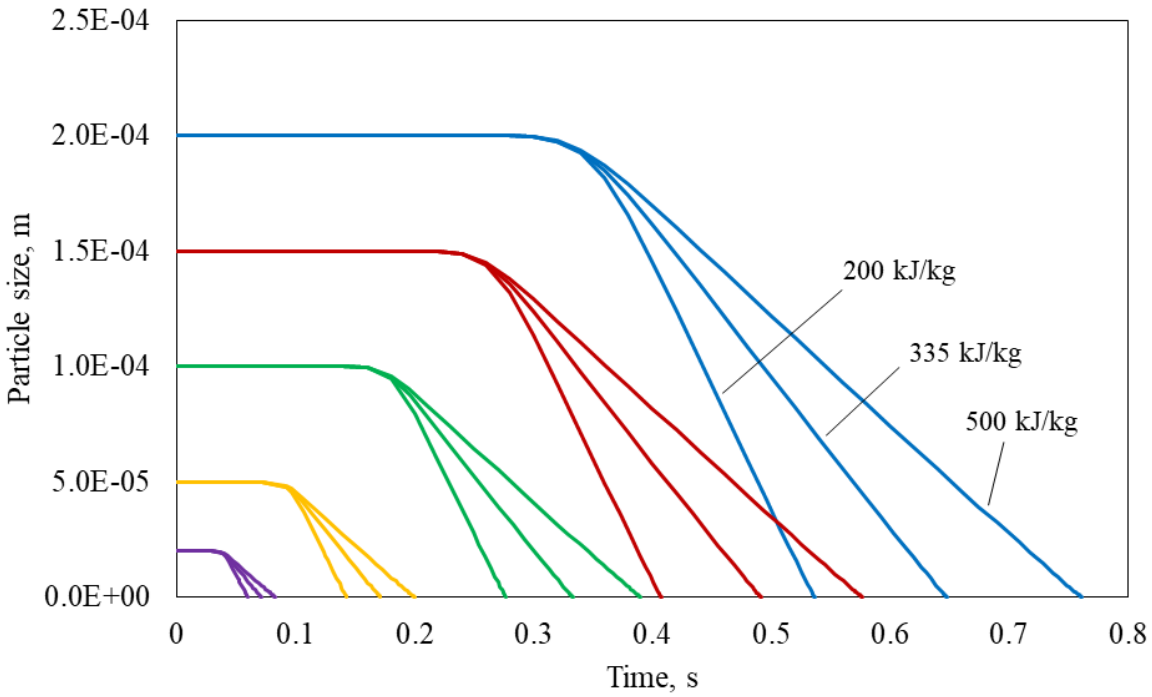

Figure S 9 - Study of the influence of the pyrolysis reaction enthalpy on the particle size profile over time, for five different initial particle sizes at 1173K

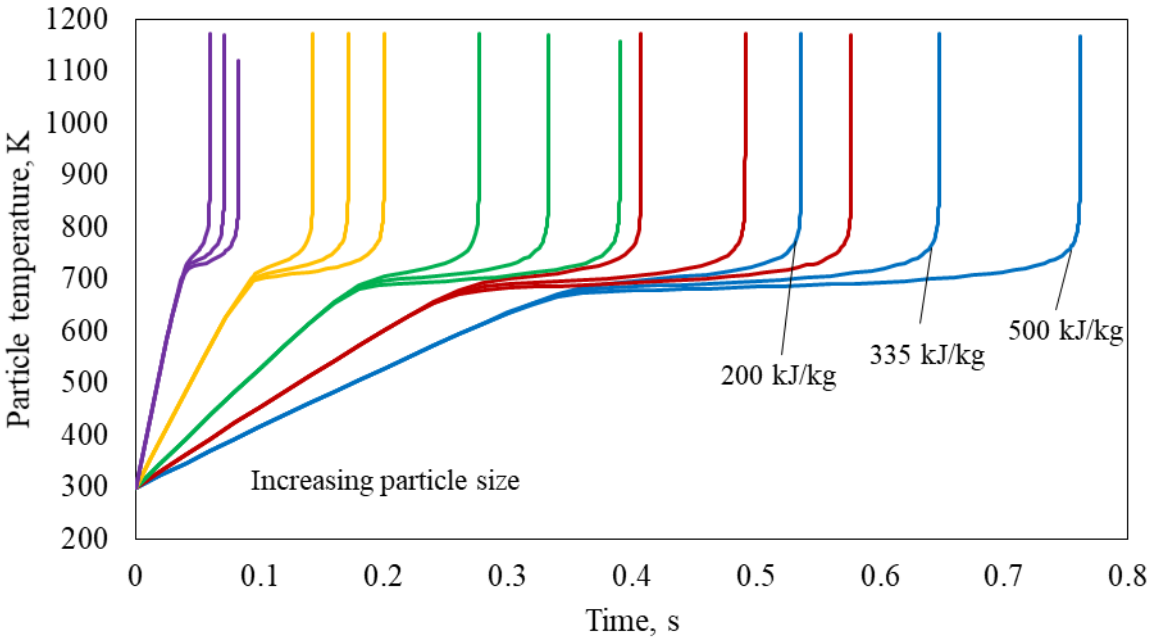

Figure S 10 - Study of the influence of the pyrolysis reaction enthalpy on the particle temperature profile over time, for five different initial particle sizes at 1173 K.

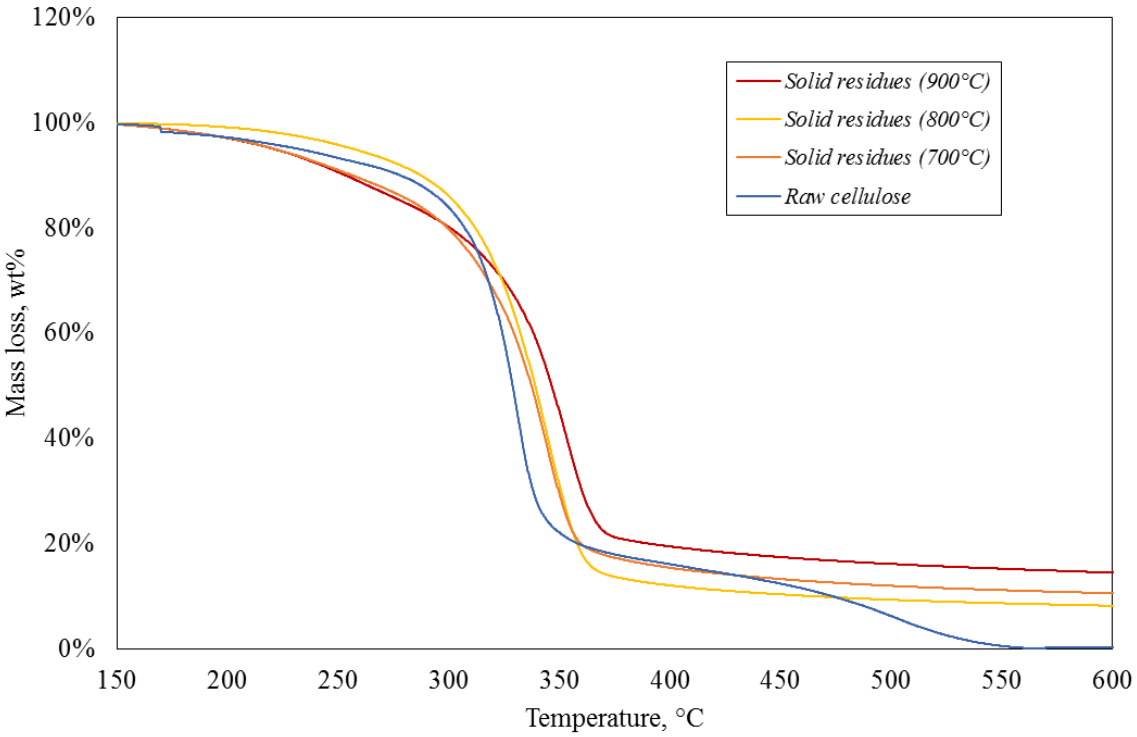

Figure S 11 - TGA curves for raw cellulose and for the three solid residues of cellulose pyrolysis tests, sampled in the modified GG furnace at 700, 800 and 900°C.

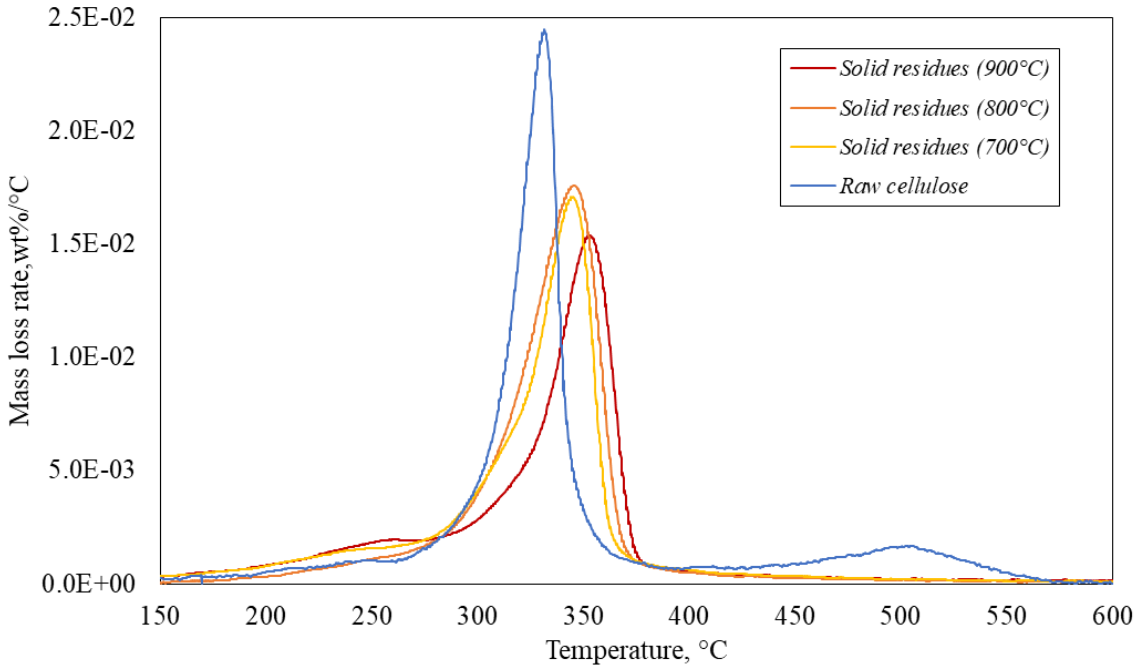

Figure S 12 - dTG curves for raw cellulose and for the three solid residues of cellulose pyrolysis tests, sampled in the modified GG furnace at 700, 800 and 900°C.

Annex 3

Making hybrid mixture explosions a common case

Matteo Pietraccini [a], Pierre-Alexandre Glaude [a], Anthony Dufour [a] & Olivier Dufaud [a]

[a] Université de Lorraine, CNRS, LRGP, F-54000 Nancy, France

E-mail: olivier.dufaud@univ-lorraine.fr

Supporting information

1. Modified Godbert-Greenwald furnace

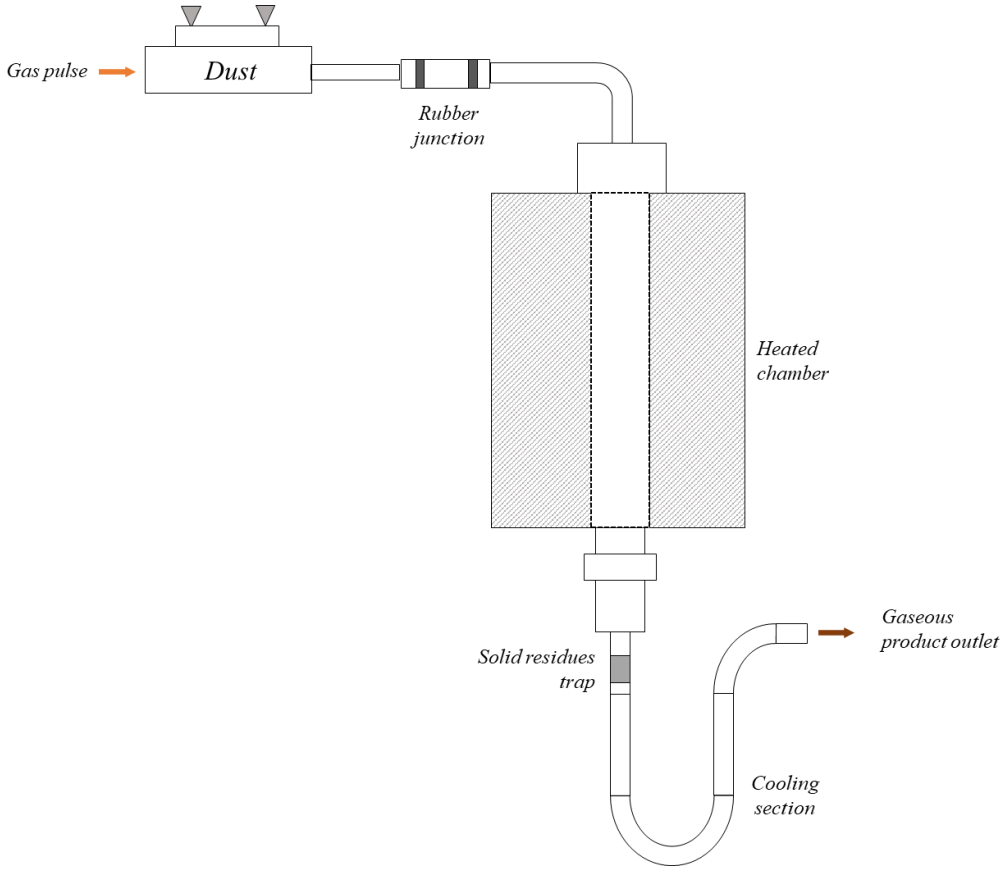

Figure S 13 - The scheme of the modified Godbert-Greenwald furnace used to collect the pyrolysis gases

2. Tar synthesis

2.1 Micro-fluidised bed reactor

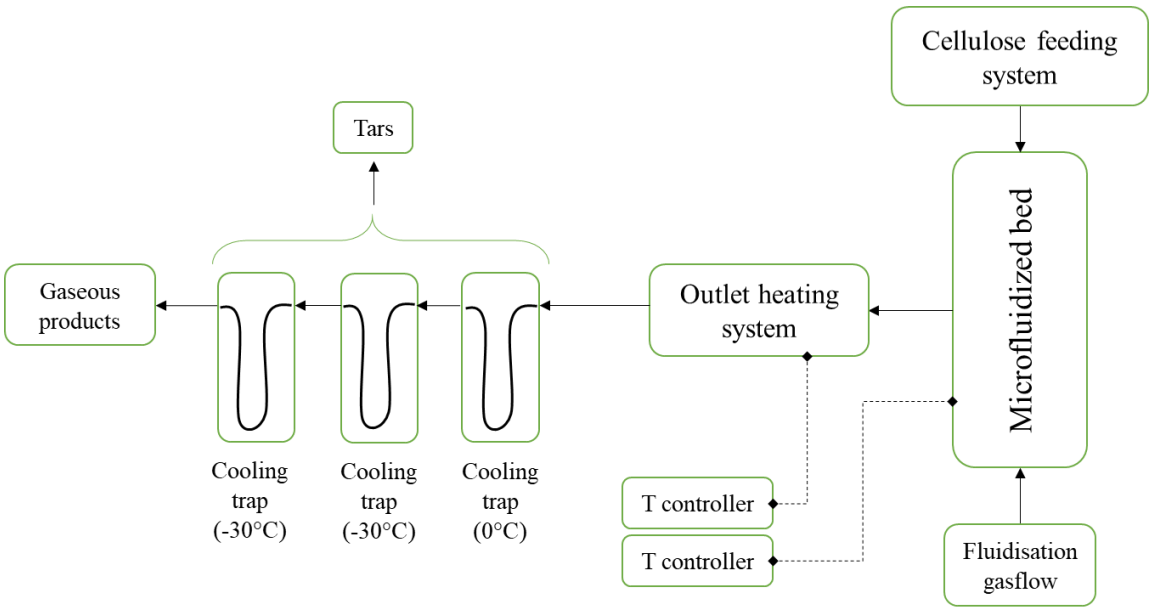

Figure S 14 - Schematic representation of the micro-fluidised bed reactor used to synthetise the tars, subsequently used for tar-coating the cellulose powder

3. Cellulose tar-coating

3.1 Tar analysis

The GC-MS-FID spectrum allowed to identify the main components of the tars synthesised in the micro-fluidised bed**.** Table S 2 resumes its composition (calculated neglecting the solvent and the traces of other compounds).

Table S 2 - Composition of the condensable product fraction used for tar-coating the cellulose powder

Species	**Formula**	**Molar fraction, mol%**
Hydroxyacetaldehyde	$C_2H_4O_2$	2.42%
Dihydroxyacetone	$C_3H_6O_3$	1.40%
2-Furanone	$C_2H_4O_2$	1.44%
Furfural	$C_5H_4O_2$	0.66%
(2-Hydroxy-1-methoxy)ethylfuran	$C_6H_6O_3$	3.37%
Levoglucosenone	$C_6H_6O_3$	3.18%

1,4:3,6-Dianhydro-alfa-d-glucopyranose	$C_6H_8O_4$	2.20%
Trans-1,2-Cyclohexanediol	$C_6H_{12}O_2$	1.32%
1-tetradecene	$C_{14}H_{28}$	0.05%
Levoglucosan	$C_6H_{10}O_5$	78.95%
1,6-Anhydro-alfa-d-galactofuranose	$C_6H_{10}O_6$	5.01%

3.2 Cellulose coating procedure

The tar collected in the bubbling condenser, dissolved in water, was dehydrated in a lyophilizer for about 48h. The sticky and highly viscous material thus obtained was first weighted and then dissolved in approximately 22 mL of ethanol (the lowest volume possible to avoid a subsequent long drying step) to allow a homogeneous dispersion in the powder. Four coated cellulose samples were prepared to simulate the progress of the pyrolysis reaction in a dust explosion. A tar yield of 40wt% was considered to determine the mass of cellulose to add to the tar-ethanol solution (Piskorz et al. 2000b). The pyrolysis product yields considered in the calculations were extracted from Piskorz (Piskorz et al. 2000b). They are reported in Table S 3. The tar-cellulose mixes were dried for 12h at 35°C and 30%RH to remove the ethanol, then they were slightly mixed to be homogenised. Results are reported in

Table S 4 and Figure S 14 shows the tar-coated cellulose samples.

Table S 3 - Cellulose pyrolysis product yields

	Yield, wt%	**Yield, wt%**
Gas	11%	13%
Water vapour	8%	9%
Tar	36%	40%
Char	34%	38%
	From Piskorz et al. 2000	100% basis

Table S 4 - Coated cellulose mixes used in the hybrid mixtures explosion tests, and their tar concentration

Mix	**Tar solution, mL**	**Tar mass, g**	**Cellulose, g**	**Tar concentration, %wt**
A	0.00	0.00	10.00	0.0%
B	2.20	0.37	9.07	4.1%
C	4.40	0.75	8.14	9.2%
D	6.60	1.12	7.20	15.6%
E	8.80	1.50	6.27	23.9%

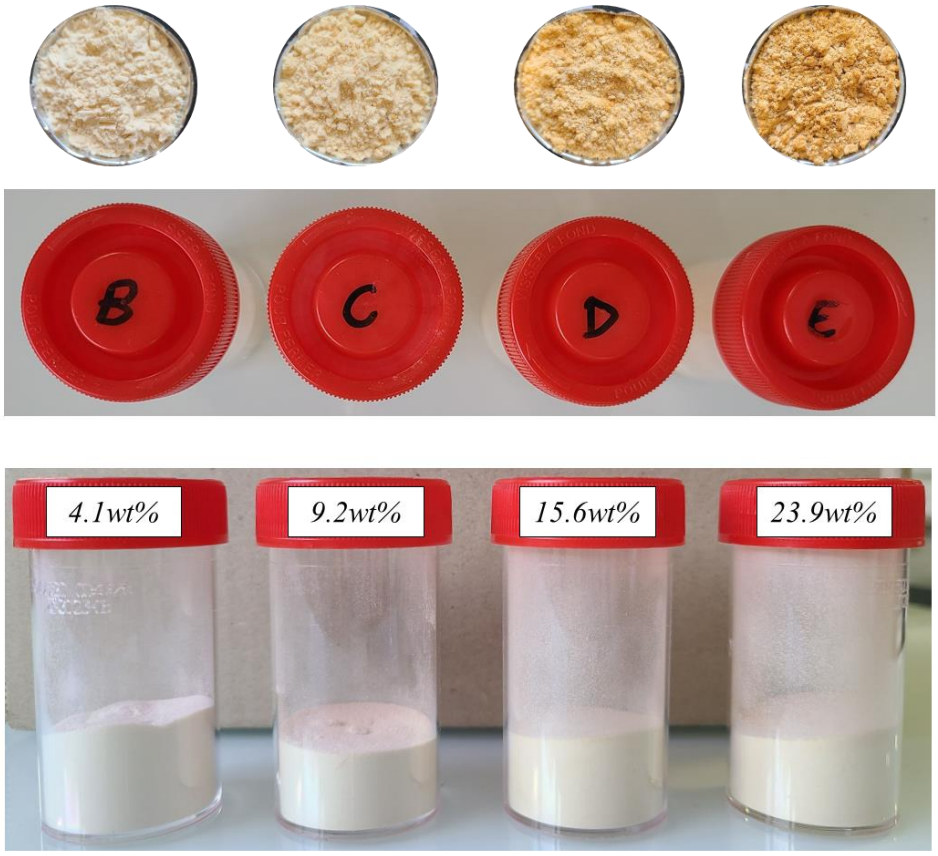

Figure S 15 - Tar-coated cellulose samples: after the drying (top) and after mixing (bottom)

4. Time scale analysis

4.1 Particle heating step

The particle temperature profile was calculated as a function of the time, using the following equation:

$$\frac{1}{6}\pi {d_p}^3 \rho_s c_{ps} \frac{dT_p}{dt} = F\sigma\varepsilon\pi {d_p}^2 \left(T_{Zr}^4 - T_p^4\right)$$

The time scale related to this step was estimated by considering the time necessary for the particle to attain the pyrolysis onset temperature (approximately 583K), determined during the thermogravimetric analysis. Since the particle temperature profile strongly depends on the particle diameter, this last was varied from 20 to 200 µm to establish a range of values. Table S 5 and S 5 report the parameters used, Figure S 16 the results.

Table S 5 - List of parameters used to calculate the particle temperature profile

Parameter	Symbol	Value	Source
Particle diameter, µm	d_p	20-50-100-150-200	-
Density, kg.m^{-3}	ρ_s	700	Piskorz et al. 2000b
Specific heat, J.kg^{-1}.K^{-1}	c_{ps}	1757	Piskorz et al. 2000b
View factor	F	1	
Stefan-Boltzmann, W.m^{-2}.K^{-4}	Σ	$5.67 \cdot 10^{-8}$	-
Zirconium flame temperature, K	T_{Zr}	4930	Doyle et al. 1958

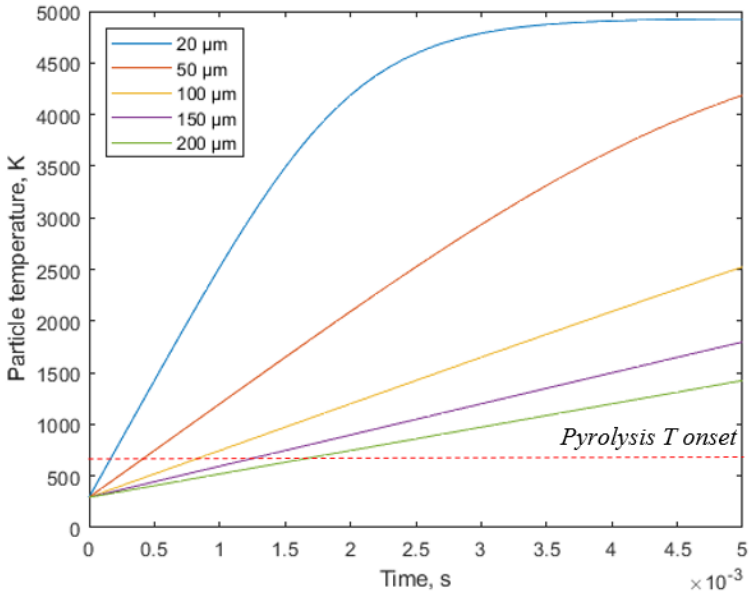

Figure S 16 - Cellulose particle temperature profile considering pyrotechnical igniters as ignition source, for different particle sizes

Table S 6 - Results of the particle heating time scale study

Particle size, µm	Characteristic time, ms
20	0.13
50	0.32
100	0.64
150	1.0
200	1.3

4.2 Pyrolysis step

The kinetic constants of each mechanism (all reported in Table S 7) were used to calculate a time scale associated with each reaction. Since the pyrolysis step is part of a global dust explosion phenomenon, only the reactions involving the volatilisation of a solid phase were considered. Cellulose activation and secondary reactions in the gaseous phase were thus excluded from this study. An average characteristic time was finally calculated considering parallel and consecutive conformations of the selected systems. Moreover, cellulose pyrolysis thermally stabilises around 450-500°C (Piskorz et al. 2000b) due to the endothermicity of the process. A temperature range between 673 and 873K was then considered to determine a range for the final results.

Table S 7 - Cellulose pyrolysis mechanisms used to calculate the characteristic time scales associated with this step

Ranzi (Ranzi et al. 2017)

	Reaction	**A, s^{-1}**	**Ea, $J.mol^{-1}$**
1	CELL → CELLA	1.50E+14	197000
2	CELLA → 0.4 HAA + 0.05 GLYOX + 0.15 CH3CHO + 0.25 HMFU + 0.35 ALD3 + 0.15 CH3OH + 0.3 CH2O + 0.61 CO + 0.36 CO2 + 0.05 H2 + 0.93 H2O + 0.02 HCOOH + 0.05 C3H6O2 + 0.05 G{CH4}	2.50E+06	80000
3	CELLA → LVG	3.3*T	42000
4	CELL → 5H2O + 6 CHAR	6.00E+07	130000
5	G{CH4} → CH4	5.00E+12	300000

Piskorz (Piskorz et al. 2000b)

	Reaction	**A, s^{-1}**	**Ea, $J.mol^{-1}$**
1	Cellulose → Pyrolysis products	1.90E+16	197300

Miller (Miller and Bellan 1996)

	Reaction	**A, s^{-1}**	**Ea, $J.mol^{-1}$**
1	From active cellulose to char + gases	1.3E+10	151000
2	From active cellulose to tar	3.28E+14	197000
3	From tar to gaseous products	4280000	108000

Lédé (Lédé 2012)

Reaction	**A, s^{-1}**	**Ea, $J.mol^{-1}$**

1	Cellulose → Pyrolysis products	2.83E+19	242000

Piskorz (Piskorz et al. 1988a)			
Reaction		**A, s^{-1}**	**Ea, $J.mol^{-1}$**
1	From cellulose to active cellulose	1.7E+21	242788
2	From active cellulose to volatiles	1.9E+16	197997.8
3	From active cellulose to char and gases	7.9E+11	150696
4	From tar and gases to gases	3.40E+08	104650

Table S 8 - Particle heating time scale ranges extracted from the profiles presented

Source		**Time scale, ms**
Ranzi et al. (2017)	min	20
	max	356
Piskorz et al. (2000)	min	0.03
	max	108
Miller et al. (1996)	min	1.86
	max	5385
Lédé et al. (2015)	min	0.01
	max	215
Piskorz et al. (1986)	min	0.04
	max	81

4.3 Oxidation step

The characteristic time scale associated with the oxidation step was divided into two parts. The first one considered the gaseous species involved (CO, CO_2, H_2, CH_4, H_2O and O_2), while the second one aimed to estimate the characteristic time of the oxidation of levoglucosan (LVG), the main condensable product of cellulose pyrolysis. Data were taken from Wang (Wang et al. 2012) for the first part, and from Peterson and Brown (Peterson and Brown 2021) for the second one. The reactions considered are reported in Table S 2. The temperature range considered was 1000-2000K. Around 600K, the pyrolysis onset temperature for cellulose, the LVG oxidation reactions are slow and likely do not occur in a cellulose combustion phenomenon. On the other hand, reactions involving permanent gases occur at these temperatures and take over the oxidation step. As the temperature increases and reaches approximately 1000K, the LVG oxidation characteristic time decreases, allowing the LVG to react

during an organic dust explosion. 2000K is approximately the adiabatic flame temperature of cellulose (Salgansky et al. 2016), representing the temperature's upper limit. 2000K is approximately the adiabatic flame temperature of cellulose [245], representing the temperature's upper limit.

Table S 9 - Kinetic parameters considered in the oxidation step characteristic time analysis

Reaction	**A, s^{-1}**	**$E.R^{-1}$, K**
$CH_4 + 0.5\ O_2 = CO + 2\ H_2$	4.40E+11	15095
$CH_4 + H_2O = CO + 3H_2$	3.00E+08	15095
$CH_4 + 1.5\ O_2 = CO + 2\ H_2O$	5.03E+11	24056
$CO + H_2O = CO_2 + H_2$	2.75E+09	10065
$CO_2 + H_2 = CO + H_2O$	6.71E+10	13688
$CO + 0.5\ O_2 = CO_2$	2.24E+12	20484
$CO_2 = CO + 0.5\ O_2$	5.00E+08	20484
$CO + 0.5\ O_2 = CO_2$	2.24E+06	5032
$CO_2 = CO + 0.5\ O_2$	1.10E+13	39452
$H_2 + 0.5\ O_2 = H_2O$	5.69E+11	17609
$H_2O = H_2 + 0.5\ O_2$	2.51E+14	47859
$H_2 + 0.5\ O_2 = H_2O$	7.91E+10	17609
$H_2O = H_2 + 0.5\ O_2$	3.48E+13	47907
Levoglucosan oxidation	1.06E+05	74000

4.4 Flame propagation with no dust

The flame propagation in homogenous mixtures of air, mix A, and mix B was studied by employing Chemkin. Table S 10 resumes the main information set for the simulations. Figure S 17 reports the characteristic time relative to this step, calculated by considering the radius of the 20L vessel as the path of the flame front during its propagation. (Santandrea et al. 2020)

Table S 10 - Principal parameters used in the simulations on Chemkin

Parameter	Value
Initial temperature, K	298
Pressure, torr	760
Central temperature, K	1200
Max number of points	3000
Min number of points	12
Initial flame thickness, mm	3
Initial mass flux through the flame front, $g.cm^{-2}.s^{-1}$	0.035

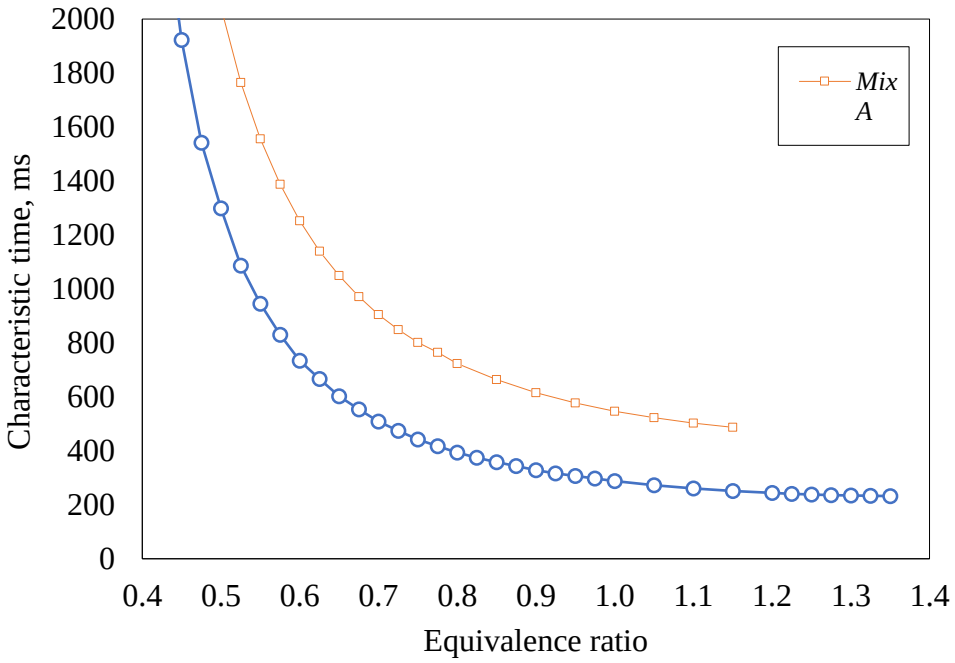

Figure S 17 - Flame propagation characteristic time, in a hypothetical mixture with no dust

4.5 Flame propagation with dust

Table S 11 - Calculation of the unstretched burning velocity via the Silvestrini relationship (Silvestrini et al. 2008) and adopting the modifications proposed by Santandrea et al. 2020

Conc, $g.m^{-3}$	P_m, bar	$(dP/dt)_m$, $bar.s^{-1}$	Unstretched burning velocity, $cm.s^{-1}$
0	0	0	0.00
125	3	36	14.02
160	3.7	60	15.83
250	5.2	134	18.81
500	6.4	220	21.02
750	7.1	265	20.89
1000	6.4	263	25.13
1250	6.2	250	25.33
1500	6	281	30.26
1750	4.8	205	33.39

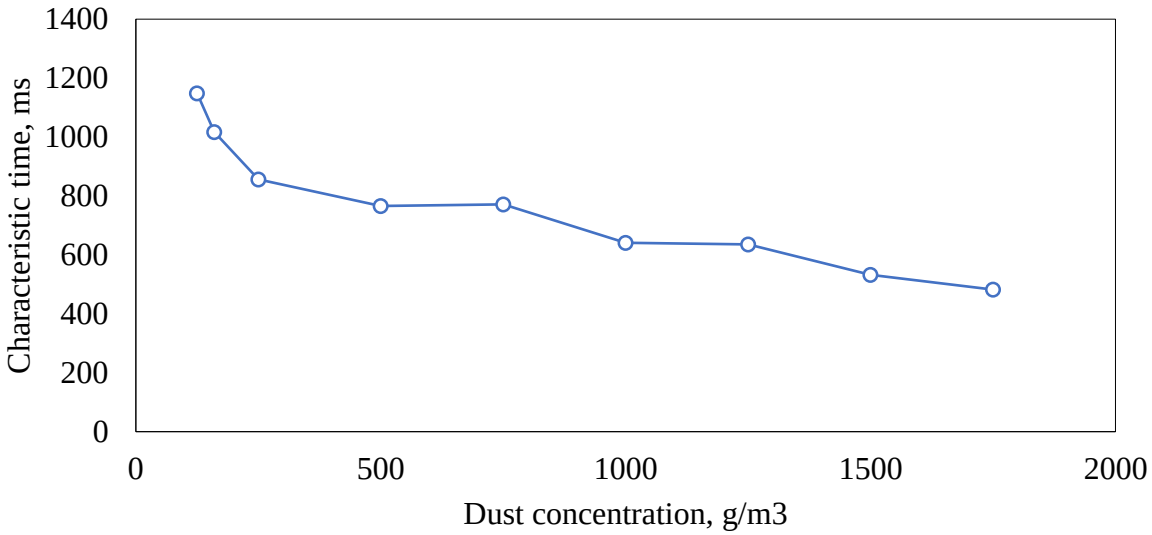

Figure S 18 - Flame propagation characteristic time within the dust cloud, calculated with the Silvestrini relationship (Silvestrini et al. 2008)

Annex 4

Effect of air on the operability of biomass pyrolysis in a micro-fluidized bed

Matteo Pietraccini [1], Olivier Dufaud [1], Pierre-Alexandre Glaude [1], Anthony Dufour [1,*]

[1] *Université de Lorraine, CNRS, LRGP, F-54000 Nancy, France*

* *corresponding author: anthony.dufour@univ-lorraine.fr*

Supporting information

1. Geldart classification

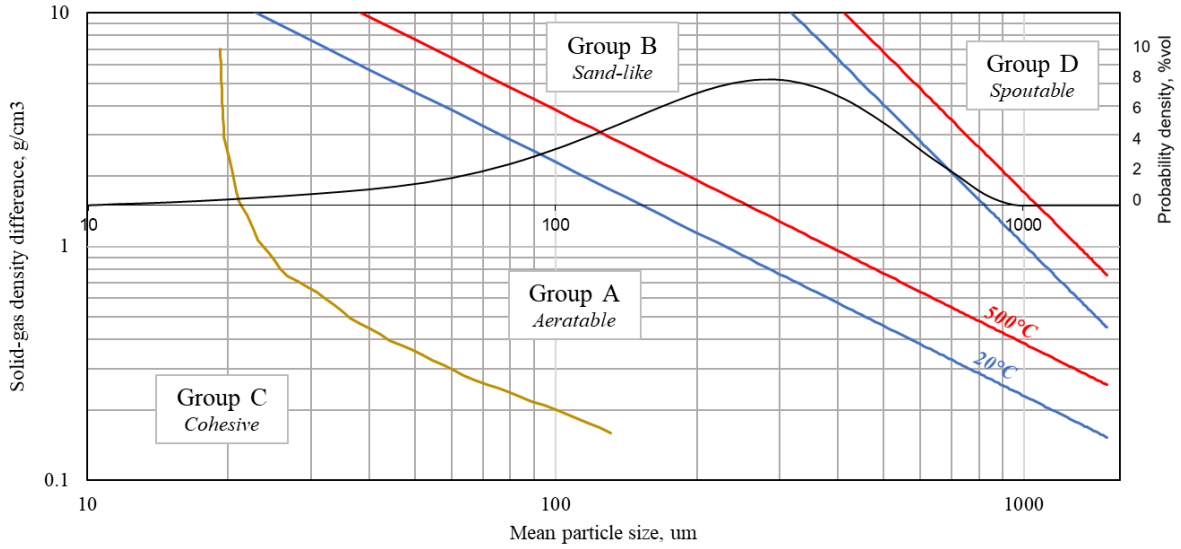

Figure S 19 - Geldart classification applied to the Fontainebleau sand used in the micro-fluidised bed reactor

2. Reactor temperature profiles

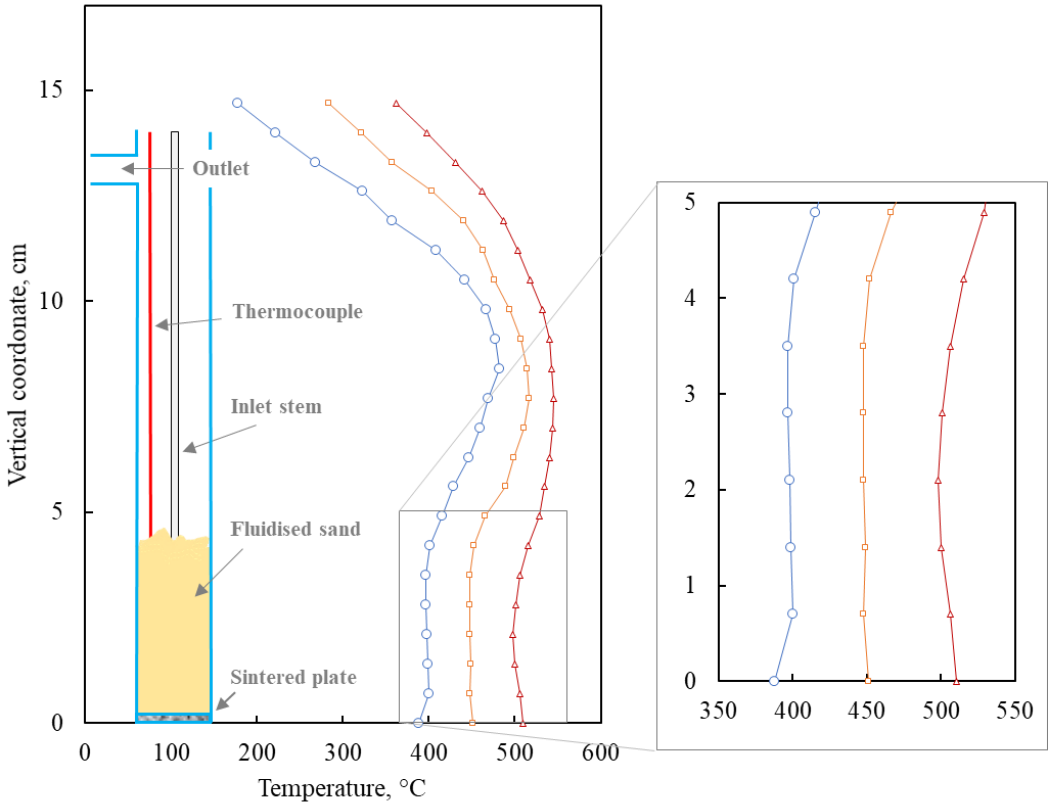

Figure S 20 – Vertical temperature profile along the reactor

3. Temperature profiles

The sand temperature during the cellulose and oak wood tests was measured and recorded over time. In Figure S 21 and Figure S 22, t = 0 corresponds to the starting of the feeding, while the purple points represent the test endpoint.

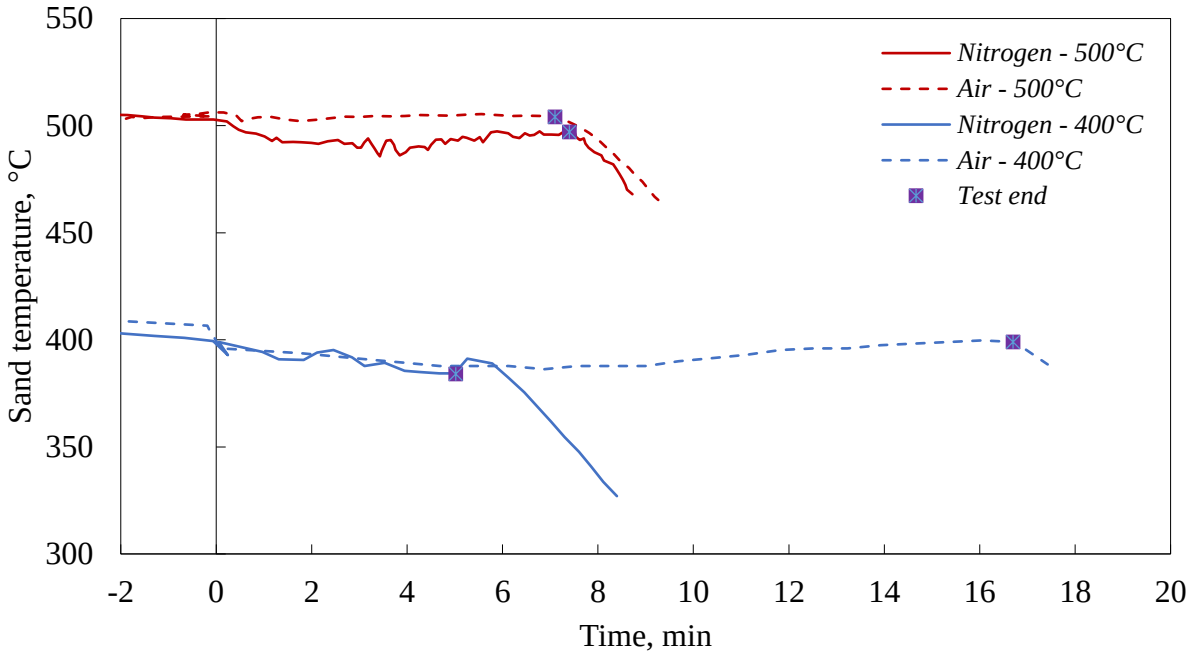

Figure S 21 - Sand temperature profiles during the tests with cellulose

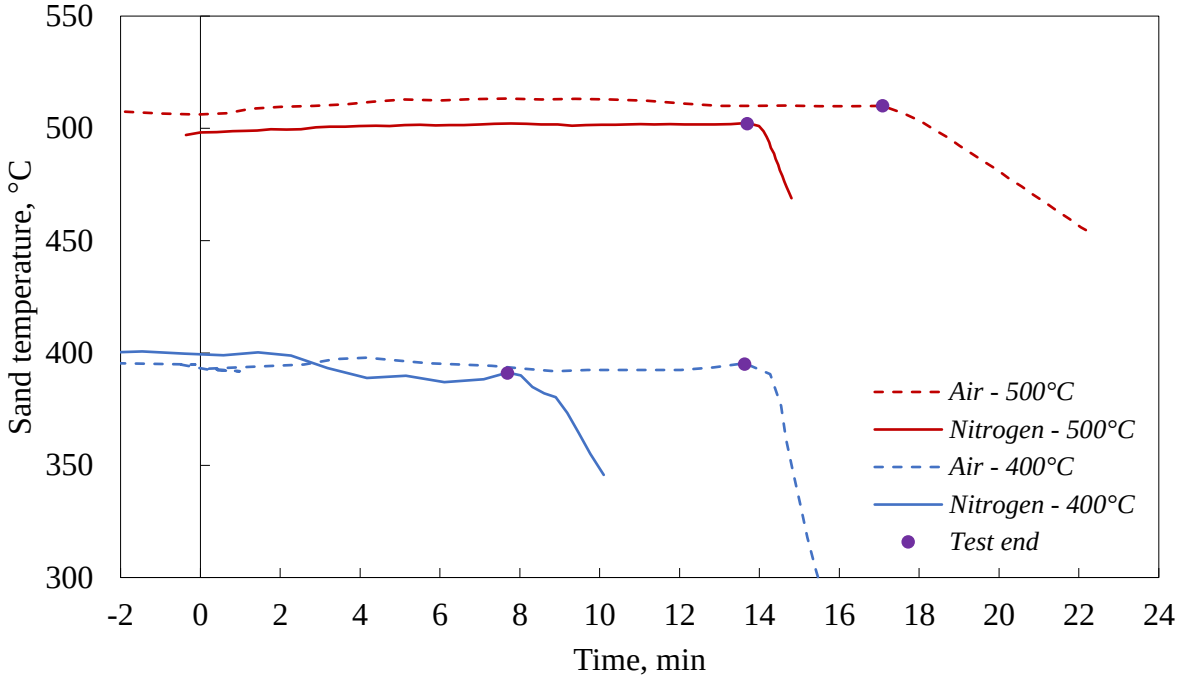

Figure S 22 - Sand temperature profiles during the tests with oak wood

4. Char residues

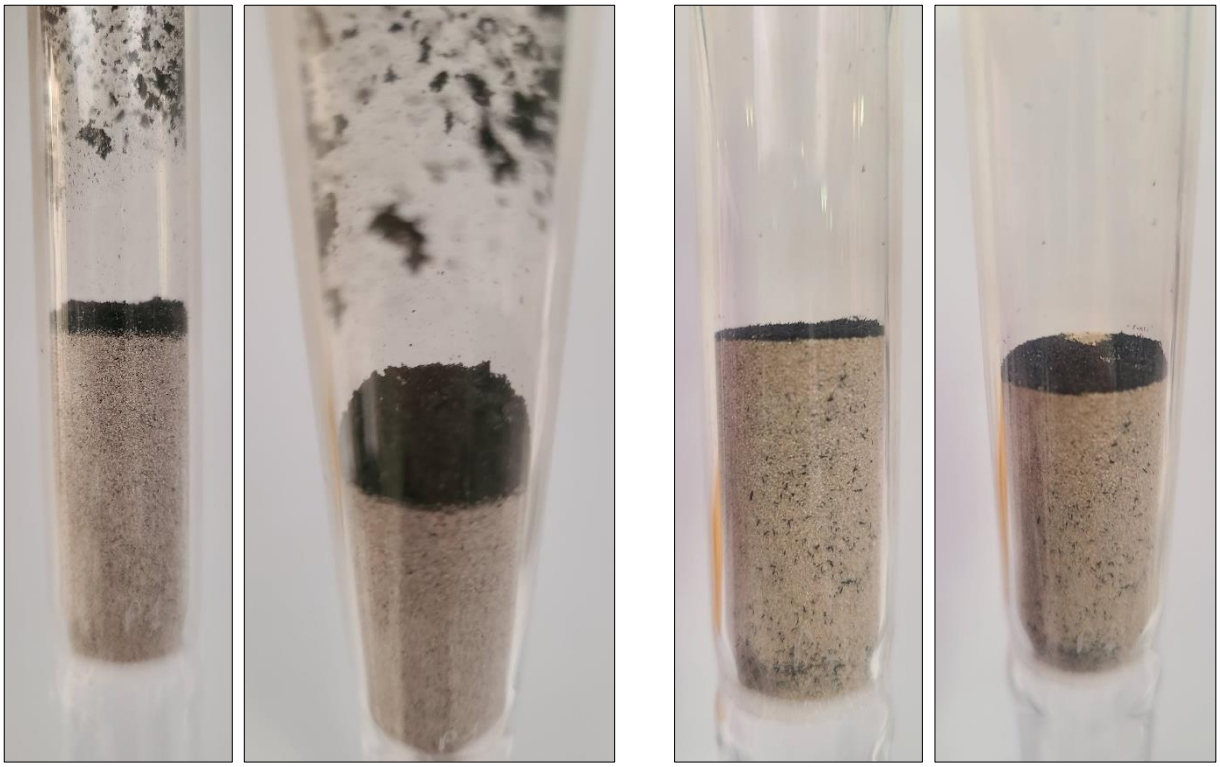

Figure S 23 - Char residues (cellulose to the left, oak wood to the right) at the surface of the sand bed after the tests at 400°C under nitrogen

Annex 5

A three-way experimental method to determine the laminar flame speed of organic powders

Matteo Pietraccini [1], Olivier Dufaud [1], Pierre-Alexandre Glaude [1], Anthony Dufour [1,*]

[1] *Université de Lorraine, CNRS, LRGP, F-54000 Nancy, France*

* *corresponding author: anthony.dufour@univ-lorraine.fr*

Supporting information

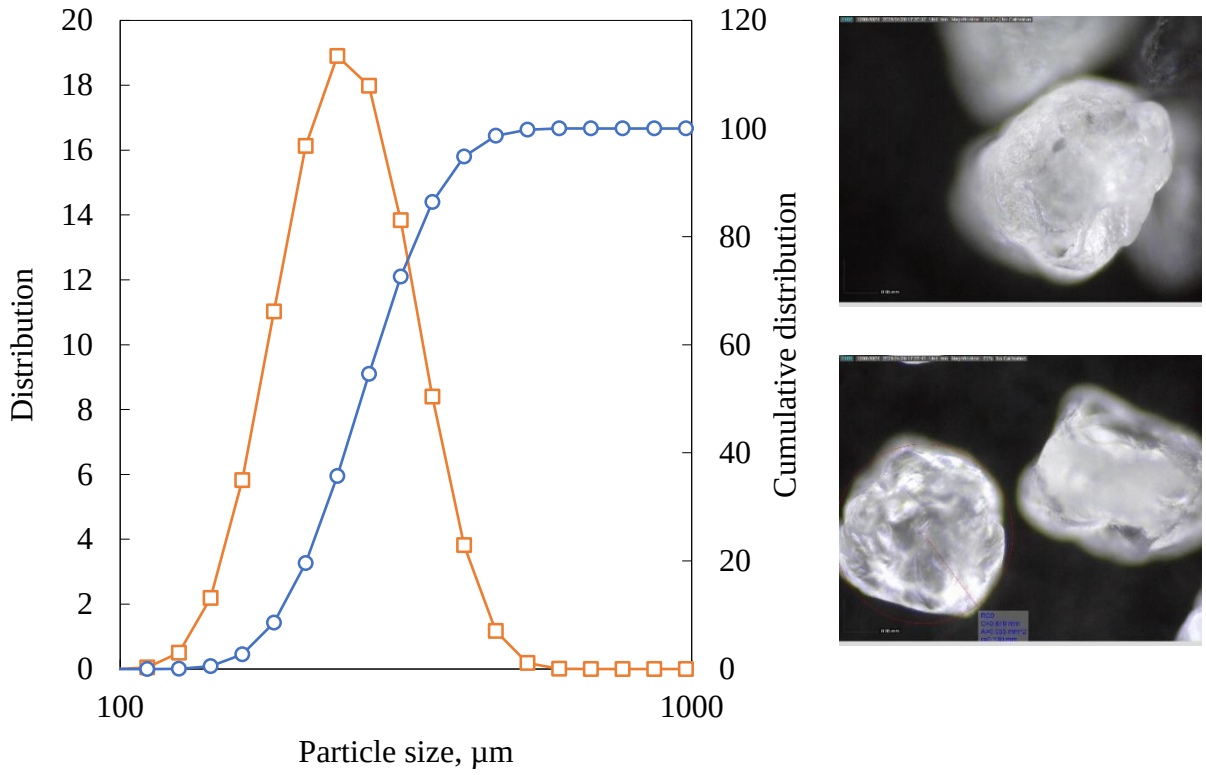

Figure S 24 - Particle size distribution (left) and appearance (right) of the Fontainebleau sand used in the micro-fluidised bed

Table S 12 - Oxygen demand for the complete oxidation of the flash pyrolysis products obtained feeding 100 g/h of cellulose

	Yield %wt of sample fed	**Mass flow g/h**	**Molar flow mol/h**	**Oxygen demand mol/h**
H_2	0.14	0.1	0.07	0.035
CO	2.69	2.7	0.10	0.048
CO_2	1.53	1.5	0.03	0.000
CH_4	0.20	0.2	0.01	0.025
C_2H_4	0.14	0.1	0.00	0.015
C_3H_6	0.35	0.4	0.01	0.037
Hydroxyacetaldehyde (gas)	7.60	7.6	0.13	0.253
Acetol (gas)	0.70	0.7	0.01	0.033
Hydroxyacetaldehyde (liquid)	0.08	0.1	0.00	0.003
Acetol (liquid)	0.01	0.0	0.00	0.000
Methanol	1.73	1.7	0.05	0.081
Acetic acid	1.73	1.7	0.03	0.058
Furfural + furfural alcohol	1.73	1.7	0.02	0.090
Levoglucosan	25.20	25.2	0.16	0.933

Table S 13 - Design procedure to calculate the nozzle diameter for the MFB burner

Umf	4.0	cm/s
Coefficient	2.0	-
Air velocity	8.0	cm/s
Reactor diameter	20	mm
Reactor section	3.1	cm^2
Sand bed temperature	400	°C
Pressure	1.0	atm
Air flow rate	0.000455	mol/s
O_2 flow rate	0.005733	mol/h de O_2
Air flow rate @ 450°C	1508	mL/min
Air flow rate @ 20°C	657	mL/min
Oxygen flow rate @ 20°C	131	mL/min
Oxygen molar flow rate @ 20°C	0.35	mol/h
Nitrogen molar flow rate @ 20°C	1.3	mol/h de N_2
Mixture richness	1	-
Oxygen demand for cellulose oxidation	1.61	mol/h
Cellulose mass flow rate (to feed)	21.6	g/h
Combustion temperature	1000	°C
Combustion products molar flow rate	3.07	mol/h
Combustion products flow rate @ T comb	193.23	L/h
Combustion products flow rate @ T comb	54	cm^3/s
Laminar burning velocity estimation	10	cm/s
Flame alfa angle	60	°
Burning velocity	12	cm/s
Flame front surface	4.6	cm^2
Nozzle diameter	5.92	mm

	Parameters
	Results

Table S 14 - Composition of the surrogate pyrolysis product mixture used in the simulation

Species	**Molar fraction**
Levoglucosan	0.758
Acetaldehyde	0.016
C_2H_4	0.003
CO_2	0.124
CO	0.096
H_2	0.000
CH_4	0.003

Table S 15 - Parameters used in the pyrolysis mixture flame propagation simulation on ChemkinII

Parameter	**Value**	**Unity**
Room temperature	298	K
Fresh mixture temperature	773	K
Fresh mixture pressure	760	torr
Initial central temperature of T gradient	1200	K
Max number of points	3000	-
Min number of points	12	-
Intial thickness flame	3	mm
Initial mass flow through flame front	0.035	$g.cm^{-2}.s^{-1}$
Initial mixture richness	1	-